3D MANEUVERS FOR ASYMMETRIC UNDER-ACTUATED RIGID BODY

A Dissertation

by

DONG HOON KIM

Submitted to the Office of Graduate Studies of
Texas A&M University
in partial fulfillment of the requirements for the degree of

DOCTOR OF PHILOSOPHY

Chair of Committee,	John L. Junkins
Co-Chair of Committee,	James D. Turner
Committee Members,	John E. Hurtado
	Aniruddha Datta
Head of Department,	Rodney Bowersox

August 2013

Major Subject: Aerospace Engineering

ABSTRACT

Most spacecraft are designed to be maneuvered to achieve pointing goals. This is generally accomplished by designing a three-axis control system. This work explores new maneuver strategies when only two control inputs are available: (i) sequential single-axis maneuvers and (ii) three-dimensional (3D) coupled maneuvers.

The sequential single-axis maneuver strategies are established for torque, time, and fuel minimization applications. The resulting control laws are more complicated than the equivalent results for three-axis control because of the highly nonlinear control switch-times. Classical control approaches lead to optimal, but discontinuous control profiles. This problem is overcome by introducing a torque-rate penalty for the torque minimization case. Alternative approaches are also considered for achieving smooth continuous control profiles by introducing a cubic polynomial multiplicative control switch smoother for the time and fuel minimization cases. Numerical and analytical results are presented to compare optimal maneuver strategies for both nominal and failed actuator cases.

The 3D maneuver strategy introduces a homotopy algorithm to achieve optimal nonlinear maneuvers minimizing the torque. Two cases are considered: (i) one of the three-axis control actuators fails and (ii) two control actuators fail among four control actuators. The solution strategy first solves the case when all three actuators are available. Then, the failed actuator case is recovered by introducing a homotopy embedding parameter, ε, into the nonlinear dynamics equation. By sweeping ε, a sequence of neighboring optimal control problems is solved that starts with the original maneuver problem and arrives at the solution for the under-actuated case. As ε approaches 1, the designated actuator no longer provides control inputs to the space-

craft, effectively modeling the failed actuator condition. This problem is complex for two reasons: (i) the governing equations are nonlinear and (ii) ε fundamentally alters the spacecraft's controllability. Davidenko's method is introduced for developing an ordinary differential equation for the costate variable as a function of ε. For each value of ε, the costate initial conditions are iteratively adjusted so that the terminal boundary conditions for the 3D maneuver are achieved. Optimal control applications are presented for both rest-to-rest and motion-to-rest cases that demonstrate the effectiveness of the proposed algorithm.

DEDICATION

To all my professors and colleagues, in particular, Professor John L. Junkins for his career contributions and Professor James D. Turner for exceptional mentorship.

To my family for their infinite trust and unconditional love.

ACKNOWLEDGEMENTS

I would like to express gratitude to my advisor Dr. John L. Junkins. His motivation, encouragement, discussions, financial support, and patience during my graduate study are sincerely appreciated. Also, Dr. Junkins has always given me perfect guidance to move forward when I encountered difficulties during my studies.

I also would like to thanks to Dr. James D. Turner. His discussions and collaboration made this dissertation possible. I also want to extend my gratitude to my committee members: Dr. John E. Hurtado and Dr. Aniruddha Datta. Additionally, I wish to convey this thanks to Dr. Srinivas R. Vadali who gave me a chance to start to work on the problem for the dissertation and Dr. Daniele Mortari who let me enter Bézier world. Thanks also go to Lisa Jordan for all her help during my studies and my friends and colleagues and the department faculty and staff for making my time at Texas A&M University a great experience.

Finally, thanks to my family for their encouragement, patience, and love.

TABLE OF CONTENTS

Page

ABSTRACT ii

DEDICATION iv

ACKNOWLEDGEMENTS v

TABLE OF CONTENTS vi

LIST OF FIGURES ix

LIST OF TABLES xv

1. INTRODUCTION 1

2. DYNAMICS AND KINEMATICS FOR RIGID BODY 8

2.1 Rigid Body Dynamics 8
2.2 Rigid Body Kinematics 9
2.2.1 Euler Angles 9
2.2.2 Quaternion 10
2.2.3 Modified Rodrigues Parameters 11

3. SINGLE-AXIS MANEUVERS OF RIGID BODY 12

3.1 Dynamics and Kinematics for Single-Axis Maneuvers 12
3.2 Minimum-Torque Maneuver 13
3.2.1 Derivations of Optimality Conditions 13
3.2.2 Analytical Solutions for States and Control 14
3.2.3 Numerical Examples 16
3.2.4 Concluding Remarks 19
3.3 Minimum-Time Maneuver 19
3.3.1 Derivations of Optimality Conditions 19
3.3.2 Analytical Solutions for States and Control 21
3.3.3 Analytical Solution for a Switch-Time 23
3.3.4 Numerical Examples 25
3.3.5 Concluding Remarks 27
3.4 Minimum-Fuel Maneuver 28
3.4.1 Derivations of Optimality Conditions 28
3.4.2 Analytical Solutions for States and Control 30
3.4.3 Analytical Solutions for Switch-Times 32

3.4.4 Numerical Examples 34
3.4.5 Concluding Remarks 37

4. JUMP DISCONTINUITY AVOIDANCE FOR CONTROL PROFILES . . 38

4.1 Torque-Rate Performance Index Technique: Torque Minimization . . 38
4.1.1 Derivations of Optimality Conditions 39
4.1.2 Analytical Solutions for States and Control 40
4.1.3 Numerical Examples 45
4.1.4 Concluding Remarks 48
4.2 Cubic Polynomial Technique: Maneuver Time Minimization 48
4.2.1 Analytical Solutions for States and Control 50
4.2.2 Numerical Example 51
4.2.3 Concluding Remarks 52
4.3 Cubic Polynomial Technique: Fuel Minimization 53
4.3.1 Analytical Solutions for States and Control 54
4.3.2 Numerical Example 56
4.3.3 Concluding Remarks 57

5. THREE-DIMENSIONAL MANEUVERS OF RIGID BODY 58

5.1 Introduction 58
5.2 Problem Formulations for Nominal Case 61
5.2.1 Optimal Control Formulations Using the Euler Angles 61
5.2.2 Optimal Control-Rate Formulations Using the Euler Angles . 63
5.2.3 Numerical Example 64
5.2.4 Concluding Remarks 68
5.3 Problem Formulations for Failed Actuator Case: Classical Method . . 69
5.3.1 Optimal Control Formulations Using the Euler Angles 71
5.3.2 Optimal Control-Rate Formulations Using the Euler Angles . 73
5.3.3 Numerical Example 74
5.3.4 Concluding Remarks 82
5.4 Problem Formulations for Failed Actuator Case: Reduced Method . . 83
5.4.1 Initial Costate Formulations Using the Euler Angles (Torque Minimization) 83
5.4.2 Initial Costate Formulations Using the Euler Angles (Torque-Rate Minimization) 86
5.4.3 Concluding Remarks 89
5.5 Analytical Solutions for Failed Actuator Case: Resultant Method . . 89
5.5.1 Hamiltonian Formulations Using the Euler Angles (Torque Minimization) 89
5.5.2 Hamiltonian Formulations Using the Euler Angles (Torque-Rate Minimization) 91
5.5.3 Classical Resultant Method 92
5.5.4 Numerical Example 97
5.5.5 Concluding Remarks 99

5.6 Closed-Form Solutions for Failed Actuator Case . . . 99
5.6.1 Switch-Times and Performance Index (Torque Minimization) . 99
5.6.2 Switch-Times and Performance Indices (Torque-Rate Minimization) . . . 100
5.6.3 Numerical Example . . . 102
5.6.4 Concluding Remarks . . . 103
5.7 Result Comparisons . . . 103

6. HOMOTOPY APPROACH FOR RIGID BODY MOTION ANALYSIS . . 105

6.1 Introduction . . . 105
6.2 Overview of the Homotopy Method . . . 107
6.3 Davidenko's Method . . . 109
6.4 Body-Axis Aligned Torque Distribution . . . 110
6.4.1 Problem Formulations and Solutions . . . 110
6.4.2 Homotopy Method Differential Equation . . . 112
6.4.3 Numerical Examples . . . 116
6.4.4 Concluding Remarks . . . 126

7. SUMMARY AND CONCLUSION . . . 128

REFERENCES . . . 132

APPENDIX A. DERIVATIONS FOR SMOOTHING FUNCTIONS . . . 137

A.1 Smoothing Function for Maneuver Time Minimization Problem . . . 137
A.2 Smoothing Function for Fuel Minimization Problem . . . 138

APPENDIX B. OPTIMAL CONTROL AND CONTROL-RATE FORMULATIONS AND RESULTS . . . 141

B.1 Formulations for Nominal Case . . . 141
B.1.1 Optimal Control Formulation Using the Quaternion . . . 141
B.1.2 Optimal Control Formulation Using the MRPs . . . 142
B.1.3 Optimal Control-Rate Formulation Using the Quaternion . . . 144
B.1.4 Optimal Control-Rate Formulation Using the MRPs . . . 145
B.2 Numerical Examples . . . 146

APPENDIX C. THREE-DIMENSIONAL MANEUVERS OF RIGID BODY . 162

C.1 Minimum-Time Maneuver . . . 162
C.2 Cubic Polynomial Technique: Maneuver Time Minimization . . . 166
C.3 Minimum-Fuel Maneuver . . . 170
C.4 Cubic Polynomial Technique: Fuel Minimization . . . 174

APPENDIX D. STATE TRANSITION MATRIX AND PARAMETER INFLUENCE VECTOR . . . 178

APPENDIX E. BODY-AXIS SKEWED TORQUE DISTRIBUTION . . . 180

LIST OF FIGURES

FIGURE Page

1.1 Illustration for three sequential maneuvers with two switch-times . . . 5

3.1 Minimum-torque time trajectories for the states, costates, and control; and phase portrait (rest-to-rest) . . . 17

3.2 Minimum-torque time trajectories for the states, costates, and control; and phase portrait (motion-to-rest) . . . 18

3.3 Minimum-time time trajectories for the states and control; and phase portrait (rest-to-rest) . . . 26

3.4 Minimum-time time trajectories for the states and control; and phase portrait (motion-to-rest) . . . 27

3.5 Minimum-fuel time trajectories for the states and control; and phase portrait (rest-to-rest) . . . 35

3.6 Minimum-fuel time trajectories for the states and control; and phase portrait (motion-to-rest) . . . 36

4.1 Near minimum-torque time trajectories for the states, costates, and control; and phase portrait (rest-to-rest) . . . 46

4.2 Near minimum-torque time trajectories for the states, costates, and control; and phase portrait (motion-to-rest) . . . 47

4.3 Near minimum-time time trajectories for the states and control; and phase portrait (rest-to-rest) . . . 52

4.4 Near minimum-fuel time trajectories for the states and control; and phase portrait (rest-to-rest) . . . 57

5.1 Nominal: Time trajectories for the states and control based on the Euler angles (torque minimization) . . . 66

5.2 Nominal: Time trajectories for the costates based on the Euler angles (torque minimization) . . . 67

5.3 Nominal: Time trajectories for the states based on the Euler angles (torque-rate minimization) . . . 67

5.4 Nominal: Time trajectories for the costates based on the Euler angles (torque-rate minimization) . . . 68

5.5 Failed: Time trajectories for the states based on the Euler angles (torque minimization) . . . 77

5.6 Failed: Time trajectories for the costates based on the Euler angles (torque minimization) . . . 78

5.7 Failed: Time trajectories for the Hamiltonian and performance index based on the Euler angles (torque minimization) . . . 78

5.8 Failed: Time trajectories for the states based on the Euler angles (torque-rate minimization) . . . 79

5.9 Failed: Time trajectories for the costates based on the Euler angles (torque-rate minimization) . . . 79

5.10 Failed: Time trajectories for the Hamiltonian and performance indices based on the Euler angles (torque-rate minimization) . . . 80

5.11 Time trajectories for the principal angles based on the Euler angles (torque minimization) . . . 80

5.12 Time trajectories for the principal angles based on the Euler angles (torque-rate minimization) . . . 81

6.1 Flowchart for obtaining TPBVP solutions . . . 115

6.2 Aligned: Time trajectories for the MRPs (rest-to-rest) . . . 118

6.3 Aligned: Time trajectories for the angular velocity (rest-to-rest) . . . 119

6.4 Aligned: Time trajectories for the costates associated with the MRPs (rest-to-rest) . . . 119

6.5 Aligned: Time trajectories for the costates associated with the angular velocity (rest-to-rest) . . . 120

6.6 Aligned: Time trajectories for the control torque (rest-to-rest) . . . 120

6.7 Aligned: 3D trajectory for the MRPs (rest-to-rest) . . . 121

6.8 Aligned: 3D trajectory for the angular velocity (rest-to-rest) . . . 121

6.9 Aligned: Time trajectories for the MRPs (motion-to-rest) . . . 122

6.10 Aligned: Time trajectories for the angular velocity (motion-to-rest) . . . 123

6.11 Aligned: Time trajectories for the costates associated with the MRPs (motion-to-rest) . . . 123

6.12 Aligned: Time trajectories for the costates associated with the angular velocity (motion-to-rest) . . . 124

6.13 Aligned: Time trajectories for the control torque (motion-to-rest) . . 124

6.14 Aligned: 3D trajectory for the MRPs (motion-to-rest) . . . 125

6.15 Aligned: 3D trajectory for the angular velocity (motion-to-rest) . . . 125

B.1 Nominal: Time trajectories for the states and control based on the quaternion (torque minimization) . . . 148

B.2 Nominal: Time trajectories for the costates based on the quaternion (torque minimization) . . . 148

B.3 Failed: Time trajectories for the states and control based on the quaternion (torque minimization) . . . 149

B.4 Failed: Time trajectories for the costates based on the quaternion (torque minimization) . . . 149

B.5 Failed: Time trajectories for the Hamiltonian and performance index based on the quaternion (torque minimization) . . . 150

B.6 Failed: Time trajectories for the (3-1-3) set of Euler angles based on the quaternion (torque minimization) . . . 150

B.7 Time trajectories for the principal angles based on the quaternion (torque minimization) . . . 151

B.8 Nominal: Time trajectories for the states based on the quaternion (torque-rate minimization) . . . 151

B.9 Nominal: Time trajectories for the costates based on the quaternion (torque-rate minimization) . . . 152

B.10 Failed: Time trajectories for the states based on the quaternion (torque-rate minimization) . . . 152

B.11 Failed: Time trajectories for the costates based on the quaternion (torque-rate minimization) . . . 153

B.12 Failed: Time trajectories for the Hamiltonian and performance indices based on the quaternion (torque-rate minimization) . . . 153

B.13 Failed: Time trajectories for the (3-1-3) set of Euler angles based on the quaternion (torque-rate minimization) 154

B.14 Time trajectories for the principal angles based on the quaternion (torque-rate minimization) 154

B.15 Nominal: Time trajectories for the states and control based on the MRPs (torque minimization) 155

B.16 Nominal: Time trajectories for the costates based on the MRPs (torque minimization) 155

B.17 Failed: Time trajectories for the states and control based on the MRPs (torque minimization) 156

B.18 Failed: Time trajectories for the costates based on the MRPs (torque minimization) 156

B.19 Failed: Time trajectories for the Hamiltonian and performance index based on the MRPs (torque minimization) 157

B.20 Failed: Time trajectories for the (3-1-3) set of Euler angles based on the MRPs (torque minimization) 157

B.21 Time trajectories for the principal angles based on the MRPs (torque minimization) 158

B.22 Nominal: Time trajectories for the states based on the MRPs (torque-rate minimization) 158

B.23 Nominal: Time trajectories for the costates based on the MRPs (torque-rate minimization) 159

B.24 Failed: Time trajectories for the states based on the MRPs (torque-rate minimization) 159

B.25 Failed: Time trajectories for the costates based on the MRPs (torque-rate minimization) 160

B.26 Failed: Time trajectories for the Hamiltonian and performance indices based on the MRPs (torque-rate minimization) 160

B.27 Failed: Time trajectories for the (3-1-3) set of Euler angles based on the MRPs (torque-rate minimization) 161

B.28 Time trajectories for the principal angles based on the MRPs (torque-rate minimization) 161

C.1 Minimum-time time trajectories for the (1-3-1) set of Euler angles . . 164
C.2 Minimum-time time trajectories for the angular velocity (1-3-1) . . . 164
C.3 Minimum-time time trajectories for the control torque (1-3-1) 165
C.4 Minimum-time time trajectories for the principal angle (1-3-1) 165
C.5 Minimum-time time trajectories for the principal angle (3-1-3) 166
C.6 Near minimum-time time trajectories for the (1-3-1) set of Euler angles167
C.7 Near minimum-time time trajectories for the angular velocity (1-3-1) 168
C.8 Near minimum-time time trajectories for the control torque (1-3-1) . 168
C.9 Near minimum-time time trajectories for the principal angle (1-3-1) . 169
C.10 Near minimum-time time trajectories for the principal angle (3-1-3) . 169
C.11 Minimum-fuel time trajectories for the (1-3-1) set of Euler angles . . 171
C.12 Minimum-fuel time trajectories for the angular velocity (1-3-1) 172
C.13 Minimum-fuel time trajectories for the control torque (1-3-1) 172
C.14 Minimum-fuel time trajectories for the principal angle (1-3-1) 173
C.15 Minimum-fuel time trajectories for the principal angle (3-1-3) 173
C.16 Near minimum-fuel time trajectories for the (1-3-1) set of Euler angles 175
C.17 Near minimum-fuel time trajectories for the angular velocity (1-3-1) . 175
C.18 Near minimum-fuel time trajectories for the control torque (1-3-1) . . 176
C.19 Near minimum-fuel time trajectories for the principal angle (1-3-1) . . 176
C.20 Near minimum-fuel time trajectories for the principal angle (3-1-3) . . 177
E.1 Pyramid type of reaction wheel allocation description 181
E.2 Skewed: Time trajectories for the MRPs (rest-to-rest) 181
E.3 Skewed: Time trajectories for the angular velocity (rest-to-rest) . . . 182
E.4 Skewed: Time trajectories for the costates associated with the MRPs (rest-to-rest) 182
E.5 Skewed: Time trajectories for the costates associated with the angular velocity (rest-to-rest) 183

E.6 Skewed: Time trajectories for the control torque (rest-to-rest) 183

E.7 Skewed: 3D trajectory for the MRPs (rest-to-rest) 184

E.8 Skewed: 3D trajectory for the angular velocity (rest-to-rest) 184

E.9 Skewed: Time trajectories for the MRPs (motion-to-rest) 185

E.10 Skewed: Time trajectories for the angular velocity (motion-to-rest) . 185

E.11 Skewed: Time trajectories for the costates associated with the MRPs (motion-to-rest) 186

E.12 Skewed: Time trajectories for the costates associated with the angular velocity (motion-to-rest) 186

E.13 Skewed: Time trajectories for the control torque (motion-to-rest) . . 187

E.14 Skewed: 3D trajectory for the MRPs (motion-to-rest) 187

E.15 Skewed: 3D trajectory for the angular velocity (motion-to-rest) . . . 188

LIST OF TABLES

TABLE Page

3.1 Simulation parameters for a single-axis minimum-torque maneuver . . 16

3.2 Simulation parameters for a single-axis minimum-time maneuver . . . 25

3.3 Simulation parameters for a single-axis minimum-fuel maneuver . . . 34

5.1 Simulation parameters for a 3D minimum-torque maneuver at initial and final times 65

5.2 Nominal: found initial costates and required iterations (torque minimization) 65

5.3 Nominal: found initial costates and required iterations (torque-rate minimization) 66

5.4 Simulation parameters for a 3D minimum-torque maneuver at interior times 75

5.5 Failed: found initial costates and required iterations (torque minimization) 75

5.6 Failed: found initial costates and required iterations (torque-rate minimization) 76

5.7 Torque consumption comparison: nominal vs failed actuator 82

5.8 Torque consumption comparison: (3-1-3) set vs (1-3-1) set 103

5.9 Computational burden comparison: torque minimization vs torque-rate minimization 104

6.1 Simulation parameters for a 3D minimum-torque maneuver (rest-to-rest) 116

6.2 Simulation parameters for a 3D minimum-torque maneuver (motion-to-rest) 116

B.1 Simulation parameters for a 3D minimum-torque maneuver 147

1. INTRODUCTION

This dissertation explores under-actuated spacecraft attitude maneuver problems. This class of spacecraft maneuver applications represents a special case of general maneuver strategies. The problem, however, has great practical utility. The early part of the dissertation deals with the classical case of single-axis rigid body sub-optimal maneuvers. Subsequent developments are introduced that apply to three-axis optimal rigid body maneuvers. In these developments, the Euler angle transformation [1] is utilized to establish new insights into avoiding inputs for the failed control axis. Fully coupled three-dimensional (3D) maneuvers are achieved by introducing a homotopy approach to obtain optimal control solutions as well as analyze the optimal rigid body behavior due to numerical challenges associated with the degradation of controllability.

The dynamics and several kinematic equations are addressed in Section 2 for developing under-actuated system control strategies. Several configuration coordinates are investigated but Euler angles are mainly used in this work. In general, it is known that each set of Euler angles has a geometric singularity. For example, the standard aircraft orientation angles, the (3-2-1) set of Euler angles, yaw, pitch, and roll, are singular when the aircraft pitches up or down 90 degrees [1]. Therefore, selecting Euler angles as the orientation parameters introduces singularities for some maneuvers. However, certain analytical advantages still make Euler angle representations useful in specific problems. There exist 12 sets of Euler angle transformations based on the rotation sequences. Among the 12 sets, attention is focused on the "symmetric" sets, which have the same index for the first and third rotations as (1-3-1), (3-1-3), etc. Intuition suggests these special sets are useful for

handling under-actuated system control problems that have only two control inputs available. Alternatively, Tsiotras and Longuski introduced a new set of rigid body attitude coordinates, which has only two parameters [2]. These attitude coordinates are utilized to handle symmetric under-actuated system stabilization problems [3, 4, 5, 6, 7, 8, 9]. This work extends Tsiotras's work to handle the general (asymmetric) under-actuated system control problems, which are more general and also more challenging cases. Tsiotras's work is further extended by introducing a quadratic torque-rate penalty to the performance index to produce smooth continuous control profiles.

Section 3 reviews classical single-axis rigid body optimal maneuver problems, specifically minimum-energy, minimum-time, and minimum-fuel maneuvers. Many of theses formulations and solutions already exist with some assumptions in Refs. [10, 11], but all formulations and solutions are generalized for handling the special need of under-actuated spacecraft control. Both rest-to-rest and motion-to-rest cases are considered and simulation results are presented. Moreover, it is found that an open-loop control for the torque minimization problem has a structure somewhat analogous to a feedback control. These existing formulations are discussed to help readers understand the sequential maneuver strategy presented in Section 5 for under-actuated control problems.

While Section 3 deals with general single-axis optimal maneuver formulations and solutions, Section 4 studies two techniques for generating smooth continuous control profiles. In Section 3, the control profiles for the several optimal maneuvers are discussed. For example, the minimum-torque approach yields a smooth linear control profile, whereas the minimum-time and minimum-fuel approaches yield bang-bang and bang-off-bang control profiles, respectively. These jump discontinuities in control profiles are unattractive for some applications: in particular, for flexible struc-

tures, because their high frequency behavior can potentially excite an undesirable flexible body response. Two techniques are investigated to avoid the jump discontinuities in control profiles, specifically (i) a quadratic torque-rate penalty addition to the performance index and (ii) a cubic polynomial weight function multiplication for smoothing the control switches. The quadratic torque-rate penalty term is added to the performance index for torque minimization problems, and the cubic polynomial multiplication is applied for the control smoothing for both maneuver time and fuel minimization problems. The analytical solution for the torque minimization problem, subject to the quadratic torque-rate term in the performance index, is presented in Ref. [10]. The analytical solution is simplified by neglecting the quadratic torque term in the performance index. The analytical solution for the maneuver time minimization problem, including the cubic polynomial multiplication for the control smoothing, is presented in Refs. [12, 13], but no derivations are presented. Derivations for the analytical solution are presented in Appendix A.1 to make this dissertation self-contained. Analogous to, and motivated by, the maneuver time minimization results, the analytical solutions and derivations for the fuel minimization problem, including the cubic polynomial multiplication for the control smoothing, are presented in Appendix A.2. For flexible body cases, the jump discontinuities in control profiles cause an undesirable vibratory motion. Thus, both of these control smoothing approaches are useful for flexible system applications. As is shown in Ref. [13], smoothing of control profiles is extremely effective in reductions of vibration for both theoretically and in hardware realizations.

Section 5 extends the single-axis rigid body minimum-torque problem to the three-axis rigid body minimum-torque problem. For the nominal case, where three control inputs are available along the body axes, optimal control and control-rate formulations based on the Euler angles are derived. Again, the torque-rate mini-

mization case is studied for generating smooth continuous control profiles; however, this approach does not generate the minimum-torque solution. The optimal control and control-rate formulations utilizing the quaternion and the modified Rodrigues parameters are derived in Appendix B. For the failed actuator case, where only two control inputs are available along any arbitrary two body axes, it's extremely difficult to find optimal control solutions unless accurate initial costate guesses are given. Thus, a sequential sub-optimal maneuver strategy is suggested to avoid inputs for the failed control axis. Since the sequential maneuver strategy is utilized for the failed actuator case, one may expect longer "flight time" state trajectories than the optimal solutions for the failed actuator case given accurate initial costate guesses. Thus, this strategy provides sub-optimal solutions that are "good enough" for some applications. The main advantage of this strategy is that this will efficiently lead us to 3D maneuver solutions given two control inputs most of the time, even if accurate initial costate guesses are not available.

When only two control inputs are available, the suggested strategy is as follows: (1) transform the given initial and final attitude representations to specific attitude representations using the Euler angle transformations that avoid the input for the failed control axis; (2) define three sequential sub-maneuvers; (3) define new attitude commands at switch-times for each sub-maneuver; (4) solve for optimal switch-times for starting and ending each sub-maneuver; and (5) perform the defined single-axis sub-maneuvers. With three maneuver periods to be defined, two unknown switch-times, t_1 and t_2, must be found as shown in Fig. 1.1.

The suggested strategy gives rise to three issues that make the calculation of an optimal control solution challenging: (i) unknown switch-times must be determined to change from one sub-maneuver to the next sub-maneuver, (ii) the number of constraints is high, and (iii) the switch-times introduce jump conditions on the

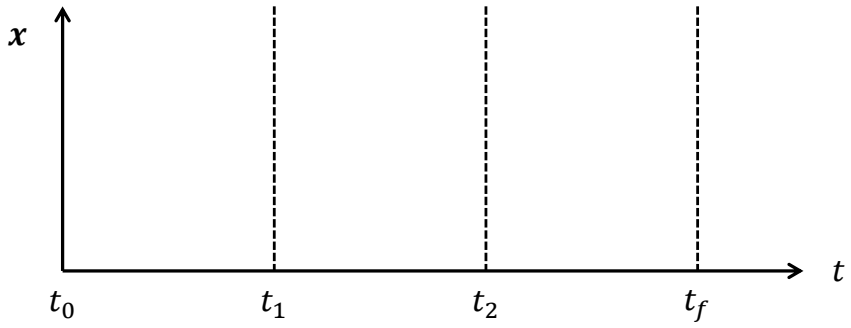

Figure 1.1: Illustration for three sequential maneuvers with two switch-times

necessary conditions that must be iteratively refined to generate the desired solution. The brute-force approach for solving the problem consists of handling the nonlinear necessary conditions by introducing a multiple shooting method [14], which enforces both the end and interior points that define the optimal solution. This method is called the *classical method* in this work; it requires expensive computational efforts.

This expensive computational cost motivates a search for simpler strategies. To this end, using the analytical solutions for the single-axis maneuvers, the unknown initial costates are reformulated as functions of two unknown switch-times. This variable transformation reduced 32 (or 47) nonlinear constraints to 2 constraints, which greatly simplified the problem. By reducing the number of unknowns, this problem becomes much less sensitive to initial guesses. For the remainder of this work, this method is called the *reduced method*; it requires less computational efforts than the classical method.

In the reduced method formulation, the initial costate are functions of two unknown switch-times. The necessary conditions defining the switch-times are defined by two Hamiltonian constraints. These constraint conditions are handled by introducing a classical algebraic resultant method [15]. The resultant method transforms the two scalar constraint conditions into a matrix equation, where one variable

is eliminated from all terms in the matrix. By evaluating the determinant of the matrix and setting the result to zero, a polynomial equation is obtained that is only a function of one of the switch-times. This equation is numerically solved for the roots of the polynomial. Extraneous root solutions are eliminated to ensure that the switch-time solutions are physically meaningful. By calculating the performance index for each remaining meaningful solution, a set of switch-times is obtained. This method is called the *resultant method* in this work; it requires post-processing but it is much less expensive than the reduced method computationally.

This approach is further refined by observing that the Hamiltonian polynomial equations can be manipulated analytically to provide *closed-form solutions* for both switch-times. Until now, a set of Euler angle sequences is implicitly assumed. However, two possible sets are available when one control axis has failed. For example, when second control axis fails, both the (1-3-1) and (3-1-3) sets are available. Using the closed-form solution for the switch-times, a closed-form solution for the performance index is also obtained. By calculating the performance index, the best Euler angle sequence for the sub-optimal maneuver solution is determined. Obviously, the closed-form solution approach provides the highest level of computational performance and enables real-time calculations for on-board spacecraft applications.

Section 6 presents a homotopy algorithm to establish an optimal nonlinear maneuver strategy minimizing torque for large-angle three-axis spacecraft. This problem is very challenging and fundamental as a rigorous optimal control solution for under-actuated control applications. As a generalization, the case when two control actuators fail among four control actuators is presented in Appendix E. For the three actuator case, the solution strategy first solves the three-axis control problem when all three actuators are available. The failed actuator case is recovered by introducing a homotopy embedding parameter, ε, into the nonlinear dynamics equation to suppress

the input from the assumed failed actuator. By sweeping ε, a sequence of neighboring optimal control problems is solved that starts with the nominal maneuver problem and arrives at the solution for the failed actuator case. For example, the nominal rotational dynamic equation is given by

$$\dot{\boldsymbol{\omega}} = \boldsymbol{p}\,(\boldsymbol{\omega},\, u_1,\, u_2,\, u_3) \tag{1.1}$$

and the Homotopy dynamic equation is given by

$$\dot{\boldsymbol{\omega}}(\varepsilon) = \tilde{\boldsymbol{p}}\,(\boldsymbol{\omega},\, u_1,\, u_2,\, (1-\varepsilon)u_3) \tag{1.2}$$

Clearly, setting $\varepsilon = 0$ defines the nominal case in Eq. (1.1). Setting $\varepsilon = 1$ defines the failed actuator case

$$\dot{\boldsymbol{\omega}}(\varepsilon = 1) = \tilde{\boldsymbol{p}}\,(\boldsymbol{\omega},\, u_1,\, u_2,\, 0) \tag{1.3}$$

where u_3 no longer contributes to the system dynamics, thereby emulating a failed actuator situation.

The governing equation is nonlinear, and the term, $1-\varepsilon$, fundamentally alters controllability of the spacecraft. Davidenko's method is introduced for developing an ordinary differential equation for the costate variable as a function of ε. For each value of ε, the costate initial condition is iteratively adjusted so that the terminal boundary conditions for the 3D maneuver are achieved. Optimal control applications are presented for both rest-to-rest and motion-to-rest cases that demonstrate the effectiveness of the proposed algorithm. The resulting solutions are very general, but expensive to obtain.

2. DYNAMICS AND KINEMATICS FOR RIGID BODY

The rotational dynamics and several kinematics for an asymmetric rigid body are discussed briefly. All details for the dynamics and kinematics are omitted. (see Ref. [1])

2.1 Rigid Body Dynamics

The rotational dynamics equations of a rigid body is given by [10, 16, 17]

$$\dot{\boldsymbol{\omega}} \triangleq \boldsymbol{p}(\boldsymbol{\omega},\, \boldsymbol{u}) = [J]^{-1}\left(-\left[\boldsymbol{\omega}^{\times}\right][J]\boldsymbol{\omega} + \boldsymbol{u}\right) \tag{2.1}$$

where $[J] \in \mathcal{R}^{3\times 3}$ is the positive definite inertia tensor for the spacecraft, $\boldsymbol{\omega} \in \mathcal{R}^3$ is the angular velocity vector of the spacecraft, $\boldsymbol{u} \in \mathcal{R}^3$ is the control torque vector, and $[\boldsymbol{\zeta}^{\times}] \in \mathcal{R}^{3\times 3}$ is the cross product of the generic vector, $\boldsymbol{\zeta} \in \mathcal{R}^3$, which is defined as

$$\left[\boldsymbol{\zeta}^{\times}\right] \triangleq \begin{bmatrix} 0 & -\zeta_3 & \zeta_2 \\ \zeta_3 & 0 & -\zeta_1 \\ -\zeta_2 & \zeta_1 & 0 \end{bmatrix}$$

By choosing a body fixed coordinate system, which is aligned with the principal body axes, the inertia tensor is diagonal and Eq. (2.1) is expressed as

$$\dot{\omega}_1 = -\frac{(J_{33} - J_{22})}{J_{11}}\omega_2\omega_3 + \frac{u_1}{J_{11}} \tag{2.2a}$$

$$\dot{\omega}_2 = -\frac{(J_{11} - J_{33})}{J_{22}}\omega_3\omega_1 + \frac{u_2}{J_{22}} \tag{2.2b}$$

$$\dot{\omega}_3 = -\frac{(J_{22} - J_{11})}{J_{33}}\omega_1\omega_2 + \frac{u_3}{J_{33}} \tag{2.2c}$$

2.2 Rigid Body Kinematics

Attitude parameters are sets of coordinates that completely describe the orientation of a rigid body relative to some reference coordinate frame. There exist infinite number of attitude coordinates [1]. Several common attitude parameters are considered for the optimal control formulations: (i) the Euler angles, (ii) the quaternion, and (iii) the modified Rodrigues parameters (MRPs).

2.2.1 Euler Angles

The Euler angles describe the attitude motion through three successive rotation angles (θ_1, θ_2, θ_3) about the body fixed axes. The governing kinematic differential equation for the Euler angles is given by

$$\dot{\boldsymbol{\theta}} \triangleq \boldsymbol{h}(\boldsymbol{\theta}, \boldsymbol{\omega}) = [B(\boldsymbol{\theta})]\,\boldsymbol{\omega} \tag{2.3}$$

where $[B(\boldsymbol{\theta})] \in \mathcal{R}^{3\times 3}$ is defined by the sequence of rotation. For aircraft and spacecraft orientations, the (3-2-1) set of Euler angles is commonly used. To define the orientation of orbit planes of the planet relative to the Earth's orbit plane, the (3-1-3) set of Euler angles is commonly used [10]. The (3-1-3) set of mapping matrix, $B[(\boldsymbol{\theta})]$, between the angular velocity vector of the spacecraft and the Euler angle rates, $\dot{\boldsymbol{\theta}}$, is given by

$$[B(\boldsymbol{\theta})] \triangleq \frac{1}{\mathrm{s}\theta_2} \begin{bmatrix} \mathrm{s}\theta_3 & \mathrm{c}\theta_3 & 0 \\ \mathrm{s}\theta_2\,\mathrm{c}\theta_3 & -\mathrm{s}\theta_2\,\mathrm{s}\theta_3 & 0 \\ -\mathrm{c}\theta_2\,\mathrm{s}\theta_3 & -\mathrm{c}\theta_2\,\mathrm{c}\theta_3 & \mathrm{s}\theta_2 \end{bmatrix}$$

where $\mathrm{s}\theta_i$ and $\mathrm{c}\theta_i$ denote $\sin\theta_i$ and $\cos\theta_i$, respectively. The (3-1-3) set of Euler angle kinematic differential equation encounters a singularity at $\theta_2 = 0$ or 180 radians. In general, all possible 12 sets of $B[(\boldsymbol{\theta})]$ encounter singularity at specific value of the

second rotation angle, θ_2, only [1]. This drawback limits the use of the Euler angle kinematic differential equations. Certain analytical advantages, however, still make Euler angle representations useful in specific problems.

2.2.2 Quaternion

The quaternion vector is a popular set of coordinates; four elements of the quaternion provide a redundant, nonsingular attitude description that is well suited to describe arbitrary and large rotations [1]. The quaternion vector, $\boldsymbol{q} \in \mathcal{R}^4$, is defined in terms of the principal rotation elements as

$$\boldsymbol{q} \triangleq \begin{Bmatrix} \boldsymbol{\rho} \\ q_4 \end{Bmatrix} = \begin{Bmatrix} \hat{\boldsymbol{e}} \sin \dfrac{\Phi}{2} \\ \cos \dfrac{\Phi}{2} \end{Bmatrix} \tag{2.4}$$

where $\hat{\boldsymbol{e}} \in \mathcal{R}^3$ is the principal vector, $\Phi \in \mathcal{R}^1$ is the principal angle, and the quaternion is constrained by the following relation

$$\boldsymbol{q}^{\mathrm{T}} \boldsymbol{q} = 1 \tag{2.5}$$

The governing kinematic differential equation for the quaternion is given by

$$\dot{\boldsymbol{q}} \triangleq \boldsymbol{f}(\boldsymbol{q}, \boldsymbol{\omega}) = \frac{1}{2} \left[\Omega(\boldsymbol{\omega})\right] \boldsymbol{q} \tag{2.6}$$

where $[\Omega(\boldsymbol{\omega})] \in \mathcal{R}^{4\times 4}$ is defined as

$$\left[\Omega(\boldsymbol{\omega})\right] \triangleq \begin{bmatrix} -\left[\boldsymbol{\omega}^{\times}\right] & \boldsymbol{\omega} \\ -\boldsymbol{\omega}^{\mathrm{T}} & 0 \end{bmatrix}$$

The time derivative of Eq. (2.5) is written as

$$\frac{\mathrm{d}}{\mathrm{d}t}\left(\boldsymbol{q}^{\mathrm{T}}\boldsymbol{q}\right) = \dot{\boldsymbol{q}}^{\mathrm{T}}\boldsymbol{q} + \boldsymbol{q}^{\mathrm{T}}\dot{\boldsymbol{q}} \tag{2.7}$$

Substituting Eq. (2.6) into Eq. (2.7) yields

$$\dot{\boldsymbol{q}}^{\mathrm{T}}\boldsymbol{q} + \boldsymbol{q}^{\mathrm{T}}\dot{\boldsymbol{q}} = \frac{1}{2}\boldsymbol{q}^{\mathrm{T}}\left[\Omega(\boldsymbol{\omega})\right]^{\mathrm{T}}\boldsymbol{q} + \frac{1}{2}\boldsymbol{q}^{\mathrm{T}}\left[\Omega(\boldsymbol{\omega})\right]\boldsymbol{q} = -\frac{1}{2}\boldsymbol{q}^{\mathrm{T}}\left[\Omega(\boldsymbol{\omega})\right]\boldsymbol{q} + \frac{1}{2}\boldsymbol{q}^{\mathrm{T}}\left[\Omega(\boldsymbol{\omega})\right]\boldsymbol{q} = 0 \tag{2.8}$$

which demonstrates that the quaternion norm constraint in Eq. (2.5) is satisfied naturally from Eq. (2.6).

2.2.3 Modified Rodrigues Parameters

The MPRs are another set of coordinates; they provide any attitude description except for a complete revolution [1]. The MRPs are defined in terms of the quaternion or the principal rotational elements as

$$\boldsymbol{\sigma} = \frac{\boldsymbol{\rho}}{1 + q_4} = \hat{\boldsymbol{e}} \tan\frac{\Phi}{4} \tag{2.9}$$

where the MRPs have a geometric singularity at $\Phi = \pm 2\pi$ radians from Eq. (2.9).

The governing kinematic differential equation for the MRPs is given by

$$\dot{\boldsymbol{\sigma}} \triangleq \boldsymbol{r}(\boldsymbol{\sigma}, \boldsymbol{\omega}) = \frac{1}{4}\left[B(\boldsymbol{\sigma})\right]\boldsymbol{\omega} \tag{2.10}$$

where $[B(\boldsymbol{\sigma})] \in \mathcal{R}^{3\times 3}$ is defined as

$$\left[B(\boldsymbol{\sigma})\right] \triangleq \left(1 - \boldsymbol{\sigma}^{\mathrm{T}}\boldsymbol{\sigma}\right) I_{3\times 3} + 2\left[\boldsymbol{\sigma}^{\times}\right] + 2\boldsymbol{\sigma}\boldsymbol{\sigma}^{\mathrm{T}}$$

3. SINGLE-AXIS MANEUVERS OF RIGID BODY

Single-axis special maneuver cases are presented for several minimization problems: (i) torque, (ii) maneuver time, and (iii) fuel.

3.1 Dynamics and Kinematics for Single-Axis Maneuvers

For a single-axis maneuver special case, the kinematic and rotational dynamic equations in Eqs. (2.1) and (2.3) are simply expressed as

$$\dot{\theta} = \omega \tag{3.1a}$$

$$\dot{\omega} = \frac{u}{J} \tag{3.1b}$$

where $\{\theta, \omega\}^{\mathrm{T}} \in \mathcal{R}^2$ is the state vector and $J \in \mathcal{R}^1$ is the inertia for the rotating axis. The scalar control input, u, is constrained by

$$|u(t)| \leq u_{\max} \tag{3.2}$$

where $u_{\max}$ is the maximum control input.

The objective is to determine a control input to bring any given initial states $\{\theta(t_0), \omega(t_0)\}^{\mathrm{T}}$ to a desired final states $\{\theta(T), \omega(T)\}^{\mathrm{T}}$. The initial and final states are defined as

$$\theta(t_0) = \theta_0 \tag{3.3a}$$

$$\omega(t_0) = \omega_0 \tag{3.3b}$$

$$\theta(T) = \theta_T \tag{3.3c}$$

$$\omega(T) = \omega_T \tag{3.3d}$$

3.2 Minimum-Torque Maneuver

A minimum-torque control solution is developed by defining the Lagrange form of a performance index given by

$$\mathcal{J} = \frac{1}{2}\int_{t_0}^{T} u^2 \, \mathrm{d}t \tag{3.4}$$

where t_0 is the *fixed* initial time and T is the *fixed* final time.

$*$ *Note that the unbounded control input is assumed for the minimum-torque maneuver.*

3.2.1 Derivations of Optimality Conditions

Using standard calculus of variations techniques, the Hamiltonian for the given problem is defined as

$$\mathcal{H} = \frac{1}{2}u^2 + \lambda_\theta \dot{\theta} + \lambda_\omega \dot{\omega} = \frac{1}{2}u^2 + \lambda_\theta \omega + \lambda_\omega \frac{u}{J} \tag{3.5}$$

where $\{\lambda_\theta, \, \lambda_\omega\}^{\mathrm{T}} \in \mathcal{R}^2$ is the costate vector, one obtains the costate equations

$$\dot{\lambda}_\theta = -\frac{\partial \mathcal{H}}{\partial \theta} = 0 \tag{3.6a}$$

$$\dot{\lambda}_\omega = -\frac{\partial \mathcal{H}}{\partial \omega} = -\lambda_\theta \tag{3.6b}$$

For the case of smooth unbounded control, Pontryagin's principle leads to the following stationarity condition

$$0 = \frac{\partial \mathcal{H}}{\partial u} = u + \frac{\lambda_\omega}{J} \tag{3.7}$$

and the optimal control is given by

$$u^*(t) = -\frac{\lambda_\omega^*(t)}{J} \tag{3.8}$$

$*$ *Note that the optimal control,* $u^*(t)$*, is determined by the optimal costate,* $\lambda_\omega^*(t)$*.*

3.2.2 Analytical Solutions for States and Control

Integrating Eq. (3.6) from t_0 to t yields

$$\lambda_\theta(t) = \text{constant} \triangleq \lambda_\theta \tag{3.9a}$$

$$\lambda_\omega(t) = \lambda_\omega(t_0) - \lambda_\theta(t - t_0) \tag{3.9b}$$

Substituting Eq. (3.8) into Eq. (3.1b) yields

$$\dot{\omega}(t) = -\frac{\lambda_\omega(t)}{J^2} \tag{3.10}$$

Using Eq. (3.9b) and integrating Eq. (3.10) from t_0 to t yields

$$\omega(t) = \omega(t_0) - \frac{\lambda_\omega(t_0)}{J^2}(t - t_0) + \frac{\lambda_\theta}{2J^2}(t - t_0)^2 \tag{3.11}$$

Using Eq. (3.11) and integrating Eq. (3.1a) from t_0 to t yields

$$\theta(t) = \theta(t_0) + \omega(t_0)(t - t_0) - \frac{\lambda_\omega(t_0)}{2J^2}(t - t_0)^2 + \frac{\lambda_\theta}{6J^2}(t - t_0)^3 \tag{3.12}$$

which is expressed in the form of a cubic polynomial equation as follows:

$$\theta(t) = \theta(t_0) + \dot{\theta}(t_0)(t - t_0) + \frac{\ddot{\theta}(t_0)}{2}(t - t_0)^2 + \frac{\theta^{(3)}(t_0)}{6}(t - t_0)^3 \tag{3.13}$$

where the superscript (#) indicates the # order derivative.

Comparing Eq. (3.12) and Eq. (3.13) gives the initial costates as follows:

$$\lambda_\omega(t_0) = -J^2\ddot{\theta}(t_0) \tag{3.14a}$$

$$\lambda_\theta = J^2\theta^{(3)}(t_0) \tag{3.14b}$$

The cubic polynomial equation in Eq. (3.13) must satisfy the initial and final boundary conditions in Eq. (3.3). Imposing these conditions upon Eq. (3.13) and solving for $\ddot{\theta}(t_0)$ and $\theta^{(3)}(t_0)$, with some algebra, yields

$$\ddot{\theta}(t_0) = \frac{6(\theta_T - \theta_0)}{(T-t_0)^2} - \frac{2(\omega_T + 2\omega_0)}{T-t_0} \tag{3.15a}$$

$$\theta^{(3)}(t_0) = -\frac{12(\theta_T - \theta_0)}{(T-t_0)^3} + \frac{6(\omega_T + \omega_0)}{(T-t_0)^2} \tag{3.15b}$$

Substituting Eq. (3.15) into Eq. (3.14) determines the initial costate constants in terms of the nontrivial initial and final boundary conditions.

Then, the solution for the open-loop control, $u^o(t)$, is given by

$$u^o(t) = -k_\theta^o(t)(\theta_0 - \theta_T) - k_\omega^o(t)(\omega_0 - \omega_T) + k_e^o(t)\omega_0 \tag{3.16}$$

where the time-varying gains are defined by

$$k_\theta^o(t) \triangleq \frac{6J}{(T-t_0)^3}(t_0 + T - 2t), \quad k_\omega^o(t) \triangleq \frac{2J}{(T-t_0)^2}(-2t_0 - T + 3t),$$
$$k_e^o(t) \triangleq \frac{6J}{(T-t_0)^2}(-t_0 - T + 2t)$$

$*$ *Note that this open-loop control has the form of a closed-loop control when the initial states are changed to current states.*

If the initial angular velocity, ω_0, is set to zero, the open-loop control becomes

$$u^o(t) = k_\theta^o(t)\,(\theta_T - \theta_0) + k_\omega^o(t)\omega_T \tag{3.17}$$

For rest-to-rest maneuvers, the open-loop control is further simply expressed as

$$u^o(t) = k_\theta^o(t)\,(\theta_T - \theta_0) \tag{3.18}$$

3.2.3 Numerical Examples

Two maneuver cases are considered: (i) rest-to-rest and (ii) motion-to-rest; and the numerical simulation parameters are listed in Table 3.1.

Table 3.1: Simulation parameters for a single-axis minimum-torque maneuver

Parameter	Symbol	(i)	(ii)	Unit
Inertia for the rotating axis	J	14.2	14.2	kg-m^2
Initial time	t_0	0	0	sec
Initial angle	$\theta\,(t_0)$	$\pi/4$	$\pi/4$	rad
Initial angular velocity	$\omega\,(t_0)$	0	-0.05	rad/s
Final time	T	10	10	sec
Final angle	$\theta(T)$	0	0	rad
Final angular velocity	$\omega(T)$	0	0	rad/s

The simulation results are shown in Figs. 3.1 and 3.2. The states satisfy the prescribed boundary conditions and smooth linear control profiles are obtained. This approach leads to jump discontinuities in control profiles, which are unattractive because they are very sensitive to high frequency behaviors when applied to flexible structures [13]. A methodology to avoid the jump discontinuity in control profile is

discussed in Section 4.1.

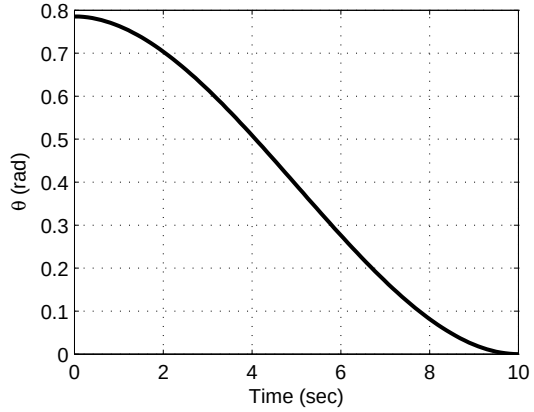

(a) Angle

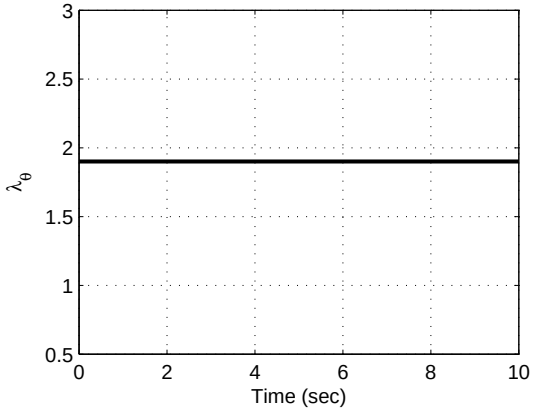

(b) Costate for the angle

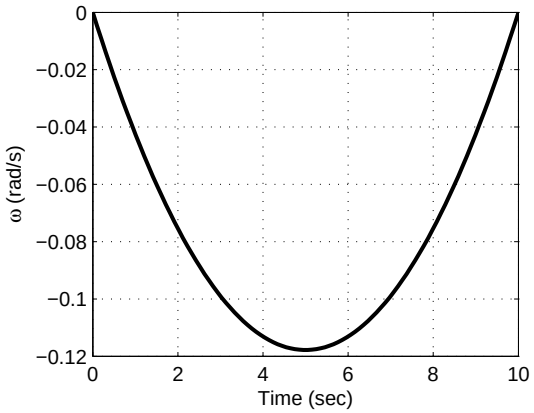

(c) Angular velocity

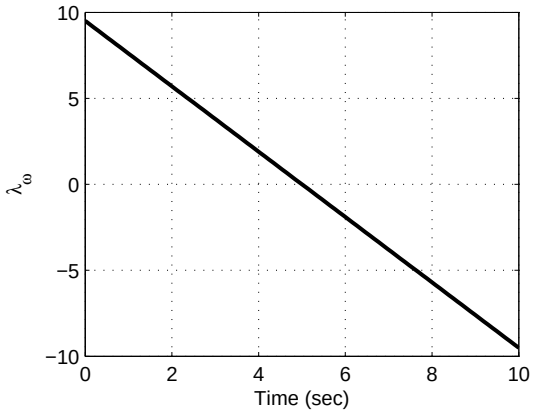

(d) Costate for the angular velocity

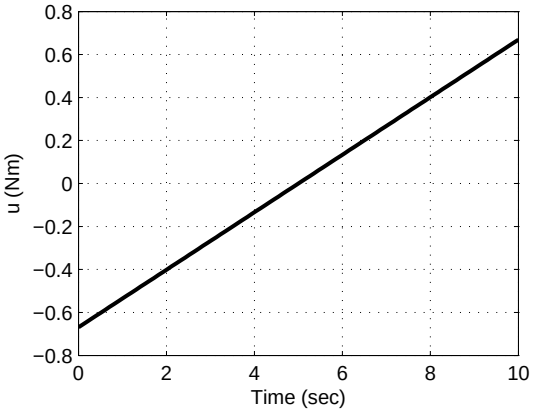

(e) Control input

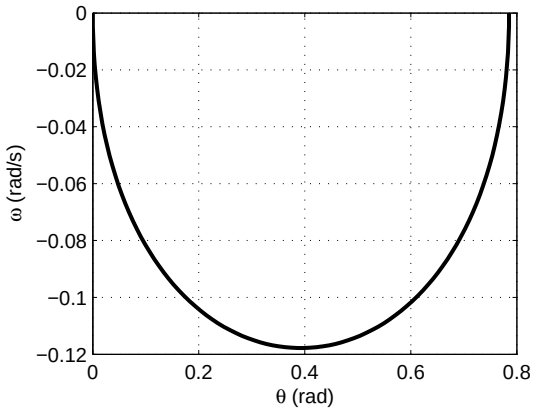

(f) Phase-plane

Figure 3.1: Minimum-torque time trajectories for the states, costates, and control; and phase portrait (rest-to-rest)

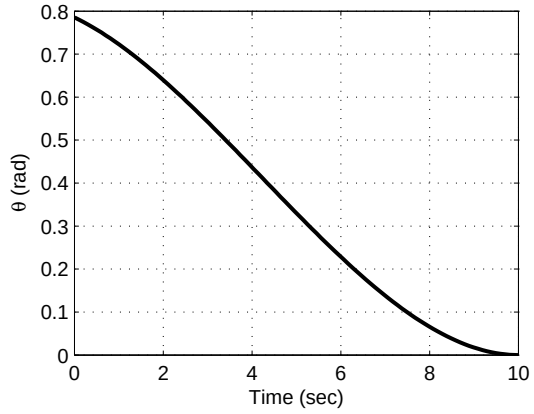

(a) Angle

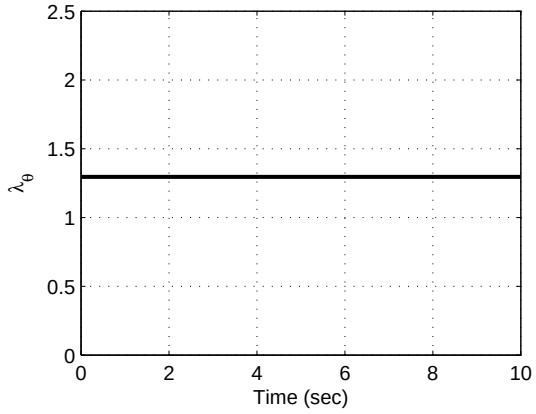

(b) Costate for the angle

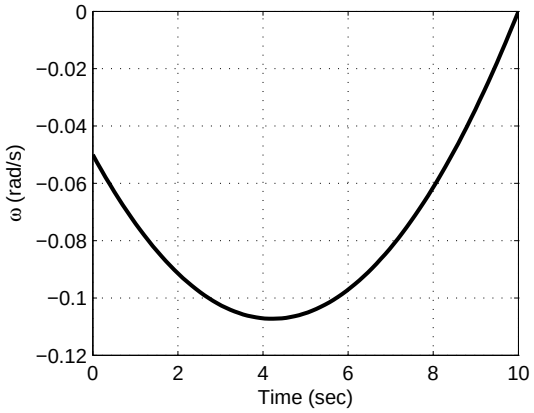

(c) Angular velocity

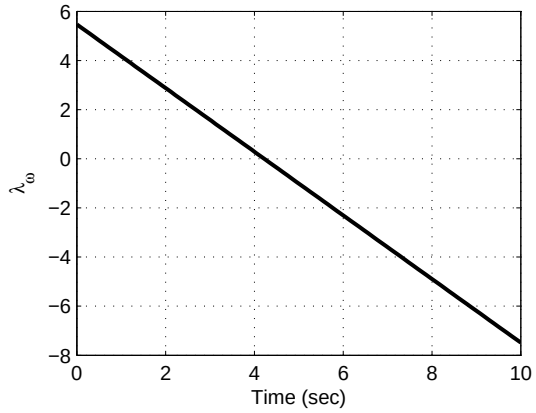

(d) Costate for the angular velocity

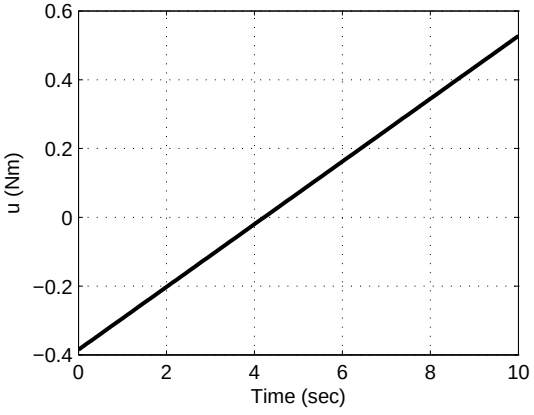

(e) Control input

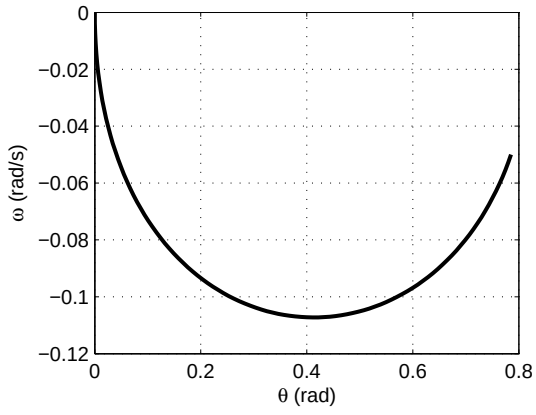

(f) Phase-plane

Figure 3.2: Minimum-torque time trajectories for the states, costates, and control; and phase portrait (motion-to-rest)

3.2.4 Concluding Remarks

This Section revisits the torque minimization problem for single-axis maneuvers. The existing formulations are revised and numerical results are demonstrated for both rest-to-rest and motion-to-rest cases. These formulations are generalized and extended for solving problems of higher dimensionality, especially for under-actuated systems, in Section 5.

3.3 Minimum-Time Maneuver

A minimum-time control solution is developed by defining the Lagrange form of a performance index given by

$$\mathcal{J} = \int_{t_0}^{T} 1 \, \mathrm{d}t \tag{3.19}$$

where t_0 is the *fixed* initial time and T is the *free* final time.

3.3.1 Derivations of Optimality Conditions

Using standard calculus of variations techniques, the Hamiltonian for the given problem is defined as

$$\mathcal{H} = 1 + \lambda_\theta \dot{\theta} + \lambda_\omega \dot{\omega} = 1 + \lambda_\theta \omega + \lambda_\omega \frac{u}{J} \tag{3.20}$$

where $\{\lambda_\theta, \, \lambda_\omega\}^{\mathrm{T}} \in \mathcal{R}^2$ is the costate vector, one obtains the costate equations

$$\dot{\lambda}_\theta = -\frac{\partial \mathcal{H}}{\partial \theta} = 0 \tag{3.21a}$$

$$\dot{\lambda}_\omega = -\frac{\partial \mathcal{H}}{\partial \omega} = -\lambda_\theta \tag{3.21b}$$

Because the final time is unspecified, the final time transversality condition

is defined by

$$0 = \mathcal{H}(T) = 1 + \lambda_\theta(T)\omega(T) + \lambda_\omega(T)\frac{u(T)}{J} \tag{3.22}$$

Substituting the final boundary condition for the angular velocity in Eq. (3.3d) with zero values (general case for the end of maneuvers) into Eq. (3.22) yields

$$\lambda_\omega(T)u(T) = -J \tag{3.23}$$

According to the Pontryagin's minimum principle, the optimal control, $u^*(t)$, must satisfy

$$\frac{\lambda_\omega^*}{J}u^* \leq \frac{\lambda_\omega^*}{J}u, \ \forall \text{ admissible } u(t) \tag{3.24}$$

To describe the relationship between the optimal control and the costates, the signum function of a real number, x, is defined as [11]

$$\text{sgn}(x) = \begin{cases} -1, & \text{if } x < 0; \\ \text{intermediate}, & \text{if } x = 0; \\ 1, & \text{if } x > 0 \end{cases} \tag{3.25}$$

Then, the optimal control is written as

$$u^*(t) = -u_{\max} \cdot \text{sgn}\left(\frac{\lambda_\omega^*(t)}{J}\right) \tag{3.26}$$

$*$ *Note that the optimal control, $u^*(t)$, is determined by the optimal costate, $\lambda_\omega^*(t)$.*

Integrating Eq. (3.21) from T to t yields

$$\lambda_\theta(t) = \text{constant} \triangleq \lambda_\theta \tag{3.27a}$$

$$\lambda_\omega(t) = \lambda_\omega(T) + (T-t)\lambda_\theta \tag{3.27b}$$

Using Eq. (3.23) and the fact that $u^*(T)$ is limited to $u_{\max}$ or $-u_{\max}$ requires either

$$u^*(T) = u_{\max} \quad \text{and} \quad \lambda_\omega^*(T) = -\frac{J}{u_{\max}} \tag{3.28}$$

or

$$u^*(T) = -u_{\max} \quad \text{and} \quad \lambda_\omega^*(T) = \frac{J}{u_{\max}} \tag{3.29}$$

3.3.2 Analytical Solutions for States and Control

Since $\lambda_\omega(t)$ is a linear function of time as shown in Eq. (3.27b), it crosses time-axis at most one time, so that there is at most one control switching [11]. Therefore, the optimal control is one of the following choices:

$$u^*(t) = \begin{cases} \text{(a)} \ -u_{\max}, \\ \text{(b) switching from} \ -u_{\max} \ \text{to} \ u_{\max}, \\ \text{(c) switching from} \ u_{\max} \ \text{to} \ -u_{\max}, \\ \text{(d)} \ u_{\max} \end{cases} \tag{3.30}$$

Now, the optimal control needs to be determined among the choices (a) through (d). Also, the switch-time, t_s, must be found when it crosses the time-axis. Let us determine the state trajectories for the two possible control inputs, (a) and (d). For the constant control input case, the solution of Eq. (3.1) is given by

$$\omega(t) = \omega(t_0) + \frac{u}{J}(t - t_0) \tag{3.31a}$$

$$\theta(t) = \theta(t_0) + \omega(t_0)(t - t_0) + \frac{u}{2J}(t - t_0)^2 \tag{3.31b}$$

or

$$\omega(t) = \omega(T) + \frac{u}{J}(t - T) \tag{3.32a}$$

$$\theta(t) = \theta(T) + \omega(T)(t - T) + \frac{u}{2J}(t - T)^2 \tag{3.32b}$$

To eliminate time variables, substituting $t - T = J[\omega(t) - \omega(T)]/u$ from Eq. (3.32a) into Eq. (3.32b) yields

$$u[\theta(t) - \theta(T)] = J\omega(T)[\omega(t) - \omega(T)] + \frac{J}{2}[\omega(t) - \omega(T)]^2 \tag{3.33}$$

which defines a parabola based on the final states. As the final states vary, a family of parabolas is defined.

Substituting the final boundary conditions in Eqs. (3.3c) and (3.3d) into Eq. (3.33) yields

$$u[\theta(t) - \theta_T] = J\omega_T[\omega(t) - \omega_T] + \frac{J}{2}[\omega(t) - \omega_T]^2 \tag{3.34}$$

Again, zero angular velocity at the final time, which is the general case, is assumed. By setting $\omega_T = 0$ in Eq. (3.34), the equation of the switching curve is given by

$$\theta(t) = \theta_T + \frac{J}{2u}\omega^2(t) \tag{3.35}$$

Let's assume that the initial states are on the switching curve. Then, the following control will bring the states to desired states:

$$u(t) = \begin{cases} u_{\max}, & \text{if } \omega < 0; \\ -u_{\max}, & \text{if } \omega > 0 \end{cases} \tag{3.36}$$

Now, the equation of the switching curve in Eq. (3.35) is rewritten as

$$\theta(t) = \theta_T - \frac{J}{2u_{\max}}\omega(t)\,|\omega(t)| \tag{3.37}$$

Finally, the feedback control law is given by

$$u(t) = \begin{cases} -u_{\max}, & \text{if } \theta(t) > \theta_T - \dfrac{J}{2u_{\max}}\omega(t)\,|\omega(t)|; \\ u_{\max}, & \text{if } \theta(t) < \theta_T - \dfrac{J}{2u_{\max}}\omega(t)\,|\omega(t)| \end{cases} \tag{3.38}$$

3.3.3 Analytical Solution for a Switch-Time

Using the boundary conditions in Eq. (3.3), let us assume the initial states follow as

$$\theta_0 > \theta_T - \frac{J}{2u_{\max}}\omega_0\,|\omega_0| \tag{3.39}$$

then the initial control input, $u = -u_{\max}$, is applied and the control input is switched to $u = u_{\max}$ at switch-time, $t = t_s$.

The switch-time curve for $\omega < 0$ is described by

$$\theta(t) = \theta_T + \frac{J}{2u_{\max}}\omega^2(t) \tag{3.40}$$

At $t = t_s$, Eq. (3.31) is expressed as

$$\omega\,(t_s) = \omega_0 - \frac{u_{\max}}{J}\,(t_s - t_0) \tag{3.41a}$$

$$\theta\,(t_s) = \theta_0 + \omega_0\,(t_s - t_0) - \frac{u_{\max}}{2J}(t_s - t_0)^2 \tag{3.41b}$$

Comparing Eq. (3.40) at $t = t_s$ and Eq. (3.41b) yields the quadratic equation

as follows:

$$a(t_s - t_0)^2 + b\,(t_s - t_0) + c = 0 \tag{3.42}$$

where the coefficients are

$$a = \frac{u_{\max}}{J}, \quad b = -2\omega_0, \quad c = \theta_T - \theta_0 + \frac{J\omega_0^2}{2u_{\max}}$$

Solving the quadratic equation in Eq. (3.42) gives the positive switch-time, t_s, as follows:

$$t_s = t_0 + \frac{J}{u_{\max}}\left[\omega_0 + \sqrt{\frac{\omega_0^2}{2} - \frac{u_{\max}}{J}\,(\theta_T - \theta_0)}\right] \tag{3.43}$$

At $t = t_s$, Eq. (3.32a) is expressed as

$$\omega_T = \omega\,(t_s) + \frac{u_{\max}}{J}\,(T - t_s) \tag{3.44}$$

Substituting Eq. (3.41a) into Eq. (3.44) yields

$$\omega_T = \omega_0 + \frac{u_{\max}}{J}\,(t_0 - 2t_s + T) \tag{3.45}$$

With zero angular velocity at the final time, the final time, T, is given by

$$T = -t_0 + 2t_s - \frac{J\omega_0}{u_{\max}} \tag{3.46}$$

Substituting Eq. (3.43) into Eq. (3.46) yields the final time in terms of initially given values as follows:

$$T = t_0 + \frac{J}{u_{\max}}\left[\omega_0 + 2\sqrt{\frac{\omega_0^2}{2} - \frac{u_{\max}}{J}\,(\theta_T - \theta_0)}\right] \tag{3.47}$$

3.3.4 Numerical Examples

Two maneuver cases are considered: (i) rest-to-rest and (ii) motion-to-rest; and the numerical simulation parameters are listed in Table 3.2.

Table 3.2: Simulation parameters for a single-axis minimum-time maneuver

Parameter	Symbol	(i)	(ii)	Unit
Inertia for the rotating axis	J	14.2	14.2	kg-m^2
Maximum value of control torque	$u_{\max}$	1	1	Nm
Initial time	t_0	0	0	sec
Initial angle	$\theta(t_0)$	$\pi/4$	$\pi/4$	rad
Initial angular velocity	$\omega(t_0)$	0	-0.05	rad/s
Final angle	$\theta(T)$	0	0	rad
Final angular velocity	$\omega(T)$	0	0	rad/s

For the case (i), the switch-time, t_s, and the final time, T, are obtained by

$$(t_s,\, T) = (3.3396,\, 6.6791) \text{ sec}$$

For the case (ii), the switch-time, t_s, and the final time, T, are obtained by

$$(t_s,\, T) = (2.6671,\, 6.0042) \text{ sec}$$

The simulation results are shown in Figs. 3.3 and 3.4. The states satisfy the prescribed boundary conditions and bang-bang control profiles are obtained. These jump discontinuities in control profiles are unattractive because they induce high frequency, which leads to excite a flexible body response [13]. A methodology to avoid the jump discontinuity in control profile is discussed in Section 4.2.

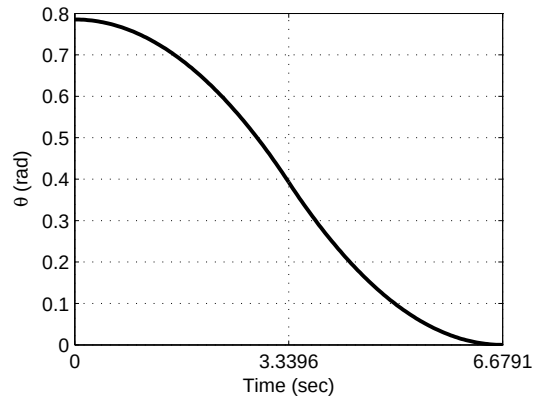

(a) Angle

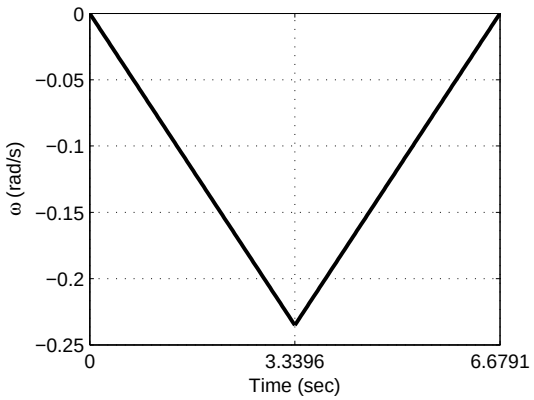

(b) Angular velocity

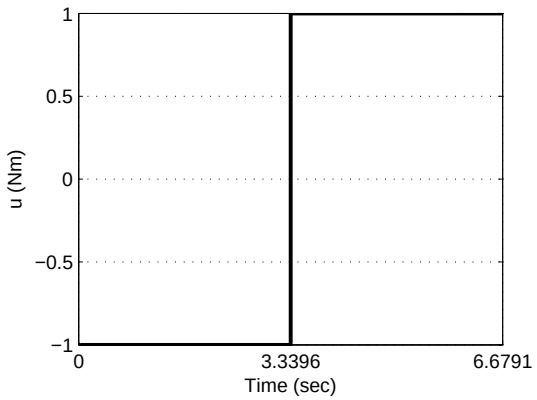

(c) Control input

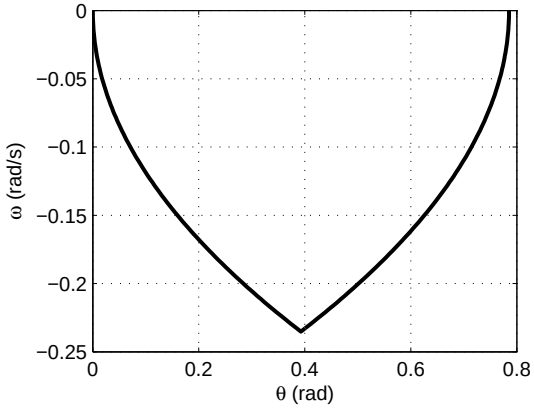

(d) Phase-plane

Figure 3.3: Minimum-time time trajectories for the states and control; and phase portrait (rest-to-rest)

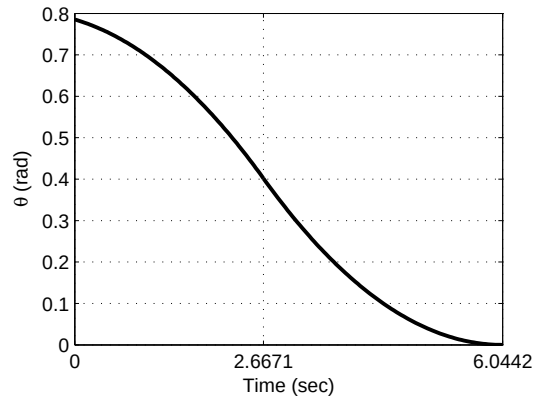

(a) Angle

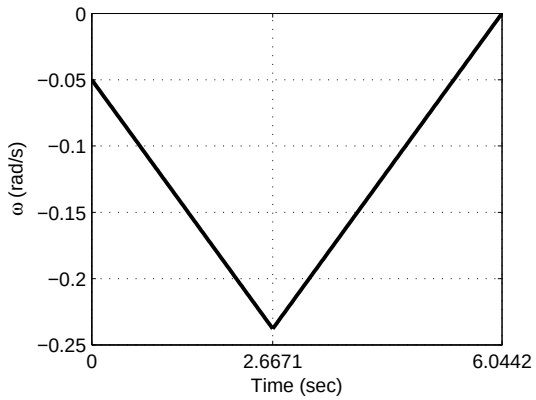

(b) Angular velocity

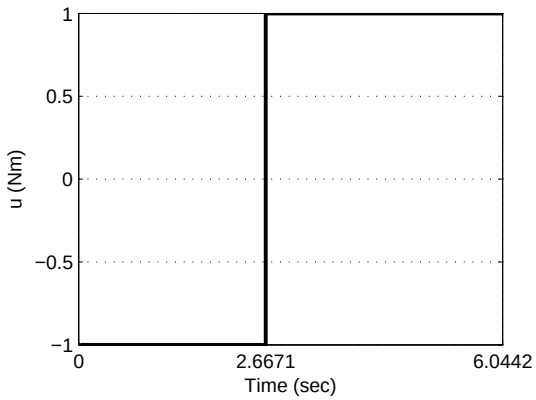

(c) Control input

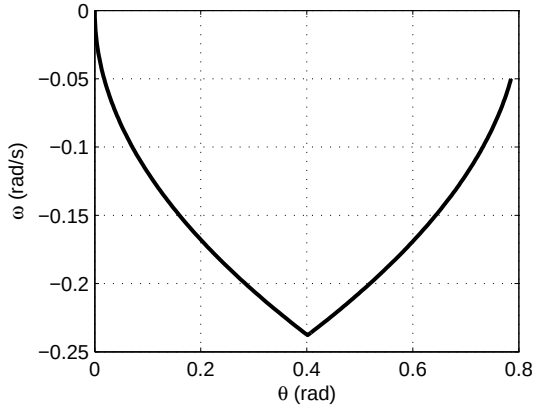

(d) Phase-plane

Figure 3.4: Minimum-time time trajectories for the states and control; and phase portrait (motion-to-rest)

3.3.5 Concluding Remarks

This Section revisits the maneuver time minimization problem for single-axis maneuvers. The existing formulations are revised and numerical results are demonstrated for both rest-to-rest and motion-to-rest cases. These formulations are generalized and extended for solving problems of higher dimensionality, especially for under-actuated systems, in Appendix C.1.

3.4 Minimum-Fuel Maneuver

A minimum-fuel control solution is developed by defining the Lagrange form of a performance index given by

$$\mathcal{J} = \int_{t_0}^{T} |u| \, \mathrm{d}t \tag{3.48}$$

where t_0 is the *fixed* initial time and T is the *free* final time.

3.4.1 Derivations of Optimality Conditions

Using standard calculus of variations techniques, the Hamiltonian for the given problem is defined as

$$\mathcal{H} = |u| + \lambda_\theta \dot{\theta} + \lambda_\omega \dot{\omega} = |u| + \lambda_\theta \omega + \lambda_\omega \frac{u}{J} \tag{3.49}$$

where $\{\lambda_\theta, \, \lambda_\omega\}^{\mathrm{T}} \in \mathcal{R}^2$ is the costate vector, one obtains the costate equations

$$\dot{\lambda}_\theta = -\frac{\partial \mathcal{H}}{\partial \theta} = 0 \tag{3.50a}$$

$$\dot{\lambda}_\omega = -\frac{\partial \mathcal{H}}{\partial \omega} = -\lambda_\theta \tag{3.50b}$$

Because the final time is unspecified, the final time transversality condition is defined by

$$0 = \mathcal{H}(T) = |u(T)| + \lambda_\theta(T)\omega(T) + \lambda_\omega(T)\frac{u(T)}{J} \tag{3.51}$$

Substituting the final boundary condition for the angular velocity in Eq. (3.3d) with zero values (general case for the end of maneuvers) into Eq. (3.51) yields

$$\lambda_\omega(T)u(T) = -J \, |u(T)| \tag{3.52}$$

According to the Pontryagin's minimum principle, the optimal control, $u^*(t)$, must satisfy

$$|u^*| + \frac{\lambda_\omega^*}{J} u^* \leq |u| + \frac{\lambda_\omega^*}{J} u, \ \forall \text{ admissible } u(t) \tag{3.53}$$

The quantity, which needs to be minimized by selection of $u(t)$, is defined as

$$q(t) \triangleq |u| + \frac{\lambda_\omega}{J} u = \begin{cases} \left(1 + \dfrac{\lambda_\omega}{J}\right) |u|, & u \geq 0; \\ \left(1 - \dfrac{\lambda_\omega}{J}\right) |u|, & u \leq 0 \end{cases} \tag{3.54}$$

To describe the relationship between the optimal control and the costate, the dead-zone function of a real number, x, is defined as [11]

$$\text{dez}(x) = \begin{cases} -1, & x < -1; \\ \text{between } -1 \text{ and } 0, & x = -1; \\ 0, & -1 < x < 1; \\ \text{between } 0 \text{ and } 1, & x = 1; \\ 1, & x > 1 \end{cases} \tag{3.55}$$

Then, the optimal control is written as

$$u^*(t) = -u_{\max} \cdot \text{dez}\left(\frac{\lambda_\omega^*(t)}{J}\right) \tag{3.56}$$

$*$ *Note that the optimal control, $u^*(t)$, is determined by the optimal costate, $\lambda_\omega^*(t)$.*

Integrating Eq. (3.50) from T to t yields

$$\lambda_\theta(t) = \text{constant} \triangleq \lambda_\theta \tag{3.57a}$$

$$\lambda_\omega(t) = \lambda_\omega(T) + (T - t)\lambda_\theta \tag{3.57b}$$

Using Eq. (3.52) and the fact that $u^*(T)$ is limited to $u_{\max}$ or $-u_{\max}$ requires either

$$u^*(T) = u_{\max} \quad \text{and} \quad \lambda_\omega^*(T) = -J \tag{3.58}$$

or

$$u^*(T) = -u_{\max} \quad \text{and} \quad \lambda_\omega^*(T) = J \tag{3.59}$$

3.4.2 Analytical Solutions for States and Control

Since $\lambda_\omega(t)$ is a linear function of time as shown in Eq. (3.57b), it crosses time-axis at most two times, so that there is at most two control switching [11]. Therefore, the optimal control expressed with costate is one of the following choices:

$$u^*(t) = \begin{cases} \text{(a)}\, u_{\max}, & \lambda_\omega < -J; \\ \text{(b)}\, \text{non-negative}, & \lambda_\omega = -J; \\ \text{(c)}\, 0, & -J < \lambda_\omega < J; \\ \text{(d)}\, \text{non-positive}, & \lambda_\omega = J; \\ \text{(e)}\, -u_{\max}, & \lambda_\omega > J \end{cases} \tag{3.60}$$

Now, the optimal control needs to be determined among the choices (a) through (e). Also, the switch-times, t_1 and t_2, must be found when it crosses the time-axis. Let us determine the state trajectories for the three possible control inputs, (a), (c), and (e) excluding singular intervals (b) and (d). For the constant control input case, the solution of Eq. (3.1) is given by

$$\omega(t) = \omega(t_0) + \frac{u}{J}(t - t_0) \tag{3.61a}$$

$$\theta(t) = \theta(t_0) + \omega(t_0)(t - t_0) + \frac{u}{2J}(t - t_0)^2 \tag{3.61b}$$

or

$$\omega(t) = \omega(T) + \frac{u}{J}(t - T) \tag{3.62a}$$

$$\theta(t) = \theta(T) + \omega(T)(t - T) + \frac{u}{2J}(t - T)^2 \tag{3.62b}$$

To eliminate time variables, substituting $t - T = J[\omega(t) - \omega(T)]/u$ from Eq. (3.62a) into Eq. (3.62b) yields

$$u[\theta(t) - \theta(T)] = J\omega(T)[\omega(t) - \omega(T)] + \frac{J}{2}[\omega(t) - \omega(T)]^2 \tag{3.63}$$

which defines a parabola based on the final states. As the final states vary, a family of parabolas is defined.

Substituting the final boundary conditions in Eqs. (3.3c) and (3.3d) into Eq. (3.63) yields

$$u[\theta(t) - \theta_T] = J\omega_T[\omega(t) - \omega_T] + \frac{J}{2}[\omega(t) - \omega_T]^2 \tag{3.64}$$

Again, zero angular velocity at the final time, which is the general case, is assumed. By setting $\omega_T = 0$ in Eq. (3.64), the equation of the switching curve is given by

$$\theta(t) = \theta_T + \frac{J}{2u}\omega^2(t) \tag{3.65}$$

Let's assume that the initial states are on the switching curve. Then, the following control will bring the states to desired states:

$$u(t) = \begin{cases} u_{\max}, & \text{if } \omega < 0; \\ -u_{\max}, & \text{if } \omega > 0 \end{cases} \tag{3.66}$$

Now, the equation of the switching curve in Eq. (3.65) is rewritten as

$$\theta(t) = \theta_T - \frac{J}{2u_{\max}}\omega(t)\,|\omega(t)| \tag{3.67}$$

3.4.3 Analytical Solutions for Switch-Times

Using the boundary conditions in Eq. (3.3), let us assume the initial states follow as

$$\theta_0 > \theta_T - \frac{J}{2u_{\max}}\omega_0\,|\omega_0| \tag{3.68}$$

then the initial control input, $u = -u_{\max}$, is applied and the control input is switched to $u = 0$ at switch-time, $t = t_1$. Let the system drift until at switch-time, $t = t_2$, and the control input, $u = u_{\max}$, is applied until $t = T$. For free final time, it is shown that minimum-fuel control laws do not generally exist [11]. Let's suppose that the final time is fixed.

For $t_0 < t < t_1$, $u(t) = -u_{\max}$ and Eq. (3.61) is expressed as

$$\omega(t_1) = \omega_0 - \frac{u_{\max}}{J}(t_1 - t_0) \tag{3.69a}$$

$$\theta(t_1) = \theta_0 + \omega_0(t_1 - t_0) - \frac{u_{\max}}{2J}(t_1 - t_0)^2 \tag{3.69b}$$

For $t_1 < t < t_2$, $u(t) = 0$ and Eq. (3.61) is expressed as

$$\omega(t_2) = \omega(t_1) \tag{3.70a}$$

$$\theta(t_2) = \theta(t_1) + \omega(t_1)(t_2 - t_1) \tag{3.70b}$$

For $t_2 < t < T$, $u(t) = u_{\max}$ and Eq. (3.61) is expressed as

$$\omega(T) = \omega(t_2) + \frac{u_{\max}}{J}(T - t_2) \tag{3.71a}$$

$$\theta(T) = \theta(t_2) + \omega(t_2)(T - t_2) + \frac{u_{\max}}{2J}(T - t_2)^2 \tag{3.71b}$$

Substituting Eqs. (3.69a) and (3.70a) into Eq. (3.71a) yields

$$\omega_T = \omega_0 - \frac{u_{\max}}{J}(t_1 - t_0) + \frac{u_{\max}}{J}(T - t_2) \tag{3.72}$$

With zero angular velocity at the final time, the switch-time, t_2, is given by

$$t_2 = \frac{J\omega_0}{u_{\max}} + T - t_1 + t_0 \tag{3.73}$$

Substituting Eqs. (3.69), (3.70), and (3.73) into Eq. (3.71b) yields

$$J^2\omega_0^2 + 2u_{\max}\left[J(\theta_0 - \theta_T) + (t_0 - t_1)u_{\max}(T - t_1)\right] + 2J\omega_0 u_{\max}(T - t_1) = 0 \tag{3.74}$$

After some algebra, the switch-time, t_1, is found by

$$t_1 = \frac{J\omega_0}{2u_{\max}} + \frac{t_0 + T}{2} \mp \frac{\mathcal{D}}{2u_{\max}} \tag{3.75}$$

where

$$\mathcal{D} \triangleq \sqrt{-J\omega_0(J\omega_0 - 2t_0u_{\max} + 2u_{\max}T) - 4Ju_{\max}(\theta_0 - \theta_T) + u_{\max}^2(t_0 - T)^2}$$

Using Eq. (3.73) and the fact that $t_1 < t_2$, the switch-times are obtained by

$$t_1 = \frac{J\omega_0 - \mathcal{D}}{2u_{\max}} + \frac{t_0 + T}{2} \tag{3.76a}$$

$$t_2 = \frac{J\omega_0 + \mathcal{D}}{2u_{\max}} + \frac{t_0 + T}{2} \tag{3.76b}$$

Then, the minimum-fuel control in open-loop form is given by

$$u^*(t) = \begin{cases} -u_{\max}, & t < t_1; \\ 0, & t_1 \leq t < t_2; \\ u_{\max}, & t \geq t_2 \end{cases} \tag{3.77}$$

3.4.4 Numerical Examples

Two maneuver cases are considered: (i) rest-to-rest and (ii) motion-to-rest; and the numerical simulation parameters are listed in Table 3.3.

Table 3.3: Simulation parameters for a single-axis minimum-fuel maneuver

Parameter	Symbol	(i)	(ii)	Unit
Inertia for the rotating axis	J	14.2	14.2	kg-m^2
Maximum value of control torque	$u_{\max}$	1	1	Nm
Initial time	t_0	0	0	sec
Initial angle	$\theta\,(t_0)$	$\pi/4$	$\pi/4$	rad
Initial angular velocity	$\omega\,(t_0)$	0	-0.05	rad/s
Final time	T	10	10	sec
Final angle	$\theta(T)$	0	0	rad
Final angular velocity	$\omega(T)$	0	0	rad/s

For the case (i), the switch-times, t_1 and t_2, are obtained by

$$(t_1,\, t_2) = (1.2788,\, 8.7212) \text{ sec}$$

For the case (ii), the switch-times, t_1 and t_2, are obtained by

$$(t_1,\, t_2) = (0.4891,\, 8.8009) \text{ sec}$$

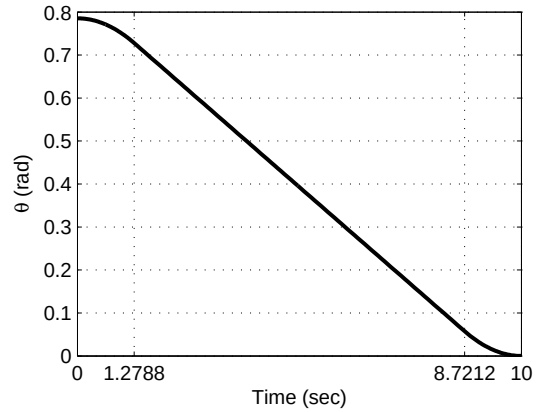

(a) Angle

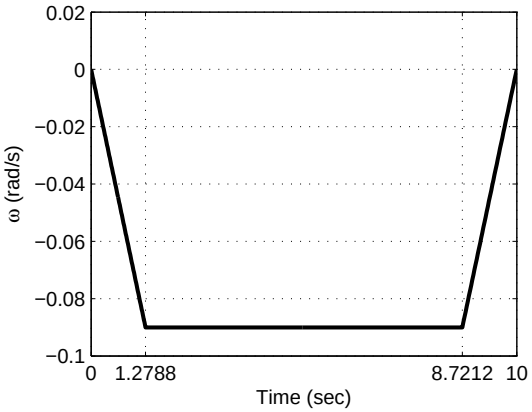

(b) Angular velocity

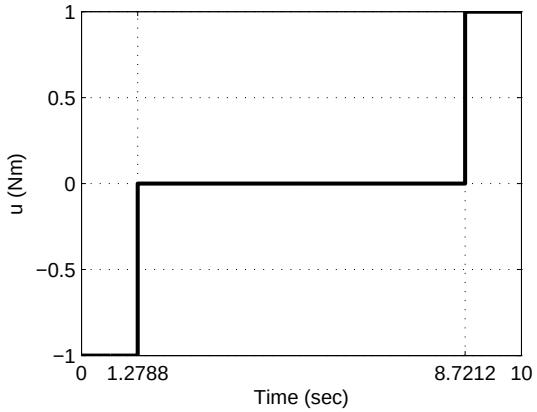

(c) Control input

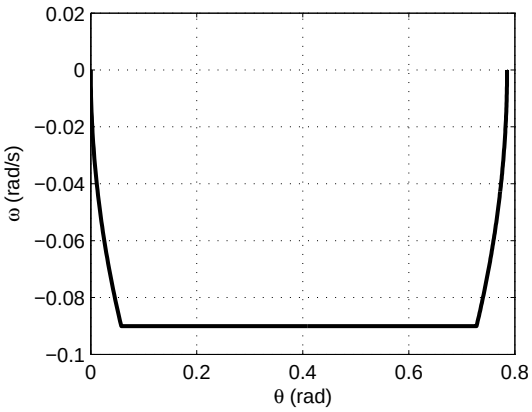

(d) Phase-plane

Figure 3.5: Minimum-fuel time trajectories for the states and control; and phase portrait (rest-to-rest)

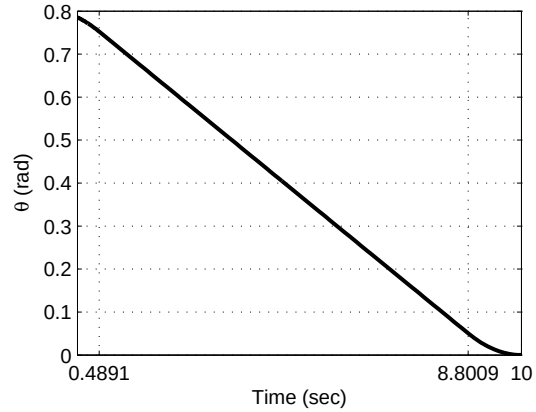

(a) Angle

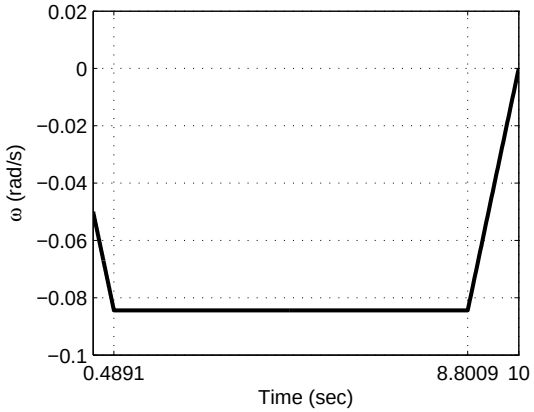

(b) Angular velocity

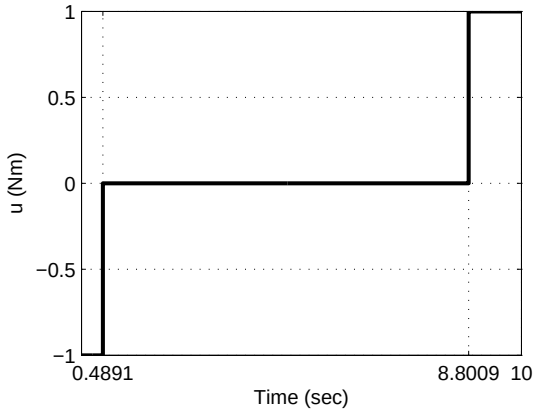

(c) Control input

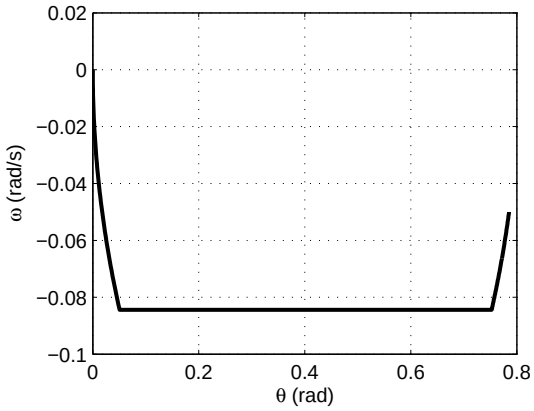

(d) Phase-plane

Figure 3.6: Minimum-fuel time trajectories for the states and control; and phase portrait (motion-to-rest)

The simulation results are shown in Figs. 3.5 and 3.6. The states satisfy the prescribed boundary conditions and bang-off-bang control profiles are obtained. These jump discontinuities in control profiles are unattractive to control highly flexible structures because they introduce high frequency distributions [13]. A methodology to avoid the jump discontinuity in control profile is discussed in Section 4.3.

3.4.5 Concluding Remarks

This Section revisits the fuel minimization problem for single-axis maneuvers. The existing formulations are revised and numerical results are demonstrated for both rest-to-rest and motion-to-rest cases. These formulations are generalized and extended for solving problems of higher dimensionality, especially for under-actuated systems, in Appendix C.3.

4. JUMP DISCONTINUITY AVOIDANCE FOR CONTROL PROFILES

Two methods to avoid jump discontinuities in control profiles are presented for single-axis maneuvers. First, for the torque minimization problem, a quadratic torque-rate is introduced into the performance index. Second, for the maneuver time and fuel minimization problems, a cubic polynomial equation is multiplied to the maximum control input.

4.1 Torque-Rate Performance Index Technique: Torque Minimization

The kinematic and rotational dynamic equations in Eq. (3.1) and time derivative of control are

$$\dot{\theta} = \omega \tag{4.1a}$$

$$\dot{\omega} = \frac{u}{J} \tag{4.1b}$$

$$\dot{u} = \bar{u} \tag{4.1c}$$

where $\{\theta,\, \omega,\, u\}^{\mathrm{T}} \in \mathcal{R}^3$ is the state vector and the control input is assumed to be unbounded.

The objective is to determine a time derivative of control input to bring given initial state $\{\theta\,(t_0)\,,\, \omega\,(t_0)\,,\, u\,(t_0)\}^{\mathrm{T}}$ to a desired final state $\{\theta(T),\, \omega(T),\, u(T)\}^{\mathrm{T}}$. Given the initial and final boundary conditions in Eq. (3.3), additional initial and final control inputs are defined as

$$u\,(t_0) = u_0 \tag{4.2a}$$

$$u(T) = u_T \tag{4.2b}$$

$*$ *Note that the control boundary conditions,* $u(t_0)$ *and* $u(T)$*, are free to choose.*

A minimum-torque control solution is developed by defining the Lagrange form of a performance index given by

$$\mathcal{J} = \frac{1}{2}\int_{t_0}^{T} \left(k^2 u^2 + \dot{u}^2\right)\, \mathrm{d}t \tag{4.3}$$

where t_0 is the *fixed* initial time, T is the *fixed* final time, $k \geq 0$ is the weight for trade-off between penalizing quadratic torque and smoothing control profiles, and u is assumed to have two continuous time derivatives.

4.1.1 Derivations of Optimality Conditions

Using standard calculus of variations techniques, the Hamiltonian for the given problem is defined as

$$\mathcal{H} = \frac{1}{2}\left(k^2 u^2 + \bar{u}^2\right) + \lambda_\theta\, \dot{\theta} + \lambda_\omega\, \dot{\omega} + \lambda_u \bar{u} = \frac{1}{2}\left(k^2 u^2 + \bar{u}^2\right) + \lambda_\theta\, \omega + \lambda_\omega \frac{u}{J} + \lambda_u \bar{u} \tag{4.4}$$

where $\{\lambda_\theta,\, \lambda_\omega,\, \lambda_u\}^{\mathrm{T}} \in \mathcal{R}^3$ is the costate vector, one obtains the costate equations

$$\dot{\lambda}_\theta = -\frac{\partial \mathcal{H}}{\partial \theta} = 0 \tag{4.5a}$$

$$\dot{\lambda}_\omega = -\frac{\partial \mathcal{H}}{\partial \omega} = -\lambda_\theta \tag{4.5b}$$

$$\dot{\lambda}_u = -\frac{\partial \mathcal{H}}{\partial u} = -\frac{\lambda_\omega}{J} - k^2 u \tag{4.5c}$$

Pontryagin's principle leads to the following stationarity condition

$$0 = \frac{\partial \mathcal{H}}{\partial \bar{u}} = \bar{u} + \lambda_u \tag{4.6}$$

and the optimal control-rate is given by

$$\bar{u}^*(t) = -\lambda_u^*(t) \tag{4.7}$$

$*$ *Note that the optimal control-rate,* $\bar{u}^*(t)$*, is determined by the optimal costate,* $\lambda_u^*(t)$.

4.1.2 Analytical Solutions for States and Control

Introducing Eq. (4.7) into Eq. (4.1) provides the necessary conditions for the optimal control solution given by

$$\dot{\theta} = \omega \tag{4.8a}$$

$$\dot{\omega} = \frac{u}{J} \tag{4.8b}$$

$$\dot{u} = -\lambda_u \tag{4.8c}$$

The solution is obtained by defining the state-costate vector

$$\boldsymbol{z} = \{\theta,\, \omega,\, u,\, \lambda_\theta,\, \lambda_\omega,\, \lambda_u\}^{\mathrm{T}} \tag{4.9}$$

Collecting the state and costate equations in Eqs. (4.5) and (4.8), the linear state space form is obtained as follows:

$$\dot{\boldsymbol{z}}(t) = [A]\boldsymbol{z}(t) \tag{4.10}$$

where the constant matrix, $[A] \in \mathcal{R}^{6\times 6}$, is defined by

$$[A] = \begin{bmatrix} 0 & 1 & 0 & 0 & 0 & 0 \\ 0 & 0 & 1/J & 0 & 0 & 0 \\ 0 & 0 & 0 & 0 & 0 & -1 \\ 0 & 0 & 0 & 0 & 0 & 0 \\ 0 & 0 & 0 & -1 & 0 & 0 \\ 0 & 0 & -k^2 & 0 & -1/J & 0 \end{bmatrix}$$

The standard approach for solving Eq. (4.10) is to determine the state-costate transition matrix, $[\Phi(t,\, t_0)] \in \mathcal{R}^{6\times 6}$, which maps the initial state-costate vector into the current state-costate as [18]

$$\boldsymbol{z}(t) = [\Phi(t,\, t_0)]\, \boldsymbol{z}(t_0) \tag{4.11}$$

where $[\Phi(t,\, t_0)]$ is often written compactly as

$$[\Phi(t,\, t_0)] = e^{[A](t-t_0)} \text{ for } [A] = \text{constant matrix} \tag{4.12}$$

The boundary conditions for the maneuver are

$$\boldsymbol{z}(t_0) = \{\theta(t_0),\, \omega(t_0),\, u(t_0),\, \lambda_\theta(t_0),\, \lambda_\omega(t_0),\, \lambda_u(t_0)\}^{\mathrm{T}} \tag{4.13a}$$

$$\boldsymbol{z}(T) = \{\theta(T),\, \omega(T),\, u(T),\, \lambda_\theta(T),\, \lambda_\omega(T),\, \lambda_u(T)\}^{\mathrm{T}} \tag{4.13b}$$

where the boundary conditions for the costates are unknown.

Substituting the boundary conditions in Eq. (4.13) into Eq. (4.11) gives

$$\boldsymbol{z}(T) = [\Phi\,(T,\, t_0)]\,\boldsymbol{z}\,(t_0) \tag{4.14}$$

where the state-costate transition matrix at the final time, $[\Phi\,(T,\, t_0)]$, is partitioned as

$$[\Phi\,(T,\, t_0)] = \begin{bmatrix} [\Phi_{11}] & [\Phi_{12}] \\ [\Phi_{21}] & [\Phi_{22}] \end{bmatrix} \tag{4.15}$$

and the partitioned state-costate transition matrices are presented on page 43.

Imposing the initial and final boundary conditions for the states and control in Eqs. (3.3) and (4.2) into Eq. (4.14) gives the following initial costates

$$\begin{Bmatrix} \lambda_\theta\,(t_0) \\ \lambda_\omega\,(t_0) \\ \lambda_u\,(t_0) \end{Bmatrix} = [\Phi_{12}]^{-1} \left(\begin{Bmatrix} \theta_T \\ \omega_T \\ u_T \end{Bmatrix} - [\Phi_{11}] \begin{Bmatrix} \theta_0 \\ \omega_0 \\ u_0 \end{Bmatrix} \right) \tag{4.16}$$

which completes the solution for the TPBVP for the torque-rate appended control formulation.

By choosing large k, a near minimum-torque solution is obtained with smooth continuous control profiles. Let's assume that $k = 0$ for simply generating smooth continuous control profiles. Then, this problem becomes a torque-rate minimization problem. As shown in the partition matrices of the state-costate transition matrix, however, a singular problem is caused when $k = 0$ is selected.

$$[\Phi_{11}] = \begin{bmatrix} 1 & T-t_0 & \frac{e^{k(t_0-T)}\left(-1+e^{k(T-t_0)}\right)^2}{2Jk^2} \\ 0 & 1 & \frac{e^{k(t_0-T)}\left(-1+e^{2k(T-t_0)}\right)}{2Jk} \\ 0 & 0 & \frac{1}{2}e^{k(t_0-T)}\left(1+e^{2k(T-t_0)}\right) \end{bmatrix},$$

$$[\Phi_{12}] = \begin{bmatrix} \frac{k^3(T-t_0)^3+6k(T-t_0)-3e^{k(T-t_0)}+3e^{k(t_0-T)}}{6J^2k^5} & -\frac{T^2k^2+t_0^2k^2-2Tt_0k^2-e^{k(T-t_0)}-e^{k(t_0-T)}+2}{2J^2k^4} & \frac{2kT-e^{k(T-t_0)}+e^{k(t_0-T)}-2kt_0}{2Jk^3} \\ -\frac{-T^2k^2-t_0^2k^2+2Tt_0k^2+e^{k(T-t_0)}+e^{k(t_0-T)}-2}{2J^2k^4} & \frac{-2kT+e^{k(T-t_0)}-e^{k(t_0-T)}+2kt_0}{2J^2k^3} & -\frac{e^{k(t_0-T)}\left(-1+e^{k(T-t_0)}\right)^2}{2Jk^2} \\ \frac{2kT-e^{k(T-t_0)}+e^{k(t_0-T)}-2kt_0}{2Jk^3} & \frac{e^{k(t_0-T)}\left(-1+e^{k(T-t_0)}\right)^2}{2Jk^2} & -\frac{e^{k(t_0-T)}\left(-1+e^{2k(T-t_0)}\right)}{2k} \end{bmatrix},$$

$$[\Phi_{21}] = \begin{bmatrix} 0 & 0 & 0 \\ 0 & 0 & 0 \\ 0 & 0 & -\frac{1}{2}e^{k(t_0-T)}\left(-1+e^{2k(T-t_0)}\right)k \end{bmatrix},$$

$$[\Phi_{22}] = \begin{bmatrix} 1 & 0 & 0 \\ t_0-T & 1 & 0 \\ \frac{e^{k(t_0-T)}\left(-1+e^{k(T-t_0)}\right)^2}{2Jk^2} & -\frac{e^{k(t_0-T)}\left(-1+e^{2k(T-t_0)}\right)}{2Jk} & \frac{1}{2}e^{k(t_0-T)}\left(1+e^{2k(T-t_0)}\right) \end{bmatrix}$$

For this special case, where $k = 0$, the same procedure is required to be conducted for obtaining solutions of the torque-rate minimization problem.

From the linear state space form in Eq. (4.10), $[A] \in \mathcal{R}^{6\times 6}$ becomes

$$[A] = \begin{bmatrix} 0 & 1 & 0 & 0 & 0 & 0 \\ 0 & 0 & 1/J & 0 & 0 & 0 \\ 0 & 0 & 0 & 0 & 0 & -1 \\ 0 & 0 & 0 & 0 & 0 & 0 \\ 0 & 0 & 0 & -1 & 0 & 0 \\ 0 & 0 & 0 & 0 & -1/J & 0 \end{bmatrix}$$

At the final time, the partitioned state-costate transition matrices become

$$[\Phi_{11}] = \begin{bmatrix} 1 & T-t_0 & \frac{(T-t_0)^2}{2J} \\ 0 & 1 & \frac{T-t_0}{J} \\ 0 & 0 & 1 \end{bmatrix}, \quad [\Phi_{12}] = \begin{bmatrix} -\frac{(T-t_0)^5}{120J^2} & \frac{(T-t_0)^4}{24J^2} & -\frac{(T-t_0)^3}{6J} \\ -\frac{(T-t_0)^4}{24J^2} & \frac{(T-t_0)^3}{6J^2} & -\frac{(T-t_0)^2}{2J} \\ -\frac{(T-t_0)^3}{6J} & \frac{(T-t_0)^2}{2J} & t_0 - T \end{bmatrix}$$

$$[\Phi_{21}] = \begin{bmatrix} 0 & 0 & 0 \\ 0 & 0 & 0 \\ 0 & 0 & 0 \end{bmatrix}, \quad [\Phi_{22}] = \begin{bmatrix} 1 & 0 & 0 \\ t_0 - T & 1 & 0 \\ \frac{(T-t_0)^2}{2J} & \frac{t_0-T}{J} & 1 \end{bmatrix}$$

Imposing the initial and final boundary conditions for the states and control in Eqs. (3.3) and (4.2) into Eq. (4.14) gives the following initial costates

$$\lambda_u(t_0) \triangleq \lambda_{u_0} = -\frac{60J(\theta_T - \theta_0)}{(T-t_0)^3} + \frac{12J(2\omega_T + 3\omega_0)}{(T-t_0)^2} - \frac{3(u_T - 3u_0)}{T-t_0} \tag{4.17a}$$

$$\lambda_\omega(t_0) \triangleq \lambda_{\omega_0} = \frac{-360J^2(\theta_T - \theta_0)}{(T-t_0)^4} + \frac{24J^2(7\omega_T + 8\omega_0)}{(T-t_0)^3} - \frac{12J(2u_T - 3u_0)}{(T-t_0)^2} \tag{4.17b}$$

$$\lambda_\theta(t_0) \triangleq \lambda_\theta = -\frac{720J^2(\theta_T - \theta_0)}{(T-t_0)^5} + \frac{360J^2(\omega_T + \omega_0)}{(T-t_0)^4} - \frac{60J(u_T - u_0)}{(T-t_0)^3} \tag{4.17c}$$

Substituting the obtained initial costates in Eq. (4.17) into Eq. (4.11) provides the solutions of costates

$$\lambda_\theta(t) = \lambda_\theta = \text{constant} \tag{4.18a}$$

$$\lambda_\omega(t) = \lambda_{\omega_0} - \lambda_\theta (t - t_0) \tag{4.18b}$$

$$\lambda_u(t) = \lambda_{u_0} - \frac{\lambda_{\omega_0}}{J}(t - t_0) + \frac{\lambda_\theta}{2J}(t - t_0)^2 \tag{4.18c}$$

and states

$$u(t) = u_0 - \lambda_{u_0}(t - t_0) + \frac{\lambda_{\omega_0}}{2J}(t - t_0)^2 - \frac{\lambda_\theta}{6J}(t - t_0)^3 \tag{4.19a}$$

$$\omega(t) = \omega_0 + \frac{u_0}{J}(t - t_0) - \frac{\lambda_{u_0}}{2J}(t - t_0)^2 + \frac{\lambda_{\omega_0}}{6J^2}(t - t_0)^3 - \frac{\lambda_\theta}{24J^2}(t - t_0)^4 \tag{4.19b}$$

$$\theta(t) = \theta_0 + \omega_0(t - t_0) + \frac{u_0}{2J}(t - t_0)^2 - \frac{\lambda_{u_0}}{6J}(t - t_0)^3 + \frac{\lambda_{\omega_0}}{24J^2}(t - t_0)^4 - \frac{\lambda_\theta}{120J^2}(t - t_0)^5 \tag{4.19c}$$

4.1.3 Numerical Examples

Two maneuver cases are considered: (i) rest-to-rest and (ii) motion-to-rest; and the numerical simulation is performed using the numerical simulation parameters in Table 3.1. The initial and final control inputs are assumed to be zero.

The simulation results are shown in Figs. 4.1 and 4.2. Note that the "Linear" indicates the results described in Figs. 3.1 and 3.2. The states satisfy the prescribed boundary conditions and smooth continuous control profiles are obtained but more torque is required. This is because $k = 0$ is assumed for simply generating smooth continuous control profiles. By increasing the value of k, less torque is required but this case is not discussed here. (See Ref. [10])

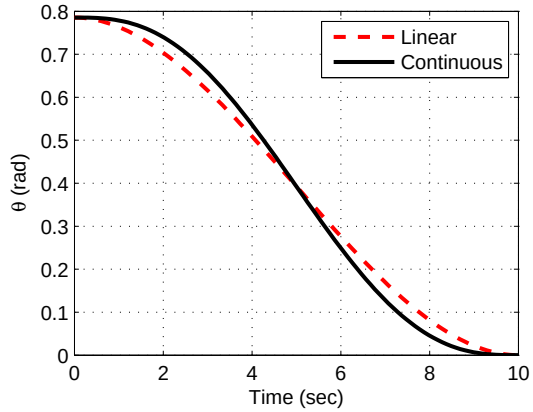

(a) Angle

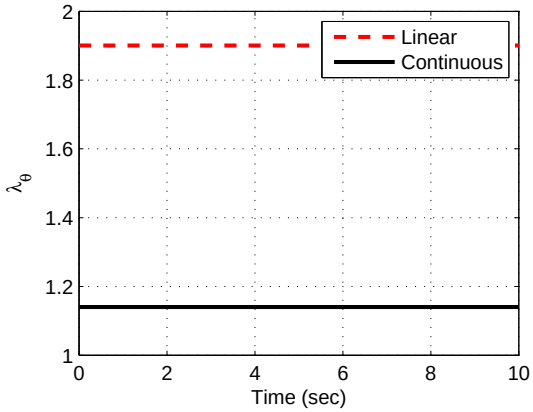

(b) Costate for the angle

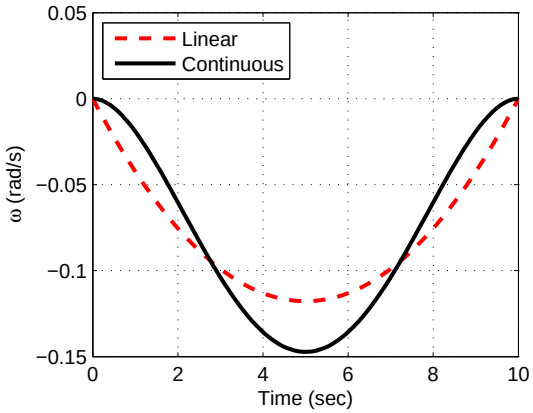

(c) Angular velocity

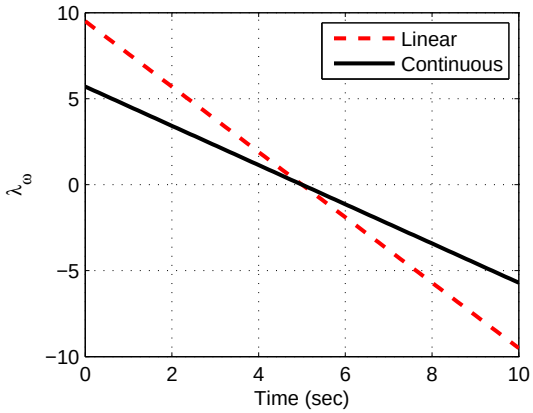

(d) Costate for the angular velocity

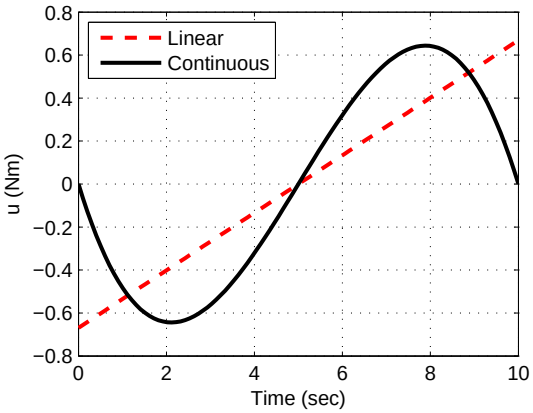

(e) Control input

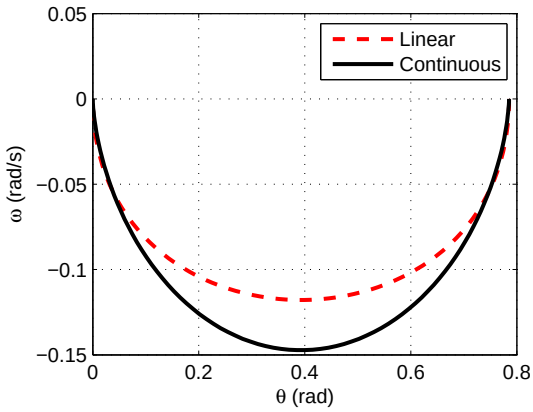

(f) Phase-plane

Figure 4.1: Near minimum-torque time trajectories for the states, costates, and control; and phase portrait (rest-to-rest)

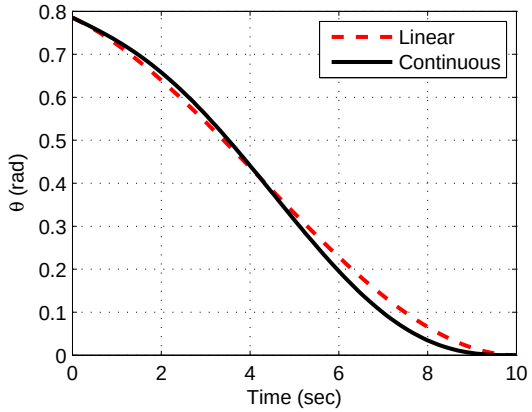

(a) Angle

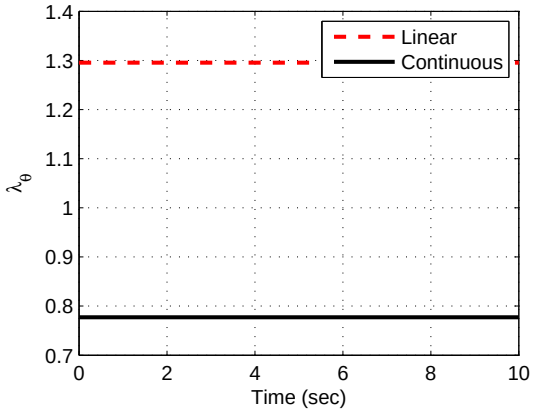

(b) Costate for the angle

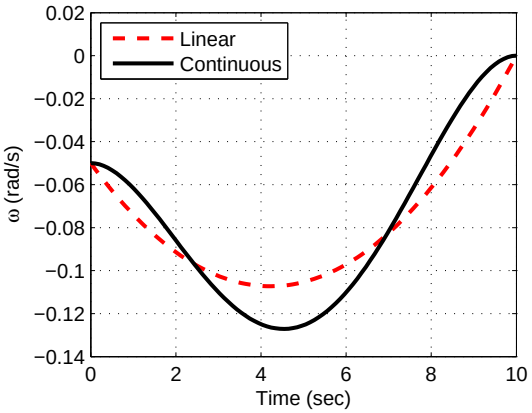

(c) Angular velocity

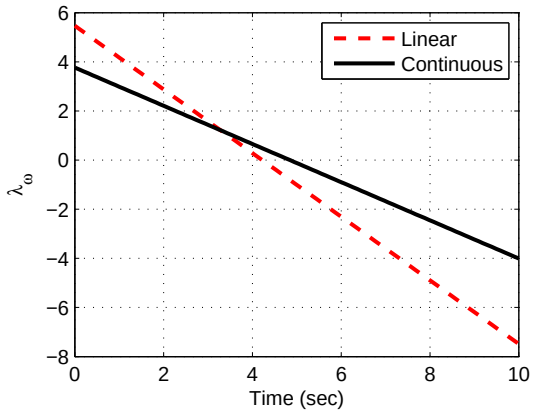

(d) Costate for the angular velocity

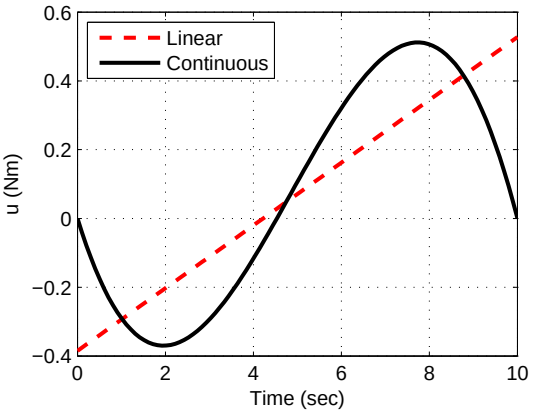

(e) Control input

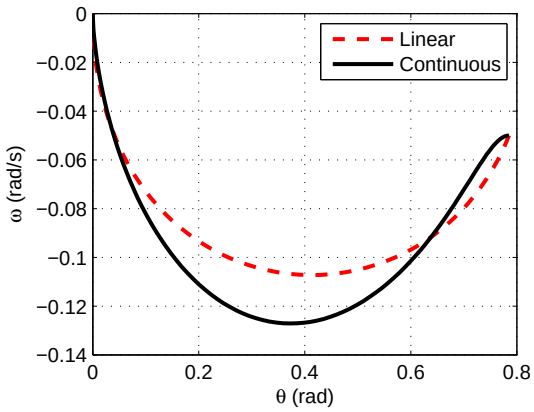

(f) Phase-plane

Figure 4.2: Near minimum-torque time trajectories for the states, costates, and control; and phase portrait (motion-to-rest)

Note that the 5^{th} order polynomial is the lowest degree polynomial, which satisfy the boundary conditions

$\underline{@t = t_0}$	$\underline{@t = T}$
$\theta(t_0) = \theta_0$	$\theta(T) = \theta_T$
$\dot{\theta}(t_0) = \dot{\theta}_0 \triangleq \omega_0$	$\dot{\theta}(T) = \dot{\theta}_T \triangleq \omega_T$
$\ddot{\theta}(t_0) = \frac{u_0}{J}$	$\ddot{\theta}(T) = \frac{u_T}{J}$

because u is assumed to have two continuous time derivatives.

For a "non-optimal" spline from the initial states to the final states must be equivalent to this optimal trajectory.

4.1.4 Concluding Remarks

This Section reviews a classical methodology to generate smooth continuous control profiles for the torque minimization problem for single-axis maneuvers. By selecting $k = 0$, this problem actually is not a torque minimization problem but rather a torque-rate minimization problem. However, by increasing the value of k, the torque-rate minimization problem becomes to the torque minimization problem. The existing formulations are revised and numerical results are demonstrated for both rest-to-rest and motion-to-rest cases. These formulations are generalized and extended for solving problems of higher dimensionality, especially for under-actuated systems, in Section 5.

4.2 Cubic Polynomial Technique: Maneuver Time Minimization

For the minimum-time maneuver, a bang-bang control profile is shown in Section 3.3. Given the kinematic and rotational dynamic equations in Eq. (3.1), a

second order differential equation (or double integrator model) is given by

$$J\ddot{\theta} = u = u_{\max}\, a(t) \tag{4.20}$$

where $a(t)$ is the cubic polynomial equation defined by

$$a(t) = b + ct + dt^2 + et^3 \tag{4.21}$$

where b, c, d, and e are the constant coefficients.

To provide a smooth transition between $-u_{\max}$ and $u_{\max}$, $a(t)$ needs to be determined for each time interval. Assuming that the initial angular velocity and time are zero, the cubic polynomial equation is found as [12, 13]

$$a(t) = \begin{cases} -\dfrac{t^2}{\delta^2}\left(3 - \dfrac{2t}{\delta}\right), & \text{if } t_0 \le t \le \delta; \\ -1, & \text{if } \delta \le t \le t_1; \\ -1 + \dfrac{(t-t_1)^2}{2\delta^2}\left(3 - \dfrac{t-t_1}{\delta}\right), & \text{if } t_1 \le t \le t_2; \\ 1, & \text{if } t_2 \le t \le t_3; \\ 1 - \dfrac{(t-t_3)^2}{\delta^2}\left[3 - \dfrac{2\,(t-t_3)}{\delta}\right], & \text{if } t_3 \le t \le T \end{cases} \tag{4.22}$$

where

$$\delta \triangleq \alpha T, \quad t_1 \triangleq \frac{T}{2} - \delta, \quad t_2 \triangleq \frac{T}{2} + \delta, \quad t_3 \triangleq T - \delta$$

$*$ *Note that the parameter, δ, should be less than or equal to $T/4$. However, an unpleasing sharp control profile is given when $\delta = T/4$.*

The sharp control profile case is not considered as a smoothing solution. Thus, the smoothing parameter, α, determining δ has to satisfy the condition $0 < \alpha < 1/4$.

4.2.1 Analytical Solutions for States and Control

Given the initial and final angles; maximum control input; and arbitrarily selected smoothing parameter, α; the final maneuver time, T, is given by [12, 13]

$$T = \sqrt{\frac{J\left(\theta_0 - \theta_T\right)}{u_{\max}\left(1/4 - \alpha/2 + \alpha^2/10\right)}} \tag{4.23}$$

The angular acceleration is calculated as

$$\ddot{\theta}(t) = \frac{u_{\max}}{J}\, a(t) \tag{4.24}$$

The angular velocity is calculated as

$$\omega(t) = \frac{u_{\max}}{J}\, v(t) \tag{4.25}$$

where

$$v(t) = \begin{cases} -\dfrac{t^3}{\delta^2}\left(1 - \dfrac{t}{2\delta}\right), & \text{if } t_0 \le t \le \delta; \\ -(t-\delta) + v(\delta), & \text{if } \delta \le t \le t_1; \\ -\left(t - t_1\right) - \dfrac{\left(t - t_1\right)^4}{8\delta^3} + \dfrac{\left(t - t_1\right)^3}{2\delta^2} + v\left(t_1\right), & \text{if } t_1 \le t \le t_2; \\ \left(t - t_2\right) + v\left(t_2\right), & \text{if } t_2 \le t \le t_3; \\ \left(t - t_3\right) - \dfrac{\left(t - t_3\right)^3}{\delta^2} + \dfrac{\left(t - t_3\right)^4}{2\delta^3} + v\left(t_3\right), & \text{if } t_3 \le t \le T \end{cases}$$

The angle is calculated as

$$\theta(t) = \frac{u_{\max}}{J}\, p(t) \tag{4.26}$$

where

$$p(t) = \begin{cases} -\dfrac{t^4}{\delta^2}\left(\dfrac{1}{4} - \dfrac{t}{10\delta}\right), & \text{if } t_0 \le t \le \delta; \\ -\dfrac{1}{2}(t-\delta)^2 + v(\delta)(t-\delta) + p(\delta), & \text{if } \delta \le t \le t_1; \\ -\dfrac{(t-t_1)^2}{2} - \dfrac{(t-t_1)^5}{40\delta^3} + \dfrac{(t-t_1)^4}{8\delta^2} + v(t_1)(t-t_1) + p(t_1), & \text{if } t_1 \le t \le t_2; \\ \dfrac{(t-t_2)^2}{2} + v(t_2)(t-t_2) + p(t_2), & \text{if } t_2 \le t \le t_3; \\ \dfrac{(t-t_3)^2}{2} - \dfrac{(t-t_3)^4}{4\delta^2} + \dfrac{(t-t_3)^5}{10\delta^3} + v(t_3)(t-t_3) + p(t_3), & \text{if } t_3 \le t \le T \end{cases}$$

Then, the smoothing control is calculated as

$$u(t) = u_{\max}\, a(t) \tag{4.27}$$

Derivation for the smoothing function, $a(t)$, is shown in Appendix A.1. Also, $v(t)$ and $p(t)$ are calculated by integrating $a(t)$ and $v(t)$, respectively.

4.2.2 Numerical Example

A rest-to-rest case is considered and numerical simulation is performed using the numerical simulation parameters in Table 3.2. The smoothing parameter, α, is assumed as 1/7.

Using Eq. (4.23), the final time is calculated as

$$T = 7.8581 \text{ sec}$$

Then, the switch-times are calculated as

$$(\delta,\, t_1,\, t_2,\, t_3) = (1.1226,\, 2.8065,\, 5.0516,\, 6.7355) \text{ sec}$$

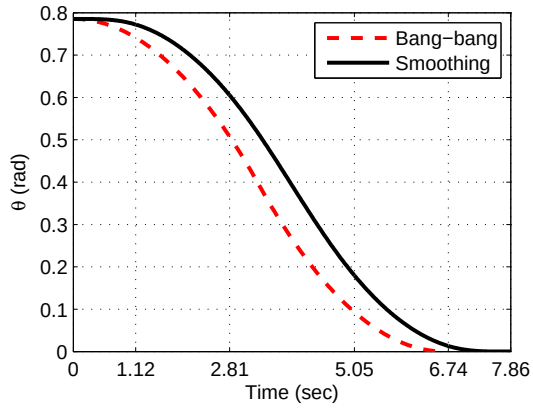

(a) Angle

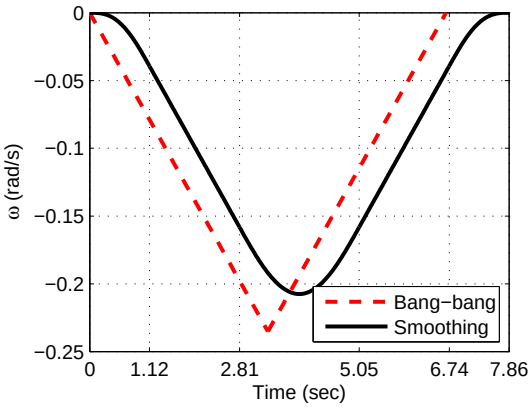

(b) Angular velocity

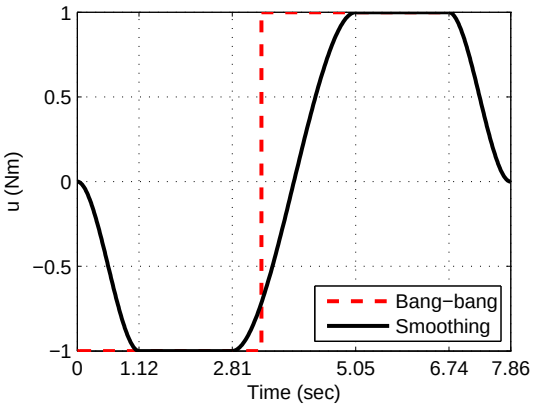

(c) Control input

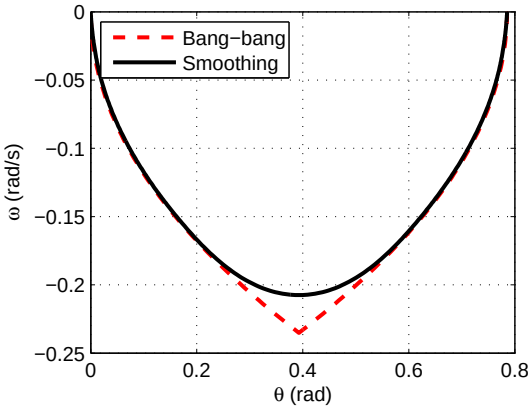

(d) Phase-plane

Figure 4.3: Near minimum-time time trajectories for the states and control; and phase portrait (rest-to-rest)

The simulation results are shown in Fig. 4.3. Note that the "Bang-bang" indicates the results described in Fig. 3.3. The states satisfy the prescribed boundary conditions and a smooth continuous control profile is obtained but a large final time is required. By decreasing the value of α, the final time for the smooth continuous control profile approaches to the final time for the bang-bang control profile.

4.2.3 Concluding Remarks

This Section shows a methodology to generate a smooth continuous control profile for the maneuver time minimization problem for single-axis maneuvers. The

existing formulations are revised and numerical results are demonstrated for a rest-to-rest case. These formulations are generalized and extended for solving problems of higher dimensionality, especially for under-actuated systems, in Appendix C.2.

4.3 Cubic Polynomial Technique: Fuel Minimization

For the minimum-fuel maneuver, a bang-off-bang control profile is shown in Section 3.4. The second order differential equation is given by

$$J\ddot{\theta} = u = u_{\max}\, a(t) \tag{4.28}$$

where $a(t)$ is the cubic polynomial equation defined by

$$a(t) = b + ct + dt^2 + et^3 \tag{4.29}$$

where b, c, d, and e are the constant coefficients.

To provide a smooth transition between $-u_{\max}$ and $u_{\max}$, $a(t)$ needs to be determined for each time interval. Assuming that the initial angular velocity and time are zeros, the cubic polynomial equation is found as

$$a(t) = \begin{cases} -\dfrac{t^2}{\delta^2}\left(3 - \dfrac{2t}{\delta}\right), & \text{if } t_0 \le t \le \delta; \\ -1, & \text{if } \delta \le t \le t_1; \\ -1 + \dfrac{(t-t_1)^2}{\delta^2}\left[3 - \dfrac{2\,(t-t_1)}{\delta}\right], & \text{if } t_1 \le t \le t_2; \\ 0, & \text{if } t_2 \le t \le t_3; \\ \dfrac{(t-t_3)^2}{\delta^2}\left[3 - \dfrac{2\,(t-t_3)}{\delta}\right], & \text{if } t_3 \le t \le t_4; \\ 1, & \text{if } t_4 \le t \le t_5; \\ 1 - \dfrac{(t-t_5)^2}{\delta^2}\left[3 - \dfrac{2\,(t-t_5)}{\delta}\right], & \text{if } t_5 \le t \le T \end{cases} \tag{4.30}$$

where

$$
\begin{aligned}
\mathcal{K} &\triangleq T - \sqrt{T^2 - 8\left(p_0 - p_T\right)} \\
p_0 &\triangleq \frac{J}{u_{\max}}\theta_0,\ p_T \triangleq \frac{J}{u_{\max}}\theta_T \\
\delta &\triangleq \beta\mathcal{K} \\
t_1 &\triangleq \frac{T}{2} + \frac{1}{2}\left[-\delta - \sqrt{\left(T-\delta\right)^2 - 4\left(p_0 - p_T\right)}\right] \\
t_2 &\triangleq \frac{T}{2} + \frac{1}{2}\left[\delta - \sqrt{\left(T-\delta\right)^2 - 4\left(p_0 - p_T\right)}\right] \\
t_3 &\triangleq \frac{T}{2} + \frac{1}{2}\left[-\delta + \sqrt{\left(T-\delta\right)^2 - 4\left(p_0 - p_T\right)}\right] \\
t_4 &\triangleq \frac{T}{2} + \frac{1}{2}\left[\delta + \sqrt{\left(T-\delta\right)^2 - 4\left(p_0 - p_T\right)}\right] \\
t_5 &\triangleq T - \delta
\end{aligned}
$$

$*$ *Note that the term,* $8\left(p_0 - p_T\right)$*, should be less than or equal to* T^2 *and the parameter,* δ*, should be less than or equal to* $\mathcal{K}/4$*. However, an unpleasing sharp control profile is given when* $\delta = \mathcal{K}/4$*.*

The sharp control profile case is not considered as a smoothing solution. Thus, the smoothing parameter, β, has to satisfy the condition $0 < \beta < 1/4$.

4.3.1 Analytical Solutions for States and Control

The angular acceleration is calculated as

$$\ddot{\theta}(t) = \frac{u_{\max}}{J}\, a(t) \tag{4.31}$$

The angular velocity is calculated as

$$\omega(t) = \frac{u_{\max}}{J}\, v(t) \tag{4.32}$$

where

$$v(t) = \begin{cases} -\dfrac{t^3}{\delta^2}\left(1 - \dfrac{t}{2\delta}\right), & \text{if } t_0 \le t \le \delta; \\ v(\delta) - (t - \delta), & \text{if } \delta \le t \le t_1; \\ v\left(t_1\right) - (t - t_1) + \dfrac{\left(t - t_1\right)^3}{\delta^2}\left(1 - \dfrac{t - t_1}{2\delta}\right), & \text{if } t_1 \le t \le t_2; \\ v\left(t_2\right), & \text{if } t_2 \le t \le t_3; \\ v\left(t_3\right) + \dfrac{\left(t - t_3\right)^3}{\delta^2}\left(1 - \dfrac{t - t_3}{2\delta}\right), & \text{if } t_3 \le t \le t_4; \\ v\left(t_4\right) + t - t_4, & \text{if } t_4 \le t \le t_5; \\ v\left(t_5\right) + t - t_5 - \dfrac{\left(t - t_5\right)^3}{\delta^2}\left(1 - \dfrac{t - t_5}{2\delta}\right), & \text{if } t_5 \le t \le T \end{cases}$$

The angle is calculated as

$$\theta(t) = \frac{u_{\max}}{J}\, p(t) \tag{4.33}$$

where

$$p(t) = \begin{cases} p\left(t_0\right) - \dfrac{t^4}{\delta^2}\left(\dfrac{1}{4} - \dfrac{t}{10\delta}\right), & \text{if } t_0 \le t \le \delta; \\ p(\delta) + v(\delta)(t - \delta) - \dfrac{1}{2}\left(t - \delta\right)^2, & \text{if } \delta \le t \le t_1; \\ p\left(t_1\right) + v\left(t_1\right)\left(t - t_1\right) - \dfrac{\left(t - t_1\right)^2}{2} + \dfrac{\left(t - t_1\right)^4}{\delta^2}\left(\dfrac{1}{4} - \dfrac{t - t_1}{10\delta}\right), & \text{if } t_1 \le t \le t_2; \\ p\left(t_2\right) + v\left(t_2\right)\left(t - t_2\right), & \text{if } t_2 \le t \le t_3; \\ p\left(t_3\right) + v\left(t_3\right)\left(t - t_3\right) + \dfrac{\left(t - t_3\right)^4}{\delta^2}\left(\dfrac{1}{4} - \dfrac{t - t_3}{10\delta}\right), & \text{if } t_3 \le t \le t_4; \\ p\left(t_4\right) + v\left(t_4\right)\left(t - t_4\right) + \dfrac{1}{2}\left(t - t_4\right)^2, & \text{if } t_4 \le t \le t_5; \\ p\left(t_5\right) + v\left(t_5\right)\left(t - t_5\right) + \dfrac{\left(t - t_5\right)^2}{2} - \dfrac{\left(t - t_5\right)^4}{\delta^2}\left(\dfrac{1}{4} - \dfrac{t - t_5}{10\delta}\right), & \text{if } t_5 \le t \le T \end{cases}$$

Then, the smoothing control is calculated as

$$u(t) = u_{\max}\, a(t) \tag{4.34}$$

Derivation for the smoothing function, $a(t)$, is shown in Appendix A.2. Also, $v(t)$ and $p(t)$ are calculated by integrating $a(t)$ and $v(t)$, respectively.

4.3.2 Numerical Example

A rest-to-rest case is considered and numerical simulation is performed using the numerical simulation parameters in Table 3.3. The smoothing parameter, β, is assumed as 1/9.

The switch-times are calculated as

$$(\delta,\, t_1,\, t_2,\, t_3,\, t_4,\, t_5) = (0.7463,\, 1.4245,\, 2.1708,\, 7.8292,\, 8.5755,\, 9.2537)\ \text{sec}$$

The simulation results are shown in Fig. 4.4. Note that the "Bang-off-bang" indicates the results described in Fig. 3.5. The states satisfy the prescribed boundary conditions and a smooth continuous control profile is obtained but a less singular control time is required. By decreasing the value of β, the singular control time for the smooth continuous control profile approaches to the singular control time for the bang-off-bang control profile.

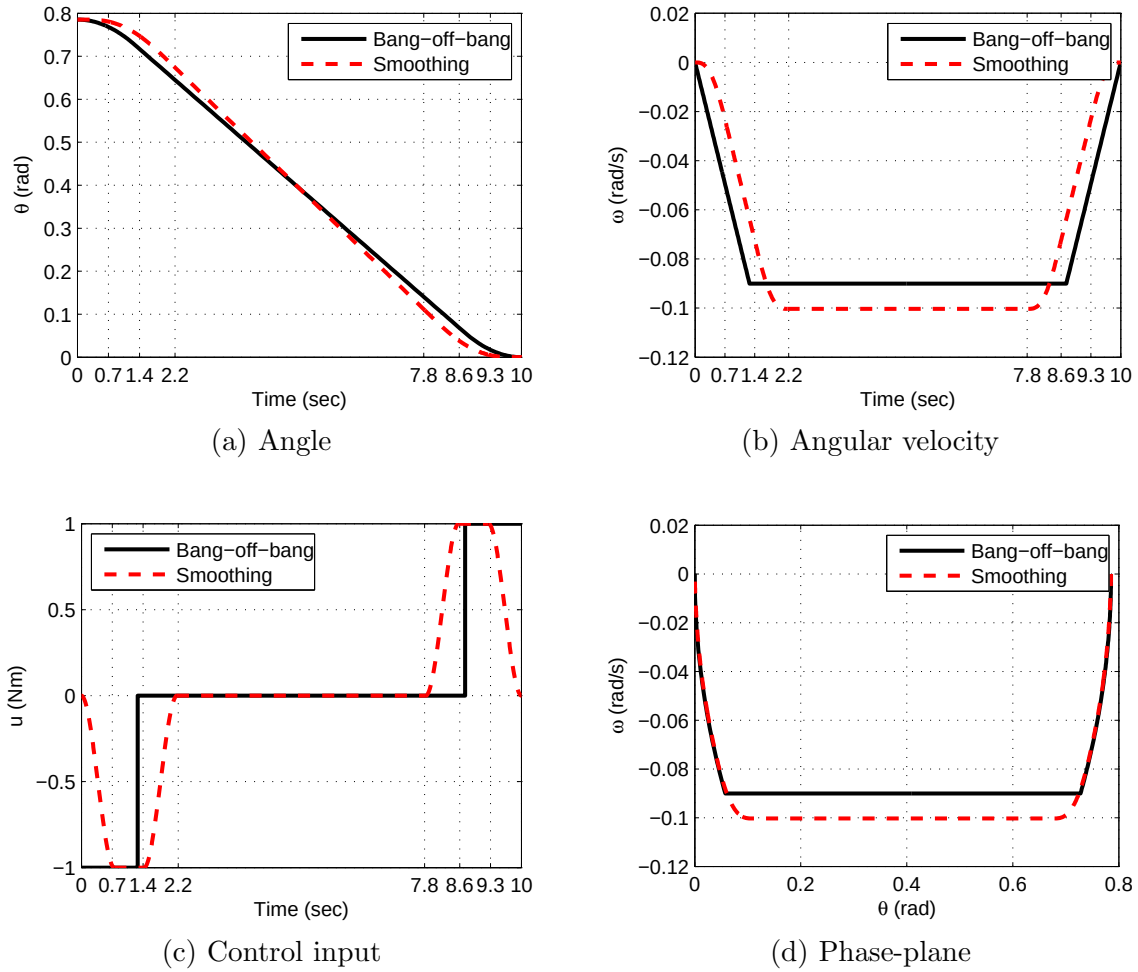

(a) Angle

(b) Angular velocity

(c) Control input

(d) Phase-plane

Figure 4.4: Near minimum-fuel time trajectories for the states and control; and phase portrait (rest-to-rest)

4.3.3 Concluding Remarks

This Section shows a methodology to generate a smooth continuous control profiles for the fuel minimization problem for single-axis maneuvers. The formulations are derived and numerical results are demonstrated for a rest-to-rest case. These formulations are generalized and extended for solving problems of higher dimensionality, especially for under-actuated systems, in Appendix C.4.

5. THREE-DIMENSIONAL MANEUVERS OF RIGID BODY

The single-axis maneuvers of a rigid body are extended to 3D general maneuvers of an asymmetric rigid body. The torque minimization problem for under-actuated systems is the focus of this Section and the maneuver time and fuel minimization problems for under-actuated systems are additionally discussed in Appendix C. *

5.1 Introduction

Extensive literature exists for controlling the attitude motion of rigid and flexible spacecraft. For a fully functioning spacecraft, it is assumed that all actuators required for completing the control task are available. Many different control strategies have been proposed for handling the nominal three-axis control case [10, 16, 17, 19, 20, 21]. More specialized literature has considered off-nominal cases where actuator failures have occurred. For example, Tsiotras and Longuski [22] have considered the case designing control strategies for handling situations in which sensor and actuator failures limit the control options available for carrying out the original mission objectives. Keraï [23] has considered a more extreme case where only a single control actuator is available, but this case is shown to be uncontrollable, which is intuitively reasonable. Brockett [24] has shown that two controls can be made asymptotically stable about the origin. Tsiotras et al. [2, 3, 4, 5, 6, 7, 8] and Shen and Tsiotras [9] have further addressed the problem of stabilizing asymmetric spacecraft including tracking control laws. Kim et al. [25, 26, 27] have introduced sequential control concepts when the actuator failure is detected by monitoring resid-

*Part of this section is reprinted with permission from "Suboptimal Asymmetric Spacecraft Maneuvers Using Two Controls" by Donghoon Kim and James D. Turner, 2013. *Journal of Guidance, Control, and Dynamics*, accepted for print, Copyright [2013] by Donghoon Kim.

uals. Others [28, 29] have presented approximate strategies that switch between two different control laws. Much of the later work has considered complex mathematical approaches for overcoming the under-actuated spacecraft control problem.

First, formulations and solutions of a rigorous nonlinear optimal control problem are presented for spacecraft maneuvers. Then, the formulations and solutions are addressed for the case when actuator failures limit the number of control inputs to two-axes, which is solved by completing three sequential sub-maneuvers. An asymmetric rigid spacecraft math model with only two available control inputs is assumed. The control design objective is to avoid inputs for the axis where the actuator failure has occurred. A spacecraft maneuver strategy is designed by formulating an optimal control problem. When only two control inputs are available, the suggested strategy is as follows: (1) transform the given initial and final attitude representations to specific attitude representations using the Euler angle transformation that is selected to avoid inputs for the failed control axis; (2) define three sequential sub-maneuvers; (3) define new attitude commands at switch-times for each sub-maneuver; (4) solve for optimal switch-times for starting and ending each sub-maneuver; and (5) perform the defined single-axis sub-maneuvers. With three maneuver periods to be defined, two unknown switch-times must be found. This approach is successful but leads to discontinuous control solutions because of jump conditions for Lagrange multipliers at switch-times. These jump discontinuities in control profiles are handled by simply changing the torque minimization problem to a torque-rate minimization problem. As discussed in Section 4.1, this approach is studied for simply generating smooth continuous control profiles and more general cases are already studied in Ref. [10]. The strategy addresses three issues that make the calculation of an optimal control solution challenging: (i) unknown switch-times must be determined to change from one sub-maneuver to the next sub-maneuver; (ii) the number of constraints is

high; and (iii) the switch-times introduce jump conditions on the necessary conditions that must be iteratively refined to generate the desired solution. The nonlinear necessary conditions are handled by introducing a multiple shooting method [14], which enforces both the end and interior points that define the optimal solution.

Second, the initial unknown costates are reformulated as functions of two unknown switch-times. By reducing the number of unknowns, this problem becomes much less sensitive to the initial unknowns and helps to reduce the computational burden.

Third, the Hamiltonian constraints are focused for obtaining analytical solutions for the switch-times. The classical resultant method [15] is utilized and several meaningful solutions for the switch-times are obtained. When more than one solution is obtained, optimality is established by calculating performance index for each meaningful solution.

Finally, the equations for describing Hamiltonian constraints are sequentially manipulated and the closed-form solution of optimal set of switch-times are obtained. To determine the optimal sequence of maneuver, the closed-form solution of performance index is also obtained.

For developing formulations, two quadratic performance indices are introduced for defining the optimal control problem for the actuator failure maneuver special case. Both the nominal and failed control maneuvers are designed to achieve the 3D rigid body boundary conditions. When only two control inputs are available for the failed actuator case, one can introduce unknown switch-times into the definition of the maneuver that must be recovered as part of the solution algorithm.

Two related control formulations are presented: (i) a quadratic penalty on torque, leading to discontinuous control profiles, and (ii) a quadratic penalty on torque-rate, leading to smooth continuous control profiles. Both performance indices

are defined as follows:

$$\mathcal{J}^{\boldsymbol{u}} \triangleq \frac{1}{2}\int_{t_0}^{t_f} \boldsymbol{u}^{\mathrm{T}}\boldsymbol{u}\,\mathrm{d}t \tag{5.1a}$$

$$\mathcal{J}^{\bar{\boldsymbol{u}}} \triangleq \frac{1}{2}\int_{t_0}^{t_f} \bar{\boldsymbol{u}}^{\mathrm{T}}\bar{\boldsymbol{u}}\,\mathrm{d}t \tag{5.1b}$$

where the *initial* time, t_0, and the *final* time, t_f, are fixed and the time derivative of control is defined as

$$\dot{\boldsymbol{u}} \triangleq \boldsymbol{g}(\bar{\boldsymbol{u}}) = \bar{\boldsymbol{u}} \tag{5.2}$$

This Section focuses on the Euler angle kinematics. Formulations for the quaternion and MRPs are presented in Appendix B.

5.2 Problem Formulations for Nominal Case

For the nominal case, minimum-torque formulations are addressed.

5.2.1 Optimal Control Formulations Using the Euler Angles

A solution for Eqs. (2.1) and (2.3) is obtained by satisfying the prescribed terminal conditions:

$$\boldsymbol{\theta}\left(t_0\right) = \boldsymbol{\theta}_{t_0}, \quad \boldsymbol{\omega}\left(t_0\right) = \boldsymbol{\omega}_{t_0}, \quad \boldsymbol{\theta}\left(t_f\right) = \boldsymbol{\theta}_{t_f}, \quad \boldsymbol{\omega}\left(t_f\right) = \boldsymbol{\omega}_{t_f} \tag{5.3}$$

where the 12 members of Eq. (5.3) are prescribed constants characterizing the attitude and angular velocity at the initial and final times.

Defining the Hamiltonian for the system

$$\mathcal{H} = \frac{1}{2}\boldsymbol{u}^{\mathrm{T}}\boldsymbol{u} + \boldsymbol{\mu}^{\mathrm{T}}\boldsymbol{p} + \boldsymbol{\gamma}^{\mathrm{T}}\boldsymbol{h} \tag{5.4}$$

where the Lagrange multipliers associated with the Euler angles and angular velocity

are $\boldsymbol{\gamma} \in \mathcal{R}^3$ and $\boldsymbol{\mu} \in \mathcal{R}^3$, respectively. The first-order necessary conditions are obtained as:

State Equations:

$$\dot{\boldsymbol{\theta}} = \frac{\partial \mathcal{H}}{\partial \boldsymbol{\gamma}} = \boldsymbol{h} = [B(\boldsymbol{\theta})]\,\boldsymbol{\omega} \tag{5.5a}$$

$$\dot{\boldsymbol{\omega}} = \frac{\partial \mathcal{H}}{\partial \boldsymbol{\mu}} = \boldsymbol{p} = [J]^{-1}\left(-\left[\boldsymbol{\omega}^{\times}\right][J]\boldsymbol{\omega} + \boldsymbol{u}\right) \tag{5.5b}$$

Costate Equations:

$$\dot{\boldsymbol{\gamma}} = -\frac{\partial \mathcal{H}}{\partial \boldsymbol{\theta}} = -\left[\frac{\partial \boldsymbol{h}}{\partial \boldsymbol{\theta}}\right]^{\mathrm{T}} \boldsymbol{\gamma} = -\left[\Delta(\boldsymbol{\theta}, \boldsymbol{\omega})\right]^{\mathrm{T}} \boldsymbol{\gamma} \tag{5.6a}$$

$$\dot{\boldsymbol{\mu}} = -\frac{\partial \mathcal{H}}{\partial \boldsymbol{\omega}} = -\left[\frac{\partial \boldsymbol{p}}{\partial \boldsymbol{\omega}}\right]^{\mathrm{T}} \boldsymbol{\mu} - \left[\frac{\partial \boldsymbol{h}}{\partial \boldsymbol{\omega}}\right]^{\mathrm{T}} \boldsymbol{\gamma} = -\left[\Sigma(\boldsymbol{\omega},\, J)\right]^{\mathrm{T}} \boldsymbol{\mu} - \left[B(\boldsymbol{\theta})\right]^{\mathrm{T}} \boldsymbol{\gamma} \tag{5.6b}$$

where

$$[\Delta(\boldsymbol{\theta},\, \boldsymbol{\omega})] \triangleq \begin{bmatrix} 0 & -\dfrac{\mathrm{c}\theta_2\left(\omega_2 \mathrm{c}\theta_3 + \omega_1 \mathrm{s}\theta_3\right)}{\mathrm{s}^2\theta_2} & \dfrac{\omega_1 \mathrm{c}\theta_3 - \omega_2 \mathrm{s}\theta_3}{\mathrm{s}\theta_2} \\ 0 & 0 & -\omega_2 \mathrm{c}\theta_3 - \omega_1 \mathrm{s}\theta_3 \\ 0 & \dfrac{\omega_2 \mathrm{c}\theta_3 + \omega_1 \mathrm{s}\theta_3}{\mathrm{s}^2\theta_2} & -\dfrac{\mathrm{c}\theta_2\left(\omega_1 \mathrm{c}\theta_3 - \omega_2 \mathrm{s}\theta_3\right)}{\mathrm{s}\theta_2} \end{bmatrix},$$

$$[\Sigma(\boldsymbol{\omega},\, J)] \triangleq \begin{bmatrix} 0 & \dfrac{J_2 - J_3}{J_1}\omega_3 & \dfrac{J_2 - J_3}{J_1}\omega_2 \\ \dfrac{J_3 - J_1}{J_2}\omega_3 & 0 & \dfrac{J_3 - J_1}{J_2}\omega_1 \\ \dfrac{J_1 - J_2}{J_3}\omega_2 & \dfrac{J_1 - J_2}{J_3}\omega_1 & 0 \end{bmatrix}$$

Stationarity Condition:

$$0 = \frac{\partial \mathcal{H}}{\partial \boldsymbol{u}} = \boldsymbol{u} + \left[\frac{\partial \boldsymbol{p}}{\partial \boldsymbol{u}}\right]^{\mathrm{T}} \boldsymbol{\mu} = \boldsymbol{u} + [J]^{-1}\boldsymbol{\mu} \tag{5.7}$$

5.2.2 Optimal Control-Rate Formulations Using the Euler Angles

A solution of Eqs. (2.1), (2.3), and (5.2) is obtained by satisfying the prescribed terminal conditions:

$$\boldsymbol{\theta}(t_0) = \boldsymbol{\theta}_{t_0}, \quad \boldsymbol{\omega}(t_0) = \boldsymbol{\omega}_{t_0}, \quad \boldsymbol{u}(t_0) = \boldsymbol{u}_{t_0} \tag{5.8a}$$

$$\boldsymbol{\theta}(t_f) = \boldsymbol{\theta}_{t_f}, \quad \boldsymbol{\omega}(t_f) = \boldsymbol{\omega}_{t_f}, \quad \boldsymbol{u}(t_f) = \boldsymbol{u}_{t_f} \tag{5.8b}$$

where the 18 members of Eq. (5.8) are prescribed constants characterizing the attitude, angular velocity, and control torque at the initial and final times.

Defining the Hamiltonian for the system

$$\mathcal{H} = \frac{1}{2}\bar{\boldsymbol{u}}^{\mathrm{T}}\bar{\boldsymbol{u}} + \boldsymbol{\mu}^{\mathrm{T}}\boldsymbol{p} + \boldsymbol{\gamma}^{\mathrm{T}}\boldsymbol{h} + \boldsymbol{\eta}^{\mathrm{T}}\boldsymbol{g} \tag{5.9}$$

where the Lagrange multiplier associated with the control torque is $\boldsymbol{\eta} \in \mathcal{R}^3$. The first-order necessary conditions are obtained as:

State Equations:

$$\dot{\boldsymbol{\theta}} = \frac{\partial \mathcal{H}}{\partial \boldsymbol{\gamma}} = \boldsymbol{h} = [B(\boldsymbol{\theta})]\,\boldsymbol{\omega} \tag{5.10a}$$

$$\dot{\boldsymbol{\omega}} = \frac{\partial \mathcal{H}}{\partial \boldsymbol{\mu}} = \boldsymbol{p} = [J]^{-1}\left(-\left[\boldsymbol{\omega}^{\times}\right][J]\boldsymbol{\omega} + \boldsymbol{u}\right) \tag{5.10b}$$

$$\dot{\boldsymbol{u}} = \frac{\partial \mathcal{H}}{\partial \boldsymbol{\eta}} = \boldsymbol{g} = \bar{\boldsymbol{u}} \tag{5.10c}$$

Costate Equations:

$$\dot{\boldsymbol{\gamma}} = -\frac{\partial \mathcal{H}}{\partial \boldsymbol{\theta}} = -\left[\frac{\partial \boldsymbol{h}}{\partial \boldsymbol{\theta}}\right]^{\mathrm{T}} \boldsymbol{\gamma} = -\left[\Delta(\boldsymbol{\theta}, \boldsymbol{\omega})\right]^{\mathrm{T}} \boldsymbol{\gamma} \tag{5.11a}$$

$$\dot{\boldsymbol{\mu}} = -\frac{\partial \mathcal{H}}{\partial \boldsymbol{\omega}} = -\left[\frac{\partial \boldsymbol{p}}{\partial \boldsymbol{\omega}}\right]^{\mathrm{T}} \boldsymbol{\mu} - \left[\frac{\partial \boldsymbol{h}}{\partial \boldsymbol{\omega}}\right]^{\mathrm{T}} \boldsymbol{\gamma} = -\left[\Sigma(\boldsymbol{\omega}, J)\right]^{\mathrm{T}} \boldsymbol{\mu} - \left[B(\boldsymbol{\theta})\right]^{\mathrm{T}} \boldsymbol{\gamma} \tag{5.11b}$$

$$\dot{\boldsymbol{\eta}} = -\frac{\partial \mathcal{H}}{\partial \boldsymbol{u}} = -\left[\frac{\partial \boldsymbol{p}}{\partial \boldsymbol{u}}\right]^{\mathrm{T}} \boldsymbol{\mu} = -J^{-1}\boldsymbol{\mu} \tag{5.11c}$$

Stationarity Condition:

$$0 = \frac{\partial \mathcal{H}}{\partial \bar{\boldsymbol{u}}} = \bar{\boldsymbol{u}} + \left[\frac{\partial \boldsymbol{g}}{\partial \bar{\boldsymbol{u}}}\right]^{\mathrm{T}} \boldsymbol{\eta} = \bar{\boldsymbol{u}} + \boldsymbol{\eta} \tag{5.12}$$

5.2.3 Numerical Example

A rest-to-rest maneuver case is considered and the numerical simulation parameters are listed in Table 5.1. Numerical simulations are performed for the nominal control case (3-axis control). The full nonlinear set of necessary conditions is solved by introducing a shooting method, which is a conventional Newton-Raphson method [30], that is found to require ~ 92 iterations for convergence. The initial unknown costates are selected arbitrarily such as zero and the converged values are listed in Tables 5.2 and 5.3.

Table 5.1: Simulation parameters for a 3D minimum-torque maneuver at initial and final times

Parameter	Symbol	Value	Unit
Moment of inertia for the spacecraft	J	diag(14.2, 17.3, 20.3)	kg·m^2
Initial time	t_0	0	sec
Initial angular velocity	$\boldsymbol{\omega}_{t_0}$	$\{0, 0, 0\}^{\mathrm{T}}$	rad/s
Initial control torque	$\boldsymbol{u}_{t_0}$	$\{0, 0, 0\}^{\mathrm{T}}$	Nm
Initial Euler angles (3-2-1 set)	$\boldsymbol{\theta}_{t_0}$	$\{24, -5, 17\}^{\mathrm{T}}$	deg
Initial Euler angles (3-1-3 set)	$\boldsymbol{\vartheta}_{t_0}$	$\{8.09, 17.7, 16.66\}^{\mathrm{T}}$	deg
Initial Euler angles (1-3-1 set)	$\boldsymbol{\varphi}_{t_0}$	$\{12.14, 24.49, 5.92\}^{\mathrm{T}}$	deg
Final time	t_f	30	sec
Final angular velocity	$\boldsymbol{\omega}_{t_f}$	$\{0, 0, 0\}^{\mathrm{T}}$	deg/s
Final control torque	$\boldsymbol{u}_{t_f}$	$\{0, 0, 0\}^{\mathrm{T}}$	Nm
Final Euler angles (3-2-1 set)	$\boldsymbol{\theta}_{t_f}$	$\{4.98, -0.44, 9.98\}^{\mathrm{T}}$	deg
Final Euler angles (3-1-3 set)	$\boldsymbol{\vartheta}_{t_f}$	$\{5, 5, 5\}^{\mathrm{T}}$	deg
Final Euler angles (1-3-1 set)	$\boldsymbol{\varphi}_{t_f}$	$\{2.51, 10, 2.51\}^{\mathrm{T}}$	deg

Table 5.2: Nominal: found initial costates and required iterations (torque minimization)

Symbol	Guess	Found	Iteration
$\boldsymbol{\gamma}(t_0)$	$\mathbf{0}_{3\times1}$	$\{0.0459, 0.0196, 0.0468\}^{\mathrm{T}}$	13
$\boldsymbol{\mu}(t_0)$	$\mathbf{0}_{3\times1}$	$\{0.2985, -0.0347, 0.7023\}^{\mathrm{T}}$	

Table 5.3: Nominal: found initial costates and required iterations (torque-rate minimization)

Symbol	Guess	Found	Iteration
$\boldsymbol{\gamma}(t_0)$	$\mathbf{0}_{3\times1}$	$\{0.0031,\ 0.0013,\ 0.0031\}^{\mathrm{T}}$	
$\boldsymbol{\mu}(t_0)$	$\mathbf{0}_{3\times1}$	$\{0.0199,\ -0.0024,\ 0.0468\}^{\mathrm{T}}$	92
$\boldsymbol{\eta}(t_0)$	$\mathbf{0}_{3\times1}$	$\{0.0070,\ -0.0008,\ 0.0115\}^{\mathrm{T}}$	

For the Euler angles, 12 sets of $B[(\theta)]$ are available. The (3-1-3) set is selected and studied for comparing under-actuated system control results later. The simulation results for minimizing torque are shown in Figs. 5.1 and 5.2. Also, the simulation results for minimizing torque-rate are shown in Figs. 5.3 and 5.4.

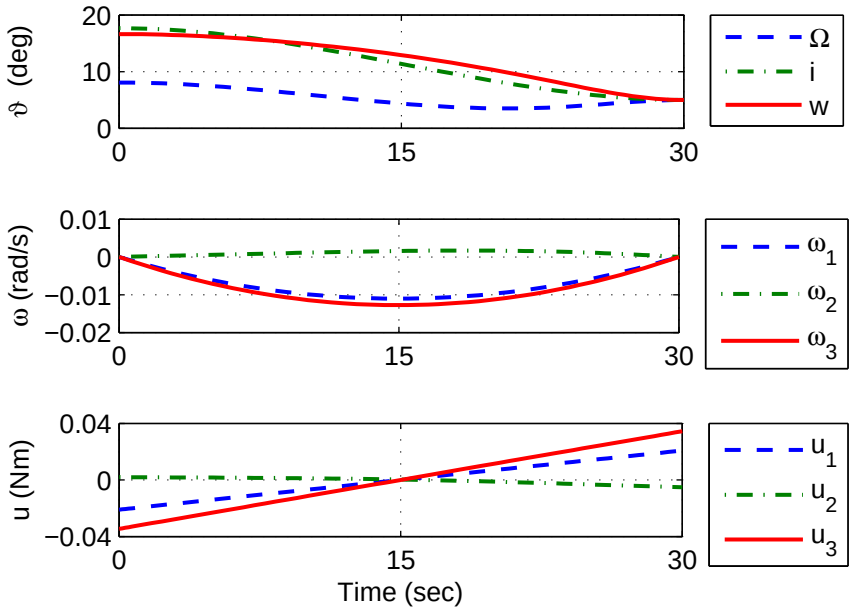

Figure 5.1: Nominal: Time trajectories for the states and control based on the Euler angles (torque minimization)

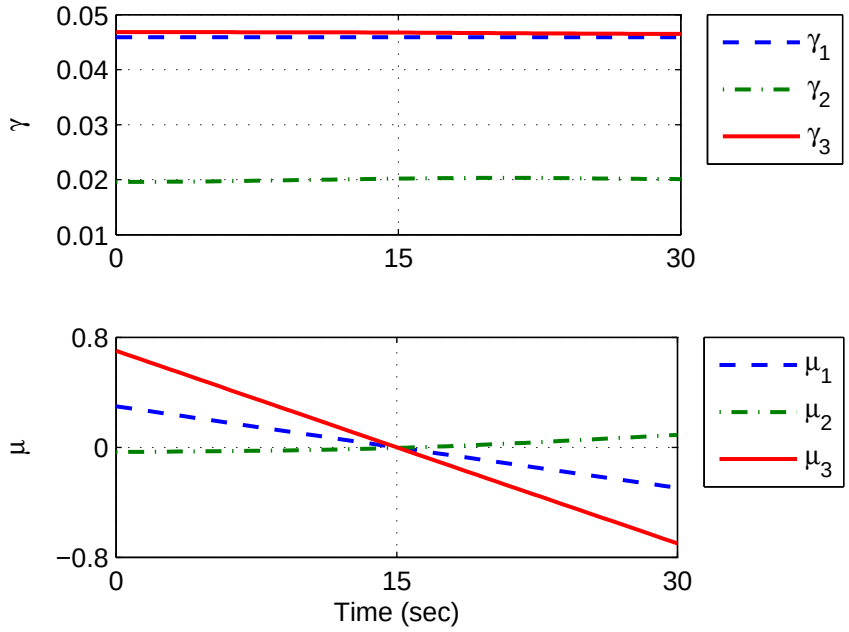

Figure 5.2: Nominal: Time trajectories for the costates based on the Euler angles (torque minimization)

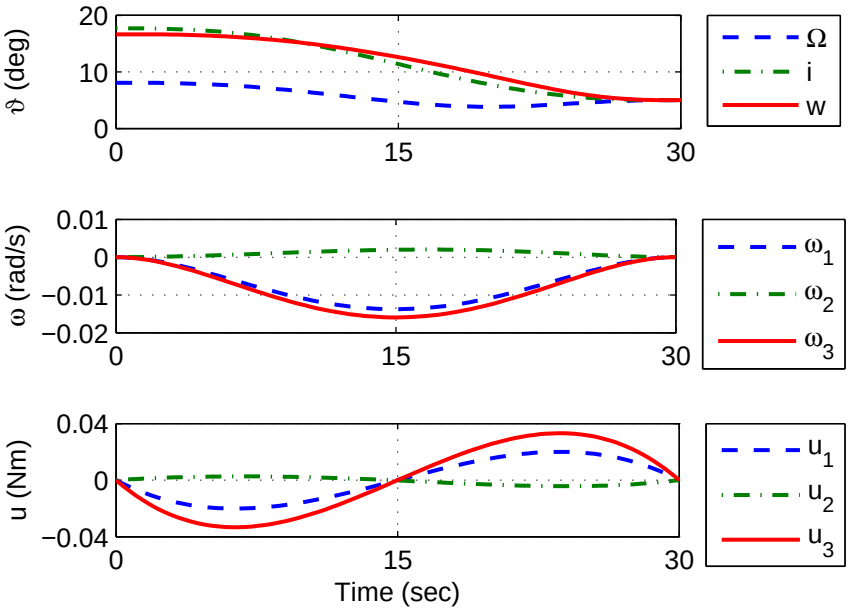

Figure 5.3: Nominal: Time trajectories for the states based on the Euler angles (torque-rate minimization)

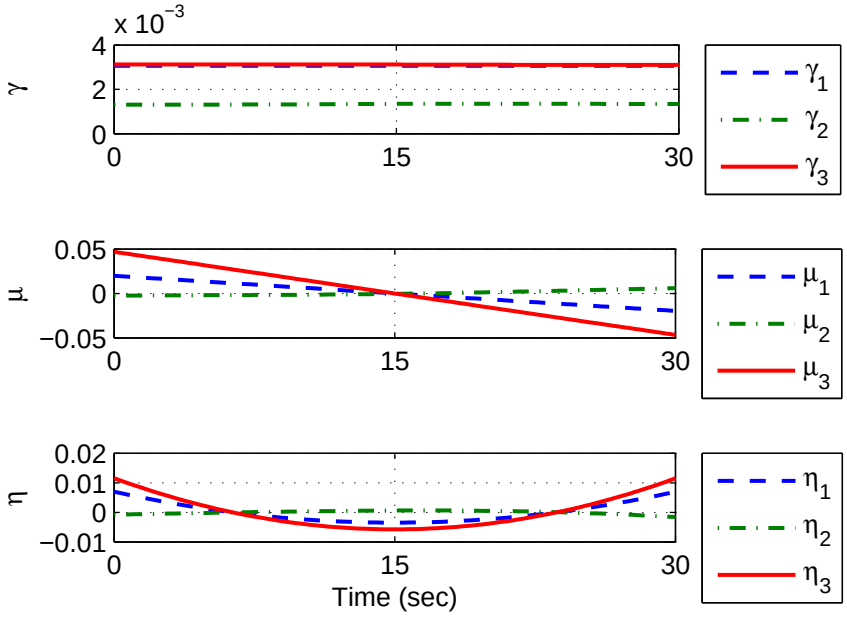

Figure 5.4: Nominal: Time trajectories for the costates based on the Euler angles (torque-rate minimization)

As shown in Figs. 5.1 and 5.2, the states satisfy the prescribed boundary conditions and the smooth linear control profiles are obtained for minimizing torque. Meanwhile, the smooth continuous control profiles are obtained for minimizing torque-rate as shown in Figs. 5.3 and 5.4. Again, the torque-rate minimization is used to generate smooth continuous control profiles while satisfying the prescribed control boundary conditions.

5.2.4 Concluding Remarks

This Section generalizes the torque minimization problem for three-axis maneuvers using the Euler angle kinematics. The numerical results are demonstrated for a rest-to-rest case using the shooting method. These formulations are continuously used for solving under-actuated system control problems in the subsequent Section.

5.3 Problem Formulations for Failed Actuator Case: Classical Method

For under-actuated systems, a sequential sub-optimal control strategy is introduced to avoid commanded inputs for the failed control axis and nonlinear spacecraft responses to the commanded control inputs. An Euler angle transformation algorithm [1] is used to define boundary conditions for the Euler angles. Unlike the nominal control, the Euler angles at switch-times also need to be determined (see Table 5.4). The boundary conditions for the Euler angles are handled by using an Euler angle rotation sequence that avoids inputs for the failed control axis. The boundary conditions for the angular velocity are set to zero at the end of each sub-maneuver; this avoids cross-axis coupling in the equations of motion for the maneuvers that follow. These control design assumptions guarantee that the constraints for the states at interior switch-times are perfectly known. Because three sequential sub-maneuvers are designed, two switch-times are specified. Failure to solve for the optimal switch-times produces large penalties in the performance index, which indicates poor maneuver performance. In general, two switch-times exist but some special cases require less than two switch-times. An example is provided to generate a reference family of direction cosine matrix.

Given the (3-2-1) set of Euler angles $(\theta_1, \theta_2, \theta_3)$, the direction cosine matrix, $[C]$, is expressed as

$$[C] = \begin{bmatrix} \mathrm{c}\theta_2\mathrm{c}\theta_1 & \mathrm{c}\theta_2\mathrm{s}\theta_1 & -\mathrm{s}\theta_2 \\ \mathrm{s}\theta_3\mathrm{s}\theta_2\mathrm{c}\theta_1 - \mathrm{c}\theta_3\mathrm{s}\theta_1 & \mathrm{s}\theta_3\mathrm{s}\theta_2\mathrm{s}\theta_1 + \mathrm{c}\theta_3\mathrm{c}\theta_1 & \mathrm{s}\theta_3\mathrm{c}\theta_2 \\ \mathrm{c}\theta_3\mathrm{s}\theta_2\mathrm{c}\theta_1 + \mathrm{s}\theta_3\mathrm{s}\theta_1 & \mathrm{c}\theta_3\mathrm{s}\theta_2\mathrm{s}\theta_1 - \mathrm{s}\theta_3\mathrm{c}\theta_1 & \mathrm{c}\theta_3\mathrm{c}\theta_2 \end{bmatrix} \tag{5.13}$$

Then, the (3-1-3) set of Euler angles (Ω, i, w) from the direction cosine matrix

are obtained by

$$\Omega = \tan^{-1}\left(\frac{C_{31}}{-C_{32}}\right) = \tan^{-1}\left(\frac{\mathrm{c}\theta_3\mathrm{s}\theta_2\mathrm{c}\theta_1 + \mathrm{s}\theta_3\mathrm{s}\theta_1}{-\mathrm{c}\theta_3\mathrm{s}\theta_2\mathrm{s}\theta_1 + \mathrm{s}\theta_3\mathrm{c}\theta_1}\right) \tag{5.14a}$$

$$i = \cos^{-1}\left(C_{33}\right) = \cos^{-1}\left(\mathrm{c}\theta_3\mathrm{c}\theta_2\right) \tag{5.14b}$$

$$w = \tan^{-1}\left(\frac{C_{13}}{C_{23}}\right) = \tan^{-1}\left(\frac{-\mathrm{s}\theta_2}{\mathrm{s}\theta_3\mathrm{c}\theta_2}\right) \tag{5.14c}$$

When $\theta_2 = 0$, the (3-1-3) Euler angles are given by $\Omega = \theta_1$, $i = \theta_3$, and $w = 0$. It indicates that only one switch-time is required to regulate the attitude. This simple case is not considered.

By introducing free interior switch-times, t_1 and t_2, for changing the control actuator, the following unknown boundary conditions are introduced:

$$\mathcal{H}\left(t_1\right) = C_1 \tag{5.15a}$$

$$\mathcal{H}\left(t_2\right) = C_2 \tag{5.15b}$$

where C_1 and C_2 are the constants. Since the Hamiltonian is not an explicit function of time, the Hamiltonian is constant over time, one concludes that C_1 equals to C_2.

Because the unknown switch-times are defined, a multiple shooting method [14] is applied to find an optimal solution, where the interior point condition [31] is given by

$$\mathcal{N}\left[\boldsymbol{z}\left(t_{\text{interior}}\right)\right] = 0 \tag{5.16}$$

where $\boldsymbol{z}$ is the total states and t_{interior} denotes t_1 and t_2. The interior point condition yields the following two additional boundary conditions that define the optimal

solution

$$\boldsymbol{\kappa}^{\mathrm{T}}\left(t^{+}_{\text{interior}}\right) = \boldsymbol{\kappa}^{\mathrm{T}}\left(t^{-}_{\text{interior}}\right) - \boldsymbol{\alpha}^{\mathrm{T}}\frac{\partial \mathcal{N}}{\partial \boldsymbol{z}}\bigg|_{t_{\text{interior}}} \tag{5.17a}$$

$$\mathcal{H}\left(t^{+}_{\text{interior}}\right) = \mathcal{H}\left(t^{-}_{\text{interior}}\right) \tag{5.17b}$$

where $\boldsymbol{\kappa}$ is the total costates and $\boldsymbol{\alpha}$ is the constant Lagrange multiplier for describing jump conditions at switch-times. The dimension of $\boldsymbol{\alpha}$ is determined by the dimension of the Lagrange multipliers associated with the states at switch-times. The Hamiltonian constraint conditions in Eqs. (5.15) and (5.17b) are shown to be the key for generating the closed-form solution for the optimal maneuver switch-times.

5.3.1 Optimal Control Formulations Using the Euler Angles

The switch-time boundary conditions, problem unknowns, and constraint conditions are presented.

5.3.1.1 Switch-Time Boundary Conditions

The total states and costates are defined as $\boldsymbol{z} \triangleq \{\boldsymbol{\theta}^{\mathrm{T}}, \boldsymbol{\omega}^{\mathrm{T}}\}^{\mathrm{T}} \in \mathcal{R}^6$ and $\boldsymbol{\kappa} \triangleq \{\boldsymbol{\gamma}^{\mathrm{T}}, \boldsymbol{\mu}^{\mathrm{T}}\}^{\mathrm{T}} \in \mathcal{R}^6$, respectively. Also, the constant Lagrange multiplier for describing jump conditions for $\boldsymbol{\gamma}(t_1)$ and $\boldsymbol{\mu}(t_1)$ are $\boldsymbol{\alpha}_1 \in \mathcal{R}^3$ and $\boldsymbol{\alpha}_2 \in \mathcal{R}^3$, respectively. Similarly, the constant Lagrange multiplier for describing jump conditions for $\boldsymbol{\gamma}(t_2)$ and $\boldsymbol{\mu}(t_2)$ are $\boldsymbol{\alpha}_3 \in \mathcal{R}^3$ and $\boldsymbol{\alpha}_4 \in \mathcal{R}^3$, respectively.

5.3.1.2 Problem Unknowns and Constraint Conditions (32)

To formulate the mathematical structure for the problem, one now collects all of the problem unknowns

$$@t_0 : \boldsymbol{\gamma}(t_0) \in \mathcal{R}^3, \quad \boldsymbol{\mu}(t_0) \in \mathcal{R}^3 \quad \Rightarrow \boxed{\text{6 unknowns}} \tag{5.18a}$$

$$@t_1 : \boldsymbol{\gamma}\left(t_1^+\right) \in \mathcal{R}^3, \quad \boldsymbol{\mu}\left(t_1^+\right) \in \mathcal{R}^3, \quad \boldsymbol{\alpha}_1 \in \mathcal{R}^3, \quad \boldsymbol{\alpha}_2 \in \mathcal{R}^3, \quad t_1 \in \mathcal{R}^1$$
$$\Rightarrow \boxed{\text{13 unknowns}} \tag{5.18b}$$

$$@t_2 : \boldsymbol{\alpha}_3 \in \mathcal{R}^3, \quad \boldsymbol{\alpha}_4 \in \mathcal{R}^3, \quad t_2 \in \mathcal{R}^1 \quad \Rightarrow \boxed{\text{7 unknowns}} \tag{5.18c}$$

$$@t_f : \boldsymbol{\gamma}(t_f) \in \mathcal{R}^3, \quad \boldsymbol{\mu}(t_f) \in \mathcal{R}^3 \quad \Rightarrow \boxed{\text{6 unknowns}} \tag{5.18d}$$

and constraint conditions

$$@t_1 : \boldsymbol{\theta}\left(t_1^+\right) = \boldsymbol{\theta}_{t_1}, \quad \boldsymbol{\omega}\left(t_1^+\right) = \boldsymbol{\omega}_{t_1}, \quad \boldsymbol{\gamma}\left(t_1^-\right) = \boldsymbol{\gamma}\left(t_1^+\right) + \boldsymbol{\alpha}_1,$$
$$\boldsymbol{\mu}\left(t_1^-\right) = \boldsymbol{\mu}\left(t_1^+\right) + \boldsymbol{\alpha}_2, \quad \mathcal{H}\left(t_1^-\right) = \mathcal{H}\left(t_1^+\right) \quad \Rightarrow \boxed{\text{13 constraints}} \tag{5.19a}$$

$$@t_2 : \boldsymbol{\theta}\left(t_2^-\right) = \boldsymbol{\theta}_{t_2}, \quad \boldsymbol{\omega}\left(t_2^-\right) = \boldsymbol{\omega}_{t_2}, \quad \boldsymbol{\theta}\left(t_2^+\right) = \boldsymbol{\theta}_{t_2}, \quad \boldsymbol{\omega}\left(t_2^+\right) = \boldsymbol{\omega}_{t_2},$$
$$\boldsymbol{\gamma}\left(t_2^-\right) = \boldsymbol{\gamma}\left(t_2^+\right) + \boldsymbol{\alpha}_3, \quad \boldsymbol{\mu}\left(t_2^-\right) = \boldsymbol{\mu}\left(t_2^+\right) + \boldsymbol{\alpha}_4, \quad \mathcal{H}\left(t_2^-\right) = \mathcal{H}\left(t_2^+\right)$$
$$\Rightarrow \boxed{\text{19 constraints}} \tag{5.19b}$$

The constraints of Eq. (5.19) are particularly challenging because jump conditions govern the optimality of the resulting solutions. The problem is characterized by both high-dimension and nonlinearity that makes it critically important to develop useful approximate starting solutions. The unknowns of Eq. (5.18) and the constraints of Eq. (5.19) are enforced by iteratively solving Eqs. (5.5)-(5.7).

5.3.2 Optimal Control-Rate Formulations Using the Euler Angles

The switch-time boundary conditions, problem unknowns, and constraint conditions are presented.

5.3.2.1 Switch-Time Boundary Conditions

The total states and costates are defined as $\boldsymbol{z} \triangleq \{\boldsymbol{\theta}^{\mathrm{T}}, \boldsymbol{\omega}^{\mathrm{T}}, \boldsymbol{u}^{\mathrm{T}}\}^{\mathrm{T}} \in \mathcal{R}^9$ and $\boldsymbol{\kappa} \triangleq \{\boldsymbol{\gamma}^{\mathrm{T}}, \boldsymbol{\mu}^{\mathrm{T}}, \boldsymbol{\eta}^{\mathrm{T}}\}^{\mathrm{T}} \in \mathcal{R}^9$, respectively. Also, the constant Lagrange multiplier for describing jump conditions for $\boldsymbol{\gamma}(t_1)$, $\boldsymbol{\mu}(t_1)$, and $\boldsymbol{\eta}(t_1)$ are $\boldsymbol{\alpha}_1 \in \mathcal{R}^3$, $\boldsymbol{\alpha}_2 \in \mathcal{R}^3$, and $\boldsymbol{\alpha}_3 \in \mathcal{R}^3$, respectively. Similarly, the constant Lagrange multiplier for describing jump conditions for $\boldsymbol{\gamma}(t_2)$, $\boldsymbol{\mu}(t_2)$, and $\boldsymbol{\eta}(t_2)$ are $\boldsymbol{\alpha}_4 \in \mathcal{R}^3$, $\boldsymbol{\alpha}_5 \in \mathcal{R}^3$, and $\boldsymbol{\alpha}_6 \in \mathcal{R}^3$, respectively.

5.3.2.2 Problem Unknowns and Constraint Conditions (47)

To formulate the mathematical structure for the problem, one now collects all of the problem unknowns

$$@t_0 : \boldsymbol{\gamma}(t_0) \in \mathcal{R}^3, \quad \boldsymbol{\mu}(t_0) \in \mathcal{R}^3, \quad \boldsymbol{\eta}(t_0) \in \mathcal{R}^3 \quad \Rightarrow \boxed{9 \text{ unknowns}} \tag{5.20a}$$

$$@t_1 : \boldsymbol{\gamma}\left(t_1^+\right) \in \mathcal{R}^3, \quad \boldsymbol{\mu}\left(t_1^+\right) \in \mathcal{R}^3, \quad \boldsymbol{\eta}\left(t_1^+\right) \in \mathcal{R}^3,$$
$$\boldsymbol{\alpha}_1 \in \mathcal{R}^3, \quad \boldsymbol{\alpha}_2 \in \mathcal{R}^3, \quad \boldsymbol{\alpha}_3 \in \mathcal{R}^3, \quad t_1 \in \mathcal{R}^1 \quad \Rightarrow \boxed{19 \text{ unknowns}} \tag{5.20b}$$

$$@t_2 : \boldsymbol{\alpha}_4 \in \mathcal{R}^3, \quad \boldsymbol{\alpha}_5 \in \mathcal{R}^3, \quad \boldsymbol{\alpha}_6 \in \mathcal{R}^3, \quad t_2 \in \mathcal{R}^1 \quad \Rightarrow \boxed{10 \text{ unknowns}} \tag{5.20c}$$

$$@t_f : \boldsymbol{\gamma}(t_f) \in \mathcal{R}^3, \quad \boldsymbol{\mu}(t_f) \in \mathcal{R}^3, \quad \boldsymbol{\eta}(t_f) \in \mathcal{R}^3 \quad \Rightarrow \boxed{9 \text{ unknowns}} \tag{5.20d}$$

and constraint conditions

$$
\begin{aligned}
@t_1 : & \boldsymbol{\theta}\left(t_1^+\right) = \boldsymbol{\theta}_{t_1}, \quad \boldsymbol{\omega}\left(t_1^+\right) = \boldsymbol{\omega}_{t_1}, \quad \boldsymbol{u}\left(t_1^+\right) = \boldsymbol{u}_{t_1}, \\
& \boldsymbol{\gamma}\left(t_1^-\right) = \boldsymbol{\gamma}\left(t_1^+\right) + \boldsymbol{\alpha}_1, \quad \boldsymbol{\mu}\left(t_1^-\right) = \boldsymbol{\mu}\left(t_1^+\right) + \boldsymbol{\alpha}_2, \quad \boldsymbol{\eta}\left(t_1^-\right) = \boldsymbol{\eta}\left(t_1^+\right) + \boldsymbol{\alpha}_3, \\
& \mathcal{H}\left(t_1^-\right) = \mathcal{H}\left(t_1^+\right) \quad \Rightarrow \boxed{\text{19 constraints}}
\end{aligned} \tag{5.21a}
$$

$$
\begin{aligned}
@t_2 : & \boldsymbol{\theta}\left(t_2^-\right) = \boldsymbol{\theta}_{t_2}, \quad \boldsymbol{\omega}\left(t_2^-\right) = \boldsymbol{\omega}_{t_2}, \quad \boldsymbol{u}\left(t_2^-\right) = \boldsymbol{u}_{t_2}, \\
& \boldsymbol{\theta}\left(t_2^+\right) = \boldsymbol{\theta}_{t_2}, \quad \boldsymbol{\omega}\left(t_2^+\right) = \boldsymbol{\omega}_{t_2}, \quad \boldsymbol{u}\left(t_2^+\right) = \boldsymbol{u}_{t_2}, \\
& \boldsymbol{\gamma}\left(t_2^-\right) = \boldsymbol{\gamma}\left(t_2^+\right) + \boldsymbol{\alpha}_4, \quad \boldsymbol{\mu}\left(t_2^-\right) = \boldsymbol{\mu}\left(t_2^+\right) + \boldsymbol{\alpha}_5, \quad \boldsymbol{\eta}\left(t_2^-\right) = \boldsymbol{\eta}\left(t_2^+\right) + \boldsymbol{\alpha}_6, \\
& \mathcal{H}\left(t_2^-\right) = \mathcal{H}\left(t_2^+\right) \quad \Rightarrow \boxed{\text{28 constraints}}
\end{aligned} \tag{5.21b}
$$

The constraints of Eq. (5.21) are particularly challenging because jump conditions govern the optimality of the resulting solutions. The problem is characterized by both high-dimension and nonlinearity that makes it critically important to develop useful approximate starting solutions. The unknowns of Eq. (5.20) and the constraints of Eq. (5.21) are enforced by iteratively solving Eqs. (5.10)-(5.12).

5.3.3 Numerical Example

The numerical simulation parameters for interior switch-times are listed in Table 5.4. Using the numerical simulation parameters in Tables 5.1 and 5.4, numerical simulations are performed for the failed control case (2-axis control). The full nonlinear set of necessary conditions is solved by introducing a multiple shooting method [14] that is found to require $\sim$ 110 iterations for convergence. The initial unknown costates are selected arbitrarily such as zero and the unknown switch-times are initialized by assuming three equal parts of total simulation time; and converged values are listed in Tables 5.5 and 5.6.

Table 5.4: Simulation parameters for a 3D minimum-torque maneuver at interior times

Parameter	Symbol	Value	Unit
Interior angular velocity	$\boldsymbol{\omega}_{t_1}$	$\{0, 0, 0\}^{\mathrm{T}}$	rad/s
Interior control torque	$\boldsymbol{u}_{t_1}$	$\{0, 0, 0\}^{\mathrm{T}}$	Nm
Interior Euler angles (3-1-3 set)	$\boldsymbol{\vartheta}_{t_1}$	$\{8.09, 17.7, 5\}^{\mathrm{T}}$	deg
Interior Euler angles (1-3-1 set)	$\boldsymbol{\varphi}_{t_1}$	$\{12.14, 24.49, 2.51\}^{\mathrm{T}}$	deg
Interior angular velocity	$\boldsymbol{\omega}_{t_2}$	$\{0, 0, 0\}^{\mathrm{T}}$	deg/s
Interior control torque	$\boldsymbol{u}_{t_2}$	$\{0, 0, 0\}^{\mathrm{T}}$	Nm
Interior Euler angles (3-1-3 set)	$\boldsymbol{\vartheta}_{t_2}$	$\{8.09, 5, 5\}^{\mathrm{T}}$	deg
Interior Euler angles (1-3-1 set)	$\boldsymbol{\varphi}_{t_2}$	$\{12.14, 10, 2.51\}^{\mathrm{T}}$	deg

Table 5.5: Failed: found initial costates and required iterations (torque minimization)

Symbol	Guess	Found	Iteration
$\boldsymbol{\gamma}(t_0)$	$\mathbf{0}_{3\times1}$	$\{0, 0, 0.5072\}^{\mathrm{T}}$	110
$\boldsymbol{\mu}(t_0)$	$\mathbf{0}_{3\times1}$	$\{0, 0, 3.1868\}^{\mathrm{T}}$	
$\boldsymbol{\gamma}(t_1)$	$\mathbf{0}_{3\times1}$	$\{0, 0.4065, 0\}^{\mathrm{T}}$	
$\boldsymbol{\mu}(t_1)$	$\mathbf{0}_{3\times1}$	$\{0, 2.2292, 0\}^{\mathrm{T}}$	
$\boldsymbol{\gamma}(t_f)$	$\mathbf{0}_{3\times1}$	$\{0.9855, 0, 0\}^{\mathrm{T}}$	
$\boldsymbol{\mu}(t_f)$	$\mathbf{0}_{3\times1}$	$\{-3.1868, 0, 0\}^{\mathrm{T}}$	
$\boldsymbol{\alpha}_1$	$\mathbf{0}_{3\times1}$	$\{0, -0.4065, 0.5072\}^{\mathrm{T}}$	
$\boldsymbol{\alpha}_2$	$\mathbf{0}_{3\times1}$	$\{0, -2.2292, -3.1868\}^{\mathrm{T}}$	
$\boldsymbol{\alpha}_3$	$\mathbf{0}_{3\times1}$	$\{-0.9855, 0.4065, 0\}^{\mathrm{T}}$	
$\boldsymbol{\alpha}_4$	$\mathbf{0}_{3\times1}$	$\{-3.1868, -2.2292, 0\}^{\mathrm{T}}$	
t_1	10	12.5651	
t_2	20	23.5329	

Table 5.6: Failed: found initial costates and required iterations (torque-rate minimization)

Symbol	Guess	Found	Iteration
$\boldsymbol{\gamma}(t_0)$	$\mathbf{0}_{3\times1}$	$\{0,\ 0,\ 0.2708\}^{\mathrm{T}}$	
$\boldsymbol{\mu}(t_0)$	$\mathbf{0}_{3\times1}$	$\{0,\ 0,\ 1.5897\}^{\mathrm{T}}$	
$\boldsymbol{\eta}(t_0)$	$\mathbf{0}_{3\times1}$	$\{0,\ 0,\ 0.1532\}^{\mathrm{T}}$	
$\boldsymbol{\gamma}(t_1)$	$\mathbf{0}_{3\times1}$	$\{0,\ 0.2271,\ 0\}^{\mathrm{T}}$	
$\boldsymbol{\mu}(t_1)$	$\mathbf{0}_{3\times1}$	$\{0,\ 1.2175,\ 0\}^{\mathrm{T}}$	
$\boldsymbol{\eta}(t_1)$	$\mathbf{0}_{3\times1}$	$\{0,\ 0.1532,\ 0\}^{\mathrm{T}}$	
$\boldsymbol{\gamma}(t_f)$	$\mathbf{0}_{3\times1}$	$\{0.6566,\ 0,\ 0\}^{\mathrm{T}}$	
$\boldsymbol{\mu}(t_f)$	$\mathbf{0}_{3\times1}$	$\{-2.4752,\ 0,\ 0\}^{\mathrm{T}}$	
$\boldsymbol{\eta}(t_f)$	$\mathbf{0}_{3\times1}$	$\{0.1532,\ 0,\ 0\}^{\mathrm{T}}$	63
$\boldsymbol{\alpha}_1$	$\mathbf{0}_{3\times1}$	$\{0,\ -0.2271,\ 0.2708\}^{\mathrm{T}}$	
$\boldsymbol{\alpha}_2$	$\mathbf{0}_{3\times1}$	$\{0,\ -1.2175,\ -1.5897\}^{\mathrm{T}}$	
$\boldsymbol{\alpha}_3$	$\mathbf{0}_{3\times1}$	$\{0,\ -0.1532,\ 0.1532\}^{\mathrm{T}}$	
$\boldsymbol{\alpha}_4$	$\mathbf{0}_{3\times1}$	$\{-0.6566,\ 0.2271,\ 0\}^{\mathrm{T}}$	
$\boldsymbol{\alpha}_5$	$\mathbf{0}_{3\times1}$	$\{-2.4752,\ -1.2175,\ 0\}^{\mathrm{T}}$	
$\boldsymbol{\alpha}_6$	$\mathbf{0}_{3\times1}$	$\{-0.1532,\ 0.1532,\ 0\}^{\mathrm{T}}$	
t_1	10	11.7390	
t_2	20	22.4608	

For the failure control simulation case, it is assumed that second axis torque cannot be generated. Thus, two possible sets of Euler transformations are available to avoid the input for the failed control axis [i.e., (3-1-3) and (1-3-1) sets]. The (3-1-3) set is selected and studied. For now, the algorithm is not including methods for selecting the optimal Euler angle rotation sequence and this indicates that the

multiple shooting method is not suitable for on-board implementation.

The simulation results for minimizing torque are shown in Figs. 5.5-5.7. Also, the simulation results for minimizing torque-rate are shown in Figs. 5.8-5.10.

As shown in Fig. 5.5, the control profiles are smooth linear functions of time for minimizing torque. The control profiles for failure control maneuver are discontinuous at the interior switch-times because the control turns off the initial control actuator and then turns on the remaining control actuator. This control design does not excite cross-axis coupling in the equations of motion. It is recognized, however, that the on-off nature of the controls is an idealization that is addressed in more complex control formulations.

Figure 5.6 presents the costate time trajectories for minimizing torque. Again, the interior switch-times are seen to generate discontinuous costate time trajectories.

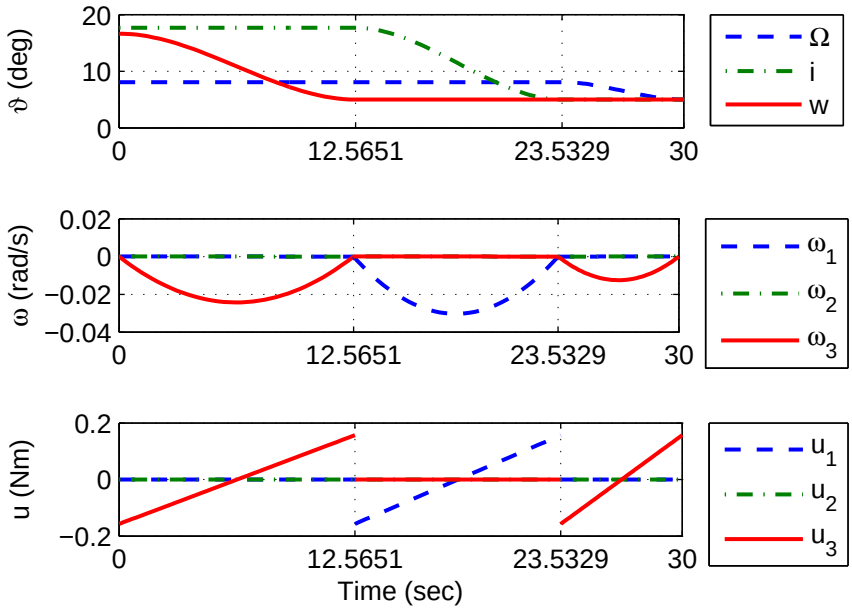

Figure 5.5: Failed: Time trajectories for the states based on the Euler angles (torque minimization)

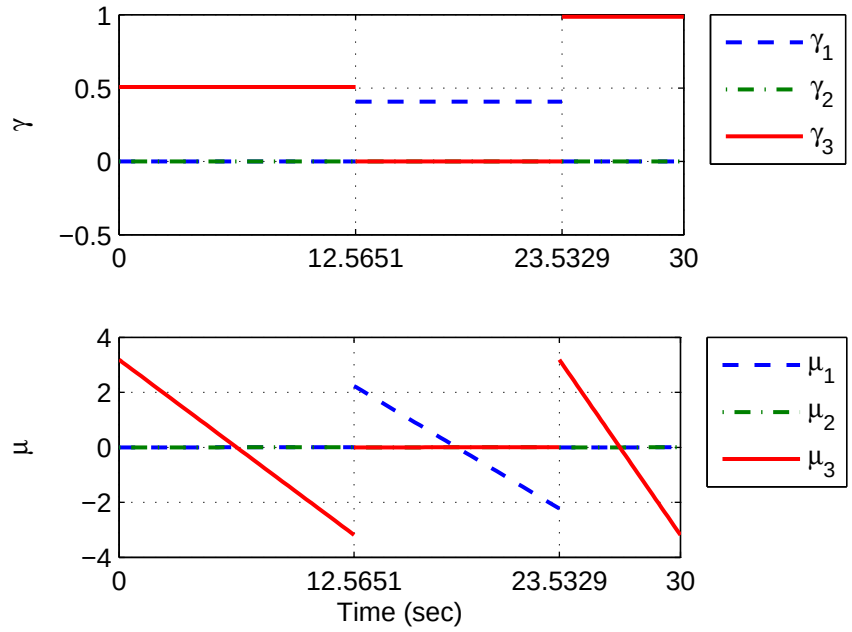

Figure 5.6: Failed: Time trajectories for the costates based on the Euler angles (torque minimization)

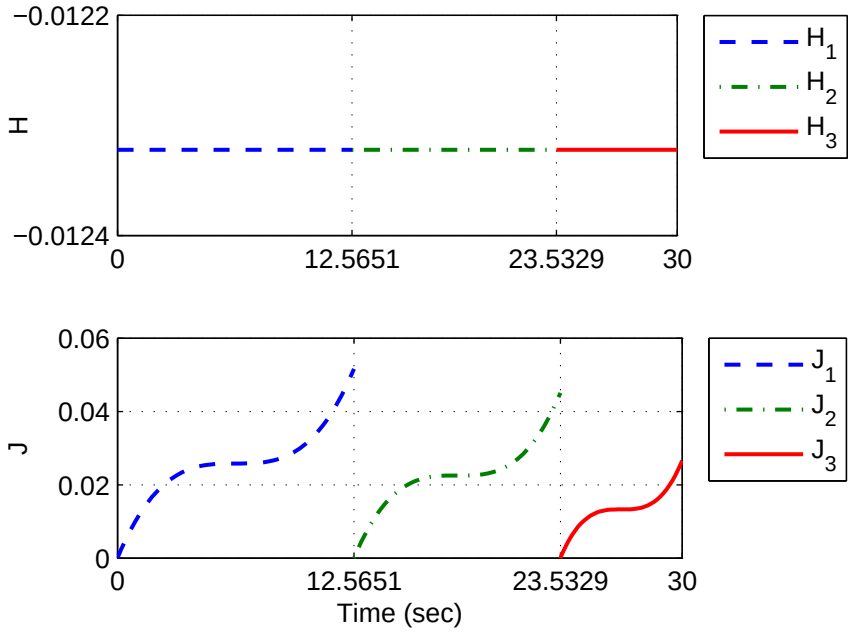

Figure 5.7: Failed: Time trajectories for the Hamiltonian and performance index based on the Euler angles (torque minimization)

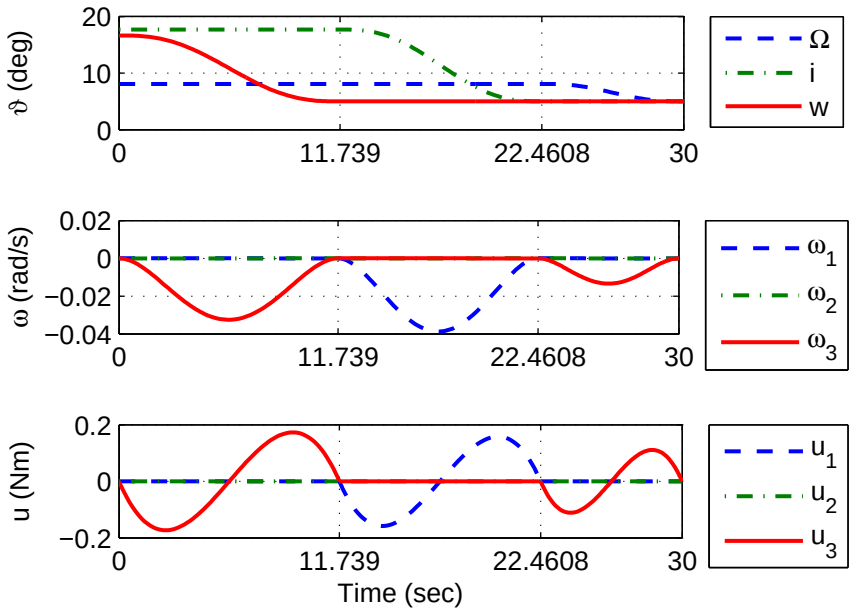

Figure 5.8: Failed: Time trajectories for the states based on the Euler angles (torque-rate minimization)

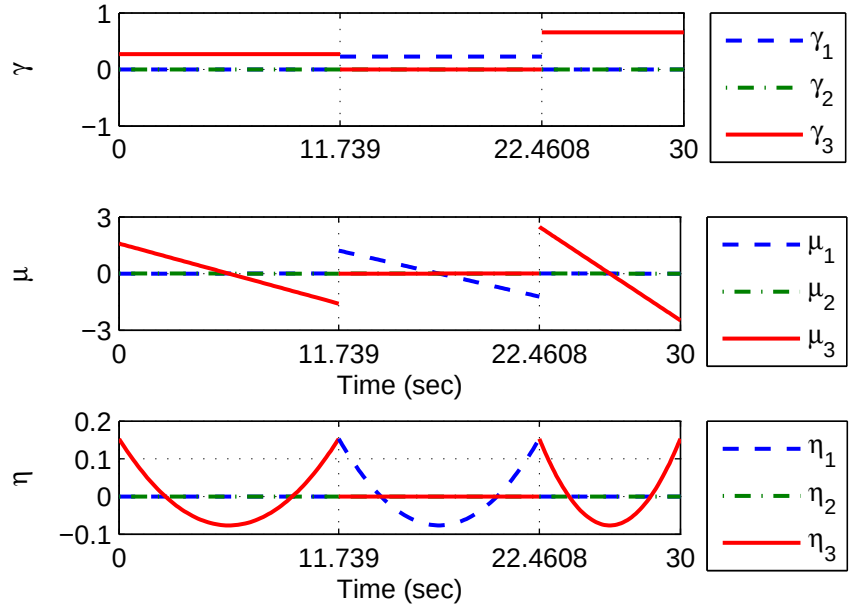

Figure 5.9: Failed: Time trajectories for the costates based on the Euler angles (torque-rate minimization)

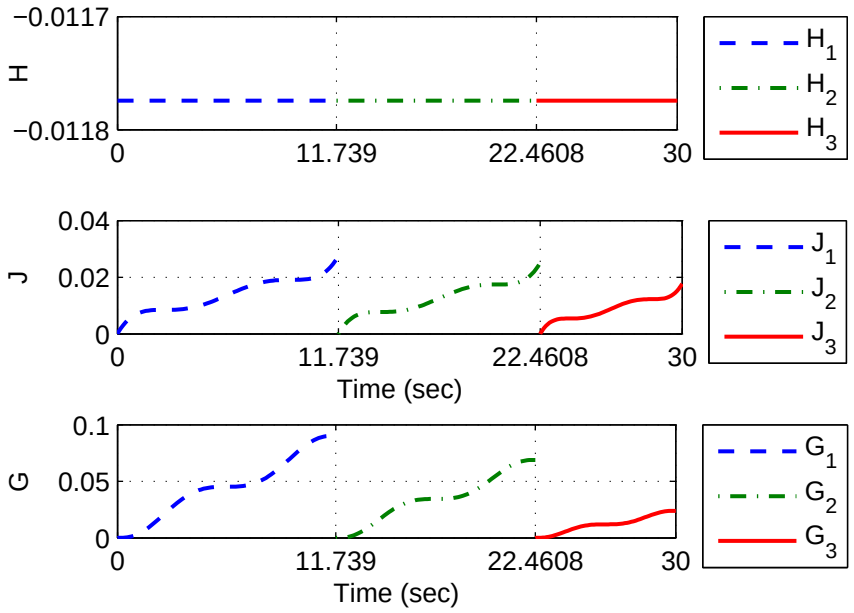

Figure 5.10: Failed: Time trajectories for the Hamiltonian and performance indices based on the Euler angles (torque-rate minimization)

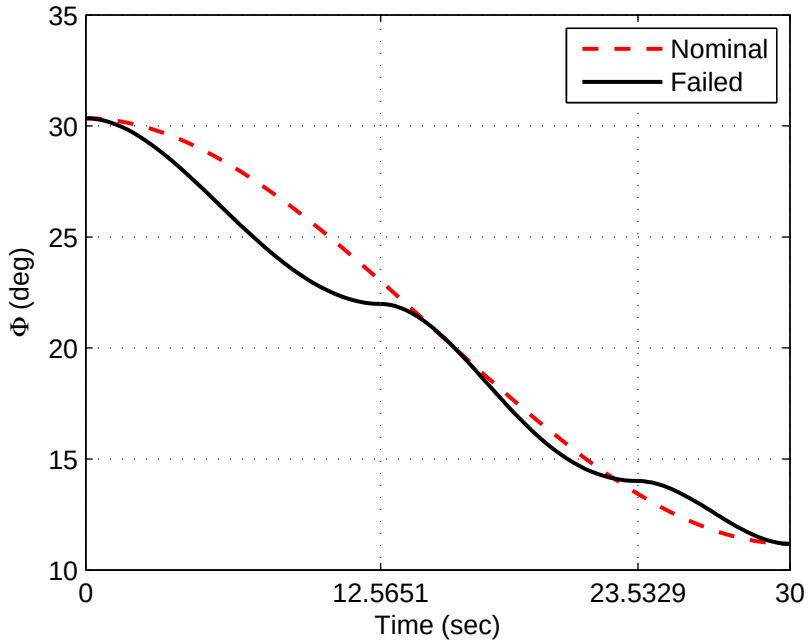

Figure 5.11: Time trajectories for the principal angles based on the Euler angles (torque minimization)

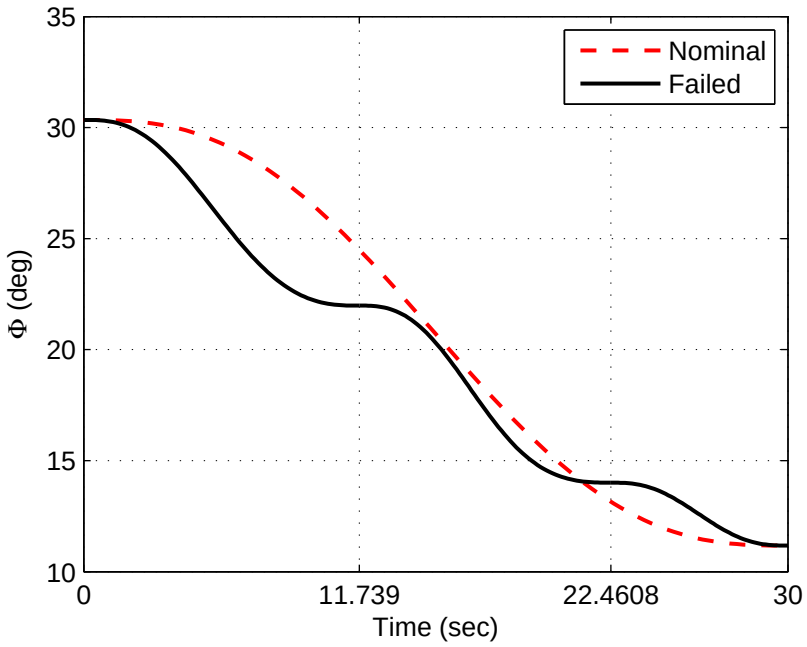

Figure 5.12: Time trajectories for the principal angles based on the Euler angles (torque-rate minimization)

As shown in Fig. 5.7, the Hamiltonian is constant over time regardless of existing control profile switches. Also, three sets of performance index time trajectories are shown and the sum of performance indices at time t_1, t_2, and t_f, is the total torque cost and it is shown that the nominal control requires less total torque cost than the failed control.

As shown in Fig. 5.8, the control profiles are smooth continuous functions of time for minimizing torque-rate. Introducing a quadratic torque-rate penalty into the problem formulations significantly increases the number of unknowns to be solved for developing the optimal control solution. Nevertheless, the overwhelming advantage of introducing the quadratic torque-rate penalty is that interior jump discontinuities are analytically eliminated from the problem, which is important for flexible body applications that are very sensitive to high-frequency behaviors in the control profiles.

Figure 5.9 presents the costate time trajectories for minimizing torque-rate.

Again, the interior switch-times are seen to generate discontinuous costate time trajectories even though the performance index minimizing torque-rate is applied.

As shown in Fig. 5.10, the Hamiltonian is constant over time regardless of existing control profile switches. Three sets of performance index time trajectories are presented and the sum of performance indices at time t_1, t_2, and t_f, generates the complete maneuver cost. A standard performance index, $\mathcal{G}^{\bar{\boldsymbol{u}}} \triangleq \frac{1}{2}\int_{t_0}^{t_f} \boldsymbol{u}^{\mathrm{T}}\boldsymbol{u}\,\mathrm{d}t$, is calculated for comparing the optimality of different solutions, which are shown in Table 5.7. Consequently, the torque consumption ratio is very similar regardless of the performance indices.

Table 5.7: Torque consumption comparison: nominal vs failed actuator

Observation	Nominal	Failed	Ratio (Failed / Nominal)
$\mathcal{J}^{\boldsymbol{u}}$	0.0082	0.1232	15.0244
$\mathcal{G}^{\bar{\boldsymbol{u}}}$	0.0117	0.1833	15.6410

Figures 5.11 and 5.12 present the principal angle time trajectories for the nominal and failed actuator cases when both torque and torque-rate minimizing performance indices are used, respectively. These results show that the failure controls minimizing both torque and torque-rate are performed successfully.

5.3.4 Concluding Remarks

This Section generalizes the torque minimization problem for three-axis maneuvers using the Euler angles. The numerical results are demonstrated for a rest-to-rest case using the multiple shooting method, which is very expensive to compute. Under-actuated systems require more unknowns and constraints. By comparing the number of unknowns and constraints between penalizing the quadratic torque and penalizing the quadratic torque-rate, the latter one has larger dimension than the for-

mer one. In Section 5.4, the problem is reformulated so that the number of necessary conditions is reduced, which leads to a substantial computational benefit.

5.4 Problem Formulations for Failed Actuator Case: Reduced Method

The general maneuver problem is now recast as three uncoupled single-axis maneuvers. The three special case solutions correspond to "pure spin" reorientations that reduce to a pure rotation about any one of the spacecraft's three principal axes of inertia. In all three cases, the initial and final states are assumed as arbitrary values except for the angular velocity about the failed control axis. To simplify the problem, the initial angular velocity for the failed control axis is assumed to be zero.

5.4.1 Initial Costate Formulations Using the Euler Angles (Torque Minimization)

The differential equations for the three special cases are expressed as:

Arbitrary Maneuver about the 1-axis:

$$\dot{\theta}_1 = \omega_1 \qquad \dot{\theta}_2 = 0 \qquad \dot{\theta}_3 = 0 \tag{5.22a}$$

$$\dot{\omega}_1 = -\mu_1 / J_1^2 \qquad \dot{\omega}_2 = 0 \qquad \dot{\omega}_3 = 0 \tag{5.22b}$$

$$\dot{\gamma}_1 = 0 \qquad \dot{\gamma}_2 = 0 \qquad \dot{\gamma}_3 = 0 \tag{5.22c}$$

$$\dot{\mu}_1 = -\gamma_1 \qquad \dot{\mu}_2 = 0 \qquad \dot{\mu}_3 = 0 \tag{5.22d}$$

Arbitrary Maneuver about the 2-axis:

$$\dot{\theta}_1 = 0 \qquad \dot{\theta}_2 = \omega_2 \qquad \dot{\theta}_3 = 0 \tag{5.23a}$$

$$\dot{\omega}_1 = 0 \qquad \dot{\omega}_2 = -\mu_2 / J_2^2 \qquad \dot{\omega}_3 = 0 \tag{5.23b}$$

$$\dot{\gamma}_1 = 0 \qquad \dot{\gamma}_2 = 0 \qquad \dot{\gamma}_3 = 0 \tag{5.23c}$$

$$\dot{\mu}_1 = 0 \qquad \dot{\mu}_2 = -\gamma_2 \qquad \dot{\mu}_3 = 0 \tag{5.23d}$$

Arbitrary Maneuver about the 3-axis:

$$\dot{\theta}_1 = 0 \qquad \dot{\theta}_2 = 0 \qquad \dot{\theta}_3 = \omega_3 \tag{5.24a}$$

$$\dot{\omega}_1 = 0 \qquad \dot{\omega}_2 = 0 \qquad \dot{\omega}_3 = -\mu_3/J_3^2 \tag{5.24b}$$

$$\dot{\gamma}_1 = 0 \qquad \dot{\gamma}_2 = 0 \qquad \dot{\gamma}_3 = 0 \tag{5.24c}$$

$$\dot{\mu}_1 = 0 \qquad \dot{\mu}_2 = 0 \qquad \dot{\mu}_3 = -\gamma_3 \tag{5.24d}$$

As shown in Section 3.2.2, the analytical solutions for the states and costates are found for single-axis maneuvers. In this Section, the costate variables λ_θ and λ_ω are changed to μ and γ, respectively.

Now, let's consider the (3-1-3) sequential rest-to-rest maneuver. The proposed methodology, however, is valid for generic maneuvers. Since three independent maneuvers are utilized, these equations are specialized by adjusting the values for t_0 and t_f to account for the current starting and stopping times for the current sub-maneuver. Of course, the initial and final angles and angular velocity as well as the moment of inertia, appearing in these equations, are also adjusted to account for the current sub-maneuver. For the (3-1-3) sequential maneuver case, the following variables are defined:

$$\mathbb{J}_1 \triangleq J_3, \quad \mathbb{J}_2 \triangleq J_1, \quad \mathbb{J}_3 \triangleq J_3 \tag{5.25a}$$

$$\vartheta_{t_1} - \vartheta_{t_0} \triangleq \text{Non-zero element of } \boldsymbol{\vartheta}_{t_1} - \boldsymbol{\vartheta}_{t_0} \tag{5.25b}$$

$$\vartheta_{t_2} - \vartheta_{t_1} \triangleq \text{Non-zero element of } \boldsymbol{\vartheta}_{t_2} - \boldsymbol{\vartheta}_{t_1} \tag{5.25c}$$

$$\vartheta_{t_f} - \vartheta_{t_2} \triangleq \text{Non-zero element of } \boldsymbol{\vartheta}_{t_f} - \boldsymbol{\vartheta}_{t_2} \tag{5.25d}$$

The analytic solutions for the maneuver necessary conditions are defined as follows:

Lagrange Multiplier Constants:

$$@t_0 : \boldsymbol{\gamma}(t_0) = \left\{ \begin{array}{c} 0 \\ 0 \\ \dfrac{-12\mathbb{J}_1^2(\vartheta_{t_1} - \vartheta_{t_0})}{(t_1 - t_0)^3} \end{array} \right\}, \quad \boldsymbol{\mu}(t_0) = \left\{ \begin{array}{c} 0 \\ 0 \\ \dfrac{-6\mathbb{J}_1^2(\vartheta_{t_1} - \vartheta_{t_0})}{(t_1 - t_0)^2} \end{array} \right\}$$

$$@t_1 : \boldsymbol{\gamma}\left(t_1^-\right) = \boldsymbol{\gamma}(t_0), \quad \boldsymbol{\mu}\left(t_1^-\right) = \boldsymbol{\mu}(t_0) - \boldsymbol{\gamma}(t_0)(t_1 - t_0) = -\boldsymbol{\mu}(t_0),$$

$$\boldsymbol{\gamma}\left(t_1^+\right) = \left\{ \begin{array}{c} 0 \\ \dfrac{-12\mathbb{J}_2^2(\vartheta_{t_2} - \vartheta_{t_1})}{(t_2 - t_1)^3} \\ 0 \end{array} \right\}, \quad \boldsymbol{\mu}\left(t_1^+\right) = \left\{ \begin{array}{c} 0 \\ \dfrac{-6\mathbb{J}_2^2(\vartheta_{t_2} - \vartheta_{t_1})}{(t_2 - t_1)^2} \\ 0 \end{array} \right\},$$

$$\boldsymbol{\alpha}_1(t_1) = \boldsymbol{\gamma}\left(t_1^-\right) - \boldsymbol{\gamma}\left(t_1^+\right), \quad \boldsymbol{\alpha}_2(t_1) = \boldsymbol{\mu}\left(t_1^-\right) - \boldsymbol{\mu}\left(t_1^+\right)$$

$$@t_2 : \boldsymbol{\gamma}\left(t_2^-\right) = \boldsymbol{\gamma}\left(t_1^+\right), \quad \boldsymbol{\mu}\left(t_2^-\right) = \boldsymbol{\mu}\left(t_1^+\right) - \boldsymbol{\gamma}\left(t_1^+\right)(t_2 - t_1) = -\boldsymbol{\mu}\left(t_1^+\right),$$

$$\boldsymbol{\gamma}\left(t_2^+\right) = \left\{ \begin{array}{c} \dfrac{-12\mathbb{J}_3^2\left(\vartheta_{t_f} - \vartheta_{t_2}\right)}{\left(t_f - t_2\right)^3} \\ 0 \\ 0 \end{array} \right\}, \quad \boldsymbol{\mu}\left(t_2^+\right) = \left\{ \begin{array}{c} \dfrac{-6\mathbb{J}_3^2\left(\vartheta_{t_f} - \vartheta_{t_2}\right)}{\left(t_f - t_2\right)^2} \\ 0 \\ 0 \end{array} \right\},$$

$$\boldsymbol{\alpha}_3(t_2) = \boldsymbol{\gamma}\left(t_2^-\right) - \boldsymbol{\gamma}\left(t_2^+\right), \quad \boldsymbol{\alpha}_4(t_2) = \boldsymbol{\mu}\left(t_2^-\right) - \boldsymbol{\mu}\left(t_2^+\right)$$

$$@t_f : \boldsymbol{\gamma}(t_f) = \boldsymbol{\gamma}\left(t_2^+\right), \quad \boldsymbol{\mu}(t_f) = \boldsymbol{\mu}\left(t_2^+\right) - \boldsymbol{\gamma}\left(t_2^+\right)(t_f - t_2) = -\boldsymbol{\mu}\left(t_2^+\right)$$

The key point is that the initial unknown costates are expressed as a function of the unknown switch-times, t_1 and t_2, *thereby reducing the number of unknowns from 32 to 2. It is important to observe that this reduction in analytic complexity yields* ~ 41*-fold boost in the computational performance.*

5.4.2 Initial Costate Formulations Using the Euler Angles (Torque-Rate Minimization)

The differential equations for the three special cases are expressed as:

Arbitrary Maneuver about the 1-axis:

$$\dot{\theta}_1 = \omega_1 \qquad \dot{\theta}_2 = 0 \qquad \dot{\theta}_3 = 0 \tag{5.26a}$$

$$\dot{\omega}_1 = u_1/J_1 \qquad \dot{\omega}_2 = 0 \qquad \dot{\omega}_3 = 0 \tag{5.26b}$$

$$\dot{u}_1 = -\eta_1 \qquad \dot{u}_2 = 0 \qquad \dot{u}_3 = 0 \tag{5.26c}$$

$$\dot{\gamma}_1 = 0 \qquad \dot{\gamma}_2 = 0 \qquad \dot{\gamma}_3 = 0 \tag{5.26d}$$

$$\dot{\mu}_1 = -\gamma_1 \qquad \dot{\mu}_2 = 0 \qquad \dot{\mu}_3 = 0 \tag{5.26e}$$

$$\dot{\eta}_1 = -\mu_1/J_1 \qquad \dot{\eta}_2 = 0 \qquad \dot{\eta}_3 = 0 \tag{5.26f}$$

Arbitrary Maneuver about the 2-axis:

$$\dot{\theta}_1 = 0 \qquad \dot{\theta}_2 = \omega_2 \qquad \dot{\theta}_3 = 0 \tag{5.27a}$$

$$\dot{\omega}_1 = 0 \qquad \dot{\omega}_2 = u_2/J_2 \qquad \dot{\omega}_3 = 0 \tag{5.27b}$$

$$\dot{u}_1 = 0 \qquad \dot{u}_2 = -\eta_2 \qquad \dot{u}_3 = 0 \tag{5.27c}$$

$$\dot{\gamma}_1 = 0 \qquad \dot{\gamma}_2 = 0 \qquad \dot{\gamma}_3 = 0 \tag{5.27d}$$

$$\dot{\mu}_1 = 0 \qquad \dot{\mu}_2 = -\gamma_2 \qquad \dot{\mu}_3 = 0 \tag{5.27e}$$

$$\dot{\eta}_1 = 0 \qquad \dot{\eta}_2 = -\mu_2/J_2 \qquad \dot{\eta}_3 = 0 \tag{5.27f}$$

Arbitrary Maneuver about the 3-axis:

$$\dot{\theta}_1 = 0 \qquad \dot{\theta}_2 = 0 \qquad \dot{\theta}_3 = \omega_3 \tag{5.28a}$$

$$\dot{\omega}_1 = 0 \qquad \dot{\omega}_2 = 0 \qquad \dot{\omega}_3 = u_3/J_3 \tag{5.28b}$$

$$\dot{u}_1 = 0 \qquad \dot{u}_2 = 0 \qquad \dot{u}_3 = -\eta_3 \tag{5.28c}$$

$$\dot{\gamma}_1 = 0 \qquad \dot{\gamma}_2 = 0 \qquad \dot{\gamma}_3 = 0 \tag{5.28d}$$

$$\dot{\mu}_1 = 0 \qquad \dot{\mu}_2 = 0 \qquad \dot{\mu}_3 = -\gamma_3 \tag{5.28e}$$

$$\dot{\eta}_1 = 0 \qquad \dot{\eta}_2 = 0 \qquad \dot{\eta}_3 = -\mu_3/J_3 \tag{5.28f}$$

As shown in Section 4.1.2, the analytical solutions for the states and costates are found for single-axis maneuvers. In this Section, the costate variables λ_θ, λ_ω, and λ_u are changed to μ, γ, and η, respectively.

Using the definitions in Eq. (5.25), the analytic solutions for the maneuver necessary conditions are defined as follows:

Lagrange Multiplier Constants:

$$@t_0 : \boldsymbol{\gamma}(t_0) = \begin{Bmatrix} 0 \\ 0 \\ \dfrac{-720\mathbb{J}_1^2(\vartheta_{t_1} - \vartheta_{t_0})}{(t_1 - t_0)^5} \end{Bmatrix}, \quad \boldsymbol{\mu}(t_0) = \begin{Bmatrix} 0 \\ 0 \\ \dfrac{-360\mathbb{J}_1^2(\vartheta_{t_1} - \vartheta_{t_0})}{(t_1 - t_0)^4} \end{Bmatrix},$$

$$\boldsymbol{\eta}(t_0) = \begin{Bmatrix} 0 \\ 0 \\ \dfrac{-60\mathbb{J}_1(\vartheta_{t_1} - \vartheta_{t_0})}{(t_1 - t_0)^3} \end{Bmatrix}$$

$$@t_1 : \boldsymbol{\gamma}\left(t_1^-\right) = \boldsymbol{\gamma}\left(t_0\right), \quad \boldsymbol{\mu}\left(t_1^-\right) = \boldsymbol{\mu}\left(t_0\right) - \boldsymbol{\gamma}\left(t_0\right)\left(t_1 - t_0\right) = -\boldsymbol{\mu}\left(t_0\right),$$

$$\boldsymbol{\eta}\left(t_1^-\right) = \boldsymbol{\eta}\left(t_0\right) - \frac{\boldsymbol{\mu}\left(t_0\right)}{\mathbb{J}_1}\left(t_1 - t_0\right) + \frac{\boldsymbol{\gamma}\left(t_0\right)}{2\mathbb{J}_1}\left(t_1 - t_0\right)^2 = \boldsymbol{\eta}\left(t_0\right),$$

$$\boldsymbol{\gamma}\left(t_1^+\right) = \left\{\begin{array}{c} 0 \\ \dfrac{-720\mathbb{J}_2^2\left(\vartheta_{t_2} - \vartheta_{t_1}\right)}{\left(t_2 - t_1\right)^5} \\ 0 \end{array}\right\}, \quad \boldsymbol{\mu}\left(t_1^+\right) = \left\{\begin{array}{c} 0 \\ \dfrac{-360\mathbb{J}_2^2\left(\vartheta_{t_2} - \vartheta_{t_1}\right)}{\left(t_2 - t_1\right)^4} \\ 0 \end{array}\right\},$$

$$\boldsymbol{\eta}\left(t_1^+\right) = \left\{\begin{array}{c} 0 \\ \dfrac{-60\mathbb{J}_2\left(\vartheta_{t_2} - \vartheta_{t_1}\right)}{\left(t_2 - t_1\right)^3} \\ 0 \end{array}\right\}, \quad \boldsymbol{\alpha}_1\left(t_1\right) = \boldsymbol{\gamma}\left(t_1^-\right) - \boldsymbol{\gamma}\left(t_1^+\right),$$

$$\boldsymbol{\alpha}_2\left(t_1\right) = \boldsymbol{\mu}\left(t_1^-\right) - \boldsymbol{\mu}\left(t_1^+\right), \quad \boldsymbol{\alpha}_3\left(t_1\right) = \boldsymbol{\eta}\left(t_1^-\right) - \boldsymbol{\eta}\left(t_1^+\right)$$

$$@t_2 : \boldsymbol{\gamma}\left(t_2^-\right) = \boldsymbol{\gamma}\left(t_1^+\right), \quad \boldsymbol{\mu}\left(t_2^-\right) = \boldsymbol{\mu}\left(t_1^+\right) - \boldsymbol{\gamma}\left(t_1^+\right)\left(t_2 - t_1\right) = -\boldsymbol{\mu}\left(t_1^+\right),$$

$$\boldsymbol{\eta}\left(t_2^-\right) = \boldsymbol{\eta}\left(t_1^+\right) - \frac{\boldsymbol{\mu}\left(t_1^+\right)}{\mathbb{J}_2}\left(t_2 - t_1\right) + \frac{\boldsymbol{\gamma}\left(t_1^+\right)}{2\mathbb{J}_2}\left(t_2 - t_1\right)^2 = \boldsymbol{\eta}\left(t_1^+\right),$$

$$\boldsymbol{\gamma}\left(t_2^+\right) = \left\{\begin{array}{c} \dfrac{-720\mathbb{J}_3^2\left(\vartheta_{t_f} - \vartheta_{t_2}\right)}{\left(t_f - t_2\right)^5} \\ 0 \\ 0 \end{array}\right\}, \quad \boldsymbol{\mu}\left(t_2^+\right) = \left\{\begin{array}{c} \dfrac{-360\mathbb{J}_3^2\left(\vartheta_{t_f} - \vartheta_{t_2}\right)}{\left(t_f - t_2\right)^4} \\ 0 \\ 0 \end{array}\right\},$$

$$\boldsymbol{\eta}\left(t_2^+\right) = \left\{\begin{array}{c} \dfrac{-60\mathbb{J}_3\left(\vartheta_{t_f} - \vartheta_{t_2}\right)}{\left(t_f - t_2\right)^3} \\ 0 \\ 0 \end{array}\right\}, \quad \boldsymbol{\alpha}_4\left(t_2\right) = \boldsymbol{\gamma}\left(t_2^-\right) - \boldsymbol{\gamma}\left(t_2^+\right),$$

$$\boldsymbol{\alpha}_5\left(t_2\right) = \boldsymbol{\mu}\left(t_2^-\right) - \boldsymbol{\mu}\left(t_2^+\right), \quad \boldsymbol{\alpha}_6\left(t_2\right) = \boldsymbol{\eta}\left(t_2^-\right) - \boldsymbol{\eta}\left(t_2^+\right)$$

$$@t_f : \boldsymbol{\gamma}\left(t_f\right) = \boldsymbol{\gamma}\left(t_2^+\right), \quad \boldsymbol{\mu}\left(t_f\right) = \boldsymbol{\mu}\left(t_2^+\right) - \boldsymbol{\gamma}\left(t_2^+\right)\left(t_f - t_2\right) = -\boldsymbol{\mu}\left(t_2^+\right),$$

$$\boldsymbol{\eta}\left(t_f\right) = \boldsymbol{\eta}\left(t_2^+\right) - \frac{\boldsymbol{\mu}\left(t_2^+\right)}{\mathbb{J}_3}\left(t_f - t_2\right) + \frac{\boldsymbol{\gamma}\left(t_2^+\right)}{2\mathbb{J}_3}\left(t_f - t_2\right)^2 = \boldsymbol{\eta}\left(t_2^+\right)$$

Now, the initial unknown costates are expressed as a function of the unknown

switch-times, t_1 and t_2, *thereby reducing the number of unknowns from 47 to 2. It is important to observe that this reduction in analytic complexity yields* ~ 86*-fold boost in the computational performance.*

5.4.3 Concluding Remarks

This Section reformulates the initial unknown costates as functions of two unknown switch-times. By examining the necessary conditions between the initial costates and the switch-times, the initial costates are reformulated as functions of two unknown switch-times. The reduction in the number of variables, one has to handle, makes real-time on-orbit applications possible.

5.5 Analytical Solutions for Failed Actuator Case: Resultant Method

To find the unknown switch-times, the Hamiltonian constraint in Eq. (5.17b) are considered.

5.5.1 Hamiltonian Formulations Using the Euler Angles (Torque Minimization)

The Hamiltonian values at right before (-) and right after (+) the switch-times are arranged as

$$\boldsymbol{u}\left(t_1^-\right) = -\frac{1}{\mathbb{J}_1}\boldsymbol{\mu}\left(t_1^-\right) \tag{5.29a}$$

$$\boldsymbol{p}\left(t_1^-\right) = \frac{1}{\mathbb{J}_1}\boldsymbol{u}\left(t_1^-\right) = -\frac{1}{\mathbb{J}_1^2}\boldsymbol{\mu}\left(t_1^-\right) \tag{5.29b}$$

$$\boldsymbol{h}\left(t_1^-\right) = \boldsymbol{\omega}\left(t_1^-\right) = \mathbf{0}_{3\times 1} \tag{5.29c}$$

$$\begin{aligned}\mathcal{H}\left(t_1^-\right) &= \frac{1}{2}\boldsymbol{u}^{\mathrm{T}}\left(t_1^-\right)\boldsymbol{u}\left(t_1^-\right) + \boldsymbol{\mu}^{\mathrm{T}}\left(t_1^-\right)\boldsymbol{p}\left(t_1^-\right) + \boldsymbol{\gamma}^{\mathrm{T}}\left(t_1^-\right)\boldsymbol{h}\left(t_1^-\right) \\ &= -\frac{18\mathbb{J}_1^2\left(\vartheta_{t_1}-\vartheta_{t_0}\right)^2}{\left(t_1-t_0\right)^4}\end{aligned} \tag{5.29d}$$

$$\boldsymbol{u}\left(t_1^+\right) = -\frac{1}{\mathbb{J}_2}\boldsymbol{\mu}\left(t_1^+\right) \tag{5.30a}$$

$$\boldsymbol{p}\left(t_1^+\right) = \frac{1}{\mathbb{J}_2}\boldsymbol{u}\left(t_1^+\right) = -\frac{1}{\mathbb{J}_2^2}\boldsymbol{\mu}\left(t_1^+\right) \tag{5.30b}$$

$$\boldsymbol{h}\left(t_1^+\right) = \boldsymbol{\omega}\left(t_1^+\right) = \mathbf{0}_{3\times 1} \tag{5.30c}$$

$$\begin{aligned}\mathcal{H}\left(t_1^+\right) =& \frac{1}{2}\boldsymbol{u}^{\mathrm{T}}\left(t_1^+\right)\boldsymbol{u}\left(t_1^+\right) + \boldsymbol{\mu}^{\mathrm{T}}\left(t_1^+\right)\boldsymbol{p}\left(t_1^+\right) + \boldsymbol{\gamma}^{\mathrm{T}}\left(t_1^+\right)\boldsymbol{h}\left(t_1^+\right) \\ =& -\frac{18\mathbb{J}_2^2\left(\vartheta_{t_2} - \vartheta_{t_1}\right)^2}{\left(t_2 - t_1\right)^4}\end{aligned} \tag{5.30d}$$

$$\boldsymbol{u}\left(t_2^-\right) = -\frac{1}{\mathbb{J}_2}\boldsymbol{\mu}\left(t_2^-\right) \tag{5.31a}$$

$$\boldsymbol{p}\left(t_2^-\right) = \frac{1}{\mathbb{J}_2}\boldsymbol{u}\left(t_2^-\right) = -\frac{1}{\mathbb{J}_2^2}\boldsymbol{\mu}\left(t_2^-\right) \tag{5.31b}$$

$$\boldsymbol{h}\left(t_2^-\right) = \boldsymbol{\omega}\left(t_2^-\right) = \mathbf{0}_{3\times 1} \tag{5.31c}$$

$$\begin{aligned}\mathcal{H}\left(t_2^-\right) =& \frac{1}{2}\boldsymbol{u}^{\mathrm{T}}\left(t_2^-\right)\boldsymbol{u}\left(t_2^-\right) + \boldsymbol{\mu}^{\mathrm{T}}\left(t_2^-\right)\boldsymbol{p}\left(t_2^-\right) + \boldsymbol{\gamma}^{\mathrm{T}}\left(t_2^-\right)\boldsymbol{h}\left(t_2^-\right) \\ =& -\frac{18\mathbb{J}_2^2\left(\vartheta_{t_2} - \vartheta_{t_1}\right)^2}{\left(t_2 - t_1\right)^4}\end{aligned} \tag{5.31d}$$

$$\boldsymbol{u}\left(t_2^+\right) = -\frac{1}{\mathbb{J}_3}\boldsymbol{\mu}\left(t_2^+\right) \tag{5.32a}$$

$$\boldsymbol{p}\left(t_2^+\right) = \frac{1}{\mathbb{J}_3}\boldsymbol{u}\left(t_2^+\right) = -\frac{1}{\mathbb{J}_3^2}\boldsymbol{\mu}\left(t_2^+\right) \tag{5.32b}$$

$$\boldsymbol{h}\left(t_2^+\right) = \boldsymbol{\omega}\left(t_2^+\right) = \mathbf{0}_{3\times 1} \tag{5.32c}$$

$$\begin{aligned}\mathcal{H}\left(t_2^+\right) =& \frac{1}{2}\boldsymbol{u}^{\mathrm{T}}\left(t_2^+\right)\boldsymbol{u}\left(t_2^+\right) + \boldsymbol{\mu}^{\mathrm{T}}\left(t_2^+\right)\boldsymbol{p}\left(t_2^+\right) + \boldsymbol{\gamma}^{\mathrm{T}}\left(t_2^+\right)\boldsymbol{h}\left(t_2^+\right) \\ =& -\frac{18\mathbb{J}_3^2\left(\vartheta_{t_f} - \vartheta_{t_2}\right)^2}{\left(t_f - t_2\right)^4}\end{aligned} \tag{5.32d}$$

Equating the Hamiltonian constraints leads to the following two coupled quar-

tic polynomial equations

$$\mathbb{J}_1^2 \left(\vartheta_{t_1} - \vartheta_{t_0}\right)^2 \left(t_2 - t_1\right)^4 = \mathbb{J}_2^2 \left(\vartheta_{t_2} - \vartheta_{t_1}\right)^2 \left(t_1 - t_0\right)^4 \tag{5.33a}$$

$$\mathbb{J}_3^2 \left(\vartheta_{t_f} - \vartheta_{t_2}\right)^2 \left(t_2 - t_1\right)^4 = \mathbb{J}_2^2 \left(\vartheta_{t_2} - \vartheta_{t_1}\right)^2 \left(t_f - t_2\right)^4 \tag{5.33b}$$

5.5.2 Hamiltonian Formulations Using the Euler Angles (Torque-Rate Minimization)

The Hamiltonian values at right before (-) and right after (+) the switch-times are arranged as

$$\boldsymbol{g}\left(t_1^-\right) = -\boldsymbol{\eta}\left(t_1^-\right) \tag{5.34a}$$

$$\boldsymbol{p}\left(t_1^-\right) = \frac{1}{\mathbb{J}_1}\boldsymbol{u}\left(t_1^-\right) = \mathbf{0}_{3\times 1} \tag{5.34b}$$

$$\boldsymbol{h}\left(t_1^-\right) = \boldsymbol{\omega}\left(t_1^-\right) = \mathbf{0}_{3\times 1} \tag{5.34c}$$

$$\begin{aligned}\mathcal{H}\left(t_1^-\right) &= \frac{1}{2}\boldsymbol{g}^{\mathrm{T}}\left(t_1^-\right)\boldsymbol{g}\left(t_1^-\right) + \boldsymbol{\mu}^{\mathrm{T}}\left(t_1^-\right)\boldsymbol{p}\left(t_1^-\right) + \boldsymbol{\gamma}^{\mathrm{T}}\left(t_1^-\right)\boldsymbol{h}\left(t_1^-\right) + \boldsymbol{\eta}^{\mathrm{T}}\left(t_1^-\right)\boldsymbol{g}\left(t_1^-\right) \\ &= -\frac{1800\mathbb{J}_1^2\left(\vartheta_{t_1} - \vartheta_{t_0}\right)^2}{\left(t_1 - t_0\right)^6}\end{aligned} \tag{5.34d}$$

$$\boldsymbol{u}\left(t_1^+\right) = -\boldsymbol{\eta}\left(t_1^+\right) \tag{5.35a}$$

$$\boldsymbol{p}\left(t_1^+\right) = \frac{1}{\mathbb{J}_2}\boldsymbol{u}\left(t_1^+\right) = \mathbf{0}_{3\times 1} \tag{5.35b}$$

$$\boldsymbol{h}\left(t_1^+\right) = \boldsymbol{\omega}\left(t_1^+\right) = \mathbf{0}_{3\times 1} \tag{5.35c}$$

$$\begin{aligned}\mathcal{H}\left(t_1^+\right) &= \frac{1}{2}\boldsymbol{g}^{\mathrm{T}}\left(t_1^+\right)\boldsymbol{g}\left(t_1^+\right) + \boldsymbol{\mu}^{\mathrm{T}}\left(t_1^+\right)\boldsymbol{p}\left(t_1^+\right) + \boldsymbol{\gamma}^{\mathrm{T}}\left(t_1^+\right)\boldsymbol{h}\left(t_1^+\right) + \boldsymbol{\eta}^{\mathrm{T}}\left(t_1^+\right)\boldsymbol{g}\left(t_1^+\right) \\ &= -\frac{1800\mathbb{J}_2^2\left(\vartheta_{t_2} - \vartheta_{t_1}\right)^2}{\left(t_2 - t_1\right)^6}\end{aligned} \tag{5.35d}$$

$$\boldsymbol{u}\left(t_2^-\right) = -\boldsymbol{\eta}\left(t_2^-\right) \tag{5.36a}$$

$$\boldsymbol{p}\left(t_2^-\right) = \frac{1}{\mathbb{J}_2}\boldsymbol{u}\left(t_2^-\right) = \mathbf{0}_{3\times 1} \tag{5.36b}$$

$$\boldsymbol{h}\left(t_2^-\right) = \boldsymbol{\omega}\left(t_2^-\right) = \mathbf{0}_{3\times 1} \tag{5.36c}$$

$$\begin{aligned}\mathcal{H}\left(t_2^-\right) &= \frac{1}{2}\boldsymbol{g}^{\mathrm{T}}\left(t_2^-\right)\boldsymbol{g}\left(t_2^-\right) + \boldsymbol{\mu}^{\mathrm{T}}\left(t_2^-\right)\boldsymbol{p}\left(t_2^-\right) + \boldsymbol{\gamma}^{\mathrm{T}}\left(t_2^-\right)\boldsymbol{h}\left(t_2^-\right) + \boldsymbol{\eta}^{\mathrm{T}}\left(t_2^-\right)\boldsymbol{g}\left(t_2^-\right) \\ &= -\frac{1800\mathbb{J}_2^2\left(\vartheta_{t_2} - \vartheta_{t_1}\right)^2}{\left(t_2 - t_1\right)^6}\end{aligned} \tag{5.36d}$$

$$\boldsymbol{u}\left(t_2^+\right) = -\boldsymbol{\eta}\left(t_2^+\right) \tag{5.37a}$$

$$\boldsymbol{p}\left(t_2^+\right) = \frac{1}{\mathbb{J}_3}\boldsymbol{u}\left(t_2^+\right) = \mathbf{0}_{3\times 1} \tag{5.37b}$$

$$\boldsymbol{h}\left(t_2^+\right) = \boldsymbol{\omega}\left(t_2^+\right) = \mathbf{0}_{3\times 1} \tag{5.37c}$$

$$\begin{aligned}\mathcal{H}\left(t_2^+\right) &= \frac{1}{2}\boldsymbol{g}^{\mathrm{T}}\left(t_2^+\right)\boldsymbol{g}\left(t_2^+\right) + \boldsymbol{\mu}^{\mathrm{T}}\left(t_2^+\right)\boldsymbol{p}\left(t_2^+\right) + \boldsymbol{\gamma}^{\mathrm{T}}\left(t_2^+\right)\boldsymbol{h}\left(t_2^+\right) + \boldsymbol{\eta}^{\mathrm{T}}\left(t_2^+\right)\boldsymbol{g}\left(t_2^+\right) \\ &= -\frac{1800\mathbb{J}_3^2\left(\vartheta_{t_f} - \vartheta_{t_2}\right)^2}{\left(t_f - t_2\right)^6}\end{aligned} \tag{5.37d}$$

Equating the Hamiltonian constraints leads to the following two coupled hexic polynomial equations

$$\mathbb{J}_1^2\left(\vartheta_{t_1} - \vartheta_{t_0}\right)^2\left(t_2 - t_1\right)^6 = \mathbb{J}_2^2\left(\vartheta_{t_2} - \vartheta_{t_1}\right)^2\left(t_1 - t_0\right)^6 \tag{5.38a}$$

$$\mathbb{J}_3^2\left(\vartheta_{t_f} - \vartheta_{t_2}\right)^2\left(t_2 - t_1\right)^6 = \mathbb{J}_2^2\left(\vartheta_{t_2} - \vartheta_{t_1}\right)^2\left(t_f - t_2\right)^6 \tag{5.38b}$$

5.5.3 Classical Resultant Method

According to the classical method of resultant, given two polynomial equations can always be written as the system of linear equations, $M\boldsymbol{y} = \mathbf{0}$, where $M = M\left(t_2\right)$ and $\boldsymbol{y} = \boldsymbol{y}\left(t_1\right) \neq 0$ [15]. Since this system must have $\det(M) = 0$, a polynomial equation only in t_2 may be determined.

For the torque minimization problem, the matrix, $M \in \mathcal{R}^{8\times 8}$, is found by the system of equations, which are multiplied by power of t_1:

$$M = \begin{bmatrix} M_{11} & M_{12} & M_{13} & M_{14} & M_{15} & 0 & 0 & 0 \\ 0 & M_{11} & M_{12} & M_{13} & M_{14} & M_{15} & 0 & 0 \\ 0 & 0 & M_{11} & M_{12} & M_{13} & M_{14} & M_{15} & 0 \\ 0 & 0 & 0 & M_{11} & M_{12} & M_{13} & M_{14} & M_{15} \\ 0 & 0 & 0 & M_{81} & M_{82} & M_{83} & M_{84} & M_{85} \\ 0 & 0 & M_{81} & M_{82} & M_{83} & M_{84} & M_{85} & 0 \\ 0 & M_{81} & M_{82} & M_{83} & M_{84} & M_{85} & 0 & 0 \\ M_{81} & M_{82} & M_{83} & M_{84} & M_{85} & 0 & 0 & 0 \end{bmatrix} \tag{5.39}$$

where the non-zero elements of M are

$$\begin{aligned} M_{11} &= A - B, \\ M_{12} &= 4Bt_0 - 4At_2, \\ M_{13} &= 6At_2^2 - 6Bt_0^2, \\ M_{14} &= 4Bt_0^3 - 4At_2^3, \\ M_{15} &= At_2^4 - Bt_0^4, \\ M_{81} &= -C, \\ M_{82} &= 4Ct_2, \\ M_{83} &= -6Ct_2^2, \\ M_{84} &= 4Ct_2^3, \\ M_{85} &= B\left(t_f - t_2\right)^4 - Ct_2^4 \end{aligned}$$

and $A \triangleq \mathbb{J}_1^2 \left(\vartheta_{t_1} - \vartheta_{t_0}\right)^2$, $B \triangleq \mathbb{J}_2^2 \left(\vartheta_{t_2} - \vartheta_{t_1}\right)^2$, and $C \triangleq \mathbb{J}_3^2 \left(\vartheta_{t_f} - \vartheta_{t_2}\right)^2$. Since $\boldsymbol{y} \neq 0$,

the determinant of M must vanish. Taking the symbolic determinant of M, and simplifying the resulting expression, it is found that t_2 satisfies a 16^{th} degree of polynomial equation, of the form:

$$\det(M) = m_{16}t_2^{16} + m_{15}t_2^{15} + \cdots + m_1 t_2 + m_0 \tag{5.40}$$

where a partial list of the polynomial coefficients are

$$\begin{aligned}
m_{16} = & -B^4\left(-A^4+4A^3B+4A^3C-6A^2B^2+124A^2BC-6A^2C^2+4AB^3-C^4\right.\\
& \left.+124AB^2C+124ABC^2+4AC^3-B^4+4B^3C-6B^2C^2+4BC^3\right)\\
m_{15} = & 16B^4\left(4AB^3t_f-B^4t_f-C^4t_0-6A^2B^2t_f-3A^2C^2t_0-3A^2C^2t_f-3B^2C^2t_0\right.\\
& -3B^2C^2t_f-A^4t_f+4A^3Bt_f+3AC^3t_0+A^3Ct_0+AC^3t_f+3A^3Ct_f\\
& +3BC^3t_0+B^3Ct_0+BC^3t_f+3B^3Ct_f+62ABC^2t_0+31AB^2Ct_0\\
& \left.+31A^2BCt_0+62ABC^2t_f+93AB^2Ct_f+93A^2BCt_f\right)\\
m_1 = & 16B^4\left(-A^4t_f^{15}+4A^3Bt_f^{15}+3A^3Ct_0^4t_f^{11}+A^3Ct_0^3t_f^{12}-6A^2B^2t_f^{15}+93A^2BCt_0^4t_f^{11}\right.\\
& +31A^2BCt_0^3t_f^{12}-3A^2C^2t_0^8t_f^7-3A^2C^2t_0^7t_f^8+4AB^3t_f^{15}+93AB^2Ct_0^4t_f^{11}\\
& +31AB^2Ct_0^3t_f^{12}+62ABC^2t_0^8t_f^7+62ABC^2t_0^7t_f^8+AC^3t_0^{12}t_f^3+3AC^3t_0^{11}t_f^4\\
& -B^4t_f^{15}+3B^3Ct_0^4t_f^{11}+B^3Ct_0^3t_f^{12}-3B^2C^2t_0^8t_f^7-3B^2C^2t_0^7t_f^8+BC^3t_0^{12}t_f^3\\
& \left.+3BC^3t_0^{11}t_f^4-C^4t_0^{15}\right)\\
m_0 = & -B^4\left(-A^4t_f^{16}+4A^3Bt_f^{16}+4A^3Ct_0^4t_f^{12}-6A^2B^2t_f^{16}+124A^2BCt_0^4t_f^{12}\right.\\
& -6A^2C^2t_0^8t_f^8+4AB^3t_f^{16}+124AB^2Ct_0^4t_f^{12}+124ABC^2t_0^8t_f^8+4AC^3t_0^{12}t_f^4\\
& \left.-B^4t_f^{16}+4B^3Ct_0^4t_f^{12}-6B^2C^2t_0^8t_f^8+4BC^3t_0^{12}t_f^4-C^4t_0^{16}\right)
\end{aligned}$$

The symbolic polynomial equation of Eq. (5.40) is evaluated numerically by first numerically evaluating the polynomial coefficients, and then calling a standard

library polynomial root solving algorithm. Because sixteen solutions are generated, one must impose constraints on the root solutions so that the switch-times are physically meaningful for the prescribed maneuver conditions. For example, the following constraints are invoked to reduce the number of roots to realistic values: (i) all roots must be real-valued; (ii) all roots must be $> t_0$; (iii) all roots must be $< t_f$; and (iv) $t_1 < t_2$.

Several solutions that are found satisfied these constraints. The optimal solution is identified by computing the performance index and then comparing numerical values. *Numerical experiments with this approach yielded performance boosts of* ~ 143*-fold when compared to the nonlinear optimization approach.*

For the torque-rate minimization problem, the matrix, $L \in \mathcal{R}^{12\times 12}$, is found by the system of equations, which are multiplied by power of t_1:

$$L = \begin{bmatrix} L_{11} & L_{12} & L_{13} & L_{14} & L_{15} & L_{16} & L_{17} & 0 & 0 & 0 & 0 & 0 \\ 0 & L_{11} & L_{12} & L_{13} & L_{14} & L_{15} & L_{16} & L_{17} & 0 & 0 & 0 & 0 \\ 0 & 0 & L_{11} & L_{12} & L_{13} & L_{14} & L_{15} & L_{16} & L_{17} & 0 & 0 & 0 \\ 0 & 0 & 0 & L_{11} & L_{12} & L_{13} & L_{14} & L_{15} & L_{16} & L_{17} & 0 & 0 \\ 0 & 0 & 0 & 0 & L_{11} & L_{12} & L_{13} & L_{14} & L_{15} & L_{16} & L_{17} & 0 \\ 0 & 0 & 0 & 0 & 0 & L_{11} & L_{12} & L_{13} & L_{14} & L_{15} & L_{16} & L_{17} \\ 0 & 0 & 0 & 0 & 0 & L_{81} & L_{82} & L_{83} & L_{84} & L_{85} & L_{86} & L_{87} \\ 0 & 0 & 0 & 0 & L_{81} & L_{82} & L_{83} & L_{84} & L_{85} & L_{86} & L_{87} & 0 \\ 0 & 0 & 0 & L_{81} & L_{82} & L_{83} & L_{84} & L_{85} & L_{86} & L_{87} & 0 & 0 \\ 0 & 0 & L_{81} & L_{82} & L_{83} & L_{84} & L_{85} & L_{86} & L_{87} & 0 & 0 & 0 \\ 0 & L_{81} & L_{82} & L_{83} & L_{84} & L_{85} & L_{86} & L_{87} & 0 & 0 & 0 & 0 \\ L_{81} & L_{82} & L_{83} & L_{84} & L_{85} & L_{86} & L_{87} & 0 & 0 & 0 & 0 & 0 \end{bmatrix} \tag{5.41}$$

where the non-zero elements of L are

$$
\begin{aligned}
L_{11} &= A - B, \\
L_{12} &= 6\left(Bt_0 - At_2\right), \\
L_{13} &= 15\left(At_2^2 - Bt_0^2\right), \\
L_{14} &= 20\left(Bt_0^3 - At_2^3\right), \\
L_{15} &= 15\left(At_2^4 - Bt_0^4\right), \\
L_{16} &= 6\left(Bt_0^5 - At_2^5\right), \\
L_{17} &= At_2^6 - Bt_0^6, \\
L_{81} &= -C, \\
L_{82} &= 6Ct_2, \\
L_{83} &= -15Ct_2^2, \\
L_{84} &= 20Ct_2^3, \\
L_{85} &= -15Ct_2^4, \\
L_{86} &= 6Ct_2^5, \\
L_{87} &= B\left(t_f - t_2\right)^6 - Ct_2^6
\end{aligned}
$$

Taking the determinant of L, it is found that t_2 satisfies a 36^{th} degree of polynomial equation. This equation has the form as follows:

$$\det(L) = l_{32}t_2^{32} + l_{31}t_2^{31} + \cdots + l_1t_2 + l_0 \tag{5.42}$$

where l_i is the coefficient and $i = 0, 1, \cdots, 32$. Analytic solutions for the coefficients are not addressed because of space limitations.

By imposing the previously mentioned maneuver conditions, several solutions

that are found satisfied these constraints.

The optimal solution is identified by computing the performance index and then comparing numerical values. *Numerical experiments with this approach yielded performance boosts of* ~ 320*-fold when compared to the nonlinear optimization approach.*

5.5.4 Numerical Example

From the determinant of M, 16 possible switch-times, t_2, are found as

$$t_2 = (5.9423,\, 23.5329,\, -9.8407,\, 41.3686) \rightarrow \text{ real} \tag{5.43a}$$

$$\begin{aligned} t_2 = (&1.7250 \pm 6.9839i,\, 37.5128 \pm 13.5124i,\, 22.3474 \pm 4.4100i, \\ &22.6761 \pm 5.2783i,\, 27.8934 \pm 7.6654i,\, 34.9017 \pm 13.6849i) \\ &\rightarrow \text{ complex} \end{aligned} \tag{5.43b}$$

By imposing two criteria into Eq. (5.43): (i) $t_0 < t_2 < t_f$ and (ii) t_2 is real, two possible switch-times, t_2, are obtained as

$$t_2 = (5.9423,\, 23.5329) \text{ sec} \tag{5.44}$$

Using the criteria, $t_1 < t_2$, and substituting Eq. (5.44) into Eq. (5.33a) provides two possible switch-times, t_1. As a result, two possible sets of switch-times are found as

$$(t_1,\, t_2) = (3.1728,\, 5.9423) \text{ sec} \tag{5.45a}$$

$$(t_1,\, t_2) = (12.5651,\, 23.5329) \text{ sec} \tag{5.45b}$$

Correspondingly, one obtains the performance index values by using all sets

of the switch-times:

$$\mathcal{J}^{\boldsymbol{u}} = 6.0041 \text{ using Eq. (5.45a)} \tag{5.46a}$$

$$\mathcal{J}^{\boldsymbol{u}} = 0.1232 \text{ using Eq. (5.45b)} \tag{5.46b}$$

Consequently, the optimal switch-times in Eq. (5.45b) provides the optimal maneuver solution.

From the determinant of L, 32 possible switch-times, t_2, are found. By imposing the same criteria mentioned previously, four possible sets of switch-times are found as

$$(t_1,\, t_2) = (10.1376,\, 19.3966) \text{ sec} \tag{5.47a}$$

$$(t_1,\, t_2) = (6.0002,\, 11.4805) \text{ sec} \tag{5.47b}$$

$$(t_1,\, t_2) = (1.8641,\, 3.5667) \text{ sec} \tag{5.47c}$$

$$(t_1,\, t_2) = (11.7390,\, 22.4608) \text{ sec} \tag{5.47d}$$

Then, performance index values are evaluated by using all sets of the switch-times as follows:

$$\mathcal{J}^{\bar{\boldsymbol{u}}} = 0.1130 \text{ using Eq. (5.47a)} \tag{5.48a}$$

$$\mathcal{J}^{\bar{\boldsymbol{u}}} = 1.5114 \text{ using Eq. (5.47b)} \tag{5.48b}$$

$$\mathcal{J}^{\bar{\boldsymbol{u}}} = 522.1901 \text{ using Eq. (5.47c)} \tag{5.48c}$$

$$\mathcal{J}^{\bar{\boldsymbol{u}}} = 0.0704 \text{ using Eq. (5.47d)} \tag{5.48d}$$

Consequently, the optimal switch-times in Eq. (5.47d) provides the optimal maneuver solution.

5.5.5 *Concluding Remarks*

This Section describes a methodology to find switch-times using the Hamiltonian constraints. A resultant method is introduced, which yields a high-order polynomial equation. The optimal maneuver is verified by computing the performance index for each physically meaningful set of switch-times and numerically ranking the performance indices.

5.6 Closed-Form Solutions for Failed Actuator Case

Closed-form solutions for the failed actuator case are derived by sequentially manipulating the Hamiltonian constraint equations.

5.6.1 *Switch-Times and Performance Index (Torque Minimization)*

A closed-form solution is obtained for the switch-times by sequentially manipulating Eq. (5.33). The final form for the switch-time solutions exploit the observation that all of the terms appearing in Eq. (5.33) are positive. An analytic solution is obtained for t_1 by dividing Eqs. (5.33a) and (5.33b) as follows:

$$t_1 = t_0 + \sqrt{\frac{\mathbb{J}_1 \left|\vartheta_{t_1} - \vartheta_{t_0}\right|}{\mathbb{J}_3 \left|\vartheta_{t_f} - \vartheta_{t_2}\right|}} \left(t_f - t_2\right) \tag{5.49}$$

which is still a function of t_2. An analytic closed-form solution is obtained for t_2 by substituting Eq. (5.49) into Eq. (5.33b) as follows:

$$t_2 = \frac{\sqrt{\mathbb{J}_3 \left|\vartheta_{t_f} - \vartheta_{t_2}\right|} t_0 + \left(\sqrt{\mathbb{J}_1 \left|\vartheta_{t_1} - \vartheta_{t_0}\right|} + \sqrt{\mathbb{J}_2 \left|\vartheta_{t_2} - \vartheta_{t_1}\right|}\right) t_f}{\sqrt{\mathbb{J}_1 \left|\vartheta_{t_1} - \vartheta_{t_0}\right|} + \sqrt{\mathbb{J}_2 \left|\vartheta_{t_2} - \vartheta_{t_1}\right|} + \sqrt{\mathbb{J}_3 \left|\vartheta_{t_f} - \vartheta_{t_2}\right|}} \tag{5.50}$$

Substituting Eq. (5.50) into Eq. (5.49) yields

$$t_1 = \frac{\left(\sqrt{\mathbb{J}_2\left|\vartheta_{t_2} - \vartheta_{t_1}\right|} + \sqrt{\mathbb{J}_3\left|\vartheta_{t_f} - \vartheta_{t_2}\right|}\right) t_0 + \sqrt{\mathbb{J}_1\left|\vartheta_{t_1} - \vartheta_{t_0}\right|} t_f}{\sqrt{\mathbb{J}_1\left|\vartheta_{t_1} - \vartheta_{t_0}\right|} + \sqrt{\mathbb{J}_2\left|\vartheta_{t_2} - \vartheta_{t_1}\right|} + \sqrt{\mathbb{J}_3\left|\vartheta_{t_f} - \vartheta_{t_2}\right|}} \tag{5.51}$$

Equations (5.50) and (5.51) are now simple analytic functions of the initial and final times, rotational angles, and inertia of the spacecraft. These results have been validated by solving necessary conditions defined by Eqs. (2.1) and (2.3) as a multiple shooting optimization problem defined by 32 constraints. *Numerical experiments with using the closed-form solutions for the switch-times yielded performance boosts of* $\sim 2.2 \times 10^6$*-fold when compared to the nonlinear optimization approach.*

Until now, the optimal sequence of rotation is not considered. To determine the optimal sequence of rotation, the cost function values must be evaluated and compared between two possible sets.

Let's consider the cost function in Eq. (5.1a). The cost function is expressed in terms of the switch-time solutions as follows:

$$\begin{aligned}\mathcal{J}^{\boldsymbol{u}} &= \frac{1}{2}\left[\int_{t_0}^{t_1} \boldsymbol{u}^{\mathrm{T}}\boldsymbol{u}\,\mathrm{d}t + \int_{t_1}^{t_2} \boldsymbol{u}^{\mathrm{T}}\boldsymbol{u}\,\mathrm{d}t + \int_{t_2}^{t_f} \boldsymbol{u}^{\mathrm{T}}\boldsymbol{u}\,\mathrm{d}t\right] \\ &= \frac{6\mathbb{J}_1^2\left(\vartheta_{t_1} - \vartheta_{t_0}\right)^2}{\left(t_1 - t_0\right)^3} + \frac{6\mathbb{J}_2^2\left(\vartheta_{t_2} - \vartheta_{t_1}\right)^2}{\left(t_2 - t_1\right)^3} + \frac{6\mathbb{J}_3^2\left(\vartheta_{t_f} - \vartheta_{t_2}\right)^2}{\left(t_f - t_2\right)^3}\end{aligned} \tag{5.52}$$

5.6.2 Switch-Times and Performance Indices (Torque-Rate Minimization)

A closed-form solution is obtained for the switch-times by sequentially manipulating Eq. (5.38). The final form for the switch-time solutions exploit the observation that all of the terms appearing in Eq. (5.38) are positive. An analytic

solution is obtained for t_1 by dividing Eqs. (5.38a) and (5.38b) as follows:

$$t_1 = t_0 + \sqrt[3]{\frac{\mathbb{J}_1 \left|\vartheta_{t_1} - \vartheta_{t_0}\right|}{\mathbb{J}_3 \left|\vartheta_{t_f} - \vartheta_{t_2}\right|}} \left(t_f - t_2\right) \tag{5.53}$$

which is still a function of t_2. An analytic closed-form solution is obtained for t_2 by introducing Eq. (5.53) into Eq. (5.38b) as follows:

$$t_2 = \frac{\sqrt[3]{\mathbb{J}_3 \left|\vartheta_{t_f} - \vartheta_{t_2}\right|} t_0 + \left(\sqrt[3]{\mathbb{J}_1 \left|\vartheta_{t_1} - \vartheta_{t_0}\right|} + \sqrt[3]{\mathbb{J}_2 \left|\vartheta_{t_2} - \vartheta_{t_1}\right|}\right) t_f}{\sqrt[3]{\mathbb{J}_1 \left|\vartheta_{t_1} - \vartheta_{t_0}\right|} + \sqrt[3]{\mathbb{J}_2 \left|\vartheta_{t_2} - \vartheta_{t_1}\right|} + \sqrt[3]{\mathbb{J}_3 \left|\vartheta_{t_f} - \vartheta_{t_2}\right|}} \tag{5.54}$$

Substituting Eq. (5.54) into Eq. (5.53) yields

$$t_1 = \frac{\left(\sqrt[3]{\mathbb{J}_2 \left|\vartheta_{t_2} - \vartheta_{t_1}\right|} + \sqrt[3]{\mathbb{J}_3 \left|\vartheta_{t_f} - \vartheta_{t_2}\right|}\right) t_0 + \sqrt[3]{\mathbb{J}_1 \left|\vartheta_{t_1} - \vartheta_{t_0}\right|} t_f}{\sqrt[3]{\mathbb{J}_1 \left|\vartheta_{t_1} - \vartheta_{t_0}\right|} + \sqrt[3]{\mathbb{J}_2 \left|\vartheta_{t_2} - \vartheta_{t_1}\right|} + \sqrt[3]{\mathbb{J}_3 \left|\vartheta_{t_f} - \vartheta_{t_2}\right|}} \tag{5.55}$$

Equations (5.54) and (5.55) are now simple analytic functions of the initial and final times, rotational angles, and inertia of the spacecraft. These results have been validated by solving necessary conditions defined by Eqs. (2.1), (2.3), and (5.2) as a multiple shooting optimization problem defined by 47 constraints. *Numerical experiments with using the closed-form solutions for the switch-times yielded performance boosts of* $\sim 6.5 \times 10^6$*-fold when compared to the nonlinear optimization approach.*

To determine the optimal sequence of rotation, let's consider the cost function in Eq. (5.1b). The cost function is expressed in terms of the found switch-times as

follows:

$$\begin{aligned}\mathcal{J}^{\bar{\boldsymbol{u}}} &= \frac{1}{2}\left[\int_{t_0}^{t_1} \bar{\boldsymbol{u}}^{\mathrm{T}}\bar{\boldsymbol{u}}\,\mathrm{d}t + \int_{t_1}^{t_2} \bar{\boldsymbol{u}}^{\mathrm{T}}\bar{\boldsymbol{u}}\,\mathrm{d}t + \int_{t_2}^{t_f} \bar{\boldsymbol{u}}^{\mathrm{T}}\bar{\boldsymbol{u}}\,\mathrm{d}t\right] \\ &= \frac{360\mathbb{J}_1^2\left(\vartheta_{t_1}-\vartheta_{t_0}\right)^2}{\left(t_1-t_0\right)^5} + \frac{360\mathbb{J}_2^2\left(\vartheta_{t_2}-\vartheta_{t_1}\right)^2}{\left(t_2-t_1\right)^5} + \frac{360\mathbb{J}_3^2\left(\vartheta_{t_f}-\vartheta_{t_2}\right)^2}{\left(t_f-t_2\right)^5}\end{aligned} \tag{5.56}$$

For the torque-rate minimization case, the torque minimizing performance index is calculated as

$$\mathcal{G}^{\bar{\boldsymbol{u}}} \triangleq \frac{1}{2}\int_{t_0}^{t_f} \boldsymbol{u}^{\mathrm{T}}\boldsymbol{u}\,\mathrm{d}t = \frac{60\mathbb{J}_1^2\left(\vartheta_{t_1}-\vartheta_{t_0}\right)^2}{7\left(t_1-t_0\right)^3} + \frac{60\mathbb{J}_2^2\left(\vartheta_{t_2}-\vartheta_{t_1}\right)^2}{7\left(t_2-t_1\right)^3} + \frac{60\mathbb{J}_3^2\left(\vartheta_{t_f}-\vartheta_{t_2}\right)^2}{7\left(t_f-t_2\right)^3} \tag{5.57}$$

which is computed for comparison with the torque penalty approach.

5.6.3 Numerical Example

From Eqs. (5.50) and (5.51), the switch-times are found as

$$(t_1,\, t_2) = (12.5651,\, 23.5329)\ \text{sec}$$

The performance index value using the found switch-times are calculated as

$$\mathcal{J}^{\boldsymbol{u}} = 0.1232$$

From Eqs. (5.54) and (5.55), the switch-times are found as

$$(t_1,\, t_2) = (11.7390,\, 22.4608)\ \text{sec}$$

The performance index value using the found switch-times are calculated as

$$\mathcal{J}^{\bar{u}} = 0.0704$$

5.6.4 Concluding Remarks

This Section derives closed-form solutions of the switch-times, performance index for selecting an optimal sequence, and new performance index for comparing torque consumption. These closed-form solutions are particularly useful for real-time applications and on-board spacecraft implementation.

5.7 Result Comparisons

Most of work is focused on the (3-1-3) set of Euler angle rotation sequence. Numerical simulations are performed for the case of actuator failure about the second axis. For the failure control simulation case, one assumes that second axis torque cannot be generated. As a result, two possible sets of Euler transformations are available [i.e., (3-1-3) and (1-3-1) sets]. By calculating the performance index and comparing values, the optimal rotation sequence is determined.

Using the closed-form solutions, the torque consumptions are calculated and listed in Table 5.8. As a result, the (1-3-1) set is the optimal set of sequence maneuver. Comparing these results allows one to select to an optimal rotation sequence for the 3D maneuver.

Table 5.8: Torque consumption comparison: (3-1-3) set vs (1-3-1) set

Observation	(3-1-3) set	(1-3-1) set
$\mathcal{J}^{\boldsymbol{u}}$	0.1232	0.1113
$\mathcal{G}^{\bar{\boldsymbol{u}}}$	0.1833	0.1710

The solutions are compared among the methods: (i) classical method; (ii) reduced method; (iii) resultant method; and (iv) closed-form solution. The maximum error between the closed-form solutions and the solutions from the classical method is $\sim 10^{-9}$, which is assumed to be numerical machine error.

The computational burden results are compared and listed in Table 5.9. Clearly, the closed-form solution has huge advantage in terms of computational efforts. Comparing the classical and closed-form run-time costs, it is clear that the closed-form solution outperforms the numerical optimization algorithm by factors of greater than 2.2×10^6-fold.

Table 5.9: Computational burden comparison: torque minimization vs torque-rate minimization

Observation	Torque minimization	Torque-rate minimization
Classical (32/47 unknowns)	43.6238	84.0878
Reduced (2 unknowns)	1.0719	0.9811
Resultant	0.3043	0.2631
Closed-Form	0.000020	0.000013

6. HOMOTOPY APPROACH FOR RIGID BODY MOTION ANALYSIS

A homotopy method is utilized to find minimum-torque solutions for under-actuated systems using the general formulation (No ad hoc and sub-optimal sequential maneuver strategy). A full 3D maneuver is executed by using up to two active controls. Unless given good initial guesses, a general formulation and the use of a shooting method to solve the resulting two point boundary value problem (TPBVP) fails to find the solutions. The homotopy method rigorously solves the under-actuated system control problem. The algorithm also makes the trend of time trajectories visible for the states as control torque capacity degrades.

6.1 Introduction

A minimum-torque solution for the failed actuator case is defined by minimizing an integral quadratic torque performance index. Motivated by historical research, many approaches are proposed for modifying traditional approaches to accommodate the failed actuator case. For example, when using an integral quadratic torque performance index, the corresponding elements of the torque weight matrix for the failed actuator can be made large, thereby penalizing the use of torque about the failed actuator axes. Based on this study, this heuristic approach has evident numerical difficulties.

The present work overcomes the local convergence nature of the iterative process for solving the TPBVPs associated with an optimal control formulation to address the failed actuator case by introducing a continuation method. The use of continuation or embedding methods as theoretical tools for the study of operator equations goes back to the last century. Ficken provides an excellent historical summary and many references [32]. The continuation method is introduced by trans-

forming the original problem necessary conditions for the optimal control problem by introducing a homotopy embedding parameter, ε. A one-parameter family of problems is defined, which contains an optimal control problem with an easily computed solution and the problem of interest. The algorithm starts by obtaining a solution when all actuators are available, then a continuation process is started by introducing a partition of ε as

$$0 = \varepsilon_0 < \varepsilon_1 < \cdots < \varepsilon_N = 1 \tag{6.1}$$

The challenge is to choose the partition steps to ensure that the unknown costate initial condition estimated for $\lambda(\varepsilon_k)$ lies in the domain of convergence of the algorithm used for updating the costate initial condition. Assuming such a partition can be found, one must obtain a feasible solution. While global convergence is generally not guaranteed, adapting the ε steps has been found to usually yield reliable results. Since the ε steps are chosen in the algorithm, the local steps are modified adaptively to respond to local convergence challenges, staying arbitrarily close to a neighboring converged solution to start the next "steppingstone" solution. Mathematically, in the limit, the homotopy approach is designed to continuously transform the equations of motion from the full control problem to the failed control case. This is analytically accomplished by multiplying the control input, which is assumed to fail, by a term, $1-\varepsilon$. Setting $\varepsilon = 0$ models the full control actuator case. Setting $\varepsilon = 1$ obviously corresponds to the failed actuator case. The continuous limit, where ε is varied smoothly, is considered and a differential equation is derived for the solution of the TPBVPs. Using the solution obtained for the three actuator case as a starting guess, Davidenko's method is introduced to develop costate differential equations that are a function of ε, which are integrated to provide estimates for changes in the initial costate as ε changes during the homotopy process. The

initial conditions are the optimal solution for the case of no actuator failures. A successive approximation strategy is introduced to refine the initial costate boundary conditions as ε is swept through the range values spanning $\varepsilon = [0, 1]$. The number of required discrete ε states is very much problem dependent but somewhat analogous to adaptive step-size control for differential equation solvers. Practical experience suggests that it is usually easy to establish a workable ε step-size adaption scheme. Provided numerical examples demonstrate that full 3D maneuvers are achieved for the case of a failed actuator.

6.2 Overview of the Homotopy Method

It is well known that nonlinear "root solving" problems require "good" starting guesses for differential correction strategies to successfully converge. The challenge, of course, is that one may not have adequate insight into the behavior of the solution for providing useful starting guesses. Homotopy methods allow one to overcome the local nature of correction strategies by structuring the problem to be defined by a sequence of neighboring problems, where the effectiveness of local iteration methods is maintained. While convergence is not mathematically guaranteed, in general, certain difficulties can arise, such as

- Turning points occur
- Non-reachable terminal states are specified

Numerical studies indicate these challenges are not usually present for the unbounded optimal control approach; however, in the presence of control saturation constraints, it is anticipated that reachability is a key challenge. One approach to that issue is to introduce another homotopic map to sweep the control saturation limit downward from an unbounded solution and discover, for a given maneuver

time, the control saturation bound that lies on the edge of the reachable control set. Sweeping maneuver final time would then provide means to map out the reachable set consistent with the actual actuator saturation bounds.

The solution of the nonlinear equation is found by introducing a homotopy algorithm. Let $f, g : X \to Y$ be continuous functions, where X and Y are any space. Let's call H a homotopy from g to f if $H : X \times I \to Y$ is a continuous map such that

$$H(x, \varepsilon = 0) = g(x), \quad H(x, \varepsilon = 1) = f(x), \quad \forall x \in X \tag{6.2}$$

where $I = [0, 1]$. Then the homotopy, H, maps from X to Y, varying continuously with ε. The homotopy map permits an analytic continuation method to be constructed that continuously transforms a starting guess into the desired solution.

To this end, given a nonlinear system root-solving problem, $F(x) = 0$, the goal is to embed $F(x) = 0$ into a homotopy transformational mapping equation for analytically continuing the initial estimate, x_0. Typical examples of useful homotopies are given by [33]

$$G(x, t) = \varepsilon G(x) + (1 - \varepsilon)(x - x_0) = 0 \tag{6.3a}$$

$$G(x, t) = F(x) + (\varepsilon - 1)F(x_0) = 0 \tag{6.3b}$$

where x_0 is the arbitrary reference value for a starting condition and $\varepsilon \in [0, 1]$. To be useful, the design of the homotopic map must satisfy two assumptions: (i) $G(x)$ is sufficiently smooth and (ii) for each $\varepsilon \in [0, 1]$, $\exists\, x(\varepsilon) \neq 0$ such that $G(x, \varepsilon) = 0$ and the Jacobian matrix $\frac{\partial G}{\partial x}\big|_{x(\varepsilon)}$ is full rank. Assuming that both of these assumptions are satisfied, one can derive differential equations governing the evolution of the zero curves. Two versions of the homotopy solution are generally available. In the

developments below, $F(x)$ is shown to be useful for any continuous differential mapping including the TPBVPs (in the form of state and costate differential equations with split boundary conditions) arising in optimal control: (i) discrete intermediate homotopy states ("steppingstone solutions") and (ii) continuous homotopy states.

For the discrete homotopy state algorithm, Lahaye [34] suggested an iterative continuation approach that uses a locally convergent iterative method for solving $H(x, \varepsilon) = 0$, $\varepsilon = [0, 1]$ with $0 = \varepsilon_0 < \varepsilon_1 < \cdots < \varepsilon_N = 1$. A starting guess for each new discrete value of ε is obtained by setting the last iteration at ε_k is equal to the initial approximation for the iteration at ε_{k+1}. The main delimiter of the step-size of ε depends on the domain of convergence of the local method used to update estimates for ε_{k+1}. For each application, a trade-off exists between balancing the number of iterations required to maintain solution accuracy and rapidly traversing the partitioned states of ε. The algorithm can fail if too large steps are attempted for ε. Larger steps are possible when the convergent domains increase. What is required is a self-adjusting algorithm, which adjusts incremental homotopy step-size to the convergent behavior of local iterations.

6.3 Davidenko's Method

For the continuous homotopy algorithm, Davidenko's approach [35] is used. This method is based on the observation that under suitable differentiability conditions, the unknown continuation curve is a solution of the initial value problem given $x(0) = x_0$, where the differential necessary condition is given by

$$\frac{\partial H\left(x(\varepsilon),\, \varepsilon\right)}{\partial x}\frac{\mathrm{d}x}{\mathrm{d}\varepsilon} + \frac{\partial H\left(x(\varepsilon),\, \varepsilon\right)}{\partial \varepsilon} = 0 \tag{6.4}$$

where $\varepsilon = [0, 1]$. This equation is called Davidenko's differential equation. The solution of this ordinary differential equation numerically approximates the entire

solution curve with an accuracy defined by the numerical integration error tolerance. Obviously, the value of $\frac{\partial H(x(\varepsilon),\varepsilon)}{\partial x}$ is a critical issue, and if this matrix loses full rank at any $0 \leq \varepsilon \leq 1$, then one has encountered a turning point. The Chow-Yorke algorithm [36] provides one method for circumventing this difficulty.

For many applications, Davidenko's method provides significant advantages when compared with the iterative methods, such as Newton's method. Specifically, the advantages include: (i) it does not depend on a good initial guess, (ii) it produces solutions over large range of the independent variables, and (iii) it overcomes the local convergence issues that often plague iterative processes. To be broadly useful, however, one must control the integration step-size to ensure that an accurate numerical solution is obtained.

6.4 Body-Axis Aligned Torque Distribution

In this Section, the open-loop optimal control solution of the rigid spacecraft is derived when one of the three-axis control actuators fails. Next, the extensions required for implementing the homotopy method are presented. Additionally, the case when two actuators fail among four control actuators is considered in Appendix E.

6.4.1 Problem Formulations and Solutions

The rotational dynamics equation of a rigid body is slightly modified as

$$\dot{\boldsymbol{\omega}} \triangleq \tilde{\boldsymbol{p}}(\boldsymbol{\omega},\, \boldsymbol{u},\, \varepsilon) = [J]^{-1}\left(-\left[\tilde{\boldsymbol{\omega}}\right][J]\boldsymbol{\omega} + [P(\varepsilon)]\boldsymbol{u}\right) \tag{6.5}$$

where $[P(\varepsilon)] \in \mathcal{R}^{3\times 3}$ is the control torque mapping matrix, which is usually $I_{3\times 3}$.

For describing a control torque degradation situation, a modified control torque mapping matrix, $[P(\varepsilon)] \triangleq \mathrm{diag}(1,\, 1,\, 1-\varepsilon)$, is defined in terms of ε. Substitut-

ing $\varepsilon = 0$ into the modified control torque mapping matrix yields $[P(\varepsilon = 0)] = I_{3\times 3}$. This is the full control actuator case description. On the other hand, substituting $\varepsilon = 1$ into the modified control torque mapping matrix yields $[P(\varepsilon = 1)] = \text{diag}(1,\, 1,\, 0)$. This is the failed actuator case description. By spanning ε from 0 to 1, a control torque input degradation situation is fully described.

Here, the MRPs are selected as an attitude parameter and the governing kinematic differential equation for the MRPs in Eq. (2.10) is selected.

The optimal control problem is defined by introducing the following performance index, which is to be minimized for generating the optimal control torque given *fixed* initial time, t_0, and *fixed* final time, t_f,

$$\mathcal{J} = \frac{1}{2}\int_{t_0}^{t_f} \boldsymbol{u}^{\mathrm{T}}\boldsymbol{u}\,\mathrm{d}t \tag{6.6}$$

with terminal state boundary conditions

$$\boldsymbol{\sigma}\left(t_0\right) = \boldsymbol{\sigma}_0, \quad \boldsymbol{\omega}\left(t_0\right) = \boldsymbol{\omega}_0, \quad \boldsymbol{\sigma}\left(t_f\right) = \boldsymbol{\sigma}_f, \quad \boldsymbol{\omega}\left(t_f\right) = \boldsymbol{\omega}_f \tag{6.7}$$

Defining the Hamiltonian for the system

$$\mathcal{H} = \frac{1}{2}\boldsymbol{u}^{\mathrm{T}}\boldsymbol{u} + \boldsymbol{\mu}^{\mathrm{T}}\tilde{\boldsymbol{p}} + \boldsymbol{\xi}^{\mathrm{T}}\boldsymbol{r} \tag{6.8}$$

The first-order necessary conditions are obtained as:

State Equations:

$$\dot{\boldsymbol{\sigma}} = \frac{\partial \mathcal{H}}{\partial \boldsymbol{\xi}} = \boldsymbol{r} = \frac{1}{4}\left[B(\boldsymbol{\sigma})\right]\boldsymbol{\omega} \tag{6.9a}$$

$$\dot{\boldsymbol{\omega}} = \frac{\partial \mathcal{H}}{\partial \boldsymbol{\mu}} = \tilde{\boldsymbol{p}} = [J]^{-1}\left(-\left[\boldsymbol{\omega}^{\times}\right][J]\boldsymbol{\omega} + [P(\varepsilon)]\boldsymbol{u}\right) \tag{6.9b}$$

Costate Equations:

$$\dot{\boldsymbol{\xi}} = -\frac{\partial \mathcal{H}}{\partial \boldsymbol{\sigma}} = -\left[\frac{\partial \boldsymbol{r}}{\partial \boldsymbol{\sigma}}\right]^{\mathrm{T}} \boldsymbol{\xi} = -\frac{1}{2}\left[\Lambda(\boldsymbol{\sigma},\, \boldsymbol{\omega})\right]^{\mathrm{T}} \boldsymbol{\xi} \tag{6.10a}$$

$$\dot{\boldsymbol{\mu}} = -\frac{\partial \mathcal{H}}{\partial \boldsymbol{\omega}} = -\left[\frac{\partial \tilde{\boldsymbol{p}}}{\partial \boldsymbol{\omega}}\right]^{\mathrm{T}} \boldsymbol{\mu} - \left[\frac{\partial \boldsymbol{r}}{\partial \boldsymbol{\omega}}\right]^{\mathrm{T}} \boldsymbol{\xi} = -\left[\Sigma(\boldsymbol{\omega},\, J)\right]^{\mathrm{T}} \boldsymbol{\mu} - \frac{1}{4}\left[B(\boldsymbol{\sigma})\right]^{\mathrm{T}} \boldsymbol{\xi} \tag{6.10b}$$

where

$$\left[\Lambda(\boldsymbol{\sigma},\, \boldsymbol{\omega})\right] \triangleq \begin{bmatrix} \sigma_1\omega_1 + \sigma_2\omega_2 + \sigma_3\omega_3 & \omega_3 - \sigma_2\omega_1 + \sigma_1\omega_2 & \sigma_1\omega_3 - \sigma_3\omega_1 - \omega_2 \\ \sigma_2\omega_1 - \omega_3 - \sigma_1\omega_2 & \sigma_1\omega_1 + \sigma_2\omega_2 + \sigma_3\omega_3 & \omega_1 - \sigma_3\omega_2 + \sigma_2\omega_3 \\ -\sigma_1\omega_3 + \sigma_3\omega_1 + \omega_2 & \sigma_3\omega_2 - \omega_1 - \sigma_2\omega_3 & \sigma_1\omega_1 + \sigma_2\omega_2 + \sigma_3\omega_3 \end{bmatrix}$$

Stationarity Condition:

$$0 = \frac{\partial \mathcal{H}}{\partial \boldsymbol{u}} = \boldsymbol{u} + \left[\frac{\partial \tilde{\boldsymbol{p}}}{\partial \boldsymbol{u}}\right]^{\mathrm{T}} \boldsymbol{\mu} = \boldsymbol{u} + \left[P(\varepsilon)\right][J]^{-1}\boldsymbol{\mu} \tag{6.11}$$

Boundary Condition:

Given the fixed initial time, t_0, and final time, t_f; the initial states, $\boldsymbol{\sigma}\left(t_0\right)$ and $\boldsymbol{\omega}\left(t_0\right)$; and the final states, $\boldsymbol{\sigma}\left(t_f\right)$ and $\boldsymbol{\omega}\left(t_f\right)$, there are no extra boundary conditions to be imposed. These fixed terminal boundary conditions define a classical TPBVP. The goal is to generate an open-loop control trajectory that defines the optimal maneuver, which satisfies the fixed terminal boundary conditions.

6.4.2 Homotopy Method Differential Equation

The state and costate vectors are combined as an augmented vector, $\boldsymbol{z} = \{\boldsymbol{y}^{\mathrm{T}},\, \boldsymbol{\lambda}^{\mathrm{T}}\}^{\mathrm{T}}$, where $\boldsymbol{y} = \{\boldsymbol{\sigma}^{\mathrm{T}},\, \boldsymbol{\omega}^{\mathrm{T}}\}^{\mathrm{T}}$ and $\boldsymbol{\lambda} = \{\boldsymbol{\xi}^{\mathrm{T}},\, \boldsymbol{\mu}^{\mathrm{T}}\}^{\mathrm{T}}$. Collecting these terms yields

the augmented differential equation for the TPBVP:

$$\dot{\boldsymbol{z}} = \boldsymbol{F}(\boldsymbol{z},\, \varepsilon,\, t) = \left\{ \begin{array}{c} \frac{1}{4}[B(\boldsymbol{\sigma})]\boldsymbol{\omega} \\ [J]^{-1}\left(-\left[\boldsymbol{\omega}^{\times}\right][J]\boldsymbol{\omega} - [P^2(\varepsilon)]\,[J]^{-1}\boldsymbol{\mu}\right) \\ -\frac{1}{2}[\Lambda(\boldsymbol{\sigma},\, \boldsymbol{\omega})]^{\mathrm{T}}\boldsymbol{\xi} \\ -[\Sigma(\boldsymbol{\omega},\, J)]^{\mathrm{T}}\boldsymbol{\mu} - \frac{1}{4}[B(\boldsymbol{\sigma})]^{\mathrm{T}}\boldsymbol{\xi} \end{array} \right\} \tag{6.12}$$

where $[P^2(\varepsilon)] = \mathrm{diag}\left(1,\, 1,\, (1-\varepsilon)^2\right)$. To derive the governing equations that determine the evolution of $\boldsymbol{\lambda}\,(t_0,\, \varepsilon)$, from $\boldsymbol{\lambda}\,(t_0,\, \varepsilon = 0)$ through $\boldsymbol{\lambda}\,(t_0,\, \varepsilon = 1)$, one must exploit the constraint equations that define the terminal boundary conditions for the maneuver. To this end, the terminal state boundary condition for an arbitrary value of ε is given by

$$\boldsymbol{y}\left(t_f,\, \boldsymbol{\lambda}\,(t_0,\, \varepsilon)\right) - \boldsymbol{y}_f = \boldsymbol{0} \tag{6.13}$$

Computing the total derivative of Eq. (6.13) leads to

$$\frac{\mathrm{d}\boldsymbol{y}\left(t_f,\, \boldsymbol{\lambda}\,(t_0,\, \varepsilon)\right)}{\mathrm{d}\varepsilon} = \frac{\partial \boldsymbol{y}\left(t_f,\, \boldsymbol{\lambda}\,(t_0,\, \varepsilon)\right)}{\partial \varepsilon} + \left[\frac{\partial \boldsymbol{y}\left(t_f,\, \boldsymbol{\lambda}\,(t_0,\, \varepsilon)\right)}{\partial \boldsymbol{\lambda}\,(t_0,\, \varepsilon)}\right] \frac{\mathrm{d}\boldsymbol{\lambda}\,(t_0,\, \varepsilon)}{\mathrm{d}\varepsilon} = \boldsymbol{0} \tag{6.14}$$

which displays the implicit dependence of the costate on ε. Solving for the costate rate term leads to the following ordinary differential equation:

$$\frac{\mathrm{d}\boldsymbol{\lambda}\,(t_0,\, \varepsilon)}{\mathrm{d}\varepsilon} = -\left[\frac{\partial \boldsymbol{y}\left(t_f,\, \boldsymbol{\lambda}\,(t_0,\, \varepsilon)\right)}{\partial \boldsymbol{\lambda}\,(t_0,\, \varepsilon)}\right]^{-1} \frac{\partial \boldsymbol{y}\left(t_f,\, \boldsymbol{\lambda}\,(t_0,\, \varepsilon)\right)}{\partial \varepsilon} \tag{6.15}$$

Equation (6.15) is identified as a partition of the state-costate transition matrix [18]

$$\frac{\mathrm{d}}{\mathrm{d}t}\left[\frac{\partial \boldsymbol{z}(t)}{\partial \boldsymbol{z}\,(t_0)}\right] = \left[\frac{\partial \boldsymbol{F}(\boldsymbol{z},\, \varepsilon,\, t)}{\partial \boldsymbol{z}(t)}\right]\left[\frac{\partial \boldsymbol{z}(t)}{\partial \boldsymbol{z}\,(t_0)}\right] \tag{6.16}$$

with the initial condition $\left[\frac{\partial \boldsymbol{z}(t)}{\partial \boldsymbol{z}(t_0)}\right]\Big|_{t_0} = I_{2n\times 2n}$ and the parameter influence vector

$$\frac{\mathrm{d}}{\mathrm{d}t}\left\{\frac{\partial \boldsymbol{z}(t)}{\partial \varepsilon}\right\} = \left[\frac{\partial \boldsymbol{F}(\boldsymbol{z}(t),\, \varepsilon,\, t)}{\partial \boldsymbol{z}}\right]\frac{\partial \boldsymbol{z}(t)}{\partial \varepsilon} + \frac{\partial \boldsymbol{F}(\boldsymbol{z},\, \varepsilon,\, t)}{\partial \varepsilon} \tag{6.17}$$

with the initial condition $\frac{\partial \boldsymbol{z}(t)}{\partial \varepsilon}\Big|_{t_0} = \mathbf{0}_{2n}$. For the augmented system, the state-costate transition matrix and parameter influence vector at $t = t_f$ are defined by

$$\left[\frac{\partial \boldsymbol{z}\,(t_f)}{\partial \boldsymbol{z}\,(t_0)}\right] = \begin{bmatrix} \dfrac{\partial \boldsymbol{y}\,(t_f)}{\partial \boldsymbol{y}\,(t_0)} & \dfrac{\partial \boldsymbol{y}\,(t_f)}{\partial \boldsymbol{\lambda}\,(t_0)} \\ \dfrac{\partial \boldsymbol{\lambda}\,(t_f)}{\partial \boldsymbol{y}\,(t_0)} & \dfrac{\partial \boldsymbol{\lambda}\,(t_f)}{\partial \boldsymbol{\lambda}\,(t_0)} \end{bmatrix} \tag{6.18}$$

$$\frac{\partial \boldsymbol{z}\,(t_f)}{\partial \varepsilon} = \begin{Bmatrix} \dfrac{\partial \boldsymbol{y}\,(t_f)}{\partial \varepsilon} \\ \dfrac{\partial \boldsymbol{\lambda}\,(t_f)}{\partial \varepsilon} \end{Bmatrix} \tag{6.19}$$

where the upper right partition of Eq. (6.18) provides the required partial derivative that is needed in Davidenko's equation. Also, the upper partition of Eq. (6.19) acts as the forcing function for Davidenko's method. Using the definitions of Eqs. (6.16)-(6.19), the homotopy embedded parameter differential equation is written as

$$\frac{\mathrm{d}\boldsymbol{\lambda}\,(t_0,\, \varepsilon)}{\mathrm{d}\varepsilon} = -\left[\frac{\partial \boldsymbol{y}\,(t_f)}{\partial \boldsymbol{\lambda}\,(t_0)}\right]^{-1}\frac{\partial \boldsymbol{y}\,(t_f)}{\partial \varepsilon} \tag{6.20}$$

Initial conditions for this set of ordinary differential equations for the costate vector are obtained from the solution for the nominal maneuver case, where all actuators are available, leading to $\boldsymbol{\lambda}\,(t_0,\, \varepsilon = 0) = \boldsymbol{\lambda}_0$. Equation (6.20) provides an elegant set of ordinary differential equations for numerically generating the failed actuator 3D maneuver initial conditions for the costate. Numerically integrating Eq.

(6.20) with respect to ε, one obtains

$$\boldsymbol{\lambda}(t_0,\, \varepsilon = 1) = \boldsymbol{\lambda}(t_0,\, \varepsilon = 0) + \int_0^1 \frac{\mathrm{d}\boldsymbol{\lambda}}{\mathrm{d}\varepsilon}\,\mathrm{d}\varepsilon \tag{6.21}$$

Clearly, this process requires many TPBVP solutions for the partitioned values of ε. This process is presented in the flowchart appearing in Fig. 6.1. The algorithm consists of two parts: (i) an outer loop that integrates Eq. (6.21) and (ii) an inner loop that generates the state-costate transition matrix and parameter influence vector partitions for each value of ε required in the outer loop integration algorithm.

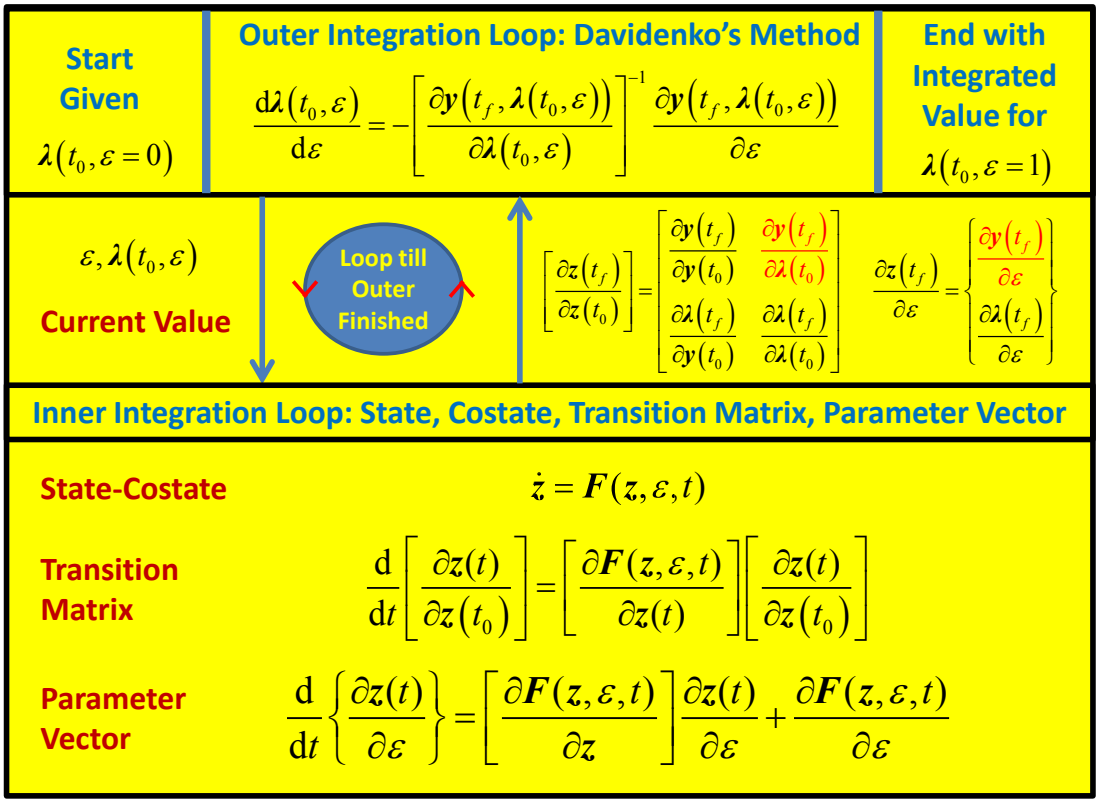

Figure 6.1: Flowchart for obtaining TPBVP solutions

6.4.3 Numerical Examples

Numerical simulation is performed for two maneuver cases: (i) rest-to-rest and (ii) motion-to-rest. Simulation parameters are listed in Tables 6.1 and 6.2.

Table 6.1: Simulation parameters for a 3D minimum-torque maneuver (rest-to-rest)

Parameter	Symbol	Value	Unit
Moment of inertia for the spacecraft	J	diag(14.2, 17.3, 20.3)	kg-m^2
Initial time	t_0	0	sec
Initial MRPs	$\boldsymbol{\sigma}_{t_0}$	$\{0.1, -0.1, 0.1\}^{\mathrm{T}}$	-
Initial angular velocity	$\boldsymbol{\omega}_{t_0}$	$\{0, 0, 0\}^{\mathrm{T}}$	rad/s
Final time	t_f	30	sec
Final MRPs	$\boldsymbol{\sigma}_{t_f}$	$\{0, 0, 0\}^{\mathrm{T}}$	-
Final angular velocity	$\boldsymbol{\omega}_{t_f}$	$\{0, 0, 0\}^{\mathrm{T}}$	rad/s

Table 6.2: Simulation parameters for a 3D minimum-torque maneuver (motion-to-rest)

Parameter	Symbol	Value	Unit
Moment of inertia for the spacecraft	J	diag(14.2, 17.3, 20.3)	kg-m^2
Initial time	t_0	0	sec
Initial MRPs	$\boldsymbol{\sigma}_{t_0}$	$\{0.1, -0.1, 0.1\}^{\mathrm{T}}$	-
Initial angular velocity	$\boldsymbol{\omega}_{t_0}$	$\{0.01, 0.01, 0.01\}^{\mathrm{T}}$	rad/s
Final time	t_f	30	sec
Final MRPs	$\boldsymbol{\sigma}_{t_f}$	$\{0, 0, 0\}^{\mathrm{T}}$	-
Final angular velocity	$\boldsymbol{\omega}_{t_f}$	$\{0, 0, 0\}^{\mathrm{T}}$	rad/s

Rest-to-Rest Maneuver Case:

For the case of the rest-to-rest maneuver, simulation results are presented in Figs. 6.2-6.8. Each line indicates the following cases: the dashed blue line represents the state and costate trajectories when three actuators are available; the bold red line represents the state and costate trajectories when only two actuators are available; and the dotted green line represents the state and costate trajectories according to the capability of the actuator by varying ε from 0 to 1.

Figure 6.2 presents the MRPs time trajectories as the optimal control problem is transformed from the original full actuator case to the failed actuator case. The dashed blue line represents the starting solution, the bold red line represents the failed actuator special case solution, and the dotted green lines represent intermediate solutions as ε is swept through its entire range from 0 to 1. As seen in the plot for $\sigma_2(t)$, the time trajectories for the intermediate trajectory solution overshoot (for $0 < \varepsilon < 1$) the final state defined by the bold red line and then return and settle (as $\varepsilon \to 1$) on the bold red line solution. This behavior results from the loss in controllability for the failed actuator case.

The angular velocity solution time trajectories presented in Fig. 6.3 display similar behavior. The solution for $\omega_3(t)$ is seen to be much smaller than the corresponding angular velocity for the two controlled axes. This behavior results from the nonlinear cross-coupling terms in Euler's equation of motion, and cannot be avoided.

The Lagrange multiplier solution time trajectories for the MRPs and angular velocities are presented in Figs. 6.4 and 6.5, respectively.

The optimal control torque time trajectories are presented in Fig. 6.6. Since the assumed failed actuator is about the 3-axis, the $u_3(t)$ solution is non-zero for the initial case, where all actuators are assumed to function, and identically zero for the final case of a failed actuator, as required by the problem definition.

Figure 6.7 presents the 3D results for tracking the MRPs solution, where it is obvious that the failed actuator case requires the longest trajectory path to achieve the 3D maneuver boundary conditions.

Figure 6.8 presents the 3D results for tracking the angular velocity solution. Like the results for the MRPs solution, the path trajectory for the angular velocity for the failed actuator case is the longest. Moreover, for both the MRPs and angular velocity, the intermediate solutions are seen to evolve over a complicated 3D surface whose shape is very difficult to predict in advance. This example clearly demonstrates the effectiveness of Davidenko's method for generating such a complicated solution for a nonlinear problem; given a starting guess that very weakly resembles the desired final solution.

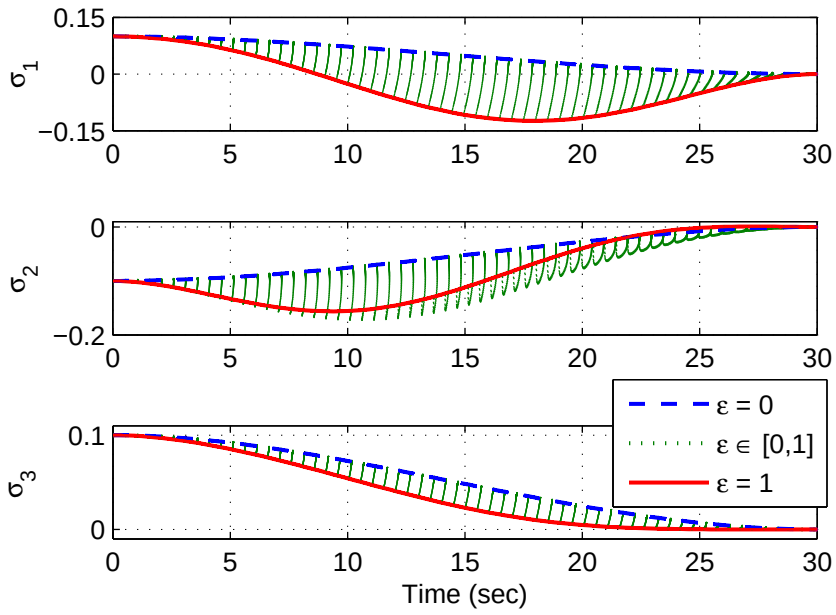

Figure 6.2: Aligned: Time trajectories for the MRPs (rest-to-rest)

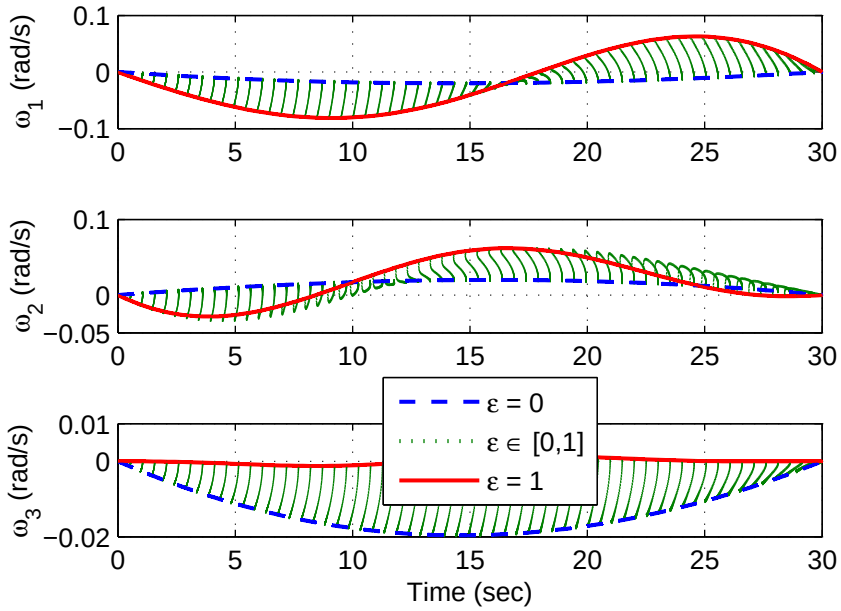

Figure 6.3: Aligned: Time trajectories for the angular velocity (rest-to-rest)

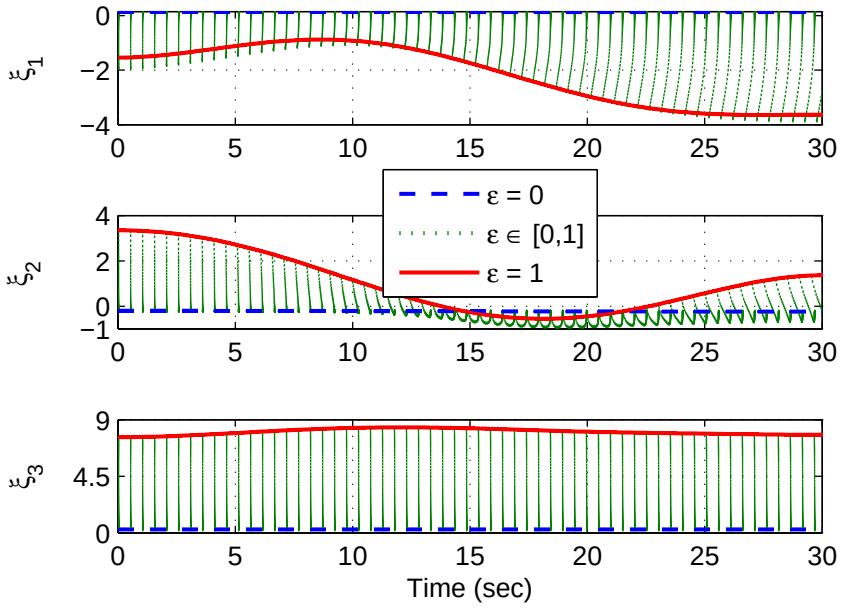

Figure 6.4: Aligned: Time trajectories for the costates associated with the MRPs (rest-to-rest)

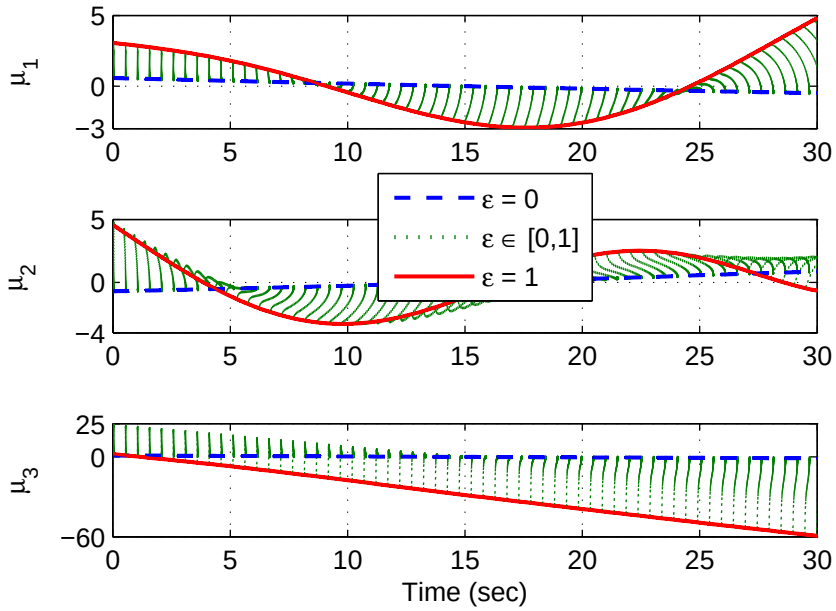

Figure 6.5: Aligned: Time trajectories for the costates associated with the angular velocity (rest-to-rest)

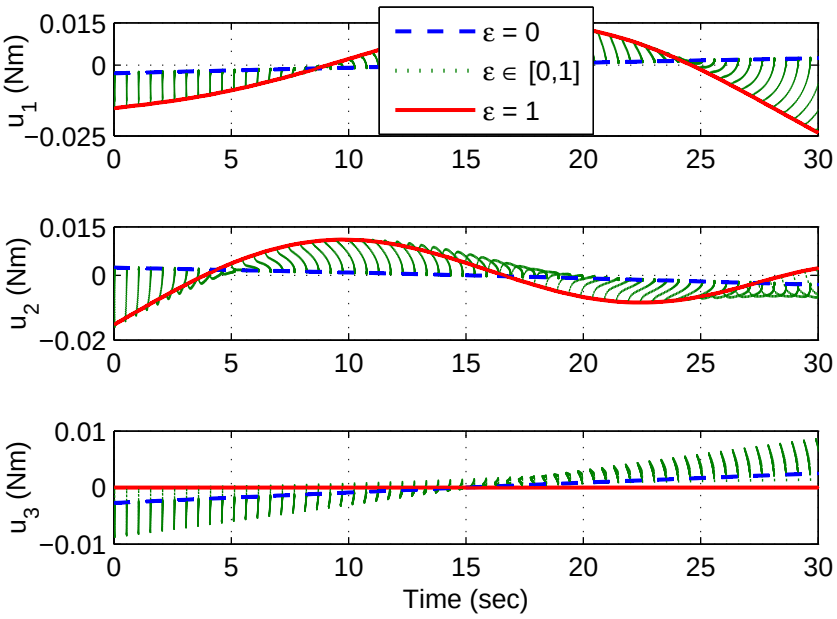

Figure 6.6: Aligned: Time trajectories for the control torque (rest-to-rest)

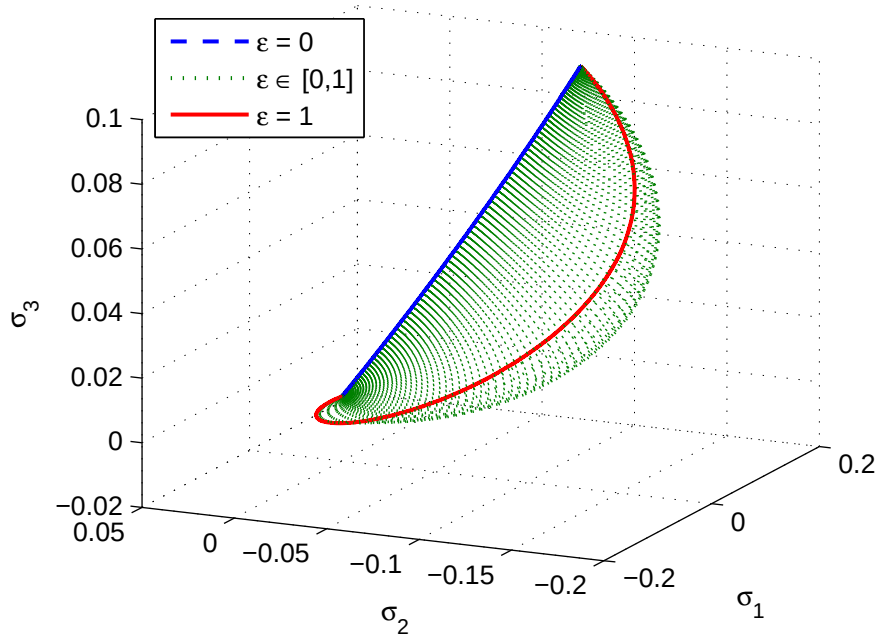

Figure 6.7: Aligned: 3D trajectory for the MRPs (rest-to-rest)

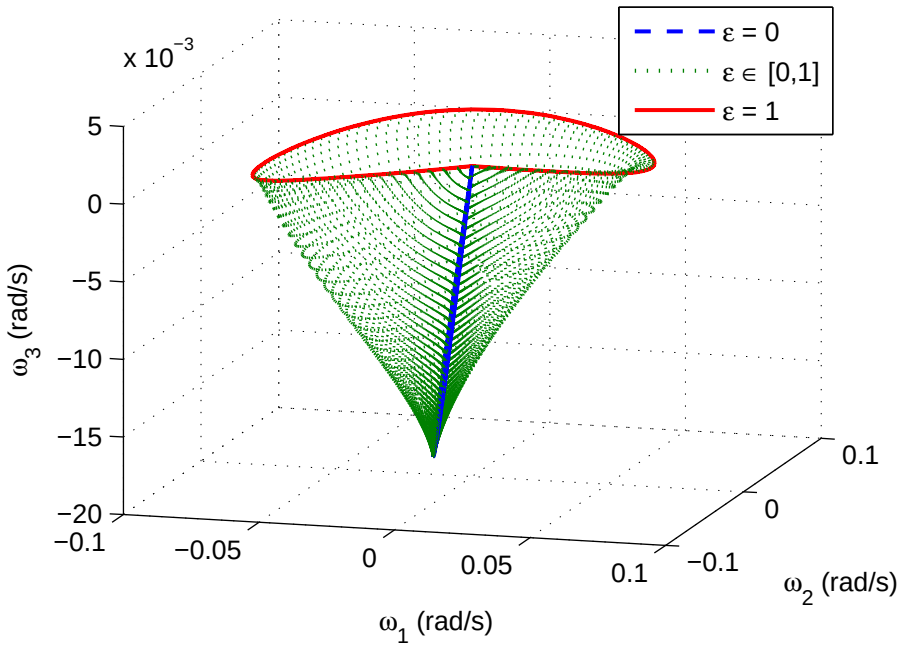

Figure 6.8: Aligned: 3D trajectory for the angular velocity (rest-to-rest)

Motion-to-Rest Maneuver Case:

For the case of the motion-to-rest maneuver, simulation results are presented in Figs. 6.9-6.14. Like the case of the rest-to-rest, quite similar state, costate, and control time trajectories are obtained. These results confirm that 3D maneuvers are successfully performed, even when only two actuators are available for maneuvering the spacecraft.

Figures 6.14 and 6.15 present the 3D results for tracking the MRPs and angular velocity solutions, where it is obvious that the failed actuator case requires the longest trajectory path to achieve the 3D maneuver boundary conditions.

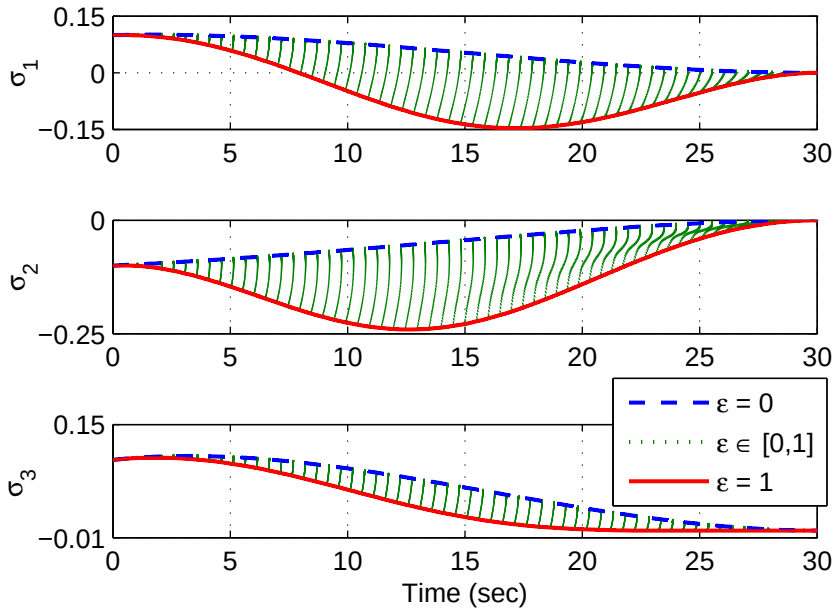

Figure 6.9: Aligned: Time trajectories for the MRPs (motion-to-rest)

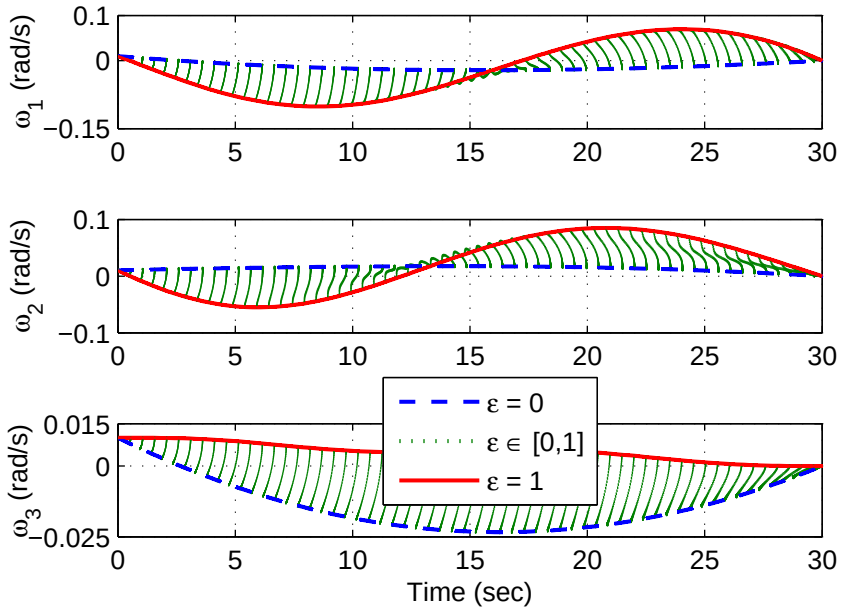

Figure 6.10: Aligned: Time trajectories for the angular velocity (motion-to-rest)

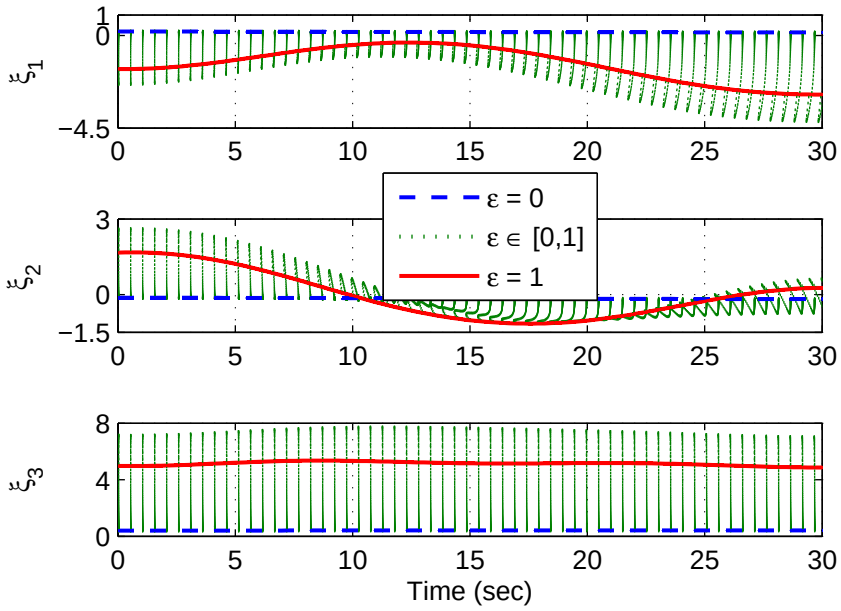

Figure 6.11: Aligned: Time trajectories for the costates associated with the MRPs (motion-to-rest)

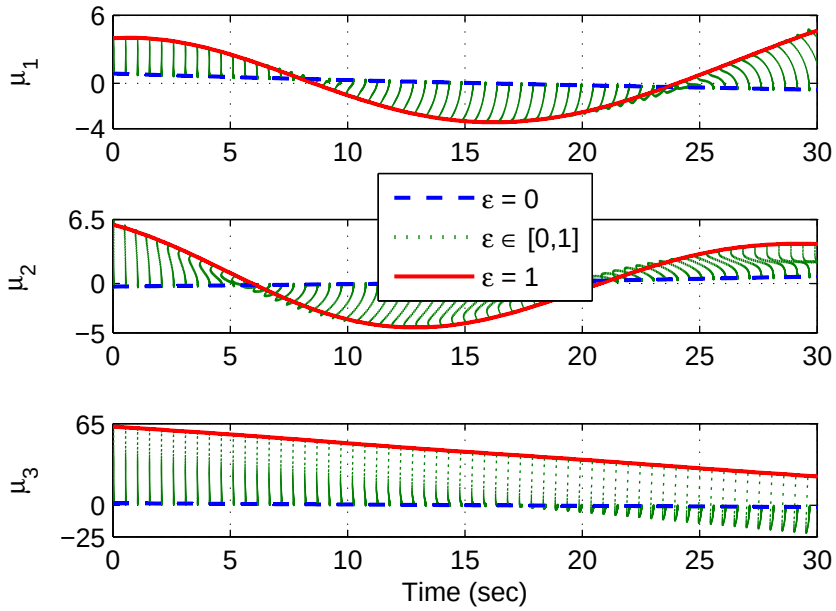

Figure 6.12: Aligned: Time trajectories for the costates associated with the angular velocity (motion-to-rest)

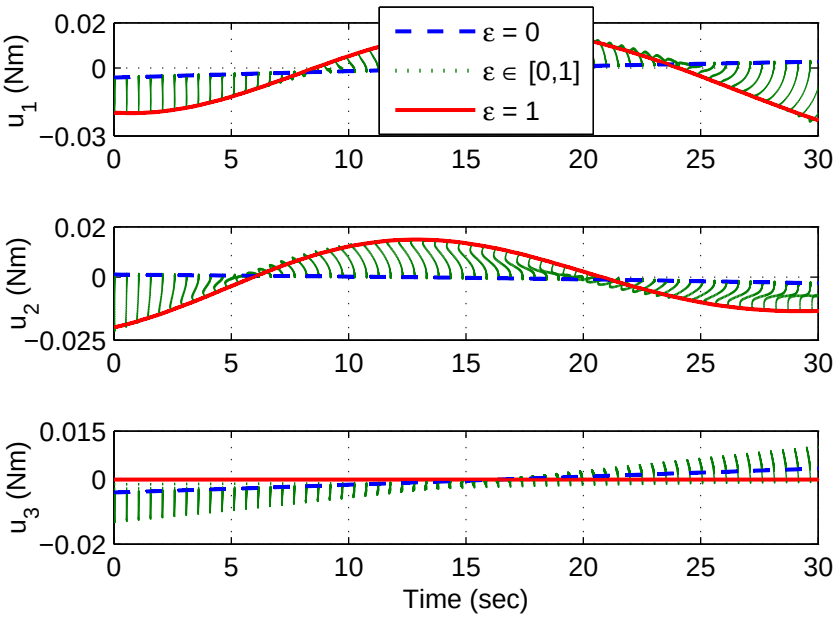

Figure 6.13: Aligned: Time trajectories for the control torque (motion-to-rest)

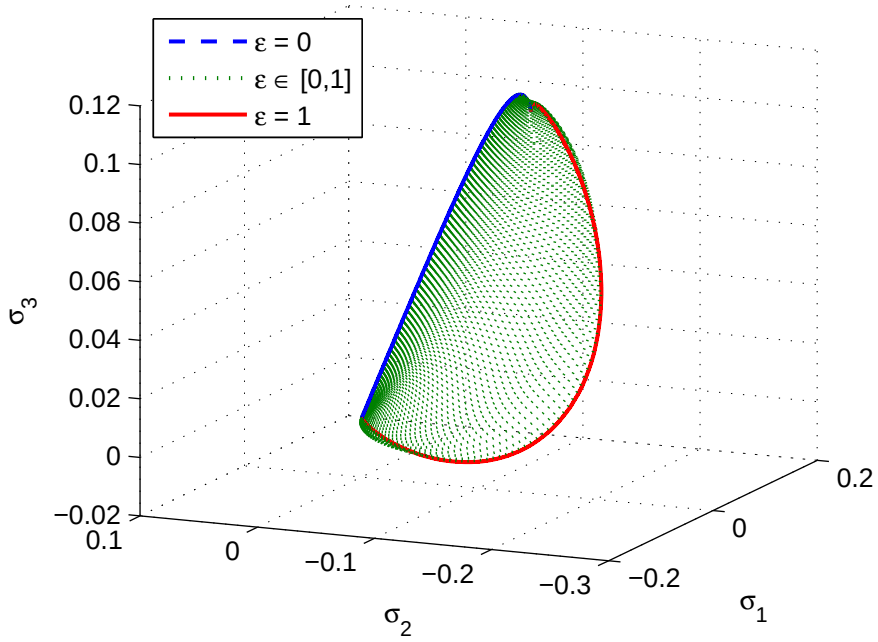

Figure 6.14: Aligned: 3D trajectory for the MRPs (motion-to-rest)

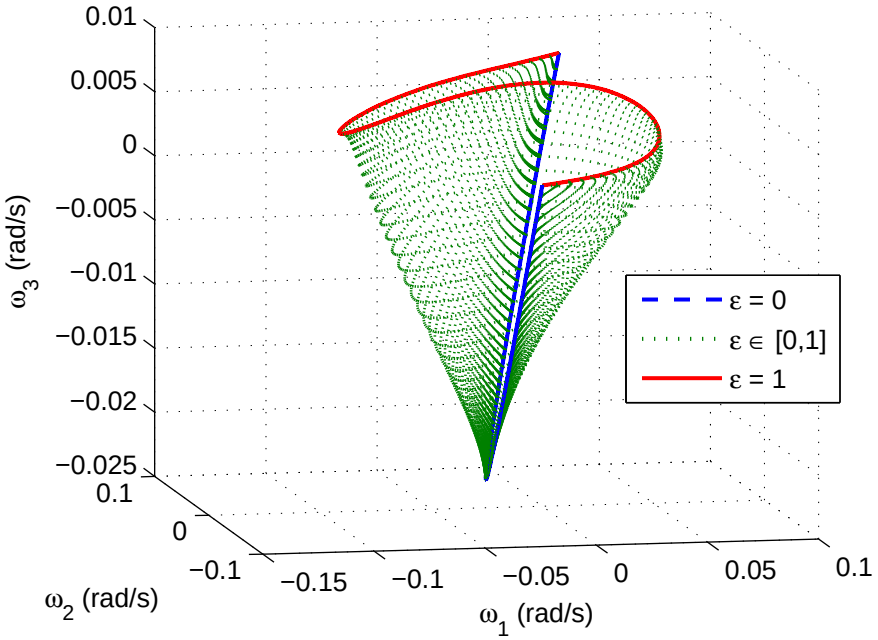

Figure 6.15: Aligned: 3D trajectory for the angular velocity (motion-to-rest)

6.4.4 Concluding Remarks

This work presents a rigorous integral-variational method for generating an optimal open-loop large-angle 3D maneuver for an asymmetric spacecraft for the case when one of the nominal maneuver actuators fails. A generalized Davidenko's classical homotopy method is introduced to develop an ordinary differential equation for the initial costate vector that permits the equation of motion to be continuously transformed from a full control problem to the failed control case. Davidenko's differential equation is assembled from partitions of the state-costate transition matrix and parameter influence vector. The homotopy transformation is introduced by multiplying the control input that is assumed to fail by a homotopy embedding parameter, ε. The starting value for the 3D maneuvers is obtained from the 3D maneuver optimal costate initial conditions, which is found for the case of no actuator failures. These initial costate variables provide the required control conditions for Davidenko's method. The differential equations for the costate, as a function of the homotopy embedding parameter, are numerically integrated to provide sensitivity data for updating estimates for the initial costate variable as the homotopy embedding parameter is swept through its entire range of values. The trajectories for the MRPs and angular velocity are seen to be very different when compared to the starting guess solutions with the failed actuator cases. The state variables are observed to experience reversal in direction as the homotopy embedding parameter changes. This is a complex behavior that is intimately tied to the loss of control input from the assumed failed actuator. The observed differences are so large that, given the nonlinear nature of the governing equations of motion and attitude kinematics, conventional solution solvers may experience difficulties in obtaining the desired solutions. Future research will investigate the observed behavior, where the intermediate

solutions overshoot the desired solution before finally returning to the failed actuator case solution. Also, the research will investigate sub-optimal solution strategies to achieve the desired 3D maneuver goals.

7. SUMMARY AND CONCLUSION

The results present two key advances for the state-of-practice in spacecraft attitude control commands, in relation to handling on-orbit hardware failure in the attitude control system. The first contribution presents a sub-optimal control strategy to avoid rotation about failed control axis. The second contribution demonstrates that optimal control solutions exist when only two controls are available.

The classic spacecraft maneuver problem is generalized to handle the special case in which an actuator failure alters the hardware capabilities available for repointing the vehicle. A key objective is to maintain an optimal solution strategy even when confronted with a degraded hardware environment. Two solution strategies are presented that enable two control inputs to complete the originally defined 3D rigid body maneuver: (i) a sequential maneuver strategy and (ii) a 3D homotopy-based strategy.

For the sequential maneuver strategy, nonlinear necessary conditions are defined for carrying out a sequence of maneuvers. In general, three single-axis submaneuvers must be introduced, where two unknown switch-times are recovered for switching between the remaining control actuators. The problem is defined by a high-dimensioned set of necessary conditions that are solved by introducing a multiple shooting method. However, this approach has been shown to be very expensive. To reduce the number of unknowns, the initial costates are transformed to be functions of the two unknown switch-times using the single-axis maneuver solutions. This step reduces the computational effort of ~ 85.7-fold but it's still expensive. Significant progress is made by working with the Hamiltonian constraints, yielding two coupled polynomial equations for solving for the two switch-times. The classical

resultant method provides a solution by uncoupling the polynomial equations, but it requires post-processing since more than one solution exists. Further significant analytic progress is made by manipulating the equations describing the Hamiltonian constraints, yielding closed-form solutions for the two switch-times. Moreover, closed-form solutions are also obtained for the performance index, which permits multiple solutions to be compared on a quantitative basis. One problem encountered with the sub-optimal sequential maneuver strategy is that it leads to discontinuous control profiles. This problem is solved by adding a quadratic torque-rate term to the performance index, which allows special boundary conditions to be specified that eliminate the discontinuities that appear in the control profiles. Simulation results indicate that the quadratic torque-rate penalty approach requires more torque consumption when compared to the quadratic torque penalty approach, but one needs to assess the impact on the performance of flexible body systems with controls designed by both approaches.

Extended studies are performed for maneuver time and fuel minimization problems. The solutions for the minimum-time 3D maneuver problem is very straightforward once the solutions for single-axis maneuvers are obtained. Unlike the minimum-time 3D maneuver problem, the minimum-fuel 3D maneuver problem is complicated because it involves many switch-times during maneuvers. Assuming that each single-axis maneuver time is given, a solution is obtained. Given that several different approaches are presented, it is natural to ask the question; which one is best? Numerical comparisons with performance index costs are easy. Other criteria associated with risk may push selected options in different directions.

The sequential maneuver case leads to a very efficient closed-form solution algorithm that outperforms the numerical optimization approach by a factor greater than 2.2×10^6-fold, which suggests that it may be useful for on-orbit real-time appli-

cations. This method is expected to be broadly useful for spacecraft applications that must deal with actuator failures on-orbit in real-time, where optimized approaches are required for maintain vehicle pointing objectives.

The homotopy approach presents a rigorous integral-variational method for generating an optimal open-loop large-angle 3D maneuvers for an asymmetric spacecraft for the cases: (i) one of three control actuators fails and (ii) two actuators fail among four actuators. The second case is more general and realistic because one more actuator is usually installed for redundancy. Greater attention is given to the first case; however, proof-of-concept maneuvers and results are demonstrated for the second case. The 3D maneuver problem is handled by introducing a generalized Davidenko's classical homotopy method, leading to an ordinary differential equation for the initial costate vector. A homotopy algorithm permits the equation of motion to be continuously transformed from a full control problem to the failed control case. This is analytically accomplished by multiplying the control input that is assumed to fail by a homotopy embedding parameter, ε. The starting value for the 3D maneuver is obtained from the 3D maneuver optimal costate initial conditions, which is found for the case of no actuator failures. Davidenko's method is used to assemble and compute the differential equations for the costate as a function of the homotopy embedding parameter, which is numerically integrated to provide sensitivity data for updating estimates for the initial costate variable as the homotopy embedding parameter is swept through its entire range of values. The trajectories for the MRPs and angular velocity are seen to be very different when comparing the starting guess solutions with the failed actuator cases. The observed differences are so large that, given the nonlinear nature of the governing equations of motion and attitude kinematics, conventional solution solvers may experience difficulties in obtaining the desired solutions. These results provide additional information for the

case when control torque capability degrades. The proposed method is expected to be useful for analyzing spacecraft behavior where the vehicle looses controllability.

REFERENCES

[1] Schaub, H. and Junkins, J. L., *Analytical Mechanics of Space Systems*, AIAA, Reston, VA, 2nd ed., 2009, pp. 103–111, 759–762.

[2] Tsiotras, P., Corless, M., and Longuski, J. M., "A Novel Approach to the Attitude Control of Axisymmetric Spacecraft," *Automatica*, Vol. 31, No. 8, August 1995, pp. 1099–1112.

[3] Tsiotras, P., "Optimal Regulation and Passivity Results for Axisymmetric Rigid Bodies Using Two Controls," *Journal of Guidance, Control, and Dynamics*, Vol. 20, No. 3, May-June 1997, pp. 457–463.

[4] Tsiotras, P. and Luo, J., "Reduced Effort Control Laws for Underactuated Rigid Spacecraft," *Journal of Guidance, Control, and Dynamics*, Vol. 20, No. 6, November-December 1997, pp. 1089–1095.

[5] Tsiotras, P. and Luo, J., "Stabilization and Tracking of Underactuated Axisymmetric Spacecraft with Bounded Control," *Proceedings of the fourth IFAC Symposium on Nonlinear Control Systems Design*, Pergamon Press, Oxford, United Kingdom, 1998, pp. 800–806.

[6] Tsiotras, P. and Luo, J., "Control of Underactuated Spacecraft with Bounded Inputs," *Automatica*, Vol. 36, No. 8, 2000, pp. 1153–1169.

[7] Tsiotras, P. and Schleicher, A., "Detumbling and Partial Attitude Stabilization of a Rigid Spacecraft Under Actuator Failure," *AIAA Guidance, Navigation, and Control Conference and Exhibit*, No. 2000-4044, AIAA, Reston, VA, August 2000, pp. 1–8.

[8] Tsiotras, P. and Doumtchenko, V., "Control of Spacecraft Subject to Actuator Failures: State-of-the-Art and Open Problems," *The Richard H. Battin Astrodynamics Conference*, No. 00-264, American Astronautical Society, San Diego, CA, 2000, pp. 1–21.

[9] Shen, H. and Tsiotras, P., "Time-Optimal Control of Axisymmetric Rigid Spacecraft Using Two Controls," *Journal of Guidance, Control, and Dynamics*, Vol. 22, No. 5, September-October 1999, pp. 682–694.

[10] Junkins, J. L. and Turner, J. D., *Optimal Spacecraft Rotational Maneuvers*, Vol. 3 of *Studies In Astronautics*, Elsevier, Amsterdam, Netherlands, 1986, pp. 52, 171–184.

[11] Lewis, F. L., Vrabie, D. L., and Syrmos, V. L., *Optimal Control*, John Wiley & Sons, Hoboken, NJ, 3rd ed., 2012, pp. 232–253.

[12] Hurtado, J. E., *Elements of Spacecraft Control*, Lulu, 2009, pp. 56–58.

[13] Junkins, J. L., Rahman, Z. H., and Bang, H., "Near-Minimum-Time Control of Distributed Parameter Systems: Analytical and Experimental Results," *Journal of Guidance, Control, and Dynamics*, Vol. 14, No. 2, March 1991, pp. 406–415.

[14] Bock, H. G. and Plitt, K. J., "A Multiple Shooting Algorithm for Direct Solution of Optimal Problems," *Proceeedings of the Ninth IFAC World Congress*, IEEE Publications, Piscataway, NJ, 1984, pp. 242–247.

[15] Mishina, A. P. and Proskuryakov, I. V., *Higher Algebra: Linear Algebra, Polynomials, General Algebra*, Pergamon Press, Oxford, United Kingdom, 1965, pp. 37–39.

[16] Junkins, J. L. and Turner, J. D., "Optimal Continuous Torque Attitude Maneuvers," *Journal of Guidance, Control, and Dynamics*, Vol. 3, No. 3, 1980, pp. 210–217.

[17] Turner, J. D. and Junkins, J. L., "Optimal Large-Angle Single Axis Rotational Maneuvers of Flexible Spacecraft," *Journal of Guidance, Control, and Dynamics*, Vol. 3, No. 6, 1980, pp. 578–585.

[18] Crassidis, J. L. and Junkins, J. L., *Optimal Estimation of Dynamic Systems*, Applied Mathematics and Nonlinear Science, Chapman & Hall/CRC, Boca Raton, Florida, 2nd ed., 2012, pp. 579–585.

[19] Kim, D. and Turner, J. D., "3D Spacecraft Attitude Control Using Two Control Inputs," *Annual Technical Symposium 2012*, No. A-3.3, AIAA, Reston, VA, May 2012, p. 26.

[20] Kim, D. and Turner, J. D., "Spacecraft Attitude Control Using Two Control Torques," *Jer-Nan Juang Astrodynamics Symposium*, No. AAS 12-640, American Astronautical Society, College Station, TX, June 2012.

[21] Kim, D. and Turner, J. D., "Suboptimal Spacecraft Maneuvers Using Two Controls," *Journal of Guidance, Control, and Dynamics*, (accepted for publication).

[22] Tsiotras, P. and Longuski, J. M., "A New Parameterization of the Attitude Kinematics," *Journal of the Astronautical Sciences*, Vol. 43, No. 3, July-September 1995, pp. 243–262.

[23] Keraï, E.-Y., "Analyis of Small Time Local Controllability of the Rigid Body Model," *Proceedings of the third IFAC Symposium on System Structure and Control*, Pergamon, Oxford, United Kingdom, 1995, pp. 597–602.

[24] Brockett, R. W., "Asymptotic Stability and Feedback Stabilization," *Differential Geometric Control Theory*, Birkhauser Boston Inc., Cambridge, MA, 1983, pp. 181–191.

[25] Kim, D., *Failure Detection and Control of Spacecraft*, Master's thesis, Department of Aerospace and Mechanical Engineering, Korea Aerospace University, Goyang, Republic of Korea, 2010.

[26] Kim, D., Choi, D., and Oh, H.-S., "Failure Diagnosis of Actuator Using the EKF and NP Theorem," *International Journal of Control, Automation, and Systems*, Vol. 11, No. 3, June 2013, pp. 450–459.

[27] Kim, D., Turner, J. D., and Leeghim, H., "A New Approach for Handling Under-Actuated System Control," *Transactions of the Japan Society for Aeronautical and Space Sciences*, (submitted for publication).

[28] Morin, P., Samson, C., Pomet, J.-B., and Jiang, Z.-P., "Time-Varying Feedback Stabilization of the Attitude of a Rigid Spacecraft with Two Controls," *Systems & Control Letters*, Vol. 25, No. 5, 1995, pp. 375–385.

[29] Coron, J.-M. and Keraï, E.-Y., "Explicit Feedbacks Stabilizing the Attitude of a Rigid Spacecraft with Two Control Torques," *Automatica*, Vol. 32, No. 5, 1996, pp. 669–677.

[30] Bryson, A. E., *Dynamic Optimization*, Addison Wesley Longman, Inc., Menlo Park, CA, 1999, pp. 82–83.

[31] Pesch, H. J., "A Practical Guide to the Solution of Real-Life Optimal Control Problems," *Control Cybernet*, Vol. 23, No. 1-2, 1994, pp. 7–60.

[32] Ficken, F. A., "The Continuation Method for Functional Equations," *Communication on Pure and Applied Mathematics*, Vol. 4, No. 4, 1951, pp. 435–356.

[33] Allgower, E. L. and K. Georg, K., *Introduction to Numerical Continuation Methods*, Society for Indestrial and Applied Mathematics, Philadelphia, PA, 2003.

[34] Lahaye, E., "Une méthode de résolution d'une catégorie d'équations transcendentes," *C. R. Acad. Sci*, Vol. 198, 1934, pp. 1840–1842.

[35] Davidenko, D., "On a New Method of Numerically Integrating a System of Nonlinear Equations," *Dokl. Akad. Nauk USSR*, Vol. 88, 1953, pp. 601–604.

[36] Chow, S. N., Mallet-Paret, J., and Yorke, J. A., "Finding Zeros of Maps: Homotopy methods that are constructive with probability one," *Mathematics of Computation*, Vol. 32, 1978, pp. 887–899.

APPENDIX A

DERIVATIONS FOR SMOOTHING FUNCTIONS

Discontinuous control profiles present real-world problems for realistic spacecraft applications. This problem is addressed by introducing a smoothing function for the maneuver time and fuel minimization problems.

A.1 Smoothing Function for Maneuver Time Minimization Problem

Given the following cubic polynomial equation

$$a(t) = b + ct + dt^2 + et^3 \tag{A.1}$$

where b, c, d, and e are the unknown constant coefficients. The time derivative of the cubic polynomial equation is given by

$$a'(t) = c + 2dt + 3et^2 \tag{A.2}$$

Four boundary conditions are required for recovering the four coefficients in Eq. (A.1).

For $t \in [0, \delta]$, the boundary conditions are

$$a(0) = 0, \quad a'(0) = 0 \tag{A.3a}$$

$$a(\delta) = -1, \quad a'(\delta) = 0 \tag{A.3b}$$

For $t \in [\delta,\, t_1]$, the boundary conditions are

$$a(\delta) = -1, \quad a'(\delta) = 0 \tag{A.4a}$$

$$a\left(t_1\right) = -1, \quad a'\left(t_1\right) = 0 \tag{A.4b}$$

For $t \in [t_1,\, t_2]$, the boundary conditions are

$$a\left(t_1\right) = -1, \quad a'\left(t_1\right) = 0 \tag{A.5a}$$

$$a\left(t_2\right) = 1, \quad a'\left(t_2\right) = 0 \tag{A.5b}$$

For $t \in [t_2,\, t_3]$, the boundary conditions are

$$a\left(t_2\right) = 1, \quad a'\left(t_2\right) = 0 \tag{A.6a}$$

$$a\left(t_3\right) = 1, \quad a'\left(t_3\right) = 0 \tag{A.6b}$$

For $t \in [t_3,\, T]$, the boundary conditions are

$$a\left(t_3\right) = 1, \quad a'\left(t_3\right) = 0 \tag{A.7a}$$

$$a(T) = 0, \quad a'(T) = 0 \tag{A.7b}$$

A.2 Smoothing Function for Fuel Minimization Problem

Given the cubic polynomial equation and the time derivative of the cubic polynomial equation in Eqs. (A.1) and (A.2), the coefficients are found for each time interval by imposing four boundary conditions.

For $t \in [0,\, \delta]$, the boundary conditions are

$$a(0) = 0, \quad a'(0) = 0 \tag{A.8a}$$

$$a(\delta) = -1, \quad a'(\delta) = 0 \tag{A.8b}$$

For $t \in [\delta,\, t_1]$, the boundary conditions are

$$a(\delta) = -1, \quad a'(\delta) = 0 \tag{A.9a}$$

$$a\left(t_1\right) = -1, \quad a'\left(t_1\right) = 0 \tag{A.9b}$$

For $t \in [t_1,\, t_2]$, the boundary conditions are

$$a\left(t_1\right) = -1, \quad a'\left(t_1\right) = 0 \tag{A.10a}$$

$$a\left(t_2\right) = 0, \quad a'\left(t_2\right) = 0 \tag{A.10b}$$

For $t \in [t_2,\, t_3]$, the boundary conditions are

$$a\left(t_2\right) = 0, \quad a'\left(t_2\right) = 0 \tag{A.11a}$$

$$a\left(t_3\right) = 0, \quad a'\left(t_3\right) = 0 \tag{A.11b}$$

For $t \in [t_3,\, t_4]$, the boundary conditions are

$$a\left(t_3\right) = 0, \quad a'\left(t_3\right) = 0 \tag{A.12a}$$

$$a\left(t_4\right) = 1, \quad a'\left(t_4\right) = 0 \tag{A.12b}$$

For $t \in [t_4,\, t_5]$, the boundary conditions are

$$a\,(t_4) = 1, \quad a'\,(t_4) = 0 \tag{A.13a}$$

$$a\,(t_5) = 1, \quad a'\,(t_5) = 0 \tag{A.13b}$$

For $t \in [t_5,\, T]$, the boundary conditions are

$$a\,(t_5) = 1, \quad a'\,(t_5) = 0 \tag{A.14a}$$

$$a(T) = 0, \quad a'(T) = 0 \tag{A.14b}$$

APPENDIX B

OPTIMAL CONTROL AND CONTROL-RATE FORMULATIONS AND RESULTS

Classical optimal control formulations lead to discontinuous control profiles when the quadratic torque penalty is included in the performance index. This problem is addressed by penalizing the quadratic torque-rate penalty in the performance index, which permits the analyst to specify control boundary conditions freely. Both approaches are compared and contrasted for the nominal and failed actuator cases.

B.1 Formulations for Nominal Case

B.1.1 Optimal Control Formulation Using the Quaternion

A solution for Eqs. (2.1) and (2.6) is obtained satisfying the prescribed terminal conditions:

$$\boldsymbol{q}\left(t_0\right)=\boldsymbol{q}_{t_0},\quad \boldsymbol{\omega}\left(t_0\right)=\boldsymbol{\omega}_{t_0},\quad \boldsymbol{q}\left(t_f\right)=\boldsymbol{q}_{t_f},\quad \boldsymbol{\omega}\left(t_f\right)=\boldsymbol{\omega}_{t_f} \tag{B.1}$$

where the 14 members of Eq. (B.1) are prescribed constants characterizing the attitude and angular velocity at the initial and final times. Observe that the prescription of the boundary conditions for the quaternion must be consistent with the constraint in Eq. (2.5), so that only 12 degrees-of-freedom exist, as expected.

Defining the Hamiltonian for the system

$$\mathcal{H}=\frac{1}{2}\boldsymbol{u}^{\mathrm{T}}\boldsymbol{u}+\boldsymbol{\mu}^{\mathrm{T}}\boldsymbol{p}+\boldsymbol{\nu}^{\mathrm{T}}\boldsymbol{f} \tag{B.2}$$

where the Lagrange multiplier associated with the quaternion is $\boldsymbol{\nu}\in\mathcal{R}^4$. The first-

order necessary conditions are obtained as:

State Equations:

$$\dot{\boldsymbol{q}} = \frac{\partial \mathcal{H}}{\partial \boldsymbol{\nu}} = \boldsymbol{f} = \frac{1}{2}\left[\Omega(\boldsymbol{\omega})\right]\boldsymbol{q} \tag{B.3a}$$

$$\dot{\boldsymbol{\omega}} = \frac{\partial \mathcal{H}}{\partial \boldsymbol{\mu}} = \boldsymbol{p} = [J]^{-1}\left(-\left[\boldsymbol{\omega}^{\times}\right][J]\boldsymbol{\omega} + \boldsymbol{u}\right) \tag{B.3b}$$

Costate Equations:

$$\dot{\boldsymbol{\nu}} = -\frac{\partial \mathcal{H}}{\partial \boldsymbol{q}} = -\left[\frac{\partial \boldsymbol{f}}{\partial \boldsymbol{q}}\right]^{\mathrm{T}}\boldsymbol{\nu} = -\frac{1}{2}\left[\Omega(\boldsymbol{\omega})\right]^{\mathrm{T}}\boldsymbol{\nu} \tag{B.4a}$$

$$\dot{\boldsymbol{\mu}} = -\frac{\partial \mathcal{H}}{\partial \boldsymbol{\omega}} = -\left[\frac{\partial \boldsymbol{p}}{\partial \boldsymbol{\omega}}\right]^{\mathrm{T}}\boldsymbol{\mu} - \left[\frac{\partial \boldsymbol{f}}{\partial \boldsymbol{\omega}}\right]^{\mathrm{T}}\boldsymbol{\nu} = -\left[\Sigma(\boldsymbol{\omega}, J)\right]^{\mathrm{T}}\boldsymbol{\mu} - \frac{1}{2}\left[\Xi(\boldsymbol{q})\right]^{\mathrm{T}}\boldsymbol{\nu} \tag{B.4b}$$

where

$$\left[\Xi(\boldsymbol{q})\right] \triangleq \begin{bmatrix} q_4 & -q_3 & q_2 \\ q_3 & q_4 & -q_1 \\ -q_2 & q_1 & q_4 \\ -q_1 & -q_2 & -q_3 \end{bmatrix}$$

Stationarity Condition:

$$0 = \frac{\partial \mathcal{H}}{\partial \boldsymbol{u}} = \boldsymbol{u} + \left[\frac{\partial \boldsymbol{p}}{\partial \boldsymbol{u}}\right]^{\mathrm{T}}\boldsymbol{\mu} = \boldsymbol{u} + [J]^{-1}\boldsymbol{\mu} \tag{B.5}$$

B.1.2 Optimal Control Formulation Using the MRPs

A solution of Eqs. (2.1) and (2.10) is obtained satisfying the prescribed terminal conditions:

$$\boldsymbol{\sigma}(t_0) = \boldsymbol{\sigma}_{t_0}, \quad \boldsymbol{\omega}(t_0) = \boldsymbol{\omega}_{t_0}, \quad \boldsymbol{\sigma}(t_f) = \boldsymbol{\sigma}_{t_f}, \quad \boldsymbol{\omega}(t_f) = \boldsymbol{\omega}_{t_f} \tag{B.6}$$

where the 12 members of Eq. (B.6) are prescribed constants characterizing the attitude and angular velocity at the initial and final times.

Defining the Hamiltonian for the system

$$\mathcal{H} = \frac{1}{2}\boldsymbol{u}^{\mathrm{T}}\boldsymbol{u} + \boldsymbol{\mu}^{\mathrm{T}}\boldsymbol{p} + \boldsymbol{\xi}^{\mathrm{T}}\boldsymbol{r} \tag{B.7}$$

where the Lagrange multiplier associated with the MRPs is $\boldsymbol{\xi} \in \mathcal{R}^3$. The first-order necessary conditions are obtained as:

State Equations:

$$\dot{\boldsymbol{\sigma}} = \frac{\partial \mathcal{H}}{\partial \boldsymbol{\xi}} = \boldsymbol{r} = \frac{1}{4}\left[B(\boldsymbol{\sigma})\right]\boldsymbol{\omega} \tag{B.8a}$$

$$\dot{\boldsymbol{\omega}} = \frac{\partial \mathcal{H}}{\partial \boldsymbol{\mu}} = \boldsymbol{p} = [J]^{-1}\left(-\left[\boldsymbol{\omega}^{\times}\right][J]\boldsymbol{\omega} + \boldsymbol{u}\right) \tag{B.8b}$$

Costate Equations:

$$\dot{\boldsymbol{\xi}} = -\frac{\partial \mathcal{H}}{\partial \boldsymbol{\sigma}} = -\left[\frac{\partial \boldsymbol{r}}{\partial \boldsymbol{\sigma}}\right]^{\mathrm{T}}\boldsymbol{\xi} = -\frac{1}{2}\left[\Lambda(\boldsymbol{\sigma},\, \boldsymbol{\omega})\right]^{\mathrm{T}}\boldsymbol{\xi} \tag{B.9a}$$

$$\dot{\boldsymbol{\mu}} = -\frac{\partial \mathcal{H}}{\partial \boldsymbol{\omega}} = -\left[\frac{\partial \boldsymbol{p}}{\partial \boldsymbol{\omega}}\right]^{\mathrm{T}}\boldsymbol{\mu} - \left[\frac{\partial \boldsymbol{r}}{\partial \boldsymbol{\omega}}\right]^{\mathrm{T}}\boldsymbol{\xi} = -\left[\Sigma(\boldsymbol{\omega},\, J)\right]^{\mathrm{T}}\boldsymbol{\mu} - \frac{1}{4}\left[B(\boldsymbol{\sigma})\right]^{\mathrm{T}}\boldsymbol{\xi} \tag{B.9b}$$

where

$$\left[\Lambda(\boldsymbol{\sigma},\, \boldsymbol{\omega})\right] \triangleq \begin{bmatrix} \sigma_1\omega_1 + \sigma_2\omega_2 + \sigma_3\omega_3 & \omega_3 - \sigma_2\omega_1 + \sigma_1\omega_2 & \sigma_1\omega_3 - \sigma_3\omega_1 - \omega_2 \\ \sigma_2\omega_1 - \omega_3 - \sigma_1\omega_2 & \sigma_1\omega_1 + \sigma_2\omega_2 + \sigma_3\omega_3 & \omega_1 - \sigma_3\omega_2 + \sigma_2\omega_3 \\ -\sigma_1\omega_3 + \sigma_3\omega_1 + \omega_2 & \sigma_3\omega_2 - \omega_1 - \sigma_2\omega_3 & \sigma_1\omega_1 + \sigma_2\omega_2 + \sigma_3\omega_3 \end{bmatrix}$$

Stationarity Condition:

$$0 = \frac{\partial \mathcal{H}}{\partial \boldsymbol{u}} = \boldsymbol{u} + \left[\frac{\partial \boldsymbol{p}}{\partial \boldsymbol{u}}\right]^{\mathrm{T}}\boldsymbol{\mu} = \boldsymbol{u} + [J]^{-1}\boldsymbol{\mu} \tag{B.10}$$

B.1.3 Optimal Control-Rate Formulation Using the Quaternion

A solution of Eqs. (2.1), (2.6), and (5.2) satisfying the prescribed terminal conditions:

$$\boldsymbol{q}\left(t_0\right)=\boldsymbol{q}_{t_0},\quad \boldsymbol{\omega}\left(t_0\right)=\boldsymbol{\omega}_{t_0},\quad \boldsymbol{u}\left(t_0\right)=\boldsymbol{u}_{t_0} \tag{B.11a}$$

$$\boldsymbol{q}\left(t_f\right)=\boldsymbol{q}_{t_f},\quad \boldsymbol{\omega}\left(t_f\right)=\boldsymbol{\omega}_{t_f},\quad \boldsymbol{u}\left(t_f\right)=\boldsymbol{u}_{t_f} \tag{B.11b}$$

where the 20 members of Eq. (B.11a) are prescribed constants characterizing the attitude, angular velocity, and control torque at the initial and final times. Observe that the prescription of the boundary conditions for the quaternion must be consistent with the constraint in Eq. (2.5), so that only 18 degrees-of-freedom exist, as expected.

Defining the Hamiltonian for the system

$$\mathcal{H}=\frac{1}{2}\bar{\boldsymbol{u}}^{\mathrm{T}}\bar{\boldsymbol{u}}+\boldsymbol{\mu}^{\mathrm{T}}\boldsymbol{p}+\boldsymbol{\nu}^{\mathrm{T}}\boldsymbol{f}+\boldsymbol{\eta}^{\mathrm{T}}\boldsymbol{g} \tag{B.12}$$

The first-order necessary conditions are obtained as:

State Equations:

$$\dot{\boldsymbol{q}}=\frac{\partial\mathcal{H}}{\partial\boldsymbol{\nu}}=\boldsymbol{f}=\frac{1}{2}\left[\Omega(\boldsymbol{\omega})\right]\boldsymbol{q} \tag{B.13a}$$

$$\dot{\boldsymbol{\omega}}=\frac{\partial\mathcal{H}}{\partial\boldsymbol{\mu}}=\boldsymbol{p}=[J]^{-1}\left(-\left[\boldsymbol{\omega}^{\times}\right][J]\boldsymbol{\omega}+\boldsymbol{u}\right) \tag{B.13b}$$

$$\dot{\boldsymbol{u}}=\frac{\partial\mathcal{H}}{\partial\boldsymbol{\eta}}=\boldsymbol{g}=\bar{\boldsymbol{u}} \tag{B.13c}$$

Costate Equations:

$$\dot{\boldsymbol{\nu}} = -\frac{\partial \mathcal{H}}{\partial \boldsymbol{q}} = -\left[\frac{\partial \boldsymbol{f}}{\partial \boldsymbol{q}}\right]^{\mathrm{T}} \boldsymbol{\nu} = -\frac{1}{2}\left[\Omega(\boldsymbol{\omega})\right]^{\mathrm{T}} \boldsymbol{\nu} \tag{B.14a}$$

$$\dot{\boldsymbol{\mu}} = -\frac{\partial \mathcal{H}}{\partial \boldsymbol{\omega}} = -\left[\frac{\partial \boldsymbol{p}}{\partial \boldsymbol{\omega}}\right]^{\mathrm{T}} \boldsymbol{\mu} - \left[\frac{\partial \boldsymbol{f}}{\partial \boldsymbol{\omega}}\right]^{\mathrm{T}} \boldsymbol{\nu} = -\left[\Sigma(\boldsymbol{\omega},\, J)\right]^{\mathrm{T}} \boldsymbol{\mu} - \frac{1}{2}\left[\Xi(\boldsymbol{q})\right]^{\mathrm{T}} \boldsymbol{\nu} \tag{B.14b}$$

$$\dot{\boldsymbol{\eta}} = -\frac{\partial \mathcal{H}}{\partial \boldsymbol{u}} = -\left[\frac{\partial \boldsymbol{p}}{\partial \boldsymbol{u}}\right]^{\mathrm{T}} \boldsymbol{\mu} = -[J]^{-1}\boldsymbol{\mu} \tag{B.14c}$$

Stationarity Condition:

$$0 = \frac{\partial \mathcal{H}}{\partial \bar{\boldsymbol{u}}} = \bar{\boldsymbol{u}} + \left[\frac{\partial \boldsymbol{g}}{\partial \bar{\boldsymbol{u}}}\right]^{\mathrm{T}} \boldsymbol{\eta} = \bar{\boldsymbol{u}} + \boldsymbol{\eta} \tag{B.15}$$

B.1.4 Optimal Control-Rate Formulation Using the MRPs

A solution of Eqs. (2.1), (2.10), and (5.2) is obtained satisfying the prescribed terminal conditions:

$$\boldsymbol{\sigma}\left(t_0\right) = \boldsymbol{\sigma}_{t_0}, \quad \boldsymbol{\omega}\left(t_0\right) = \boldsymbol{\omega}_{t_0}, \quad \boldsymbol{u}\left(t_0\right) = \boldsymbol{u}_{t_0} \tag{B.16a}$$

$$\boldsymbol{\sigma}\left(t_f\right) = \boldsymbol{\sigma}_{t_f}, \quad \boldsymbol{\omega}\left(t_f\right) = \boldsymbol{\omega}_{t_f}, \quad \boldsymbol{u}\left(t_f\right) = \boldsymbol{u}_{t_f} \tag{B.16b}$$

where the 18 members of Eq. (B.16a) are prescribed constants characterizing the attitude, angular velocity, and control torque at the initial and final times.

Defining the Hamiltonian for the system

$$\mathcal{H} = \frac{1}{2}\bar{\boldsymbol{u}}^{\mathrm{T}}\bar{\boldsymbol{u}} + \boldsymbol{\mu}^{\mathrm{T}}\boldsymbol{p} + \boldsymbol{\xi}^{\mathrm{T}}\boldsymbol{r} + \boldsymbol{\eta}^{\mathrm{T}}\boldsymbol{g} \tag{B.17}$$

The first-order necessary conditions are obtained as:

State Equations:

$$\dot{\boldsymbol{\sigma}} = \frac{\partial \mathcal{H}}{\partial \boldsymbol{\xi}} = \boldsymbol{r} = \frac{1}{4}\left[B(\boldsymbol{\sigma})\right]\boldsymbol{\omega} \tag{B.18a}$$

$$\dot{\boldsymbol{\omega}} = \frac{\partial \mathcal{H}}{\partial \boldsymbol{\mu}} = \boldsymbol{p} = [J]^{-1}\left(-\left[\boldsymbol{\omega}^{\times}\right][J]\boldsymbol{\omega} + \boldsymbol{u}\right) \tag{B.18b}$$

$$\dot{\boldsymbol{u}} = \frac{\partial \mathcal{H}}{\partial \boldsymbol{\eta}} = \boldsymbol{g} = \bar{\boldsymbol{u}} \tag{B.18c}$$

Costate Equations:

$$\dot{\boldsymbol{\xi}} = -\frac{\partial \mathcal{H}}{\partial \boldsymbol{\sigma}} = -\left[\frac{\partial \boldsymbol{r}}{\partial \boldsymbol{\sigma}}\right]^{\mathrm{T}}\boldsymbol{\xi} = -\frac{1}{2}\left[\Lambda(\boldsymbol{\sigma},\, \boldsymbol{\omega})\right]^{\mathrm{T}}\boldsymbol{\xi} \tag{B.19a}$$

$$\dot{\boldsymbol{\mu}} = -\frac{\partial \mathcal{H}}{\partial \boldsymbol{\omega}} = -\left[\frac{\partial \boldsymbol{p}}{\partial \boldsymbol{\omega}}\right]^{\mathrm{T}}\boldsymbol{\mu} - \left[\frac{\partial \boldsymbol{r}}{\partial \boldsymbol{\omega}}\right]^{\mathrm{T}}\boldsymbol{\xi} = -\left[\Sigma(\boldsymbol{\omega},\, J)\right]^{\mathrm{T}}\boldsymbol{\mu} - \frac{1}{4}\left[B(\boldsymbol{\sigma})\right]^{\mathrm{T}}\boldsymbol{\xi} \tag{B.19b}$$

$$\dot{\boldsymbol{\eta}} = -\frac{\partial \mathcal{H}}{\partial \boldsymbol{u}} = -\left[\frac{\partial \boldsymbol{p}}{\partial \boldsymbol{u}}\right]^{\mathrm{T}}\boldsymbol{\mu} = -[J]^{-1}\boldsymbol{\mu} \tag{B.19c}$$

Stationarity Condition:

$$0 = \frac{\partial \mathcal{H}}{\partial \bar{\boldsymbol{u}}} = \bar{\boldsymbol{u}} + \left[\frac{\partial \boldsymbol{g}}{\partial \bar{\boldsymbol{u}}}\right]^{\mathrm{T}}\boldsymbol{\eta} = \bar{\boldsymbol{u}} + \boldsymbol{\eta} \tag{B.20}$$

B.2 Numerical Examples

A rest-to-rest maneuver case is considered and the numerical simulation parameters are listed in Table B.1.

For the quaternion and MRPs, smooth linear control profiles are obtained for minimizing torque, whereas smooth continuous control profiles are obtained for minimizing torque-rate. The principal angle time trajectories show that the sequential maneuver strategy for the quaternion and MRPs also provides 3D maneuver solutions using only two control inputs.

Table B.1: Simulation parameters for a 3D minimum-torque maneuver

Parameter	Symbol	Value	Unit
Moment of inertia for the spacecraft	J	diag(14.2, 17.3, 20.3)	kg·m^2
Initial angular velocity	$\boldsymbol{\omega}_{t_0}$	$\{0, 0, 0\}^{\mathrm{T}}$	rad/s
Initial control torque	$\boldsymbol{u}_{t_0}$	$\{0, 0, 0\}^{\mathrm{T}}$	Nm
Initial Euler angles (3-2-1 set)	$\boldsymbol{\theta}_{t_0}$	$\{24, -5, 17\}^{\mathrm{T}}$	deg
Initial Euler angles (3-1-3 set)	$\boldsymbol{\vartheta}_{t_0}$	$\{8.09, 17.7, 16.66\}^{\mathrm{T}}$	deg
Initial quaternion	$\boldsymbol{q}_{t_0}$	$\{0.153, -0.012, 0.212, 0.965\}^{\mathrm{T}}$	-
Initial MRPs	$\boldsymbol{\sigma}_{t_0}$	$\{0.078, -0.006, 0.108\}^{\mathrm{T}}$	-
Interior angular velocity	$\boldsymbol{\omega}_{t_1}$	$\{0, 0, 0\}^{\mathrm{T}}$	rad/s
Interior control torque	$\boldsymbol{u}_{t_1}$	$\{0, 0, 0\}^{\mathrm{T}}$	Nm
Interior Euler angles (3-1-3 set)	$\boldsymbol{\vartheta}_{t_1}$	$\{8.09, 17.7, 0\}^{\mathrm{T}}$	deg
Interior quaternion	$\boldsymbol{q}_{t_1}$	$\{0.154, 0.011, 0.07, 0.986\}^{\mathrm{T}}$	-
Interior MRPs	$\boldsymbol{\sigma}_{t_1}$	$\{0.077, -0.006, 0.035\}^{\mathrm{T}}$	-
Interior angular velocity	$\boldsymbol{\omega}_{t_2}$	$\{0, 0, 0\}^{\mathrm{T}}$	rad/s
Interior control torque	$\boldsymbol{u}_{t_2}$	$\{0, 0, 0\}^{\mathrm{T}}$	Nm
Interior Euler angles (3-1-3 set)	$\boldsymbol{\vartheta}_{t_2}$	$\{8.09, 0, 0\}^{\mathrm{T}}$	deg
Interior quaternion	$\boldsymbol{q}_{t_2}$	$\{0, 0, 0.071, 0.998\}^{\mathrm{T}}$	-
Interior MRPs	$\boldsymbol{\sigma}_{t_2}$	$\{0, 0, 0.035\}^{\mathrm{T}}$	-
Final angular velocity	$\boldsymbol{\omega}_{t_f}$	$\{0, 0, 0\}^{\mathrm{T}}$	rad/s
Final control torque	$\boldsymbol{u}_{t_f}$	$\{0, 0, 0\}^{\mathrm{T}}$	Nm
Final Euler angles (3-2-1 set)	$\boldsymbol{\theta}_{t_f}$	$\{0, 0, 0\}^{\mathrm{T}}$	deg
Final Euler angles (3-1-3 set)	$\boldsymbol{\vartheta}_{t_f}$	$\{0, 0, 0\}^{\mathrm{T}}$	deg
Final quaternion	$\boldsymbol{q}_{t_f}$	$\{0, 0, 0, 1\}^{\mathrm{T}}$	-
Final MRPs	$\boldsymbol{\sigma}_{t_f}$	$\{0, 0, 0\}^{\mathrm{T}}$	-

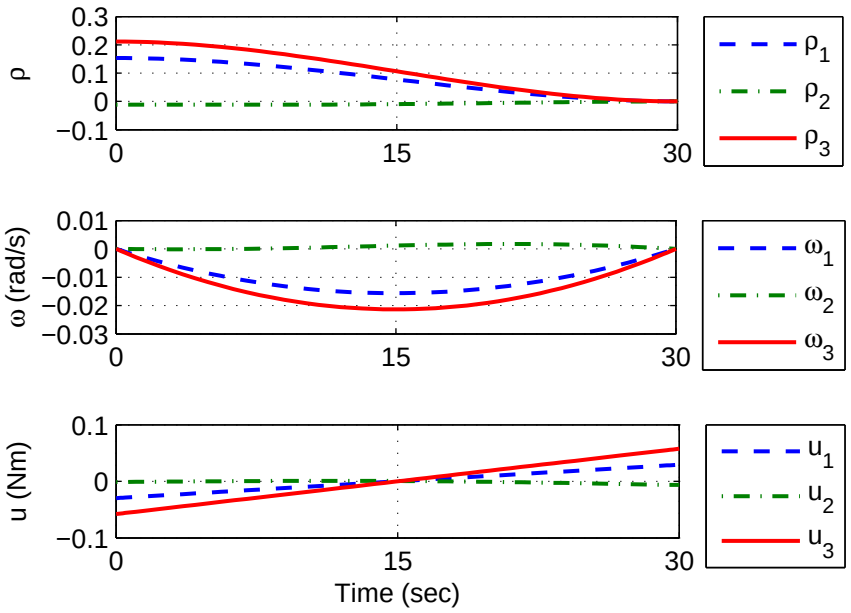

Figure B.1: Nominal: Time trajectories for the states and control based on the quaternion (torque minimization)

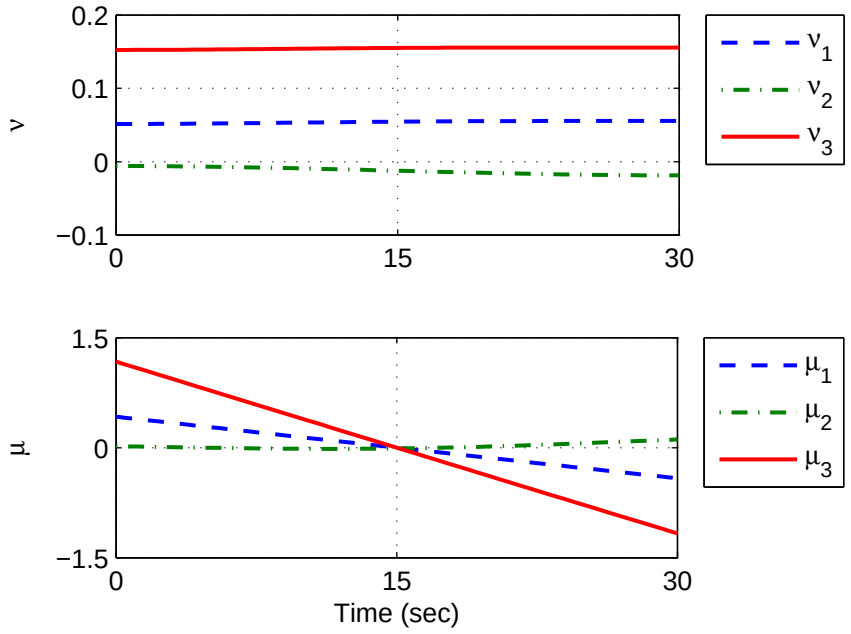

Figure B.2: Nominal: Time trajectories for the costates based on the quaternion (torque minimization)

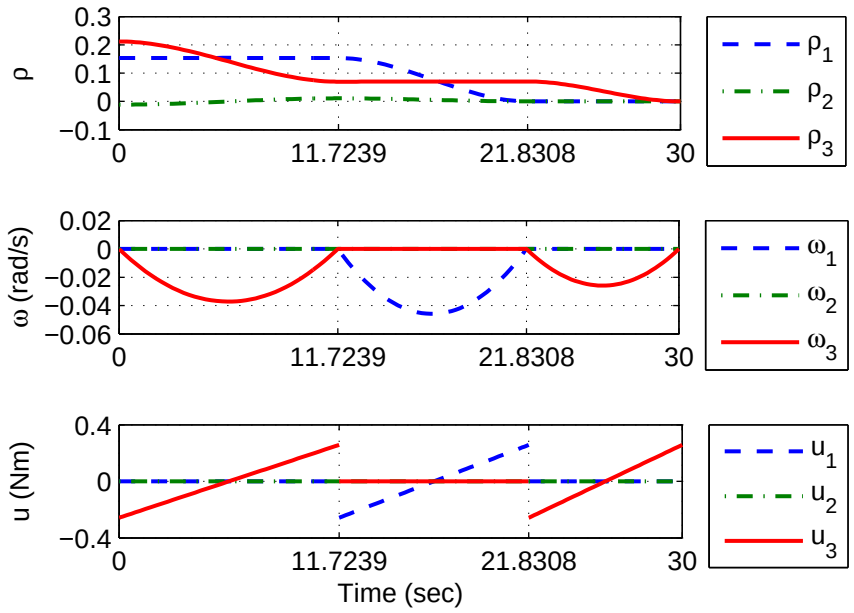

Figure B.3: Failed: Time trajectories for the states and control based on the quaternion (torque minimization)

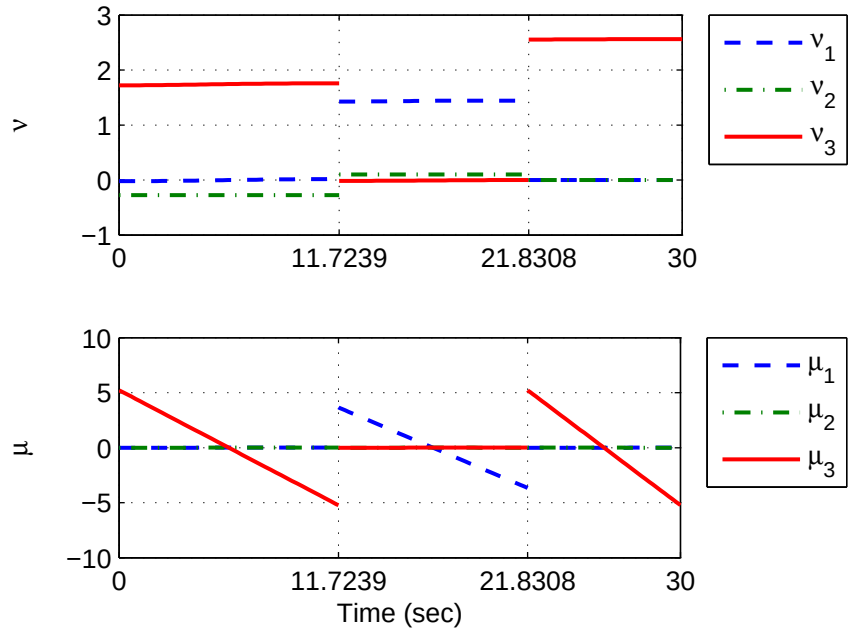

Figure B.4: Failed: Time trajectories for the costates based on the quaternion (torque minimization)

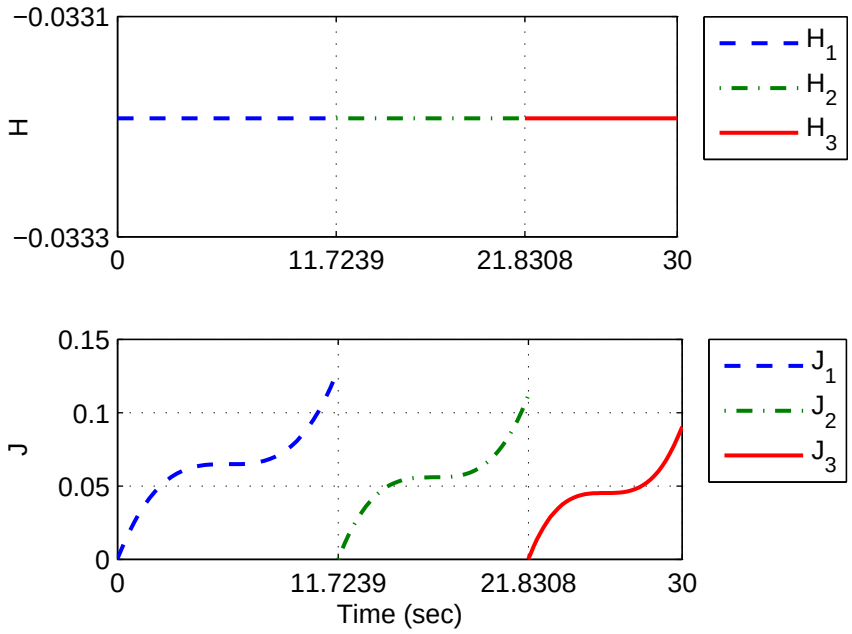

Figure B.5: Failed: Time trajectories for the Hamiltonian and performance index based on the quaternion (torque minimization)

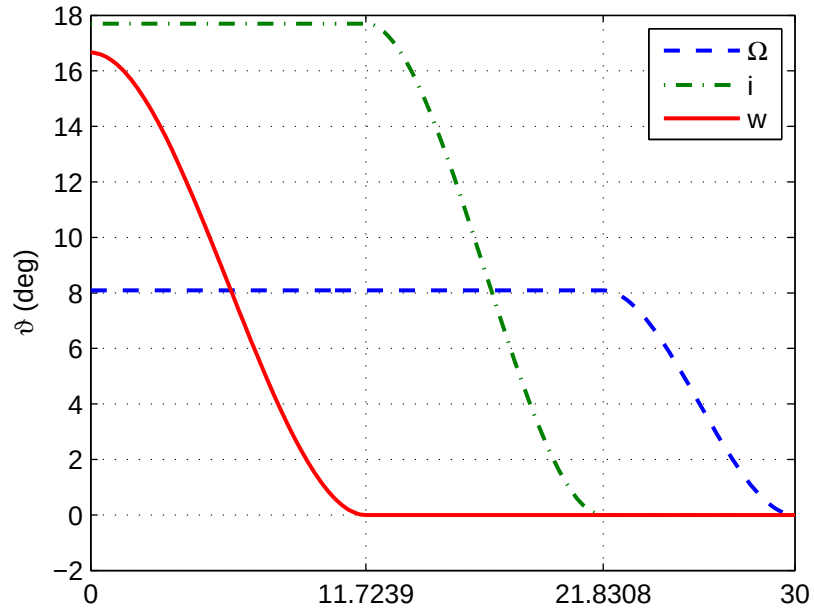

Figure B.6: Failed: Time trajectories for the (3-1-3) set of Euler angles based on the quaternion (torque minimization)

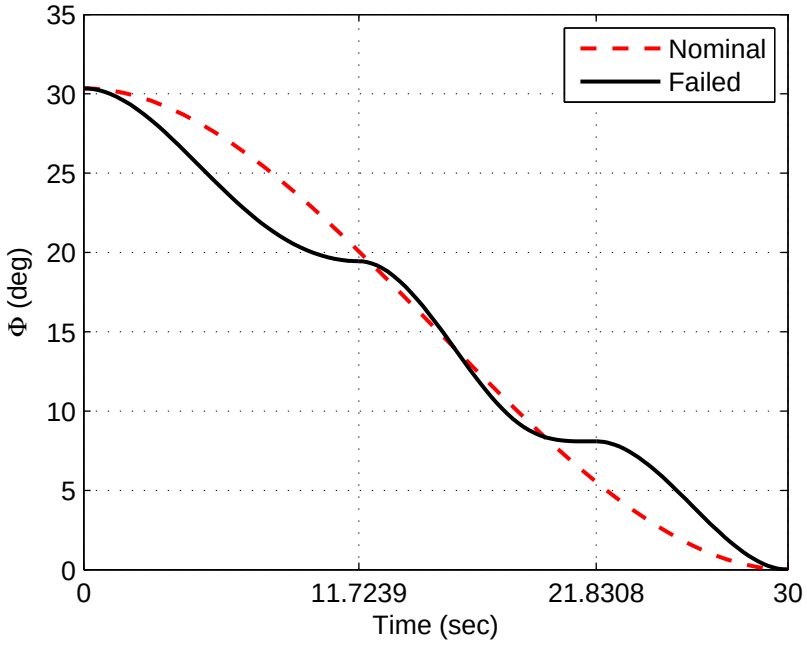

Figure B.7: Time trajectories for the principal angles based on the quaternion (torque minimization)

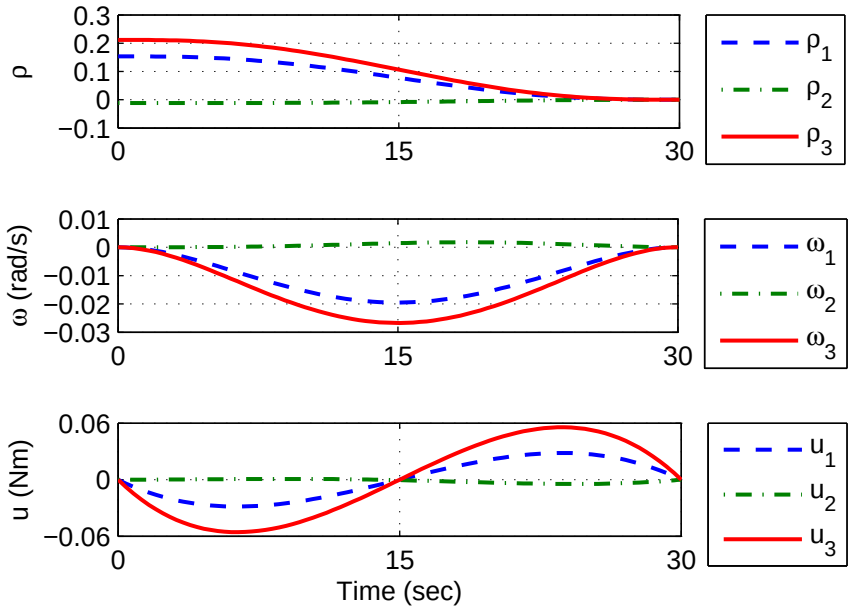

Figure B.8: Nominal: Time trajectories for the states based on the quaternion (torque-rate minimization)

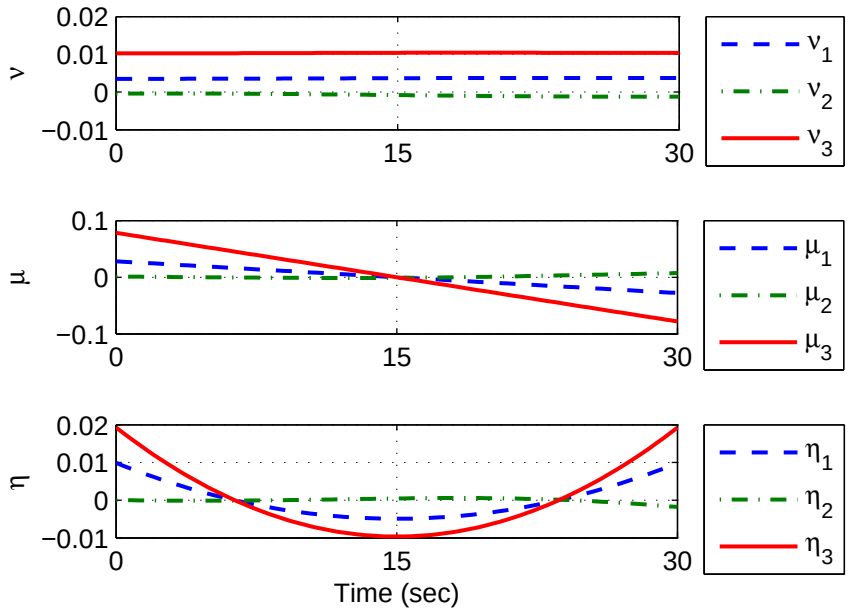

Figure B.9: Nominal: Time trajectories for the costates based on the quaternion (torque-rate minimization)

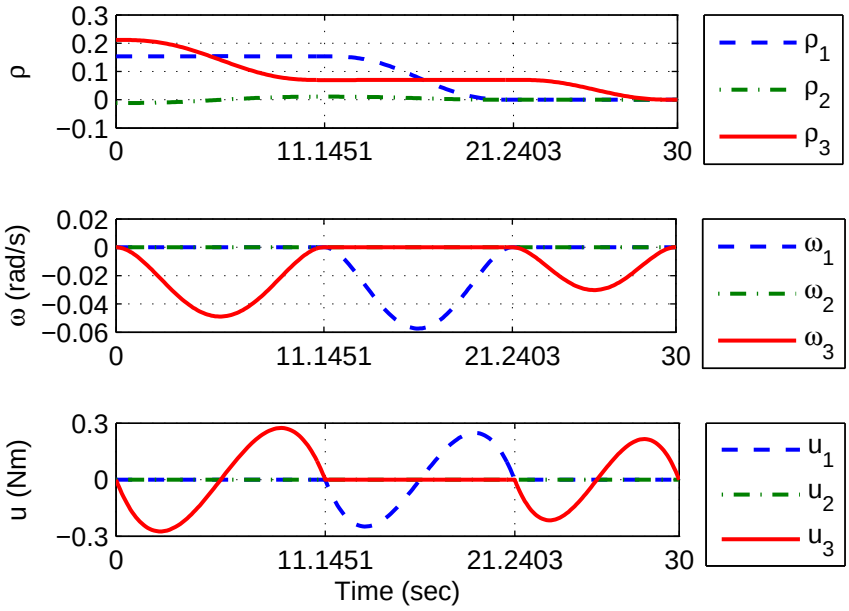

Figure B.10: Failed: Time trajectories for the states based on the quaternion (torque-rate minimization)

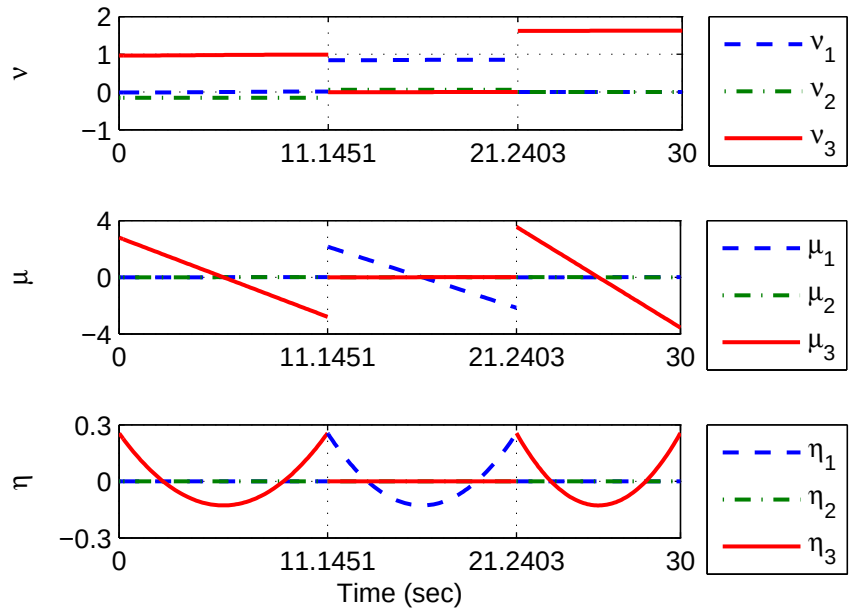

Figure B.11: Failed: Time trajectories for the costates based on the quaternion (torque-rate minimization)

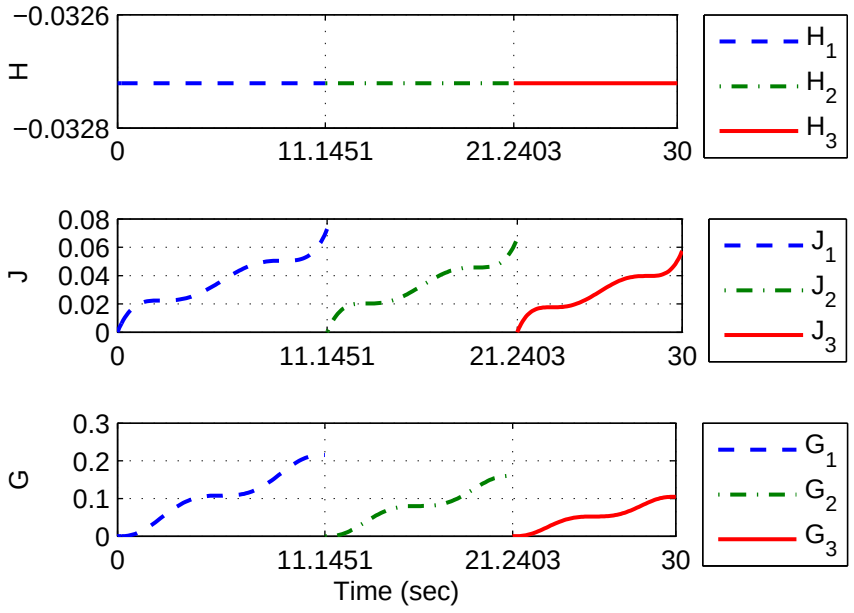

Figure B.12: Failed: Time trajectories for the Hamiltonian and performance indices based on the quaternion (torque-rate minimization)

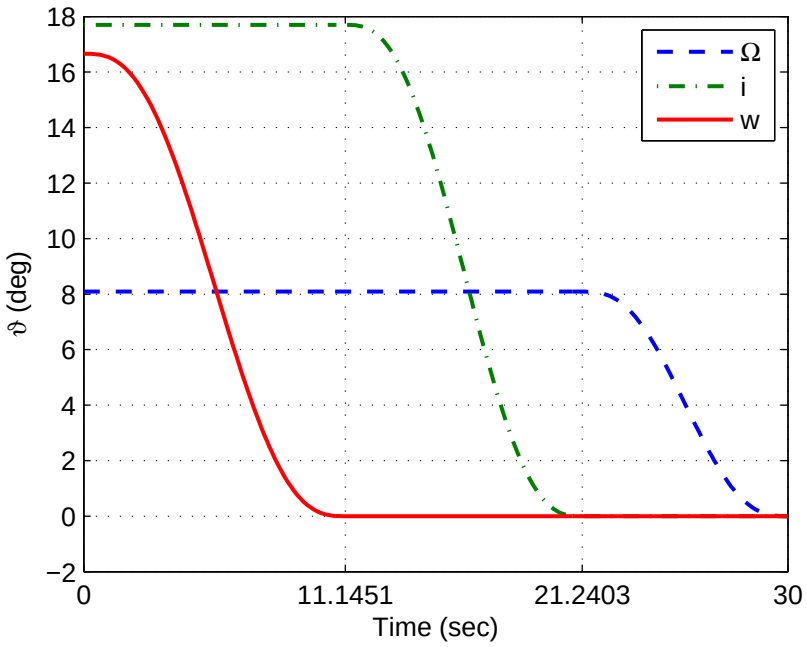

Figure B.13: Failed: Time trajectories for the (3-1-3) set of Euler angles based on the quaternion (torque-rate minimization)

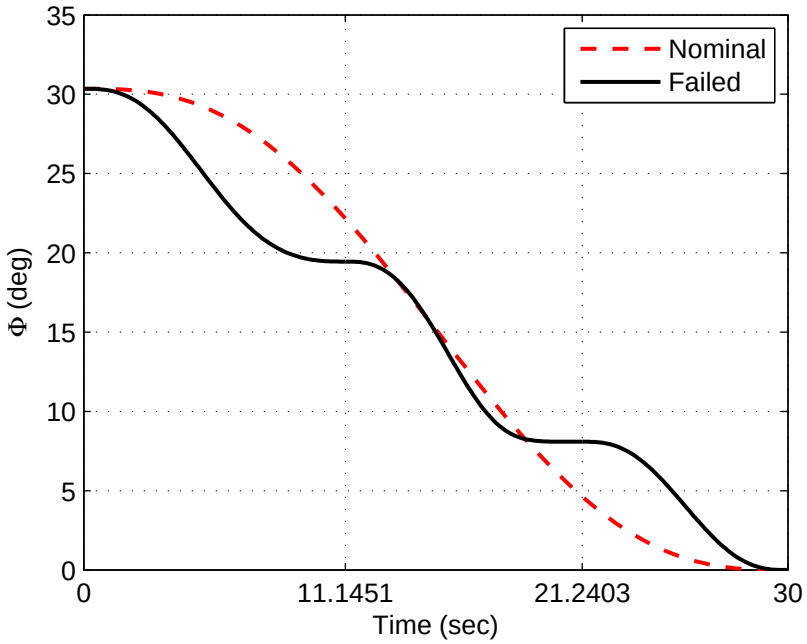

Figure B.14: Time trajectories for the principal angles based on the quaternion (torque-rate minimization)

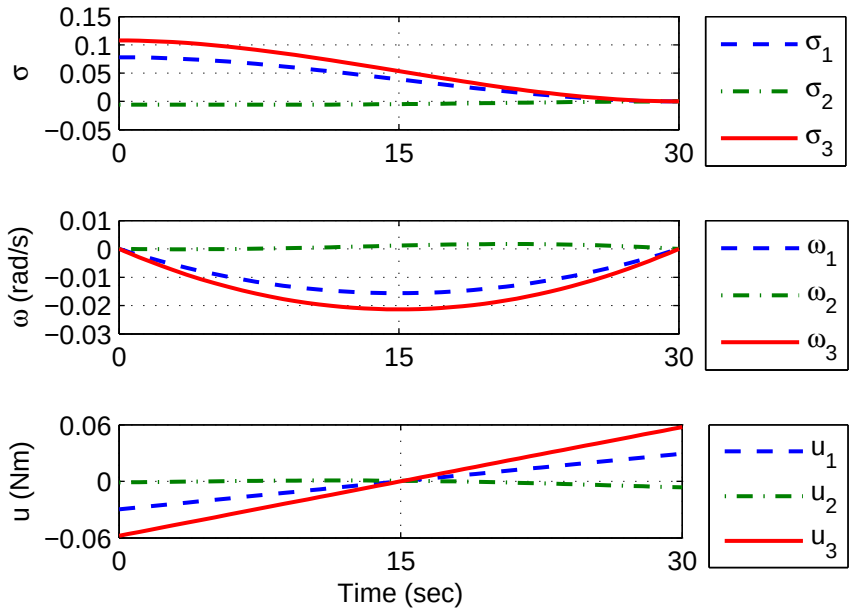

Figure B.15: Nominal: Time trajectories for the states and control based on the MRPs (torque minimization)

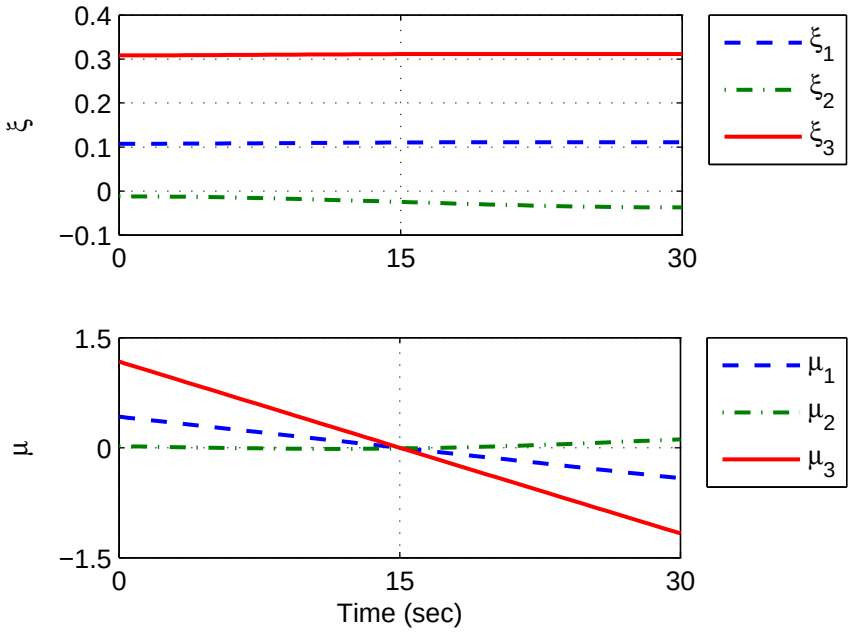

Figure B.16: Nominal: Time trajectories for the costates based on the MRPs (torque minimization)

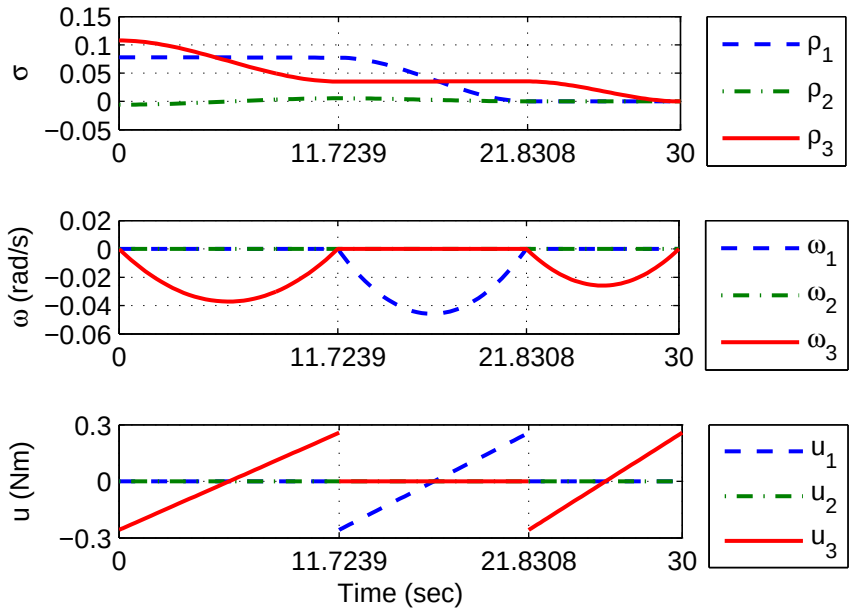

Figure B.17: Failed: Time trajectories for the states and control based on the MRPs (torque minimization)

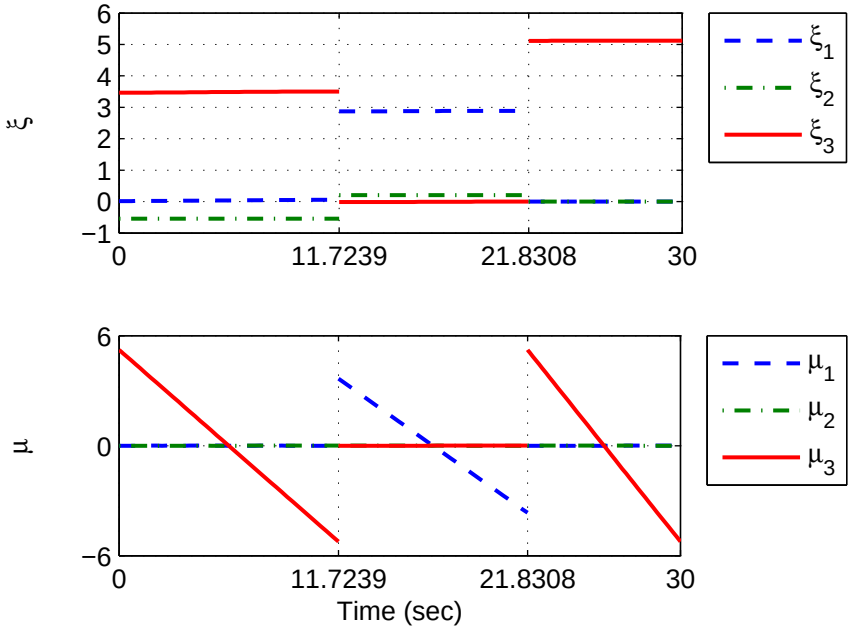

Figure B.18: Failed: Time trajectories for the costates based on the MRPs (torque minimization)

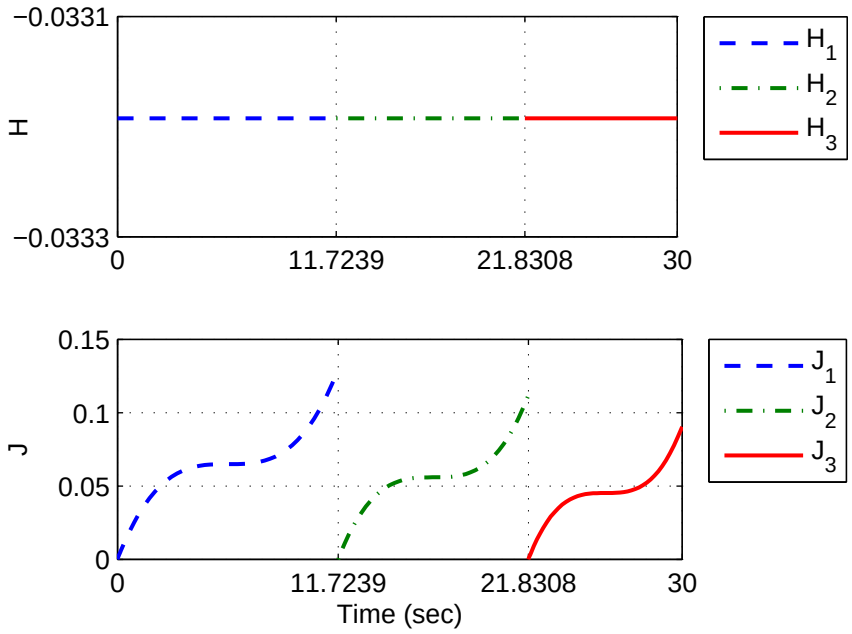

Figure B.19: Failed: Time trajectories for the Hamiltonian and performance index based on the MRPs (torque minimization)

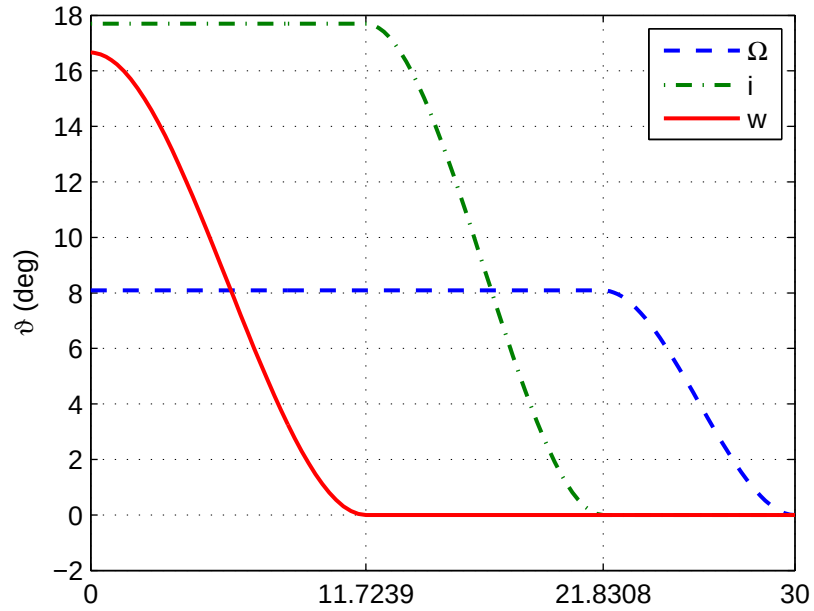

Figure B.20: Failed: Time trajectories for the (3-1-3) set of Euler angles based on the MRPs (torque minimization)

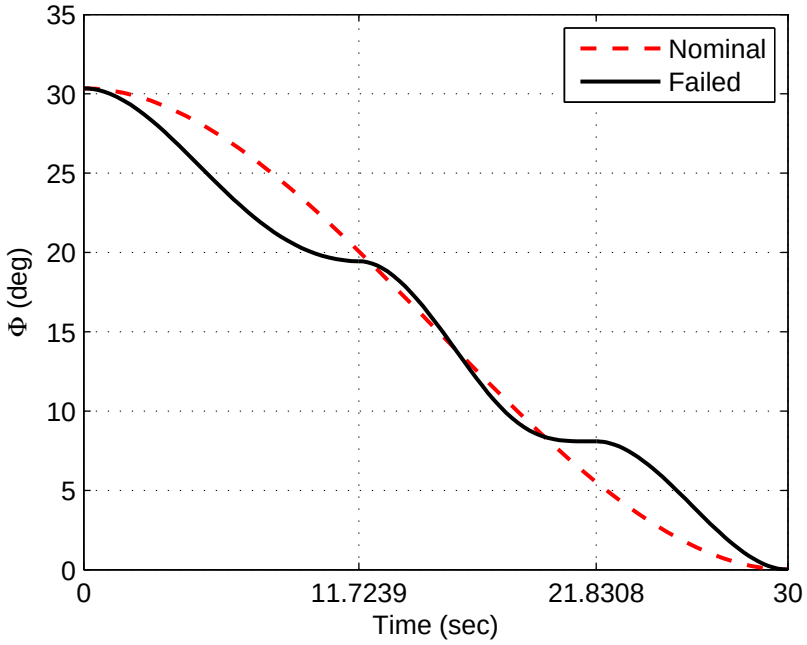

Figure B.21: Time trajectories for the principal angles based on the MRPs (torque minimization)

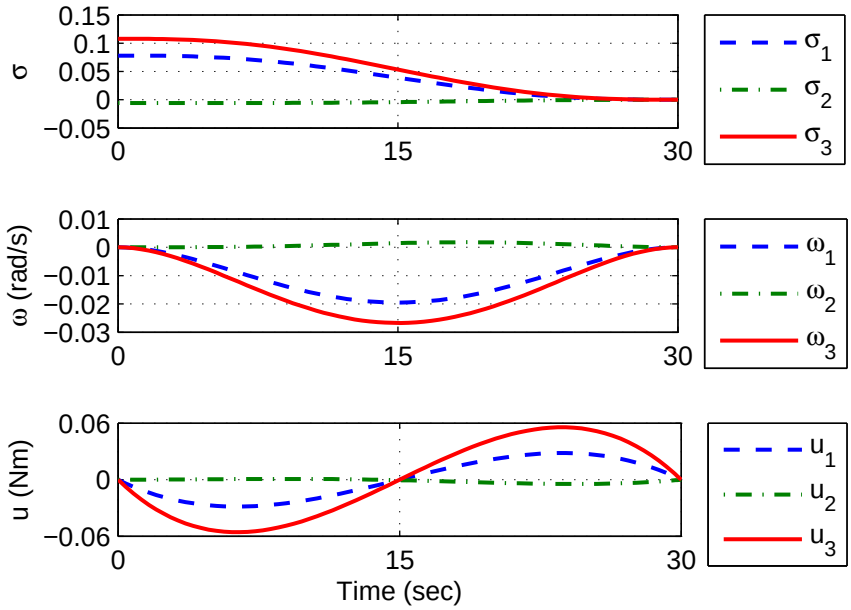

Figure B.22: Nominal: Time trajectories for the states based on the MRPs (torque-rate minimization)

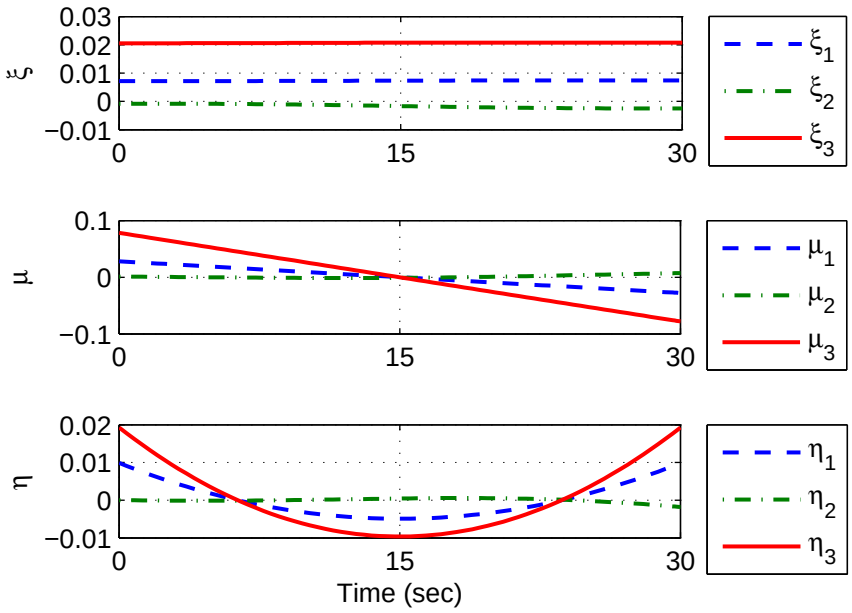

Figure B.23: Nominal: Time trajectories for the costates based on the MRPs (torque-rate minimization)

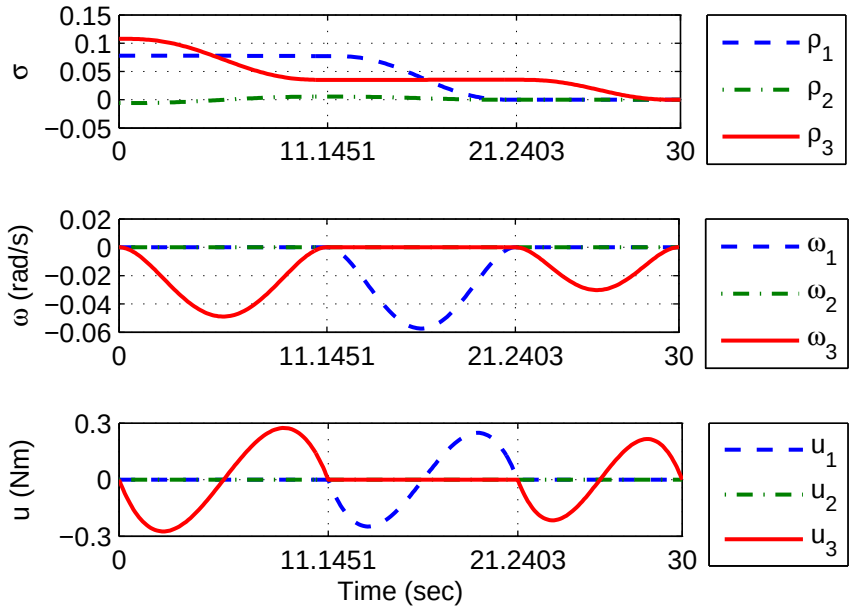

Figure B.24: Failed: Time trajectories for the states based on the MRPs (torque-rate minimization)

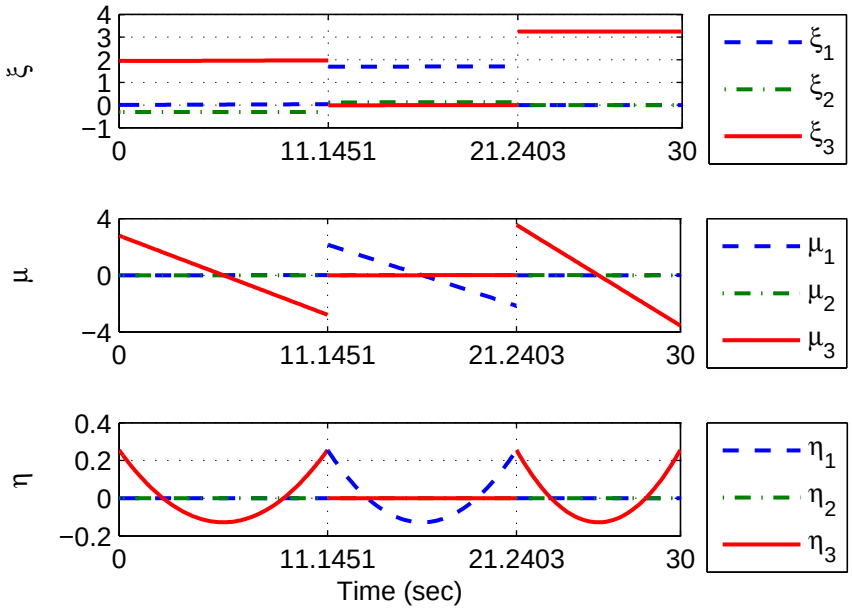

Figure B.25: Failed: Time trajectories for the costates based on the MRPs (torque-rate minimization)

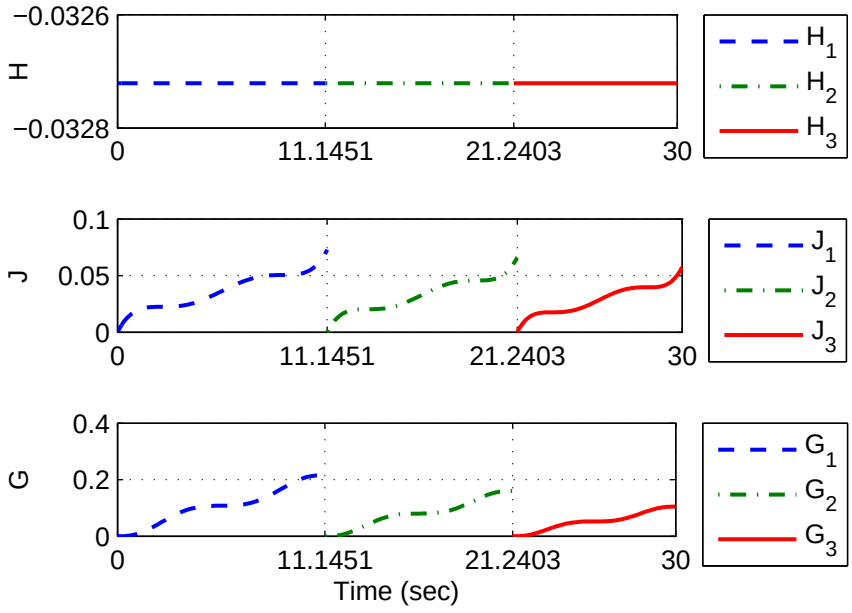

Figure B.26: Failed: Time trajectories for the Hamiltonian and performance indices based on the MRPs (torque-rate minimization)

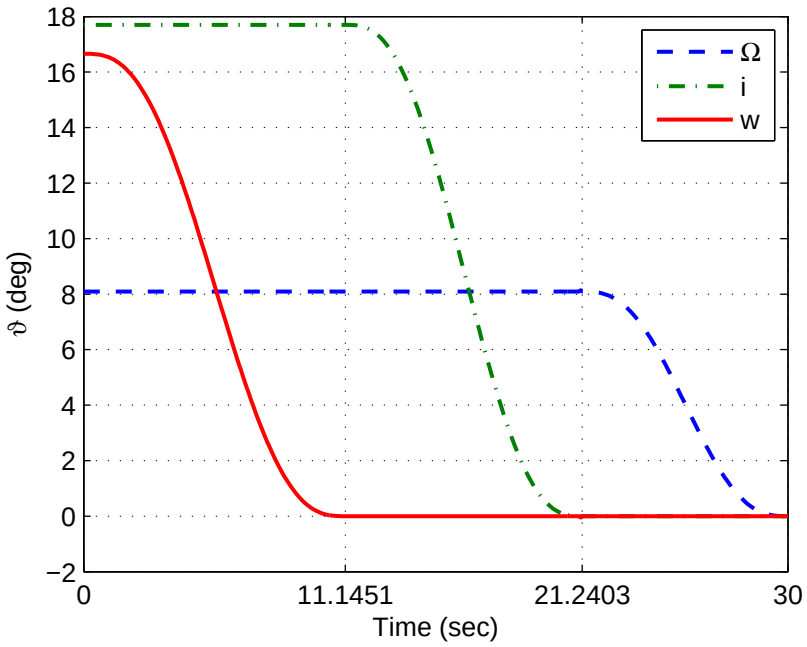

Figure B.27: Failed: Time trajectories for the (3-1-3) set of Euler angles based on the MRPs (torque-rate minimization)

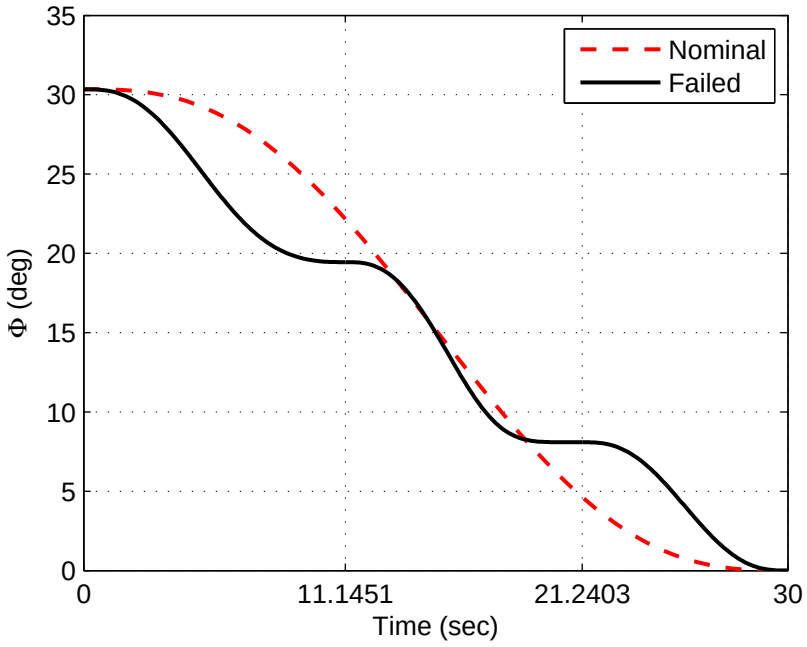

Figure B.28: Time trajectories for the principal angles based on the MRPs (torque-rate minimization)

APPENDIX C

THREE-DIMENSIONAL MANEUVERS OF RIGID BODY

Formulations for the single-axis maneuvers are presented for generalized problems with emphasis on under-actuated systems. Analytical solutions for the single-axis maneuvers are found in Sections 3.3, 3.4, 4.2, and 4.3. For 3D maneuvers for under-actuated systems, three sequential sub-maneuvers need to be performed. As a specific example for a failed actuator case, the control input along the second axis is assumed to be unavailable because of an actuator failure. Thus, two possible sets of Euler transformations are available to avoid rotation about the failed axis [i.e., (1-3-1) and (3-1-3)]. For optimally selecting the Euler angle rotation sequence between the (1-3-1) and (3-1-3) sets, the closed-form solutions for the cost function in Eqs. (5.52) and (5.56), leads to the following simple optimal selection criteria:

$$\mathcal{J}_{\text{opt}} = \min\left[\mathcal{J}_{1-3-1},\, \mathcal{J}_{3-1-3}\right] \tag{C.1}$$

C.1 Minimum-Time Maneuver

Using the numerical simulation parameters in Tables 5.1 and 5.4, numerical simulations are performed for the failed control case (2-axis control). The maximum control torque, $u_{\max}$, is assumed to be 1.

Both (1-3-1) and (3-1-3) sets of successive maneuvers are considered with Eqs. (3.43) and (3.46). For each sub-maneuver, the switch-time, t_s, and the final time, T, are slightly changed to t_{s_i} and T_i, respectively. The subscript, i, indicates the maneuver sequence and $t_f \triangleq T_3$.

For the (1-3-1) set of successive maneuver, the following set of switch-times

and the final time is computed to be

$$(t_{s_1},\, T_1,\, t_{s_2},\, T_2,\, t_{s_3},\, t_f) = (0.9199,\, 1.8398,\, 4.1060,\, 6.3722,\, 7.9170,\, 9.4619) \text{ sec}$$

For the (3-1-3) set of successive maneuver, the following set of switch-times and the final time is computed to be

$$(t_{s_1},\, T_1,\, t_{s_2},\, T_2,\, t_{s_3},\, t_f) = (2.0325,\, 4.0649,\, 5.8390,\, 7.6130,\, 8.6591,\, 9.7052) \text{ sec}$$

Comparing the obtained final time solutions, the (1-3-1) set of successive maneuver provides the minimum-time solution. The time trajectories for the (1-3-1) set, which is an optimal sequence set, of Euler angles and angular velocity are shown in Figs. C.1 and C.2, respectively. The Euler angles and angular velocity meet the prescribed boundary conditions. The bang-bang type of control profiles are shown in Fig. C.3. Three control switch-times, two maneuver switch-times, and the final time are clearly described. The principal angle time trajectories are shown in Fig. C.4. As a result, the given initial asymmetric rigid spacecraft is reoriented to the defined final state with only two control inputs.

Additionally, the principal angle time trajectories for the (3-1-3) set are shown in Fig. C.5. One can observe how the principal angles change over times for both (1-3-1) and (3-1-3) sets.

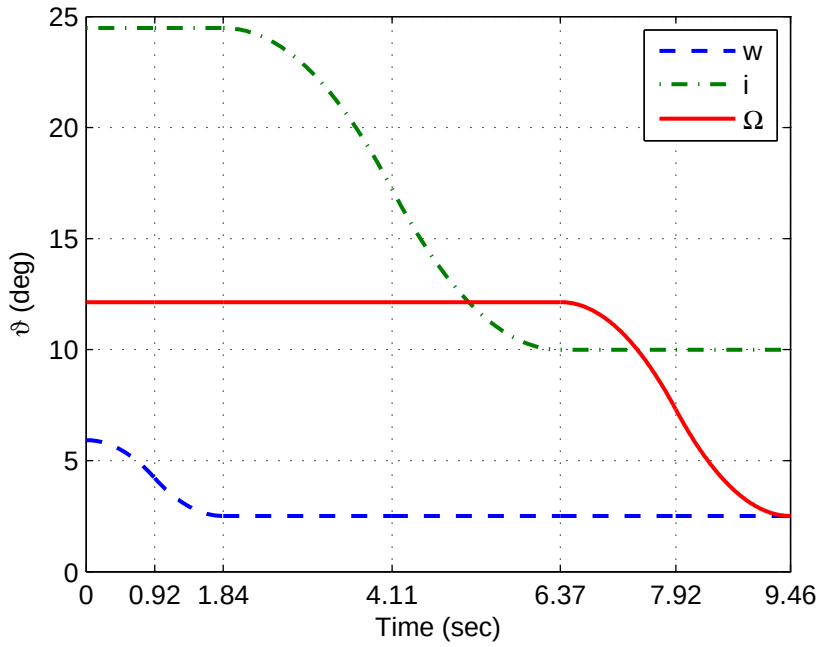

Figure C.1: Minimum-time time trajectories for the (1-3-1) set of Euler angles

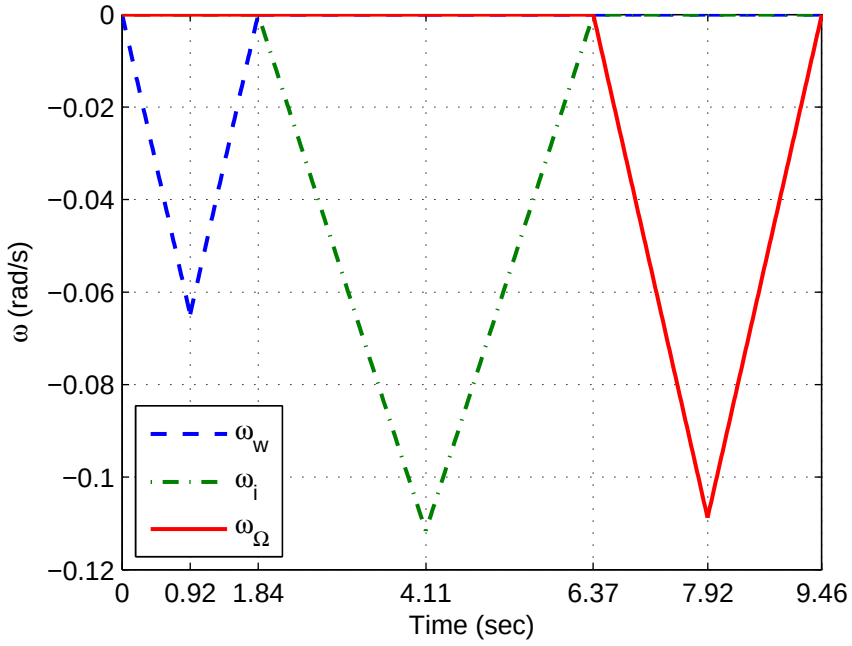

Figure C.2: Minimum-time time trajectories for the angular velocity (1-3-1)

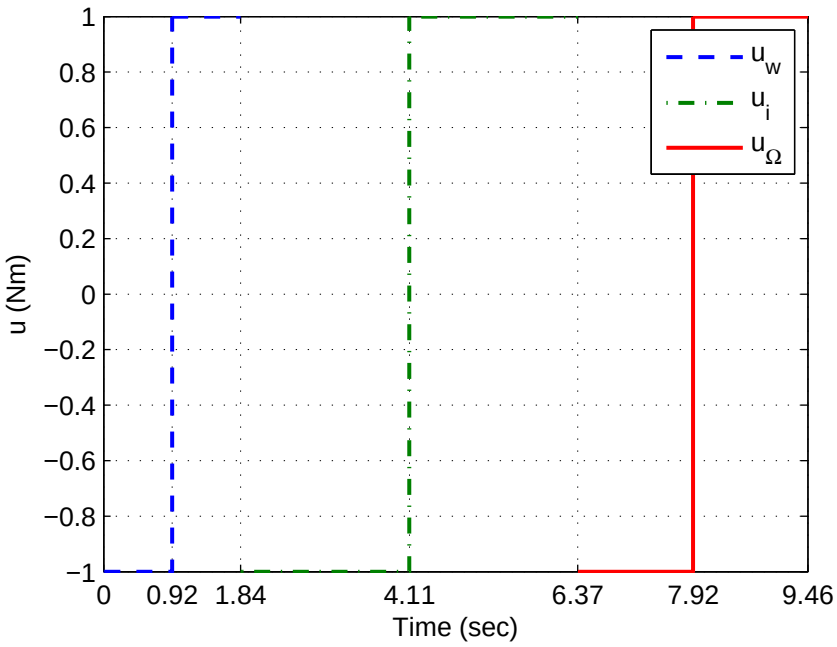

Figure C.3: Minimum-time time trajectories for the control torque (1-3-1)

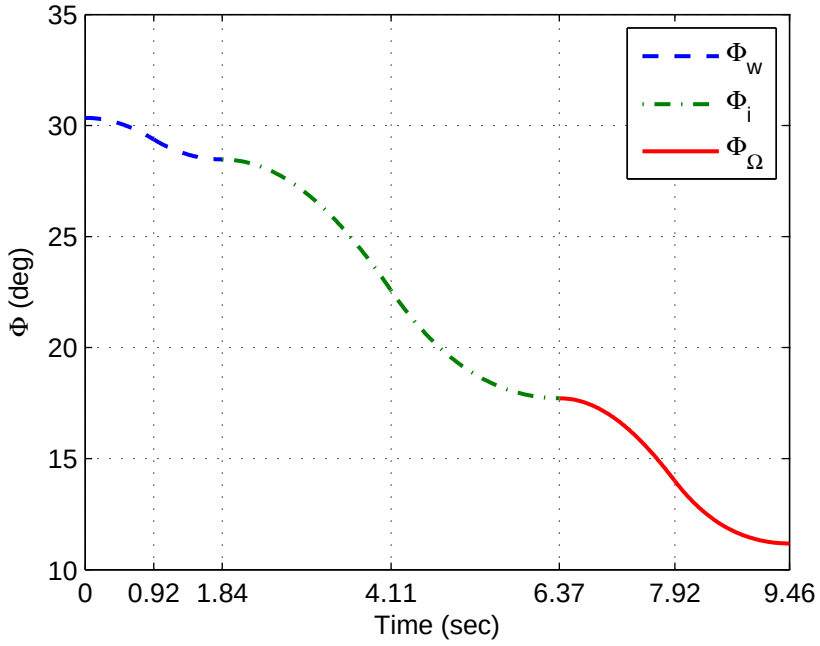

Figure C.4: Minimum-time time trajectories for the principal angle (1-3-1)

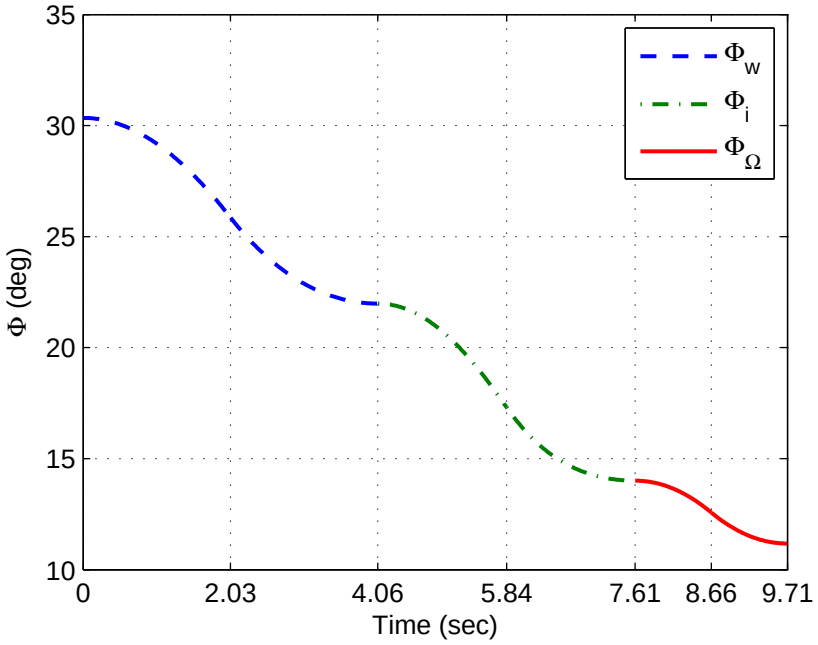

Figure C.5: Minimum-time time trajectories for the principal angle (3-1-3)

C.2 Cubic Polynomial Technique: Maneuver Time Minimization

Using the numerical simulation parameters in Tables 5.1 and 5.4, numerical simulations are performed for the failed control case (2-axis control). The maximum control torque, $u_{\max}$, is assumed to be 1 and the smoothing parameter, α, is assumed as 1/7.

The (1-3-1) set of successive maneuvers is considered with Eq. (4.23). For each sub-maneuver, the final time, T, is slightly changed to T_i. The subscript, i, indicates the maneuver sequence and $t_f \triangleq T_3$.

For the (1-3-1) set of successive maneuvers, the following set of maneuver switch-times and the final time is computed to be

$$(T_1,\, T_2,\, t_f) = (2.1646,\, 7.4969,\, 11.1320) \text{ sec}$$

For the (3-1-3) set of successive maneuvers, the following set of maneuver switch-times and the final time is computed to be

$$(T_1,\, T_2,\, t_f) = (4.7824,\, 8.9568,\, 11.4183) \text{ sec}$$

Again, it is shown that the (1-3-1) set of successive maneuver provides the minimum-time solution. The time trajectories for the (1-3-1) set, which is an optimal sequence set, of Euler angles and angular velocity are shown in Figs. C.6 and C.7, respectively. The Euler angles and angular velocity meet the prescribed boundary conditions. The smooth continuous bang-bang type of control profiles are shown in Fig. C.8. Two maneuver switch-times and the final time are clearly described. The principal angle time trajectories for the (1-3-1) and (3-1-3) sets are shown in Figs. C.9 and C.10, respectively.

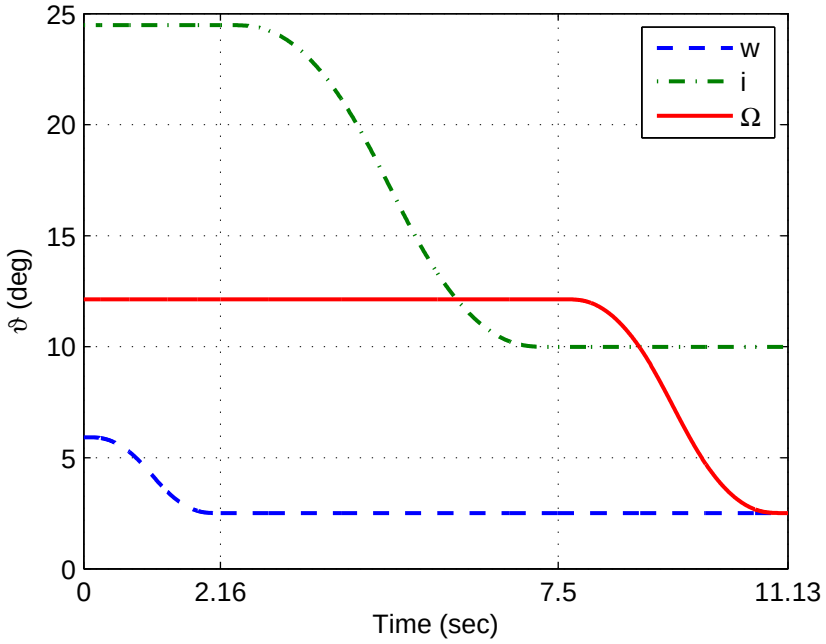

Figure C.6: Near minimum-time time trajectories for the (1-3-1) set of Euler angles

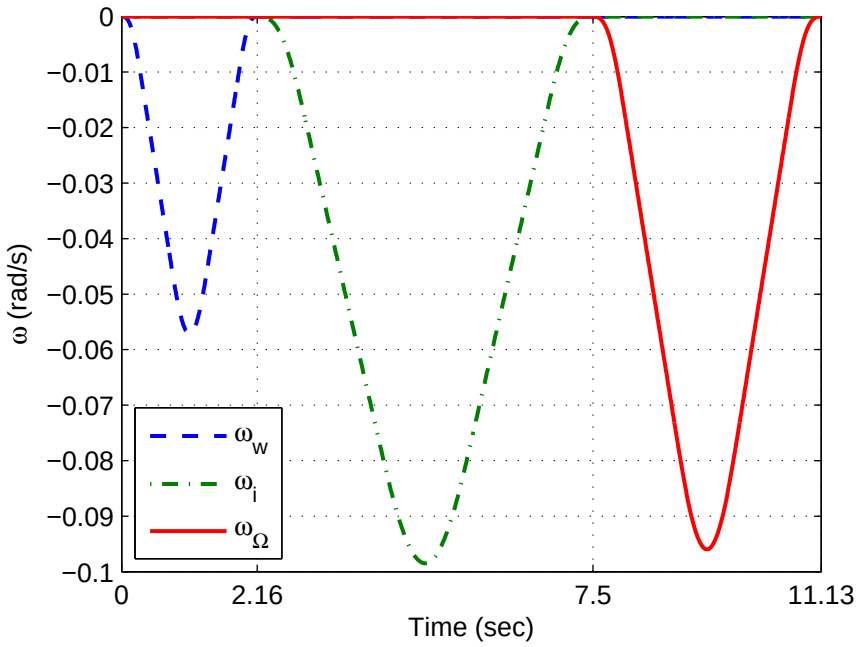

Figure C.7: Near minimum-time time trajectories for the angular velocity (1-3-1)

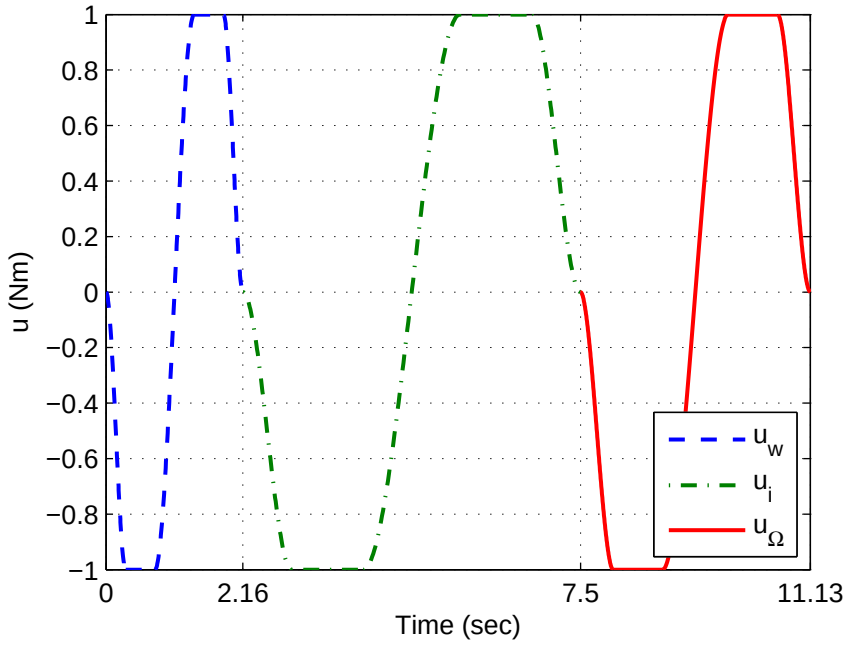

Figure C.8: Near minimum-time time trajectories for the control torque (1-3-1)

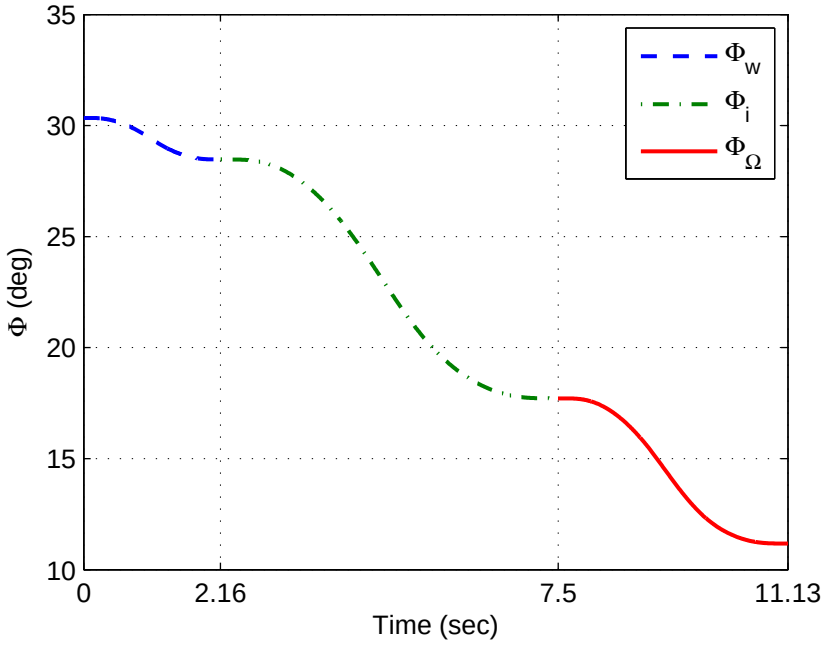

Figure C.9: Near minimum-time time trajectories for the principal angle (1-3-1)

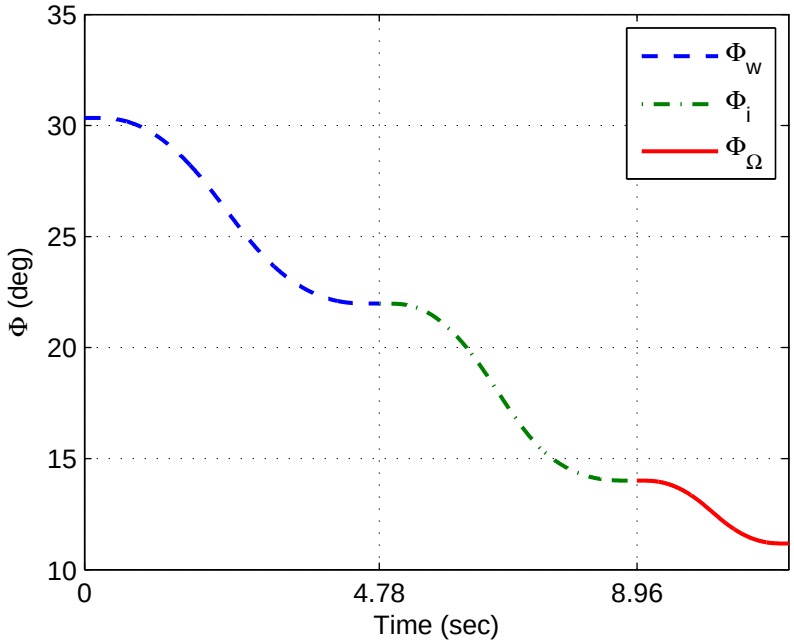

Figure C.10: Near minimum-time time trajectories for the principal angle (3-1-3)

C.3 Minimum-Fuel Maneuver

Using the numerical simulation parameters in Tables 5.1 and 5.4, numerical simulations are performed for the failed control case (2-axis control). The maximum control torque, $u_{\max}$, is assumed to be 1.

Both (1-3-1) and (3-1-3) sets of successive maneuvers are considered with Eq. (3.76). For each sub-maneuver, the switch-times, t_1 and t_2, are slightly changed to $t^i_{s_j}$. The superscript, i, indicates that i^{th} maneuver and the subscripts, j, indicate the j^{th} switch-times. Also, the final time, T, is slightly changed to T_i and $t_f \triangleq T_3$. To find a minimum-fuel solution, optimal times, T_1 and T_2, needs to be found. Here, T_1, T_2, and t_f are assumed to be 1.5 times larger than the results from the minimum-time solutions.

For the (1-3-1) set of successive maneuver, the following set of switch-times is computed to be

$$\left(t^1_{s_1},\, t^1_{s_2},\, t^2_{s_1},\, t^2_{s_2},\, t^3_{s_1},\, t^3_{s_2}\right) = (0.3513,\, 2.4087,\, 3.6262,\, 8.6888,\, 10.145,\, 13.6) \text{ sec}$$

For the (3-1-3) set of successive maneuver, the following set of switch-times is computed to be

$$\left(t^1_{s_1},\, t^1_{s_2},\, t^2_{s_1},\, t^2_{s_2},\, t^3_{s_1},\, t^3_{s_2}\right) = (0.7776,\, 5.3124,\, 6.7672,\, 10.7378,\, 11.8126,\, 14.1674) \text{ sec}$$

By comparing the performance index values, one concludes that the (1-3-1) set of successive maneuver provides the minimum-fuel solution given assumptions. The time trajectories for the (1-3-1) set, which is an optimal sequence set, of Euler angles and angular velocity are shown Figs. C.11 and C.12, respectively. The Euler angles and angular velocity meet the prescribed boundary conditions. The bang-off-

bang type of control profiles are shown in Fig. C.13. A set of switch-times is clearly described. The principal angle time trajectories are shown in Fig. C.14. As a result, the given initial asymmetric rigid spacecraft is reoriented to the defined final state with only two control inputs.

Additionally, the principal angle time trajectories for the (3-1-3) set are shown in Fig. C.15. One can observe how the principal angles change over times for both (1-3-1) and (3-1-3) sets.

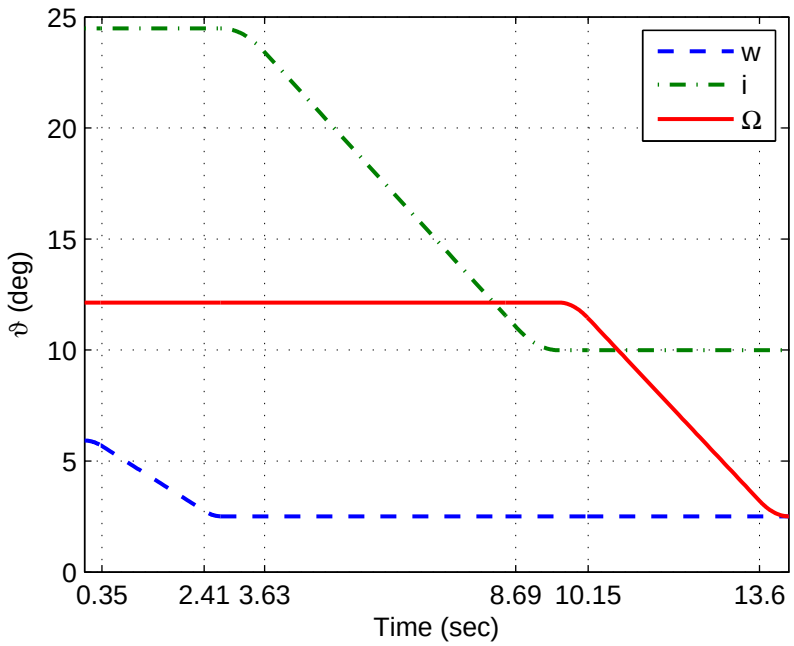

Figure C.11: Minimum-fuel time trajectories for the (1-3-1) set of Euler angles

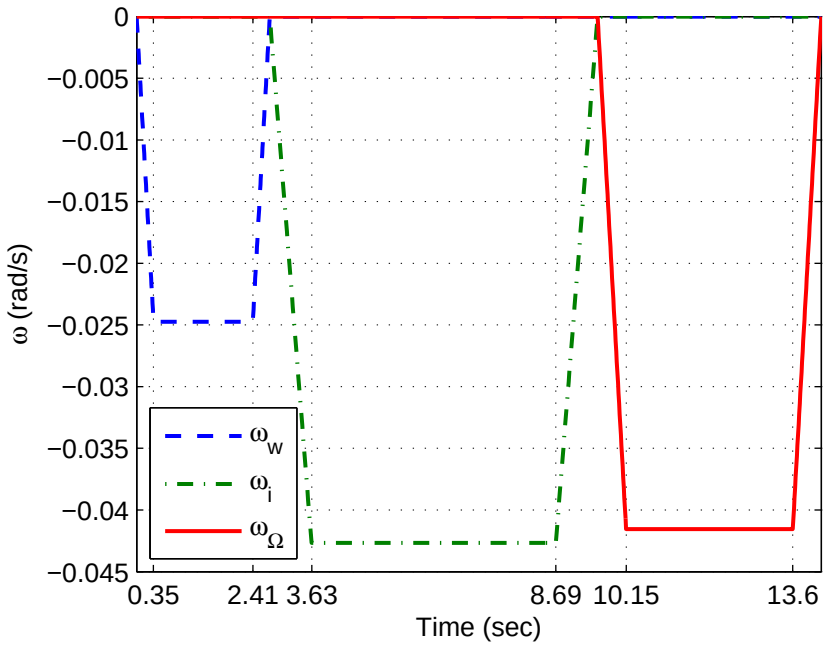

Figure C.12: Minimum-fuel time trajectories for the angular velocity (1-3-1)

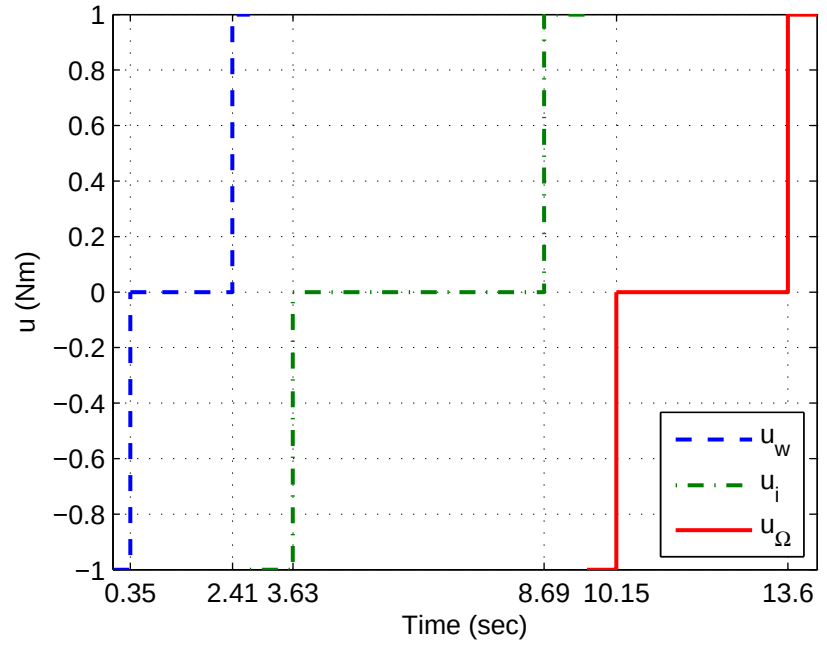

Figure C.13: Minimum-fuel time trajectories for the control torque (1-3-1)

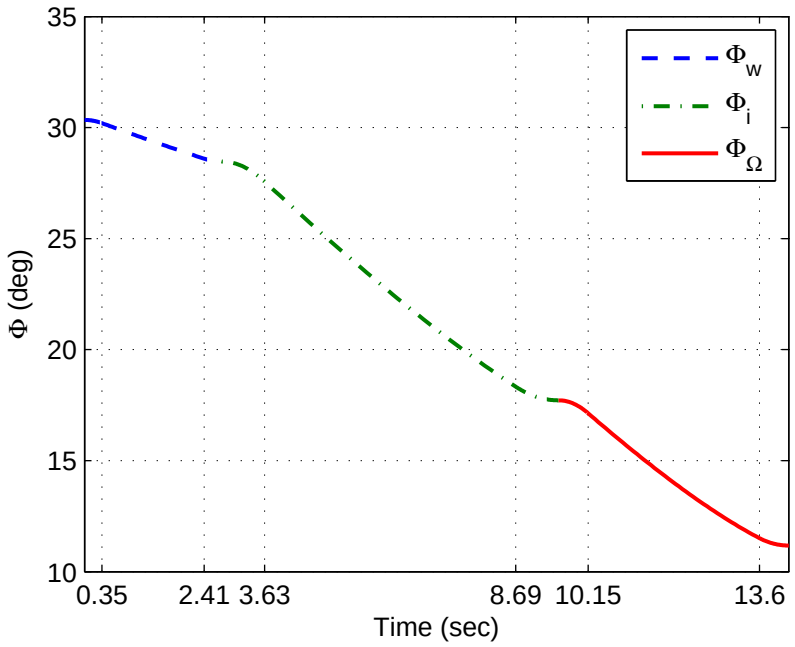

Figure C.14: Minimum-fuel time trajectories for the principal angle (1-3-1)

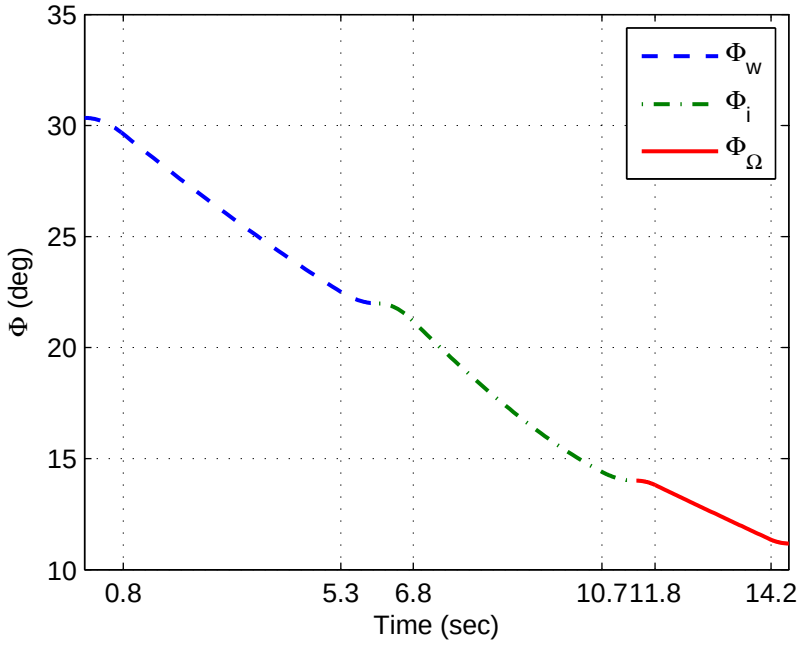

Figure C.15: Minimum-fuel time trajectories for the principal angle (3-1-3)

C.4 Cubic Polynomial Technique: Fuel Minimization

Using the numerical simulation parameters in Tables 5.1 and 5.4, numerical simulations are performed for the failed control case (2-axis control). The maximum control torque, $u_{\max}$, is assumed to be 1 and the smoothing parameter, β, is assumed as 1/5.

The (1-3-1) set of successive maneuvers is considered with the 1.5 times larger than the results from the minimum-time solutions such as T_1, T_2, and t_f.

For the (1-3-1) set of successive maneuvers, the following set of maneuver switch-times and the final time is computed to be

$$(T_1,\, T_2,\, t_f) = (2.76,\, 9.555,\, 14.19) \text{ sec}$$

For the (3-1-3) set of successive maneuvers, the following set of maneuver switch-times and the final time is computed to be

$$(T_1,\, T_2,\, t_f) = (6.09,\, 11.415,\, 14.565) \text{ sec}$$

Again, it is shown that the (1-3-1) set of successive maneuvers provides the minimum-fuel solution. The time trajectories for the (1-3-1) set, which is an optimal sequence set, of Euler angles and angular velocity are shown Figs. C.16 and C.17, respectively. The Euler angles and angular velocity meet the prescribed boundary conditions. The smooth continuous bang-off-bang type of control profiles are shown in Fig. C.18. Two maneuver switch-times and the final time are clearly described. The principal angle time trajectories for the (1-3-1) and (3-1-3) sets are shown in Figs. C.19 and C.20, respectively.

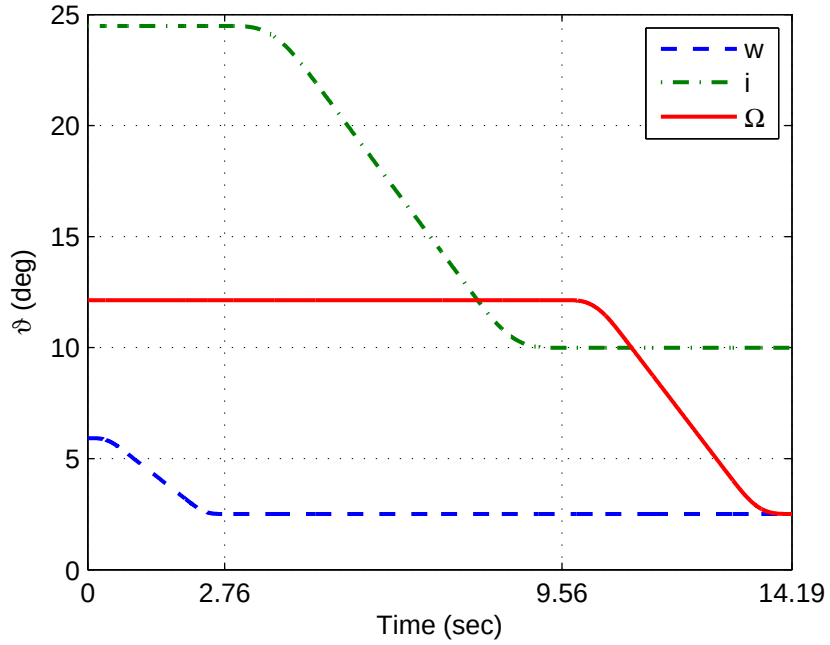

Figure C.16: Near minimum-fuel time trajectories for the (1-3-1) set of Euler angles

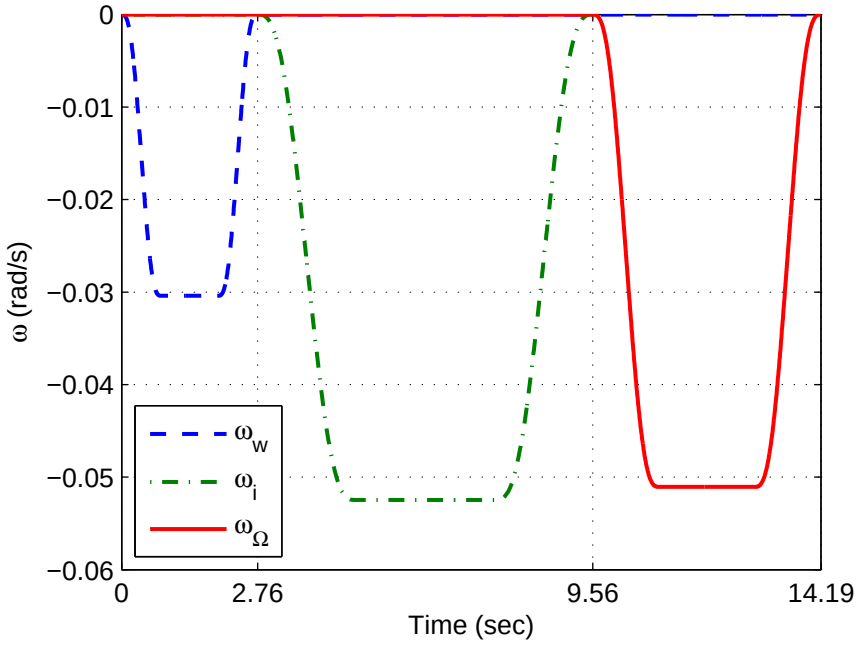

Figure C.17: Near minimum-fuel time trajectories for the angular velocity (1-3-1)

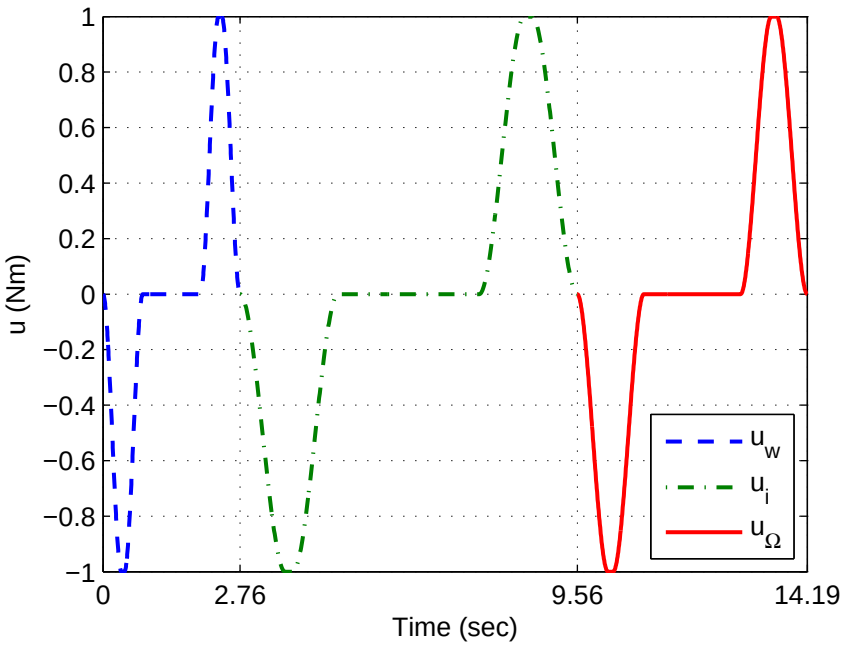

Figure C.18: Near minimum-fuel time trajectories for the control torque (1-3-1)

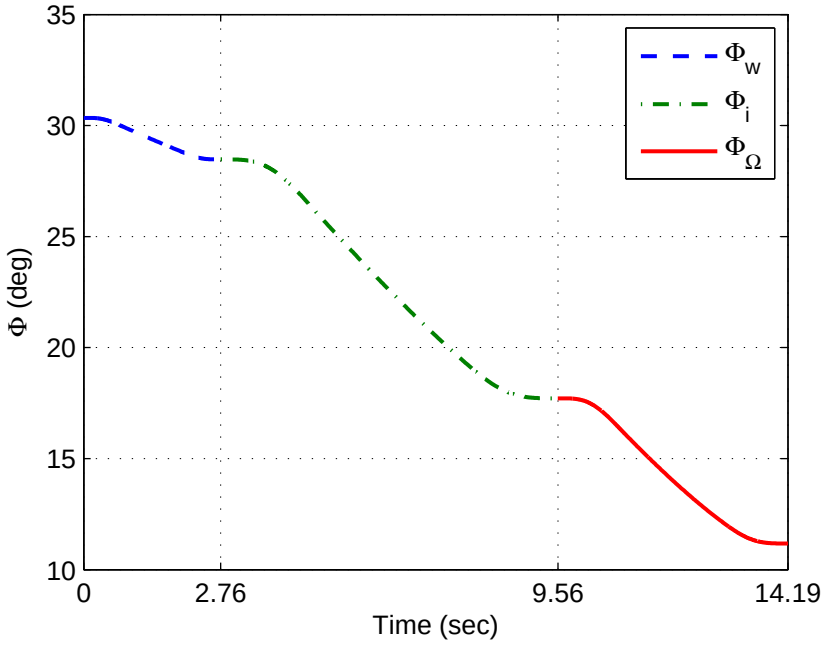

Figure C.19: Near minimum-fuel time trajectories for the principal angle (1-3-1)

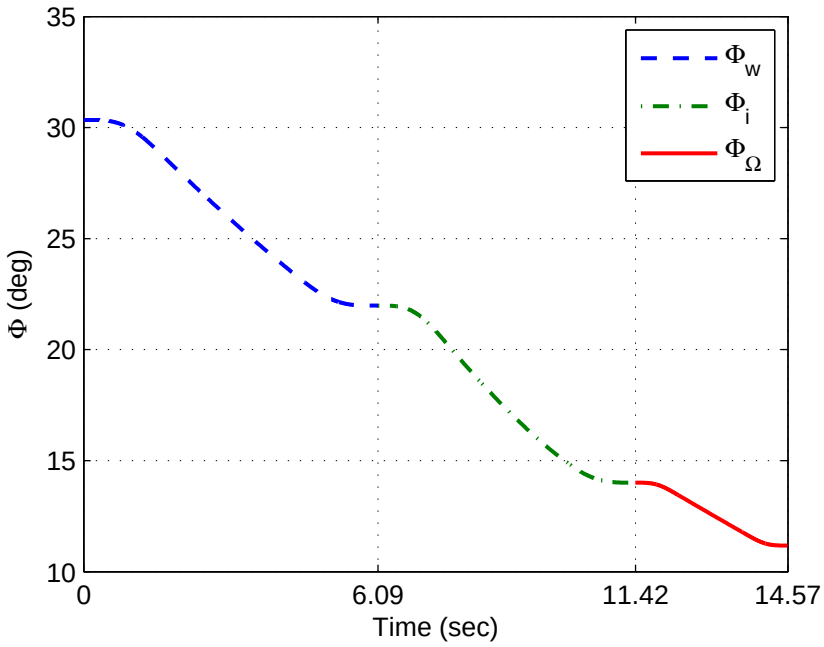

Figure C.20: Near minimum-fuel time trajectories for the principal angle (3-1-3)

APPENDIX D

STATE TRANSITION MATRIX AND PARAMETER INFLUENCE VECTOR

The state transition matrix and parameter influence vector are arranged. To find partitions of the state-costate transition matrix and parameter influence vector, the first order partials are given by

$$\frac{\partial B}{\partial \sigma_1} = 2\begin{bmatrix} \sigma_1 & \sigma_2 & \sigma_3 \\ \sigma_2 & -\sigma_1 & -1 \\ \sigma_3 & 1 & -\sigma_1 \end{bmatrix}, \quad \frac{\partial B}{\partial \sigma_2} = 2\begin{bmatrix} -\sigma_2 & \sigma_1 & 1 \\ \sigma_1 & \sigma_2 & \sigma_3 \\ -1 & \sigma_3 & -\sigma_2 \end{bmatrix}, \quad \frac{\partial B}{\partial \sigma_3} = 2\begin{bmatrix} -\sigma_3 & -1 & \sigma_1 \\ 1 & -\sigma_3 & \sigma_2 \\ \sigma_1 & \sigma_2 & \sigma_3 \end{bmatrix}$$

$$\frac{\partial \Lambda}{\partial \sigma_1} = \begin{bmatrix} \omega_1 & \omega_2 & \omega_3 \\ -\omega_2 & \omega_1 & 0 \\ -\omega_3 & 0 & \omega_1 \end{bmatrix}, \quad \frac{\partial \Lambda}{\partial \sigma_2} = \begin{bmatrix} \omega_2 & -\omega_1 & 0 \\ \omega_1 & \omega_2 & \omega_3 \\ 0 & -\omega_3 & \omega_2 \end{bmatrix}, \quad \frac{\partial \Lambda}{\partial \sigma_3} = \begin{bmatrix} \omega_3 & 0 & -\omega_1 \\ 0 & \omega_3 & -\omega_2 \\ \omega_1 & \omega_2 & \omega_3 \end{bmatrix}$$

$$\frac{\partial \Lambda}{\partial \omega_1} = \begin{bmatrix} \sigma_1 & -\sigma_2 & -\sigma_3 \\ \sigma_2 & \sigma_1 & 1 \\ \sigma_3 & -1 & \sigma_1 \end{bmatrix}, \quad \frac{\partial \Lambda}{\partial \omega_2} = \begin{bmatrix} \sigma_2 & \sigma_1 & -1 \\ -\sigma_1 & \sigma_2 & -\sigma_3 \\ 1 & \sigma_3 & \sigma_2 \end{bmatrix}, \quad \frac{\partial \Lambda}{\partial \omega_3} = \begin{bmatrix} \sigma_3 & 1 & \sigma_1 \\ -1 & \sigma_3 & \sigma_2 \\ -\sigma_1 & -\sigma_2 & \sigma_3 \end{bmatrix}$$

$$\frac{\partial \Sigma}{\partial \omega_1} = \begin{bmatrix} 0 & 0 & 0 \\ 0 & 0 & \frac{J_3 - J_1}{J_2} \\ 0 & \frac{J_1 - J_2}{J_3} & 0 \end{bmatrix}, \quad \frac{\partial \Sigma}{\partial \omega_2} = \begin{bmatrix} 0 & 0 & \frac{J_2 - J_3}{J_1} \\ 0 & 0 & 0 \\ \frac{J_1 - J_2}{J_3} & 0 & 0 \end{bmatrix}, \quad \frac{\partial \Sigma}{\partial \omega_3} = \begin{bmatrix} 0 & \frac{J_2 - J_3}{J_1} & 0 \\ \frac{J_3 - J_1}{J_2} & 0 & 0 \\ 0 & 0 & 0 \end{bmatrix}$$

The partitions of the state-costate transition matrix and parameter influence vector are shown to be

$$\frac{\partial \dot{\boldsymbol{\sigma}}}{\partial \boldsymbol{\sigma}} = \frac{1}{4}\left[\frac{\partial B}{\partial \sigma_1}\boldsymbol{\omega} \;\vdots\; \frac{\partial B}{\partial \sigma_2}\boldsymbol{\omega} \;\vdots\; \frac{\partial B}{\partial \sigma_3}\boldsymbol{\omega}\right]$$

$$\frac{\partial \dot{\boldsymbol{\xi}}}{\partial \boldsymbol{\sigma}} = -\frac{1}{2}\left[\left[\frac{\partial \Lambda}{\partial \sigma_1}\right]^{\mathrm{T}}\boldsymbol{\xi} \;\vdots\; \left[\frac{\partial \Lambda}{\partial \sigma_2}\right]^{\mathrm{T}}\boldsymbol{\xi} \;\vdots\; \left[\frac{\partial \Lambda}{\partial \sigma_3}\right]^{\mathrm{T}}\boldsymbol{\xi}\right]$$

$$\frac{\partial \dot{\boldsymbol{\xi}}}{\partial \boldsymbol{\omega}} = -\frac{1}{2}\left[\left[\frac{\partial \Lambda}{\partial \omega_1}\right]^{\mathrm{T}}\boldsymbol{\xi} \;\vdots\; \left[\frac{\partial \Lambda}{\partial \omega_2}\right]^{\mathrm{T}}\boldsymbol{\xi} \;\vdots\; \left[\frac{\partial \Lambda}{\partial \omega_3}\right]^{\mathrm{T}}\boldsymbol{\xi}\right]$$

$$\frac{\partial \dot{\boldsymbol{\mu}}}{\partial \boldsymbol{\sigma}} = -\frac{1}{4}\left[\left[\frac{\partial B}{\partial \sigma_1}\right]^{\mathrm{T}}\boldsymbol{\xi} \;\vdots\; \left[\frac{\partial B}{\partial \sigma_2}\right]^{\mathrm{T}}\boldsymbol{\xi} \;\vdots\; \left[\frac{\partial B}{\partial \sigma_3}\right]^{\mathrm{T}}\boldsymbol{\xi}\right]$$

$$\frac{\partial \dot{\boldsymbol{\mu}}}{\partial \boldsymbol{\omega}} = -\left[\left[\frac{\partial \Sigma}{\partial \omega_1}\right]^{\mathrm{T}}\boldsymbol{\mu} \;\vdots\; \left[\frac{\partial \Sigma}{\partial \omega_2}\right]^{\mathrm{T}}\boldsymbol{\mu} \;\vdots\; \left[\frac{\partial \Sigma}{\partial \omega_3}\right]^{\mathrm{T}}\boldsymbol{\mu}\right]$$

$$\frac{\partial \dot{\boldsymbol{\omega}}}{\partial \varepsilon} = -[J]^{-1}\begin{bmatrix} 0 & 0 & 0 \\ 0 & 0 & 0 \\ 0 & 0 & -2(1-\varepsilon) \end{bmatrix}[J]^{-1}\boldsymbol{\mu}$$

Finally, the state-costate transition matrix and parameter influence vector are expressed as

$$\frac{\mathrm{d}\boldsymbol{F}}{\mathrm{d}\boldsymbol{z}} = \begin{bmatrix} \begin{bmatrix} \dfrac{\partial \dot{\boldsymbol{\sigma}}}{\partial \boldsymbol{\sigma}} & \dfrac{1}{4}[B(\boldsymbol{\sigma})] \\ \mathbf{0}_{3\times 3} & [\Sigma(\boldsymbol{\omega}, J)] \end{bmatrix} & \vdots & \begin{bmatrix} \mathbf{0}_{3\times 3} & \mathbf{0}_{3\times 3} \\ \mathbf{0}_{3\times 3} & -[J]^{-1}[P^2(\varepsilon)][J]^{-1} \end{bmatrix} \\ \cdots \quad \cdots \quad \cdots & & \cdots \quad \cdots \quad \cdots \quad \cdots \\ \begin{bmatrix} \dfrac{\partial \dot{\boldsymbol{\xi}}}{\partial \boldsymbol{\sigma}} & \dfrac{\partial \dot{\boldsymbol{\xi}}}{\partial \boldsymbol{\omega}} \\ \dfrac{\partial \dot{\boldsymbol{\mu}}}{\partial \boldsymbol{\sigma}} & \dfrac{\partial \dot{\boldsymbol{\mu}}}{\partial \boldsymbol{\omega}} \end{bmatrix} & \vdots & \begin{bmatrix} -\dfrac{1}{2}[\Lambda(\boldsymbol{\sigma}, \boldsymbol{\omega})]^{\mathrm{T}} & \mathbf{0}_{3\times 3} \\ -\dfrac{1}{4}[B(\boldsymbol{\sigma})]^{\mathrm{T}} & -[\Sigma(\boldsymbol{\omega}, J)]^{\mathrm{T}} \end{bmatrix} \end{bmatrix}$$

$$\frac{\mathrm{d}\boldsymbol{F}}{\mathrm{d}\varepsilon} = \left\{\mathbf{0}_{3\times 1}^{\mathrm{T}} \quad \left\{\frac{\partial \dot{\boldsymbol{\omega}}}{\partial \varepsilon}\right\}^{\mathrm{T}} \quad \mathbf{0}_{3\times 1}^{\mathrm{T}} \quad \mathbf{0}_{3\times 1}^{\mathrm{T}}\right\}^{\mathrm{T}}$$

APPENDIX E

BODY-AXIS SKEWED TORQUE DISTRIBUTION

The open-loop optimal control solution of the rigid spacecraft is considered when two control actuators fail among four control actuators. Formulations are not shown here because only slight changes are required when compared to Section 6.4.

The rotational dynamics equation of a rigid body is slightly modified as

$$\dot{\boldsymbol{\omega}} \triangleq \tilde{\boldsymbol{p}}(\boldsymbol{\omega},\, \boldsymbol{u},\, \varepsilon) = [J]^{-1}\left(-\left[\tilde{\boldsymbol{\omega}}\right][J]\boldsymbol{\omega} + [C(\alpha,\, \beta)][P(\varepsilon)]\tilde{\boldsymbol{u}}\right) \tag{E.1}$$

where $\tilde{\boldsymbol{u}} \in \mathcal{R}^4$ is the control torque vector, $[P(\varepsilon)] \in \mathcal{R}^{4\times 4}$ is the control torque mapping matrix, and $[C(\alpha,\, \beta)] \in \mathcal{R}^{3\times 4}$ is the control torque distribution matrix from the actuator frame to the body frame. To describe the torque distribution matrix, a pyramid type of reaction wheel allocation is illustrated in Fig. E.1 and the associated torque distribution matrix is shown in Eq. (E.2).

$$[C(\alpha,\, \beta)] \triangleq \begin{bmatrix} -\mathrm{c}\beta\mathrm{c}\alpha & \mathrm{c}\beta\mathrm{c}\alpha & \mathrm{c}\beta\mathrm{c}\alpha & -\mathrm{c}\beta\mathrm{c}\alpha \\ -\mathrm{c}\beta\mathrm{s}\alpha & -\mathrm{c}\beta\mathrm{s}\alpha & \mathrm{c}\beta\mathrm{s}\alpha & \mathrm{c}\beta\mathrm{s}\alpha \\ \mathrm{s}\beta & \mathrm{s}\beta & \mathrm{s}\beta & \mathrm{s}\beta \end{bmatrix} \tag{E.2}$$

For describing a control torque degradation situation, a modified control torque mapping matrix, $[P(\varepsilon)] \triangleq \mathrm{diag}(1,\, 0,\, 1,\, 1-\varepsilon)$, is defined in terms of the homotopy embedding parameter, ε. Let's assume that one of the actuator is failed at the beginning. By spanning ε from 0 to 1, a control torque input degradation situation but two control torque inputs are unavailable at the end is fully described.

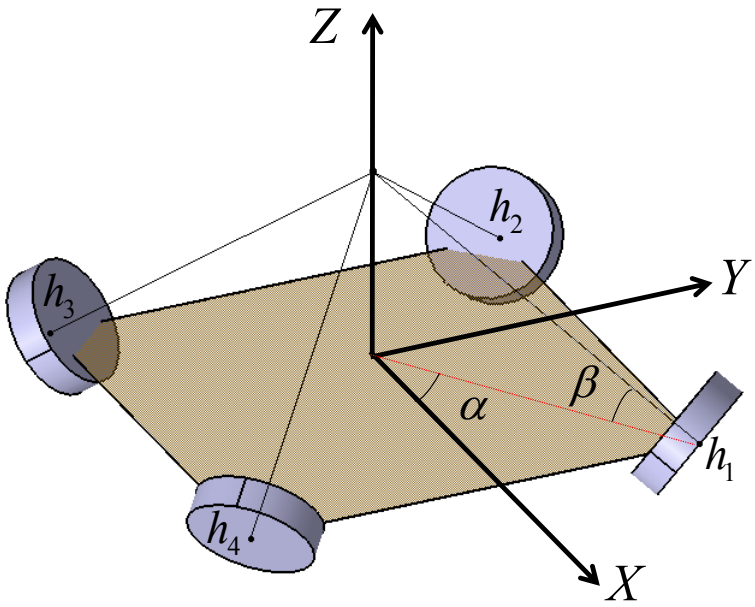

Figure E.1: Pyramid type of reaction wheel allocation description

With similar procedure in Section 6.4, the numerical simulation is performed for two maneuver cases: (i) rest-to-rest and (ii) motion-to-rest. The simulation parameters listed in Tables 6.1 and 6.2 are used and $\alpha = \beta = 45$ degrees are assumed.

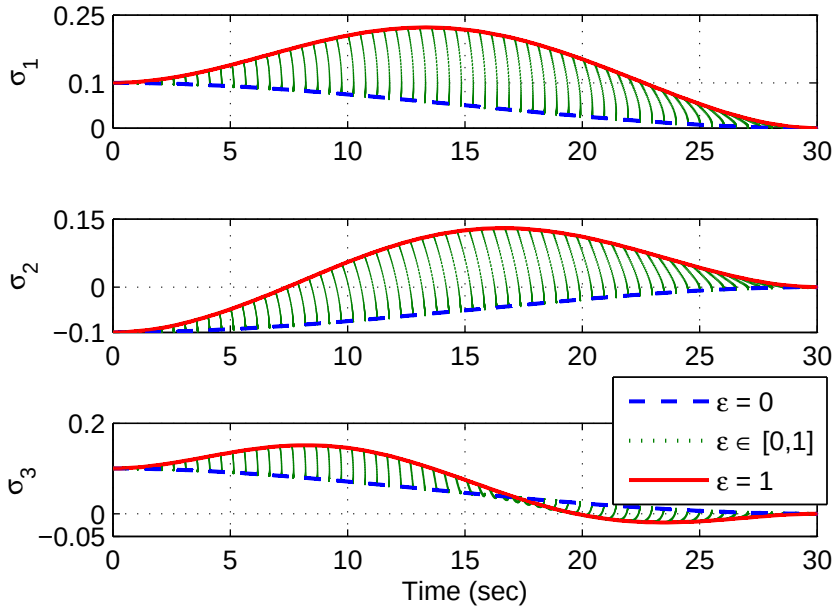

Figure E.2: Skewed: Time trajectories for the MRPs (rest-to-rest)

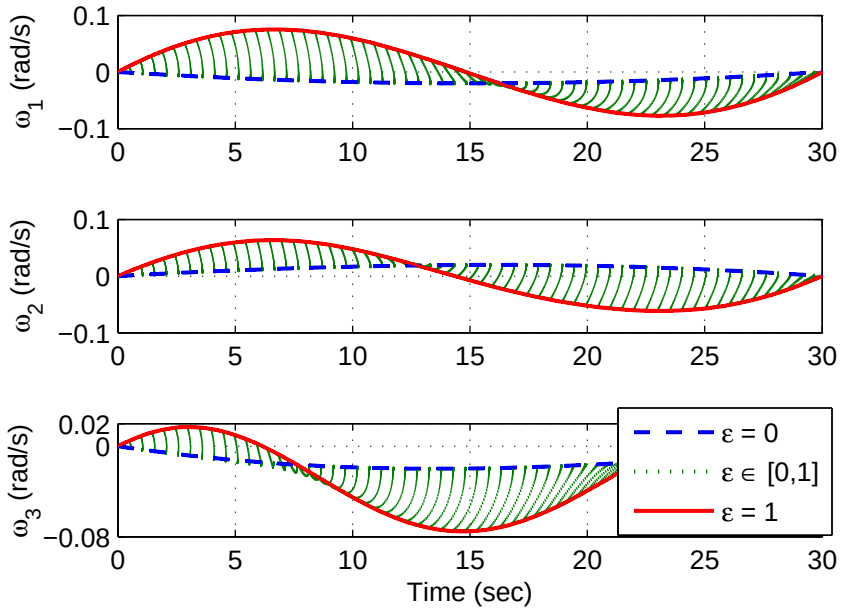

Figure E.3: Skewed: Time trajectories for the angular velocity (rest-to-rest)

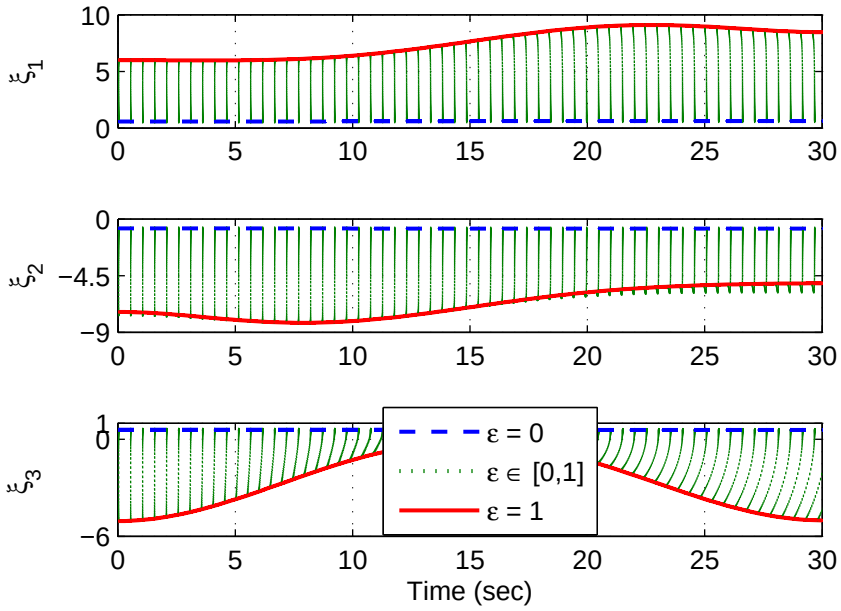

Figure E.4: Skewed: Time trajectories for the costates associated with the MRPs (rest-to-rest)

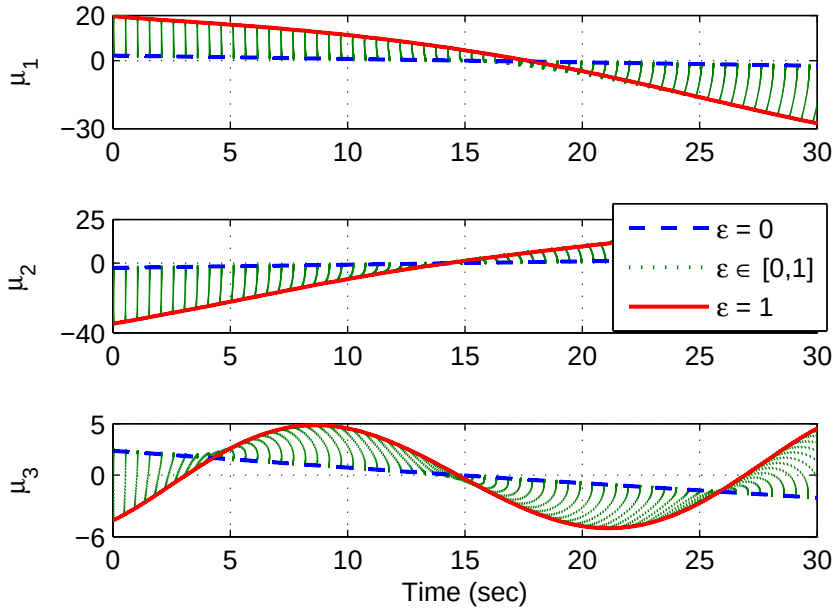

Figure E.5: Skewed: Time trajectories for the costates associated with the angular velocity (rest-to-rest)

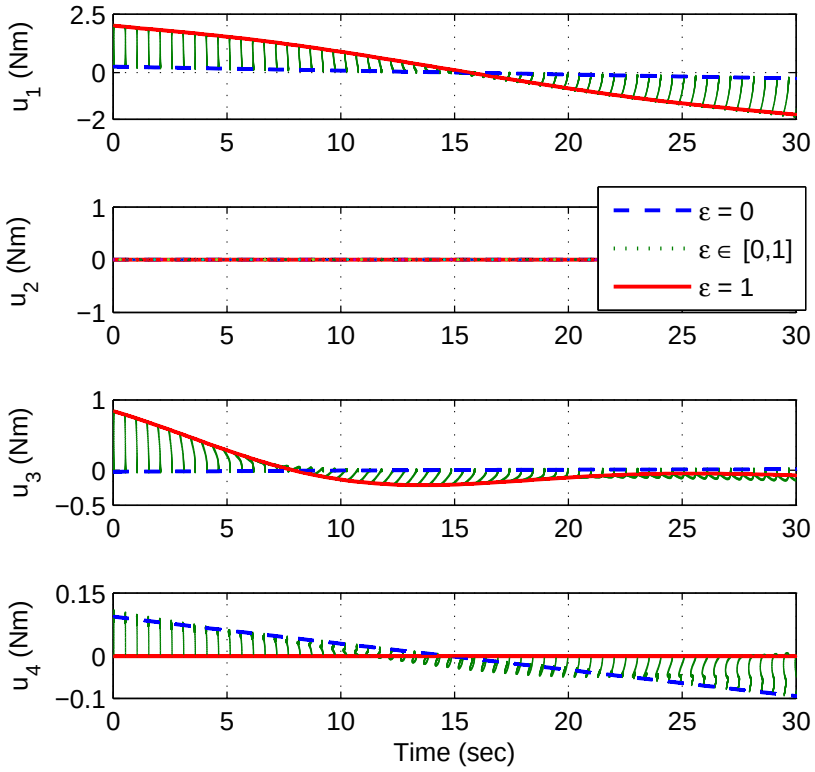

Figure E.6: Skewed: Time trajectories for the control torque (rest-to-rest)

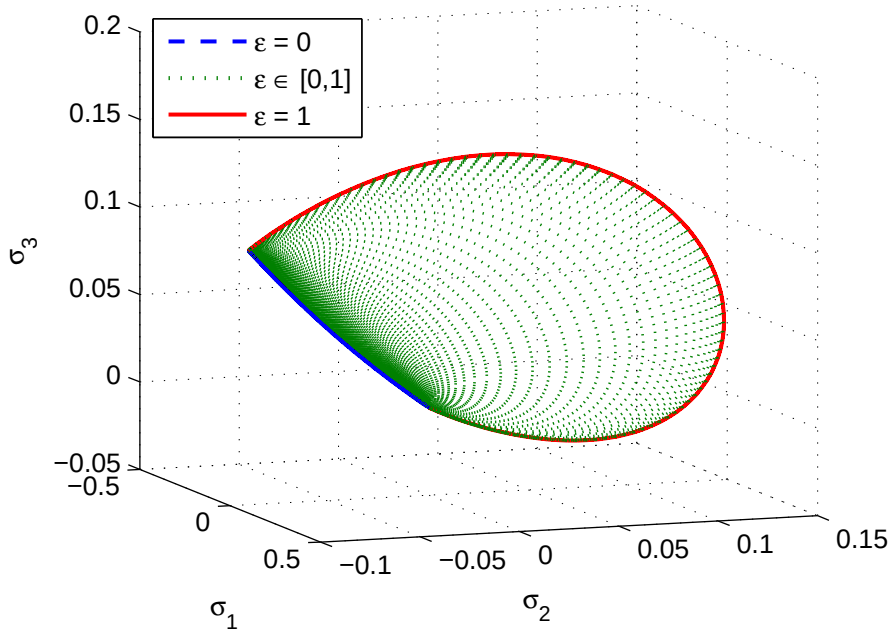

Figure E.7: Skewed: 3D trajectory for the MRPs (rest-to-rest)

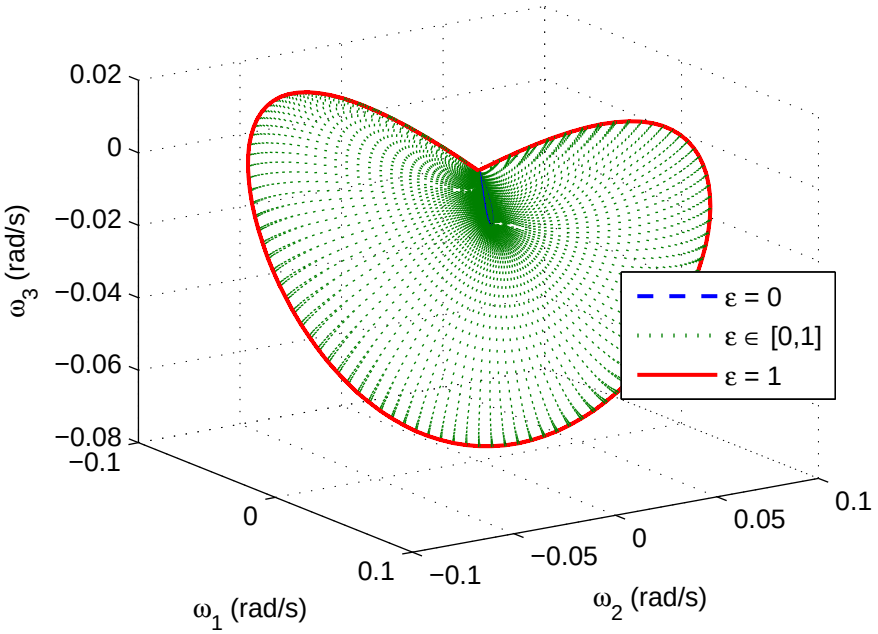

Figure E.8: Skewed: 3D trajectory for the angular velocity (rest-to-rest)

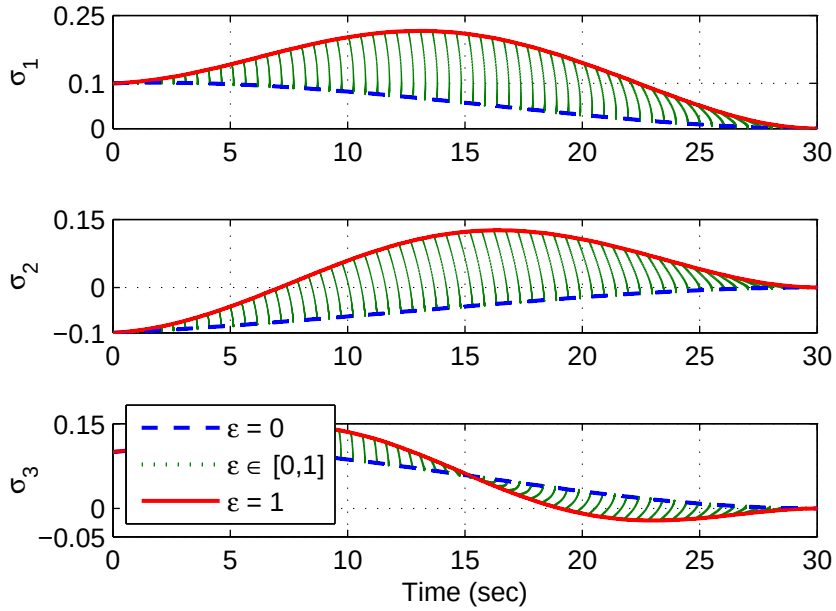

Figure E.9: Skewed: Time trajectories for the MRPs (motion-to-rest)

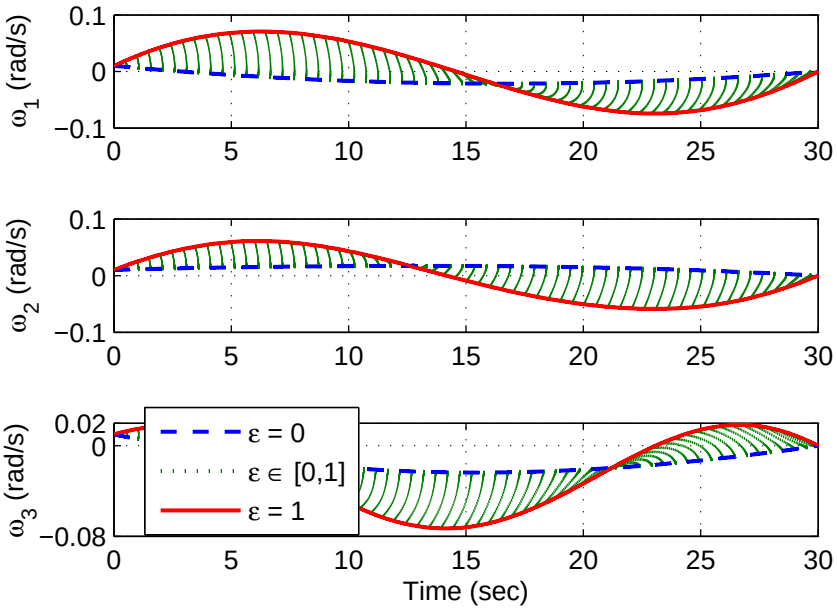

Figure E.10: Skewed: Time trajectories for the angular velocity (motion-to-rest)

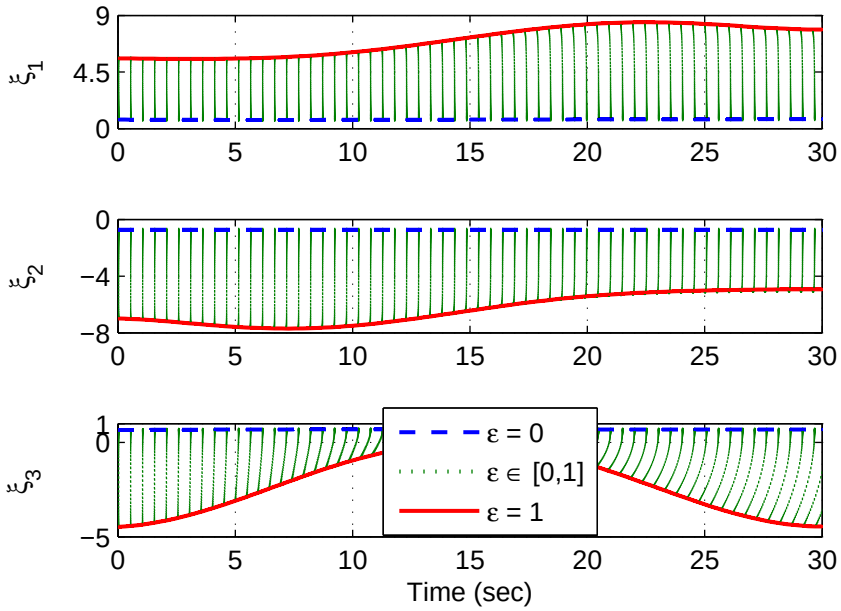

Figure E.11: Skewed: Time trajectories for the costates associated with the MRPs (motion-to-rest)

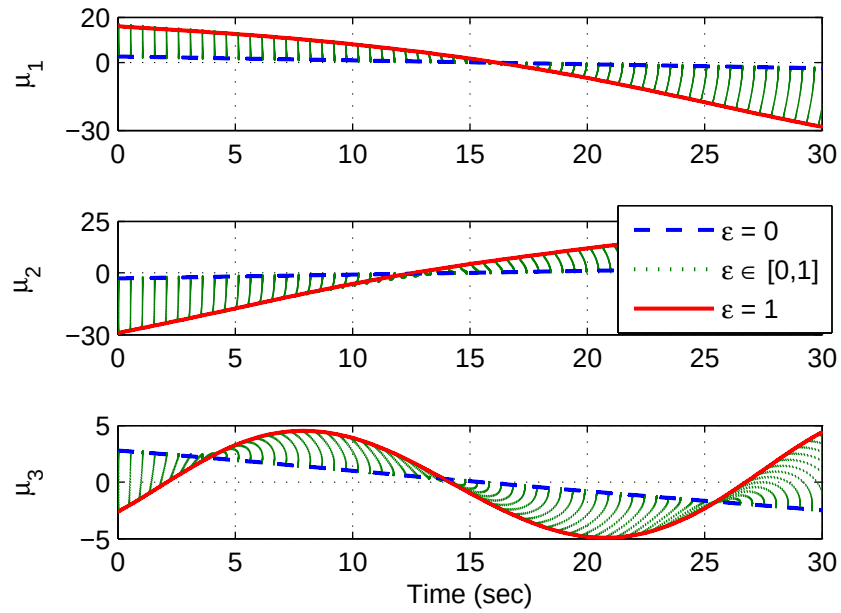

Figure E.12: Skewed: Time trajectories for the costates associated with the angular velocity (motion-to-rest)

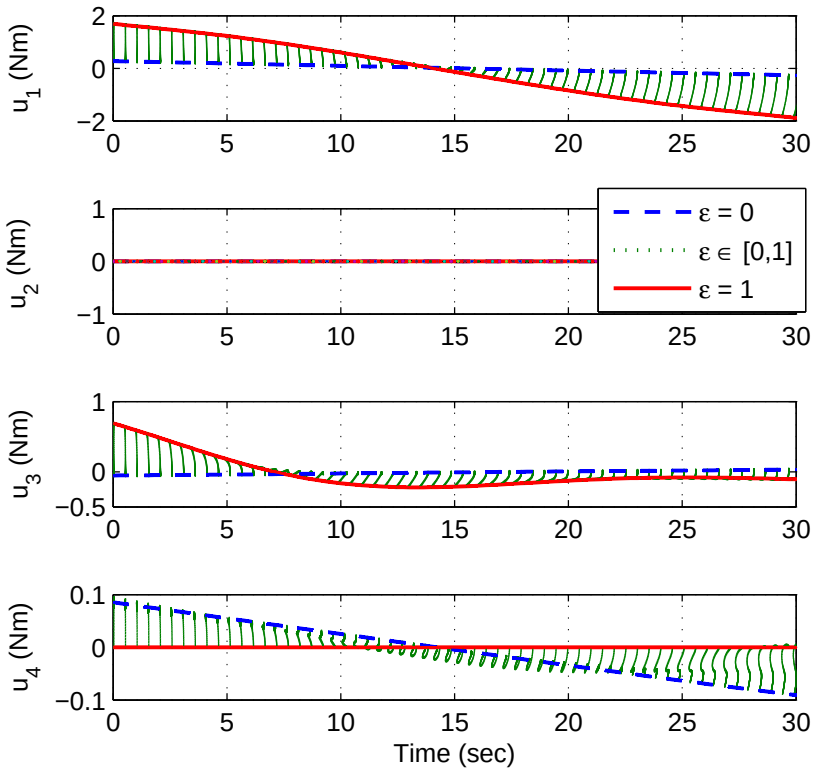

Figure E.13: Skewed: Time trajectories for the control torque (motion-to-rest)

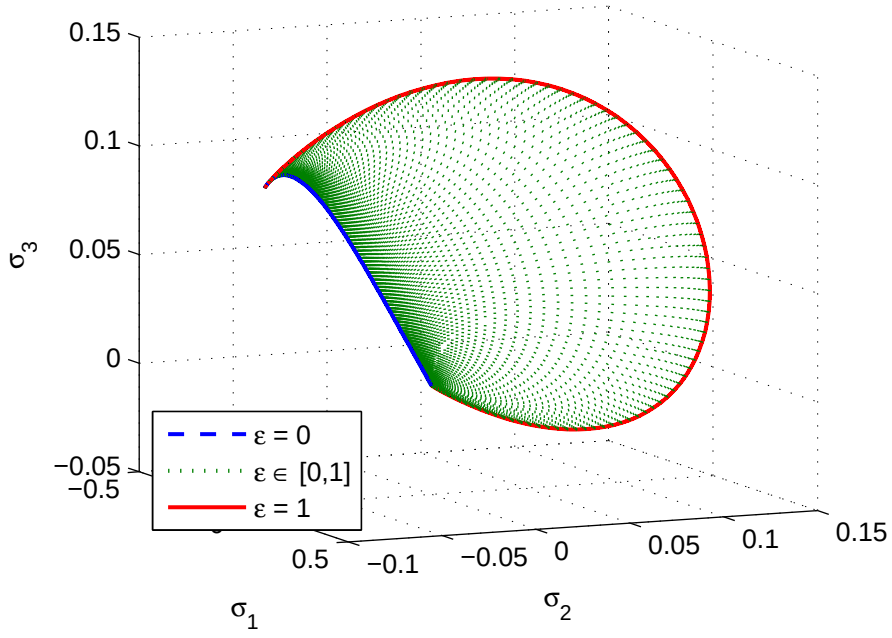

Figure E.14: Skewed: 3D trajectory for the MRPs (motion-to-rest)

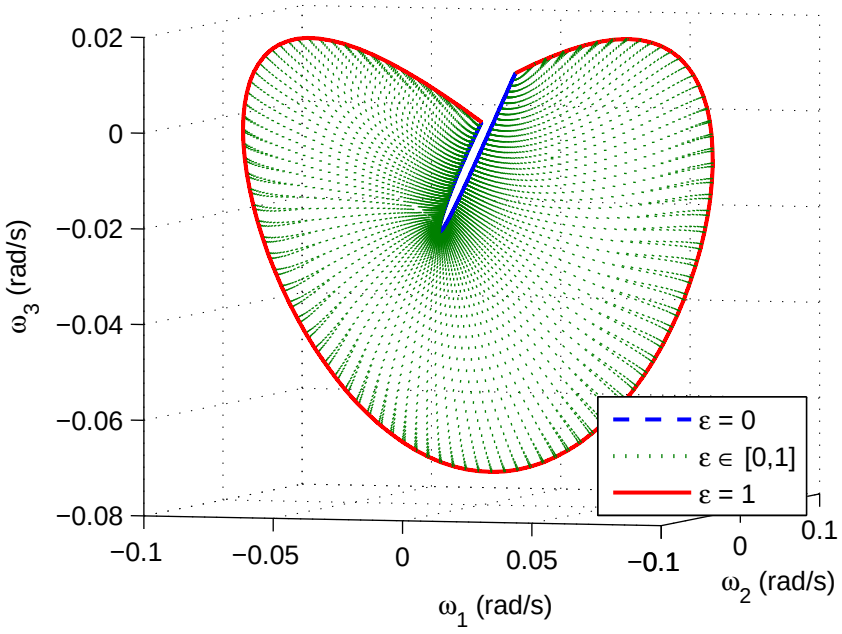

Figure E.15: Skewed: 3D trajectory for the angular velocity (motion-to-rest)